Isolation and Characterization of Natural Blue Pigments (reduced)

By Andrew Newsome

ISOLATION AND CHARACTERIZATION OF NATURAL BLUE PIGMENTS

BY

ANDREW G. NEWSOME
B.S. (West Chester University) 2007

THESIS

Submitted in partial fulfillment of the requirements
For the degree of Doctor of Philosophy in Pharmacognosy
In the Graduate College of the
University of Illinois, Chicago, 2018

Chicago, Illinois

Defense Committee:

Richard B. van Breemen, Chair and Adviser
Dr. Jimmy Orjala, Director of Graduate Studies
Dr. Brian T. Murphy
Dr. Chun-Tao Che
Dr. Stephanie Cologne

DEDICATION

This work is dedicated to science which has revolutionized nearly every aspect of human life and which in its greatest expressions often involves a well-tempered balance of reason and faith.

"To one who has faith, no explanation is necessary. To one without faith, no explanation is possible." – Thomas Aquinas

Gloria In Excelsius Deo!

ACKNOWLEDGEMENTS

This project on blue pigments was made possible primarily through the guidance and advisement of Dr. Richard van Breemen and Cathy Culver at PepsiCo. I thank PepsiCo for providing funding for the blue pigment project. I extend a special thanks to Cathy Culver at PepsiCo for working diligently against the odds for the continuation of the project. I am grateful also to the scientists at San Ei Gen F.F.I. (Osaka, Japan) for their collaboration in providing samples for the gardenia blue and kusagi berry projects. I am highly appreciative of my adviser Dr. van Breemen who has displayed consistent patience, guidance, professionalism, scientific expertise, valuable editorial feedback, and kindness.

I would like to specifically thank Dr. Gill Geesey at Montana State University for the environmental field collection of the *Zygogonium* sp. alga samples from the acidic bogs of Yellowstone National Park and for his contributions to the research on the *Zygogonium* sp. purple pigment. The carbohydrate characterization in the *Zygogonium* sp. pigment was performed by the Department of Energy funded (DE-FG02-09ER-20097) Center for Plant and Microbial Complex Carbohydrates. I also give special thanks to the condensed matter physicist Dr. Ercan Alp at Argonne National Laboratories for willingness to help with acquisition of Mössbauer and Nuclear resonance vibrational spectra for the *Zygogonium* sp. algae project. Joan Combie from Montana Polysaccharides for the work and sharing of the thermophilic microbial extract samples. The mass spectrometry instrumentation used in this work was enabled in part through the support of Shimadzu with a special thanks to Jeff Dahl.

I thank Dr. Brian Murphy also for his guidance and willingness to collaborate on the marine microbial pigments and allowed the use of his research laboratory. I thank Dr. Dejan Nikolic who over the years was an excellent source of both technical wisdom and perhaps sometimes even more

importantly, of humor. I also give thanks to the assistance and friendship of current and past members of the Dr. Richard van Breemen laboratory (Chicago Mass Spectrometry Laboratory) as well as those in other groups. These include: Joshua Henkin, Brian Wright, Zane Huack, Jordan Gunn, Ke Huang, Jerry White, Skylar Carlson, George Chlipala, and Megan Sturdy. I acknowledge the kindness and willingness of many other lab groups and members to help with specific experiments such as Jason Hickok for acquisition of the electron paramagnetic spectrum, members of the laboratories of Doug Thomas, Jimmy Orjala, Judy Bolton, and several others. I give special thanks to Michael Mallowney for his collaboration on the trichotomine project, Yongchao Li for his collaboration on the hydrolysable tannins method, and Bethany Elkington for the opportunity to collaborate on her *Polyalthia* thesis project. Finally, I would like to express deep gratitude to family and friends for their love and support through the years.

AGN

CONTRIBUTION OF AUTHORS

Chapter 1 is a literature review of natural blue pigments which was adapted from the publication almost entirely researched and authored by me with significant editing help from Catherine Culver and Richard B. van Breemen. Some limited sections of **Chapter 2** and **Chapter 3** were taken from the published *ACS sumposium* book chapter listed which was my original research and writing aside from some minor assistance and editing help. **Chapter 4** was adapted directly from the listed methods publication. This work was written by me but the research was performed in collaboration with Yong-Chao Li. The remainder of the thesis (Chapter 5, Chapter 6, and Chapter 7) is my original research and writing not based on previously published works.

TABLE OF CONTENTS

CHAPTER **PAGE**

TABLE OF CONTENTS (continued)

CHAPTER **PAGE**

TABLE OF CONTENTS (continued)

CHAPTER **PAGE**

TABLE OF CONTENTS (continued)

CHAPTER **PAGE**

LIST OF TABLES

LIST OF TABLES (continued)

LIST OF FIGURES

FIGURE **PAGE**

LIST OF FIGURES (continued)

FIGURE **PAGE**

LIST OF FIGURES (continued)

FIGURE **PAGE**

LIST OF ABBREVIATIONS

3*O*Me-G	3-*O*-methyl-gallic acid
3*O*Me-MG	3-*O*-methyl-gallic acid methyl ester
ACN	Acetonitrile
ANL	Argonne National Labs
APCI	Atmospheric pressure chemical ionization
C_{18}	Octadecylsilyl
CCRC	Complex Carbohydrate Research Center
COP	College of Pharmacy, UIC
COSY	Homonuclear correlation (NMR) spectroscopy
CSB	Center for Structural Biology, UIC
DEPTQ	Distortionless enhancement by polarization transfer, quaternary (NMR)
DFT	Density functional theory
DMSO	Dimethylsulfoxide
EA	Ellagic acid
EDTA	Ethylenediaminetetraacetic acid
EPR	Electron paramagnetic resonance
ESI	Electrospray
FD&C	Food, drug, & cosmetic
FDA	Food and drug administration
FCF	For coloring food
GA	Gallic acid
Gal	Gallic acid
Glu	Glucose
Hex	Hexose
HHDP	Hexahydroxydiphenic acid
HMBC	Heteronuclear multiple bond correlation (NMR)
HPLC	High pressure liquid chromatography
HSQC	Heteronuclear single quantum coherence (NMR) spectroscopy
HT	Hydrolysable tannin
HOMO	Highest occupied molecular orbital
HRMS	High resolution mass spectrometry
IC_{50}	Half of the maximal inhibitory concentration
ITTOF	Ion-trap Time-of-flight
L	Ligand
LUMO	Lowest unoccupied molecular orbital
MBRB	Molecular biology research building, UIC
MeCN	Acetonitrile
MeOH	Methanol
MG	Methyl gallate
mG	malonylglycoside
mGlu	malonylglucoside
MHz	Megahertz
MALDI	Matrix assisted laser desorption ionization mass spectrometry

LIST OF ABBREVIATIONS (continued)

MS	Mass spectrometry or mass spectrum
MS^2	Tandem mass spectrometry (MS/MS)
MSU	Montana State University
MTA	Material transfer agreement
NMR	Nuclear magnetic resonance
NRVS	Nuclear resonance vibrational spectroscopy
PDA	Photodiode array
RNA	Ribonucleic acid
SEC	Size-exclusion chromatography
SEM	Scanning electron microscopy
TA	Tannic acid
T_R	Retention time
TOCSY	Total correlation (NMR) spectroscopy
UHPLC	Ultra high pressure liquid chromatography
UIC	University of Illinois at Chicago
UV	Ultraviolet light
Vis	Visible light
V_0	Void volume
YNP	Yellowstone National Park

EQUIPMENT AND SUPPLIES

EQUIPMENT

The mass spectrometry laboratory (Room 550 and 552, College of Pharmacy, UIC) is jointly directed and maintained by Prof. Richard B. van Breemen and by the UIC Research Resources Center (RRC). The laboratory houses and maintains a variety of high resolution tandem mass spectrometers. The Shimadzu IT-TOF and Synapt Q-TOF will be the primary instruments of use for the dereplication and structure elucidation of small molecules. The college of pharmacy NMR facility maintains two Bruker NMR instruments (300 MHz, 400 MHz). The Center for Structural Biology (CSB) NMR facilities house a 600 MHz, 800 MHz, and 900 MHz NMR which can be used for obtaining 2D NMR data for full structure determination.

EQUIPMENT LIST:

Mass Spectrometry Laboratory:
Shimadzu IT-TOF mass spectrometer
Synapt Q-TOF mass spectrometer
Thermo Scientific LTQ Orbitrap Velos mass spectrometer
Applied Biosystems Voyager-DE Pro MALDI-TOF mass spectrometer
Thermo Finnigan LTQ Linear Ion trap mass spectrometer
Thermo Scientific LTQ FT-ICR mass spectrometer
Agilent 1946A MSD single quadrupole mass spectrometer
Shimadzu Upgraded 8030 triple quadrupole mass spectrometer
Agilent 1100 Series HPLC system with DAD-UV detector
Shimadzu UFLC with SPD-20A dual wavelength UV detector
Shimadzu UFLC with SPD-M20A photodiode array UV/Vis detector

Nuclear Magnetic Resonance (NMR) Facilities:
Bruker DXP-300 MHz NMR (COP)
Bruker DXP-400 MHz NMR (COP)
Bruker DXP-600 MHz NMR with cryogenic triple resonance inverse probe (CSB)
Bruker US2 Advance 800 MHz NMR with cryogenic triple resonance inverse probe (CSB)
Bruker US2 Advance 900 MHz NMR with cryogenic triple resonance inverse probe (CSB)

Microbiological Culture Equipment (Molecular Biology Research Building, UIC):
Innova 5000 Gyrorotary Tier Shaker table
Baker SterilGARD Class II biological safety cabinet
Amsco 3043-S and SV-120 autoclaves
Zeiss light microscopes
Cold room and incubator room

Other Equipment (College of Pharmacy, UIC):
HP 8452A Diode Array UV/Vis Spectrophotometer

EQUIPMENT AND SUPPLIES (continued)

Shimadzu IRPrestige-21 FT-IR detector with ATR crystal
RVT106 Solvent Refrigerated Vapor Trap and Speedvac Concentrator
Model Ultra AN MK2 ELGA PureLab Ultra Water Purifier
Fisher Vortex Genie 2 No. 12-812
Mettler-Toldeo AG285 Analytical Balance
Branson 2210 Sonication Heat Bath
Eppendorf 5804R 15 Amp Centrifuge
VWR 4 C refrigerator, Kenmore -20 C freezer
Fisher Scientific Accumet BASIC AB15 pH meter

SUPPLIES:

Microbiological growth nutrients and reagents, general microbiological culturing supplies and glassware, and some commercial microbial strains will be required for the isolation and cultivation of microbes. General supplies involved in the isolation, purification, and structure elucidation of pigment compounds include extraction solvents, chromatographic separation materials, chemical reagents, plastic and glass vials and tubes, HPLC grade solvents, HPLC columns, and deuterated NMR solvents.

SUMMARY

The food and beverage industry is seeking to broaden the palette of naturally derived colorants. The natural food colorant market has grown to over $1 billion dollars annually. Many approved natural food colorants are available for replacing the red, orange, and yellow synthetic dyes. However, there is still a lack of available green, blue, and violet natural colorants. The overall goal of this project is to elucidate the structures of novel blue, green, and violet pigment compounds produced within the natural products world. New blue pigment compounds may serve as patentable lead candidate compounds for future use as natural blue food colorants.

To provide a thorough and definitive framework from which to proceed with the discovery of new blue pigments, organic blue compounds from natural plant, animal, fungal, and microbial sources are first reviewed (Chapter 1). The scarcity of blue colored metabolites in the natural world relative to metabolites of other colors is discussed and structural trends common among natural blue compounds are identified. These compounds are grouped into seven structural classes and evaluated for their potential as new color additives.

Although considerable effort has been devoted to the search for new blue colorants in fruits and vegetables, less attention has been directed towards blue compounds from other sources such as bacteria and fungi. Microorganisms, especially from the marine environment, continue to be a prolific source of previously uncharacterized secondary metabolites including pigments. Chapter 2 investigates pigments from marine-derived microbes for potentially novel lead compounds and led to the dereplication of a variety of known microbial pigments. Chapter 2 also discusses a variety of established extraction, fractionation, and chromatographic purification

techniques used in this work. Known compound were dereplicated primarily using HPLC separation coupled with UV-Vis detection and high resolution tandem mass spectrometry.

Chapter 3 covers the identification of the purple pigment of acidophilic *Zygogonium sp.* algae from Yellowstone National Park. The purple pigment, found to be a macromolecular ferric oligosaccharide gallate complex, was isolated and characterized by a great variety of chemical and spectroscopic techniques. Although the purple pigment is not suitable for use in commercial products due to low color intensity and iron content, the pigment is of ecological and natural products chemistry interest. The oligosaccharide gallate species detected in this work represent a new subclass of natural product molecules. There is also evidence that the pigment may represent one of the only known ferric biological sunscreens. The need for an accurate quantitation of bound galloyl groups in this work led to the development of an improved LC/MS method for the determination of bound galloyl groups was presented in Chapter 4.

The structure elucidation of a series of novel trichotomine analogs (trichotomine G_3, trichotomine G_4, and trichotomine G_5) extracted from *Clerodendron trichotomum* (Japanese kusagi berry) is presented in Chapter 5. The intense blue hue and low toxicity of the trichotomines make them compelling as natural blue colorant lead candidates. The novel analogs contained 6-*O*-malonyl attachments. Higher molecular weight trichotomine glycosides were identified by $HRMS^n$ analysis as well. The glycosides were found to be attached to the trichotomine carboxylic acid groups (COOGlu) as opposed to the indole rings (*N*Glu) as was previously reported. Unfortunately, color stability testing indicated that the acid and heat stability of the trichotomine analogs is not sufficient for their use as consumer colorants.

Chapter 6 involves structural studies of the complex polymeric pigment "gardenia blue". The pigment is derived from the reaction of the iridoid genipin (*Gardenia jasminoides*) with a primary amine. The blue nature-derived colorant is used in few food coloring applications due to its pseudo-natural status and limited regulatory approval. Chapter 6 includes the NMR analysis of a commercial "gardenia blue" product provided by San Ei Gen F.F.I., chromatographic and spectroscopic study of "gardenia blue" pigment generated fresh by the reaction of genipin with methylamine and other amines, and theoretical (DFT) calculations of 2-pyrindine dimers. The results suggested that the chromophoric portions of the "gardenia blue" pigment involve conjugated dimers of 2-pyrindine ring systems linked by an unsaturated C_1 or C_2 bridges.

A natural blue colorant suitable for consumer beverage applications, termed the "holy grail" in the colorant field, has not yet been found. The work covered in this dissertation contributes substantially towards that goal. The pursuit of more promising research avenues, such as investigating avenues for increasing the stability of the trichotomine derivatives or searching for more heat stable versions of phycocyanin, may lead to a suitable natural blue consumer colorant in the future.

DISCLAIMER

The views expressed in this work are solely those of the authors and should not be construed as statements of position, intention, or strategy of PepsiCo or San Ei Gen F.F.I.

CHAPTER 1: INTRODUCTION

(Contains sections previously published as Newsome, A. G.; Catherine A. Culver; and Breemen, R.V.B. Nature's palette: the search for natural blue colorants. *J. Ag. Food Chem.* **2014**, *62*, 6498-6511.)

1 INTRODUCTION

Color additives are used worldwide to enhance the appearance of a wide variety of food and beverage products. Consumers express a general preference for natural food ingredients over synthetically produced ones. Consequently, the sale of natural color additives nets over $1 billion in annual revenue. Whether from natural or synthetic sources, new colorants must meet strict requirements and be approved as color additives before use in food or beverages. The US Code of Federal Regulations (1) provides details of the petitioning process. Permitted uses for colorants include replacement of color lost by processing or storage, addition of color to otherwise colorless products such as soft drinks and confectionery, and standardization of product appearance when raw materials vary in color (2). All food colorants are closely regulated to ensure that they are safe to consume and are not used in a manner to mislead consumers. These complex regulations have been summarized in a number of reviews (2-4).

1.1 Statement of the Problem

The food and beverage industry has sought to broaden the palette of naturally derived color additives for decades. Red, yellow, and orange pigments are relatively easy to produce with natural colorants such as carotenoids and anthocyanins, but product developers face a severely limited availability of naturally derived blue, green and deep purple shades. Naturally derived alternatives for these shades are unsatisfactory for use in most beverages. The synthetic colorants FD&C Blue No. 1 and FD&C Blue No. 2 (Figure 1) are approved for use in food and beverages (8). FD&C Blue No. 1 is widely used in both food and beverages. FD&C Blue No. 2 is not typically used in beverages due to unsatisfactory stability (9). To date, no direct naturally derived replacement for FD&C Blue No. 1 has

been found. Alternatives to other certified synthetic colorants have been discussed in recent reviews (2,5,6).

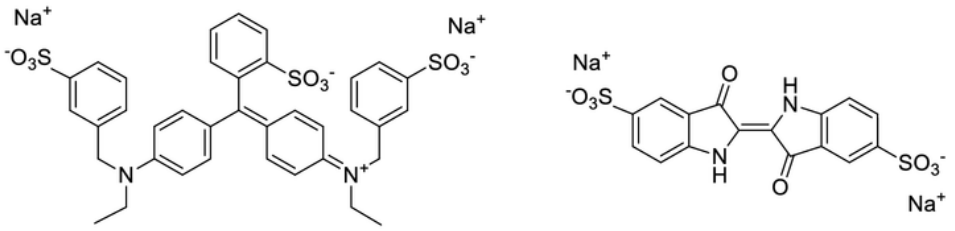

brilliant blue FCF
(FD&C blue no. 1, E133)

indigo carmine
(FD&C blue no. 2, E132)

Figure 1. The chemical structures of FD&C Blue No. 1 and FD&C Blue No. 2

Blue colors are not uncommon in nature but are extremely difficult to replicate in foods and beverages. Blue shades can be produced by some anthocyanins but only in the pH range of 5-7. These colorants turn pink or purple in typically acidic food and beverage products. A green colorant, sodium copper chlorophyllin, has been approved by the US FDA for use only in citrus-based dry beverage mixes in an amount at or below 0.2 percent wt/wt of the dry mix (7). Usage of this colorant in other products is limited by its poor stability to heat, light and acid. Blue shades can be produced by phycocyanin and iridoid-derived pigments. The US FDA recently approved phycocyanin in the form of spirulina extract for coloring candy and chewing gum (10). Unfortunately, the use of phycocyanin in other applications is limited by the lack of stability to heat, light and acid. The blue iridoid-derived colorants from *Genipa americana* and *Gardenia jasminoides* are used on a limited basis because of limited approval for use. Because bone of these blue colorants matches the shade produced by FD&C Blue No. 1, the search for naturally derived blue colorants continues.

1.1.2 Specific Objectives

The goal of the present study was to obtain and chemically characterize new pigment molecules that produce blue color shades (in solution) in an effort to find naturally derived alternatives to FD&C Blue No. 1. The specific objectives of this study were as follows:

Specific Objective A: Thoroughly review the literature to compile data on known natural blue colored molecules from plants, animals, fungi, and microbes. This review would facilitate dereplication, serve as a foundational survey of the blue chromophores produced in nature and explore whether any are suitable as color additives.

Specific Objective B: Generate or acquire lead pigmented biomass or material potentially containing novel blue or purple pigments for characterization. Pigmented lead materials may be collected from the natural environment either directly or through collaboration with other researcher and research groups.

Specific Objective C: Develop and execute dereplication procedures on pigmented lead material so that research efforts may be focused on unknown and uncharacterized pigment compounds. Dereplication would use a combination of UV/Vis spectroscopy and high resolution mass spectrometry.

Specific Objective D: Spectroscopically characterize and elucidate the structures of new blue pigments using modern chemical characterization techniques including but not limited to liquid chromatography, HRMS, tandem mass spectrometry, 2D-NMR experiments, UV-Vis spectroscopy, and FT-IR spectroscopy.

The search for new natural blue colorants begins with several fundamental questions. Perhaps most fundamentally, what is a blue pigment? What blue pigments and types of blue chromophores are found in nature, and are any of these compounds suitable for use as food colorants? And why do blue colored molecules occur far less frequently than red, orange, or yellow natural pigments? The remainder of this chapter addresses each of these questions.

1.2 Blue pigment definition

Ordinary color perception in molecules is a subtractive process where the color perceived is a result of the eye perceiving only the wavelengths of light that have passed through a molecule unabsorbed. For example, the carotenoid lycopene absorbs blue light and red is perceived. FD&C Blue No. 1 absorbs red light strongly and thereby appears intensely blue. Since α-chlorophyll absorbs both red and blue light, green is perceived. Anthocyanins appear purple (red and blue combined) because they absorb green light. There are other processes leading to perceived color. Luminescent processes like fluorescence and phosphorescence are due to emitted, not absorbed, photons. Color can also result from diffraction or scattering of light. Only pigmentation by the absorptive processes of organic molecules was within the scope of this work. A *blue pigment* is defined here as *an organic molecule that absorbs red light* (600 nm region) *and appears blue by ordinary color perception* (Figure 2). The origin of color in molecules, electron spectroscopic theory, and the processes of color perception are well known (11-13).

Blue pigments (red light absorbing molecules) are much less common in nature relative to red, orange, and yellow pigments. The reason for this may be explained using electronic absorption theory.

When the energy of an incident photon matches an energy gap ($\Delta E = h\nu$) between molecular orbitals (σ, n, or π), the photon is absorbed by an electron that is promoted to the next higher energy orbital. Most molecules absorb ultraviolet photons by $\sigma \rightarrow \sigma^*$ and $\sigma \rightarrow \pi^*$ transitions. Far fewer molecules exhibit the lower energy $\pi \rightarrow \pi^*$ and $n \rightarrow \pi^*$ transitions that are required to absorb visible light, and these molecules appear to have color. Conjugation of π-bond systems can lower the HOMO→LUMO energy gap for $\pi \rightarrow \pi^*$ transitions to occur into the blue light region (400 to 500 nm, ΔE = 3.1-2.5 eV) and this produces red, orange, and yellow colors as in carotenoids.

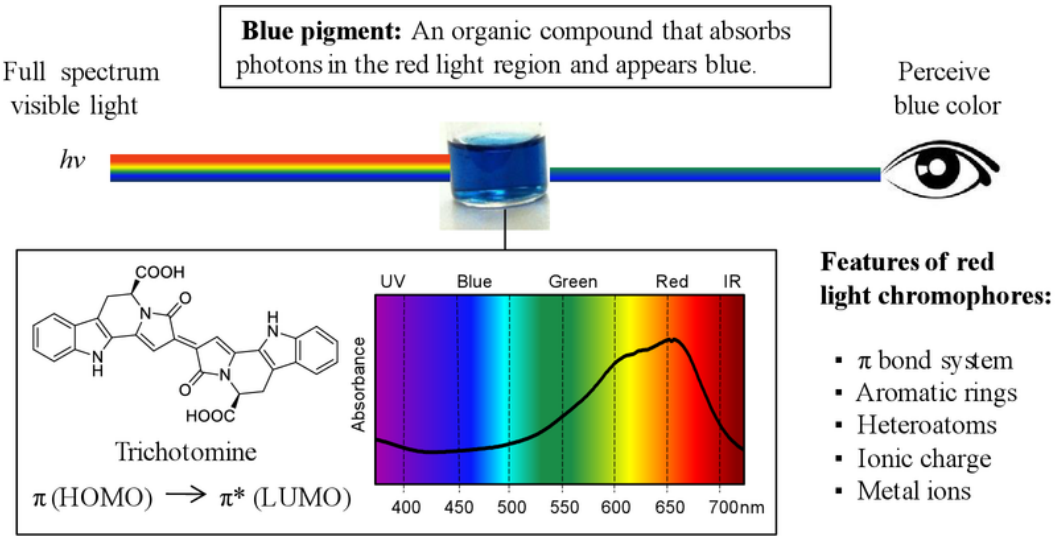

Figure 2. Color perception for a blue pigment using the visible absorbance spectrum of trichotomine (λ_{max}, methanol, 660 nm) as an example. The typical properties of red light absorbing molecules are listed.

Linear π-bond conjugation alone does not usually lead to absorption in the red light range (600 to 700 nm, ΔE = 2.1-1.8 eV). Blue pigments (red light absorbers) typically possess π bond conjugation,

aromatic ring systems, heteroatoms, and ionic charges. Also, organometallic and transition metal complexes are often brightly colored because their *d*-orbitals afford many lower energy electronic transitions. Heteroatom groups (-NH_2, -OH, =O, -Cl, etc.), sometimes called auxochromic groups, can further reduce the transition energies to produce the required bathrochromic shift. For example, red carotenoids can appear blue when complexed with iodine, converted to cations, or through interactions with amino acid side chains such as those in blue carotenoproteins (14). All of the known blue pigments presented in the forthcoming sections of this chapter contain two or more of these features. Blue pigments are less common than red, yellow, or orange ones because a more complex combination of molecular features is generally required for molecules to absorb red light.

1.3 Color Additive Properties

In addition to meeting basic criteria of the pigment definition, any new candidate colorant additives must also meet targets for specific hue, stability, suitability for the target application, and cost. Natural colorants rarely match the intensity of FD&C dyes. Most natural and synthetic color additives have ε_{max} values on the order of 10^5 or 10^6 L mol^{-1} cm^{-1} (7). Colorants with lower ε_{max} values must be used at higher levels to achieve the desired appearance, thereby increasing costs and the risk of off-flavors. Colorants must also be stable enough to avoid significant degradation throughout distribution and sales of both the ingredient and the food or beverage, which might include storage from days to years at refrigerated or ambient conditions. Common causes of instability include heat, light, oxygen, acid, and exposure to oxidants such as ascorbic acid and trace metals. Product developers might have additional requirements such as water or oil soluble formulations for specific applications. Insoluble forms may be necessary to prevent colorant migration. Finally, new natural colorants must be sourced from raw materials with a commercial supply and at levels that make extraction economically feasible.

1.4 Known Natural Blue Pigments

A thorough review and basic assessment of known organic blue compounds from plant, animal, fungal, and microbial sources is a logical first step in the pursuit of natural blue colorant alternatives. Although brilliant blue shades can be seen in flowers, berries, bird feathers and mushrooms, these colors derive from very different sources. Blue color in animals is typically caused by reflection of blue light from nanoscale structures (schemochromes). Examples include blue bird feathers (*Sialia sp.*) and iridescent butterfly wings (*Morpho sp.*). This effect is not limited to the animal kingdom. Quandong fruits (*Santalum acuminatum*) appear bright blue but contain no blue pigments (15).

Anthocyanins are the sources of most blue, red and purple colors in plant leaves, berries and roots. Plants may also contain blue copper metalloproteins for redox functions. Cyanobacteria often contain blue light harvesting proteins for photosynthesis such as phycocyanin. Some fungi and microorganisms produce a wide variety of blue secondary metabolites, which are often made in response to environmental stress or predators. Considerable effort has been devoted to the search for new blue colorants in fruits and vegetables. Less attention has been directed towards blue compounds from other sources such as from bacteria and fungi. Blue chromophores from underexplored sources such as marine microorganisms have been reviewed previously (16).

Searching natural products databases for blue pigments is not straightforward because they are organized by attributes such as molecular weight and composition instead of color. Publications often neglect to report the absorbance spectra or colors of newly identified natural products. In addition, the color of a given compound may vary with conditions such as pH, solvent, and the presence of trace metals or other compounds. Given these challenges, reviews of this subject are likely to miss some

natural blue pigments. The following sections review organic blue pigment structures according to structural class. Inorganic blue compounds, such as copper salts, are not included.

1.4.1 Flavanoids

Anthocyanidins (Figure 3) and their glycosides, anthocyanins, are ubiquitous in the plant world and are responsible for many of the colors of flowers and fruits (15,17,18). Anthocyanins from fruits and vegetables are commonly used as food colorants, but their color is highly pH dependent. The blue quinoidal form predominates under neutral or alkaline conditions, while the red flavylium cation forms under acidic conditions (Figure 3). At least 6 pH-dependent structural forms are known (1,19-21). Stability is a function of both structure and complex interactions such as acylation and co-pigmentation (21).

Research into the biosynthesis and modification of anthocyanins is extensive and has been driven by the desire for blue cultivars of flowers such as roses and carnations. A recent review summarizes these complex pathways (22). Anthocyanin color is influenced by its structure, intra- and intermolecular interactions, and pH. Increasing hydroxylation of the B-ring shifts anthocyanins to bluer shades, as seen with delphinidin, the pigment responsible for the blue color of delphiniums (21,23). The formation of complexes with co-pigments such as flavones and with metal cations can also shift the hue (21). A familiar example is the use of aluminum compounds to shift the color of hydrangea blossoms from pink to blue.

After synthesis, anthocyanins are transported to vacuoles for storage. The color of anthocyanins within the vacuole is a function of the anthocyanin type, its structural form when complexed with other components, and the vacuolar pH. These vacuoles have been suggested as food colorants (23). The

internal pH of the vacuole is higher than that of typical foods, so the anthocyanins will appear blue. It is not clear if anthocyanin vacuolar inclusions can survive the rigors of food processing and storage, or if they can be produced efficiently on a commercial scale.

Complex blue anthocyanin-derived compounds such as portisin A (Figure 3) have been isolated from aged red wine (24-26). At low pH, the portisins show a bathochromically shifted absorption maximum (portisin A, λ_{max} pH 1, 587 nm) relative to common anthocyanins such as oenin (malvidin-3-glucoside) (λ_{max} pH 1, 538 nm) (Figure 3). Portisins are purple rather than pink at low pH values (24,26). These compounds face the same challenges as other new food colorants. Additional studies will be required to determine solubility and stability. These compounds are present at such low levels that isolation from wine is not feasible; new processes for commercial production will be required.

A thorough discussion of the structural variety and stability of anthocyanins is beyond the scope of this review. The chemistry, structural diversity, biosynthesis, distribution, safety, and stability of these compounds has been reviewed extensively (1,27-29). The structures of some of these anthocyanin pigments are provided in Figure 3.

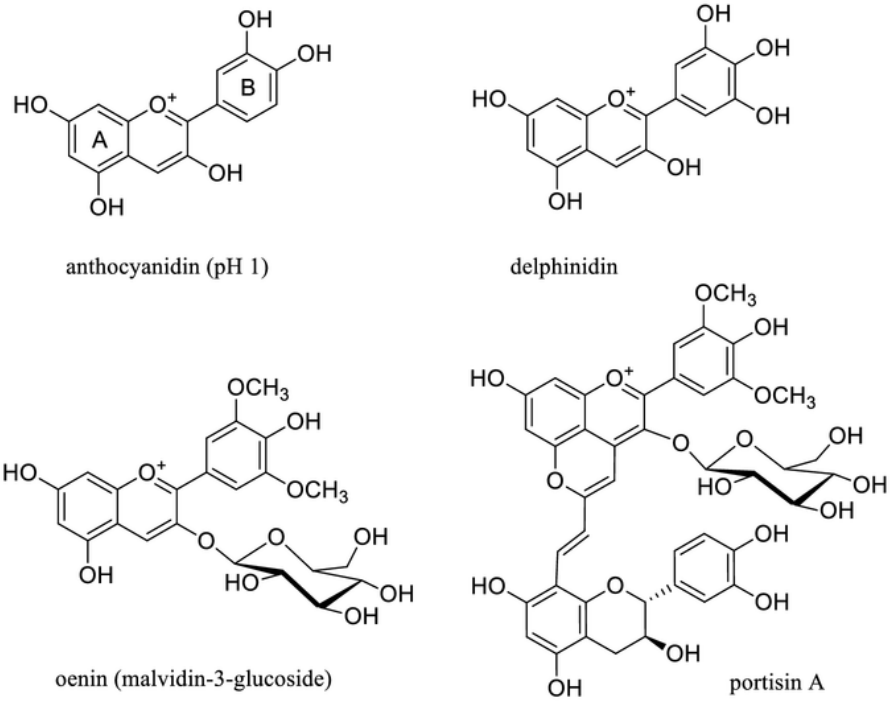

Figure 3. Chemical structures of blue flavonoid-derived natural products.

1.4.2 Quinones and Quinoids

The inclusion of carbonyl groups within an aromatic ring system can lead to the absorption of the lower energy visible spectrum photons required to produce absorption in the visible spectrum. Dyes based upon the 9,10-anthraquinone skeleton (Figure 4) were first isolated and synthesized and for commercial use in the 19th century (30,31). Varying substitutions on this skeleton for specific auxochromic effects has resulted in dyes of every color. Not all quinoid dyes are suitable for food use due to biological activity, and few are blue under acidic conditions.

Many natural blue anthraquinone or quinoid dyes are blue at alkaline pH but red or orange at neutral or acidic pH. One example is the chemotherapeutic anthraquinone drug daunorubicin. Isolated in 1964 from *Streptomyces peucetius* (32), daunorubicin (Figure 4) was among the first chemotherapeutic

compounds derived from soil microbes. Daunorubicin interchelates between DNA strands and is prescribed for acute myeloid and lymphocytic leukemia (33).

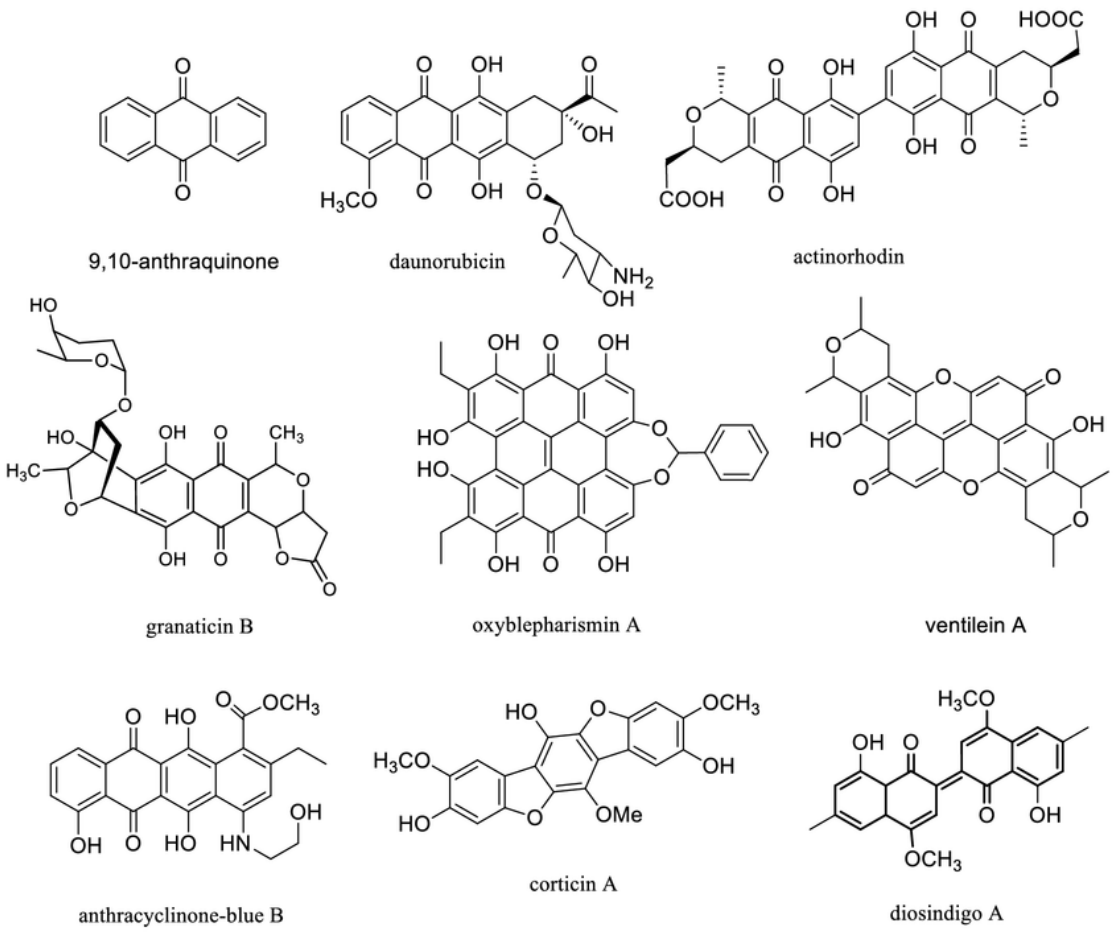

Figure 4. Chemical structures of some blue colored natural quinoids and quinones.

Streptomyces coelicolor excretes the benzoisochromaquinone actinorhodine and its analogs at yields of up to 3 g L^{-1} of fermentation media (34-36). The actinorhodins have been proposed as food colorants, but as with most anthraquinones, they are blue only under alkaline conditions, limiting their

use in foods and beverages. The actinorhodins show weak antibiotic activity but are not cytotoxic. For example, the minimum inhibitory concentration of actinorhodin (Figure 4) against *Staphylococcus aureus* is 30 μg mL^{-1} (36) whereas its LD_{50} in mice is >15 g kg^{-1} (34). Other blue benzoisochromaquinone-like antibiotics include granaticin B (Figure 4) and related analogs isolated from various *Streptomyces* species (37-39). The granaticins are cytotoxic and not blue at low pH. Diosindigo A (Figure 4) is a blue bisquinone that has been isolated from the heartwood of at least 7 *Diospyros* botanical species, but little additional information such as stability is available (40,41).

Natural anthraquinoid compounds are rarely blue under acidic conditions, but there are a few exceptions for those with an extended aromatic ring system. These include the dark blue microbial metabolites anthracyclinone-blue B (Figure 4) from a *Streptomyces galilaeus* mutant (42) and kyanomycin (λ_{max} methanol, 600 nm, ε = 11,480), from *Nonomuria* sp. NN22303 (43). Another blue compound with an extended quinone structure, ventilein A (λ_{max} methanol, 645 nm), (Figure 4) was isolated as a minor constituent from *Ventilago calyculata* root bark (44) and from *Ventilago goughii* (45). Blepharismin and stentorin are red photosensory pigments from the protists *Blepharisma japonicum* (46) and *Stentor coeruleus* (47) with a fused eight-ring conjugated quinone system identical to hypericin (bright red). Photoreaction products of the blepharismins, such as oxyblepharismin A and analogs, are blue.

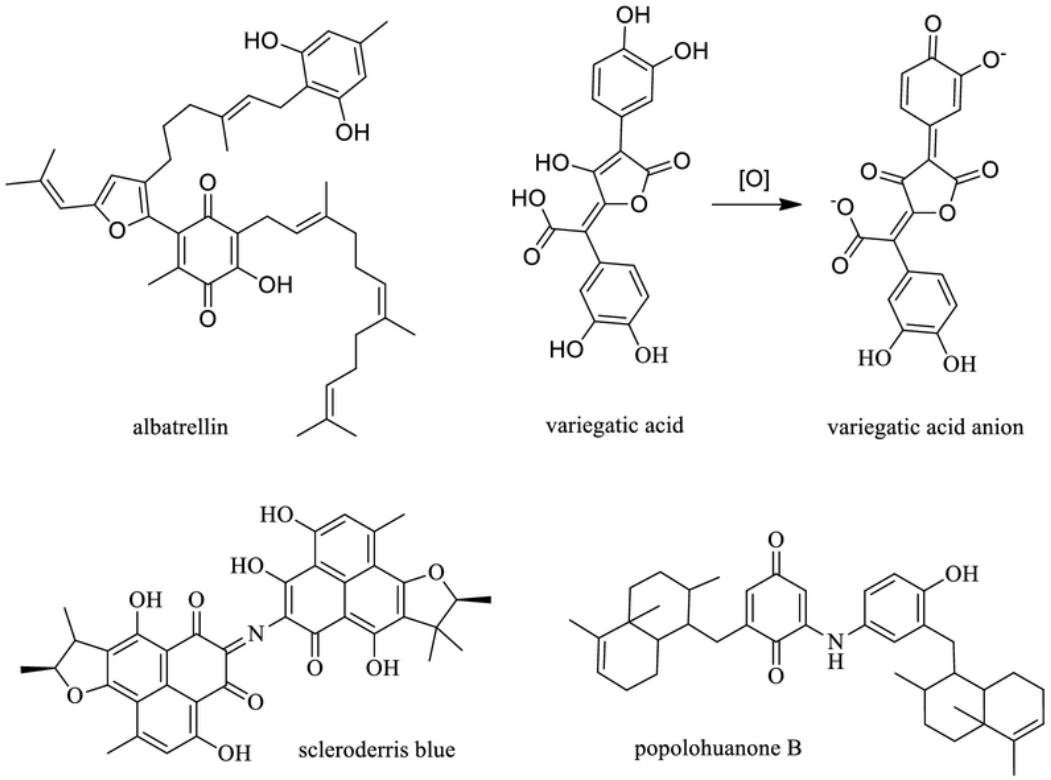

Figure 5. Chemical structures of some blue colored natural quinoids and quinones (cont.).

Quinoid pigments are responsible for the blue colors of many fungi such as *Basidiomycetes* (48). The bluing reactions of several mushroom species are due to the oxidation of conjugated furanoquinones to blue anionic compounds such as gyrocyanin (49), variegatic acid (Figure 5) (50), xerocomic acid (51), and chamonixin (52). Though relatively little research has been reported on these furanoquinone oxidation products, anecdotal evidence of subsequent fading of blue-bruising fungi suggests that these oxidation products are unstable. The variegatic acid anion fades to brown in less than 60 min (50). The meroterpenoid quinone albatrellin (Figure 5) was identified as the source of blue color in the skin of *Alabtrellus flettii* (Basidiomycete) fruiting bodies (53). The pigment is blue in chloroform or dichloromethane, but violet in methanol (λ_{max} methanol, 535 nm, ε = 3,200). Corticin A (Figure 4), a

derivative of the benzofuranoquinone fungal pigment thelephoric acid, was determined to be the blue pigment of the fungus *Corticium caeruleum* (54). A bis-quinoid fungal metabolite containing an imine linkage, scleroderris blue (Figure 5), was isolated from the canker fungus *Gremmeniella abietina* (55,56) and later from *Penicillium herquei* as a zinc complex (57). The compound is intensely blue colored (λ_{max} CH_2Cl_2, 612 nm; ε = 50,000) but relatively unstable; scleroderris blue can be converted to scleroderris green with a weak reducing agent (56). Popolohuanone B (Figure 5), a pigment containing an aminoquinone chromophore, was isolated from a blue-purple *Dysidea sp.* sponge (58). Structures of blue pigments of the quinoid or quinone class are shown in Figure 4 and Figure 5.

1.4.3 Linear Tetrapyrrole Alkaloids

Tetrapyrroles cover every color of the visible spectrum. Blue tetrapyrroles are responsible for the blue coloration of bruises (59). Biliverdins, heme degradation products found in bile, are among the few natural blue compounds in the animal kingdom. The bile pigment biliverdin-IX_a (oocyan) is responsible for the pigmentation of bird egg shells (60,61). The light harvesting protein phycocyanin in *Cyanobacteria* contains a bound linear tetrapyrrole phycocyanobilin as the blue chromophore (62,63). The difference between the intense blue phycocyanobilin and the heme byproduct urochrome, the source of yellow color in urine, is extended conjugation across four pyrrole rings via one additional unsaturation. Phycocyanin is commercially extracted from the alga *Spirulina platensis* and is used as a colorant in confections. However, phycocyanin is not stable enough for most food and beverage applications.

Bactobilin (Figure 6) (64,65), isolated from *Clostridium tetanomorphum* and *Propionibacterium shermanii* (used in Swiss cheese production), is one of the few known bacterial bile pigments (66).

Bactobilin shares the same blue chromophore as phycocyanobilin but has 8 methyl ester side chains. The stability of bactobilin has not been reported, but since alkylation or acylation enhances the stability of chromophores such as anthocyanins, bactobilin should be more stable than phycocyanobilin.

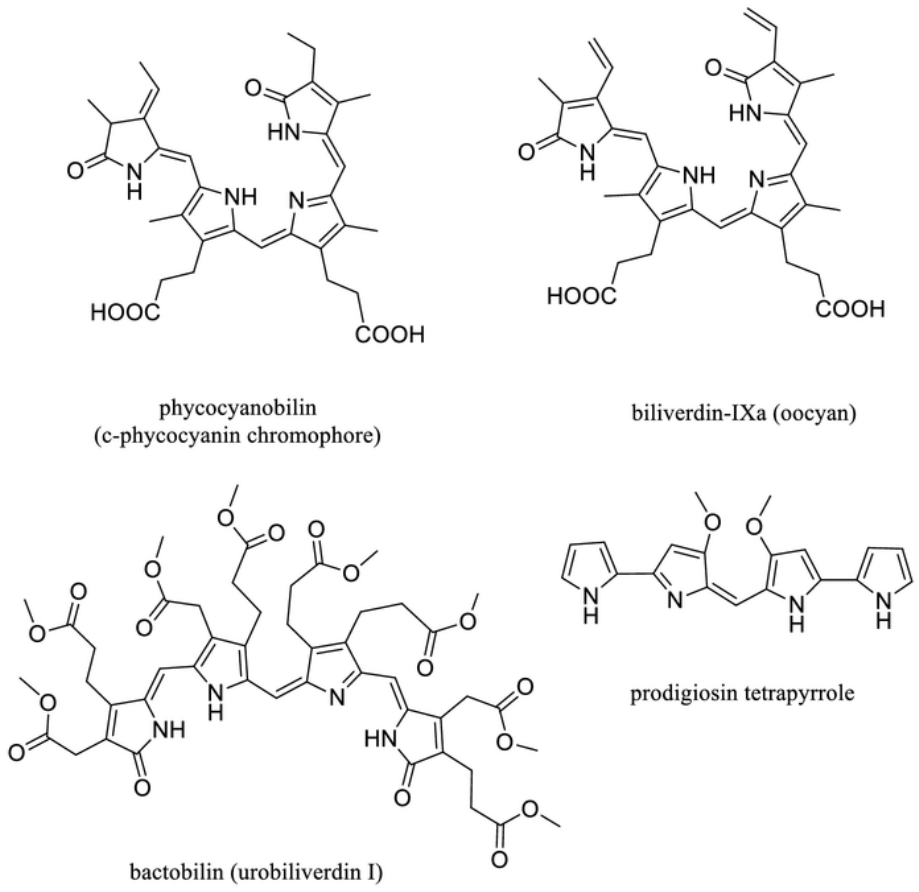

Figure 6. Chemical structures of some blue pigmented linear tetrapyrroles.

A blue prodigiosin tetrapyrrole analog of the cytotoxic microbial red pigment prodigiosin has been isolated from a variety of sources including a mutant *Serratia marcescens* strain (67), the marine bacterium *Hahella chejuensis* KCTC 2396 (68), some blue marine ascidians (69,70), a blue bryozoans

(71), and the nudibranch *Nembrotha kubaryana* (72). *N. kubaryana* might derive its color from feeding on blue ascidians and bryozoans. The prodigiosin tetrapyrrole is distinguished from bile pigments by having directly coupled pyrrole rings rather than methine spacers. Unlike the bile tetrapyrroles, prodigiosin and its analogs usually exhibit cytotoxic and antimicrobial activities (73). Structures of these blue tetrapyrrole pigments are shown in Figure 6.

1.4.4 Phenazine Alkaloids

Hundreds of natural phenazine molecules have been isolated and characterized, primarily from *Pseudomonas* and *Streptomyces* species (74,75). The colors of these compounds span the entire visible spectrum. One of the first identified and best known phenazines is the blue compound pyocyanin (Figure 7), the highly cytotoxic cystic fibrosis virulence factor from *Pseudomonas aeruginosa* (76,77). Other blue phenazines include the *N*-terpenoid substituted metabolites phenazinomycin isolated from *Streptomyces sp.* WK-2057 mycelia (78,79) and lavanducyanin from *Streptomyces aeriouvifer* (80,81). The absorption maxima and molar absorptivities of phenazinomycin (λ_{max} methanol, 745 nm, $\varepsilon = 6600$) and lavanducyanin (λ_{max} methanol, 705 nm, $\varepsilon = 1700$) are similar to that of pyocyanin (λ_{max} methanol, 746 nm, $\varepsilon = 5800$). Both show broad visible absorbance in the far red light region with relatively low molar absorptivity. Benthocyanin A from *Streptomyces prunicolor* (82,83) contains an additional lactone ring and has a higher molar absorptivity in the red light region presumably due to the larger chromophore surface area (benthocyanin A: λ_{max} methanol+HCl, 638 nm, $\varepsilon = 16200$; λ_{max} methanol+NaOH, 616 nm, $\varepsilon = 18400$). Although many blue pigments of the phenazine class are blue under acidic conditions, they are usually cytotoxic or otherwise biologically active (75,79,81) thereby

excluding them from consideration as food colorants. Structures of these blue phenazines are shown in Figure 7.

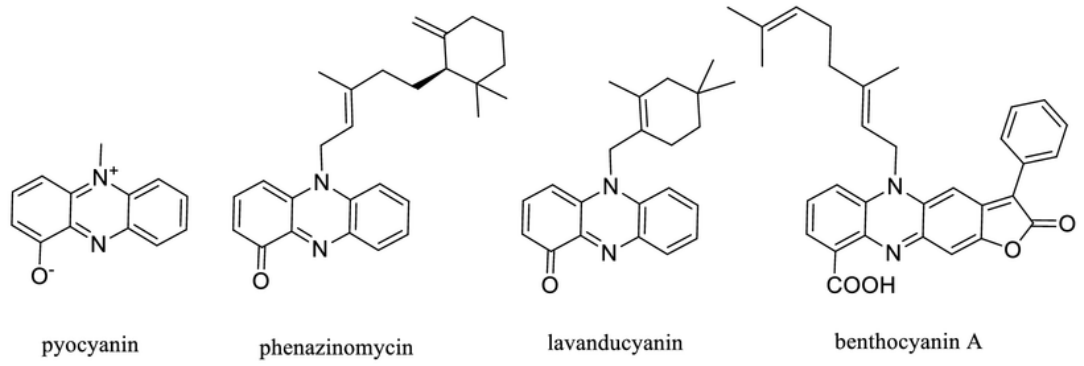

Figure 7. Chemical structures of natural blue phenazine molecules.

1.4.5 Indole Alkaloids

A small fraction of the thousands of known indole alkaloids are blue. Indigo dyes from the tropical plants woad (*Isatis tinctoria*) and true indigo (*Indigofera tinctoria*) have a long history of use in textiles (30,84). The bis-indole indigotin (Figure 8) is responsible for the blue color of indigo-based dyes (85) and today is produced synthetically. Its disulfonate sodium salt, FD&C Blue No. 2 is produced for the food and cosmetic industries (7). Indigotin and its derivatives lack the pH and light stability often required for food and beverage products. Blue 5,5'-dichlorinated analogs of indigotin, akashin A, B and C (Figure 8), were recently isolated from the marine *Streptomyces* sp. GW48/1497 (86,87). While indigotin is not cytotoxic, the akashins showed activity against cancer cell lines with IC_{50} values near 3 μg mL^{-1} (87). Candidine (Figure 8), a blue alkaloid originally isolated from *Candida lipolytica* (88,89),

is a constituent of the traditional Chinese medicinal herb qing-dai (*Indigo naturalis*) (90). Its bis-indole chromophore is similar to indigotin.

Kusagi berries from the Asian shrub *Clerodendron trichotomum* have a bright blue skin (91). Extracts of these berries have been used to dye textiles (92,93). The berry skin contains the blue *bis*-indole alkaloid trichotomine (Figure 8) and its glycosides (94-96) which are structurally more complex and intensely colored than indigotin (Figure 8). The larger absorptive surface area of the compound imparts a blue color with a molar absorptivity similar to FD&C Blue No. 1. Trichotomine and its derivatives are among the few compounds that produce the same shade of blue as FD&C Blue No. 1.

Violacein, a deep violet indole alkaloid first reported 1888, was isolated from *Chromobacterium violaceum*, a species native to the Amazon river (97). It has been studied extensively for its biological activities (98) and as a textile dye (99). Prodeoxyviolacein (Figure 8), a biosynthetic precursor of violacein, is blue in acid and red under neutral or alkaline conditions (100,101). Deep red or violet microbial and sponge pyrroloquinoline metabolites containing the indole moiety have been reported (102). Ammosamide A (Figure 8), isolated from the marine *Streptomyces* CNR-698, is similar in structure but contains an unusual thio-γ-lactam group contributing to its deep blue color (103). The thionyl group ammosamide A slowly oxidizes in air to form a carbonyl group and the red compound ammosamide B. Both compounds are active against a variety of cancer cell lines with IC_{50} values from 1 μM to 20 nM. The structurally related blue alkaloid sanguinone A has been isolated and characterized from the mushroom *Mycena sanguinolenta* (104). Data on its biological activity and stability have not been reported. See Figure 8 for the chemical structures of these indole-derived blue pigments.

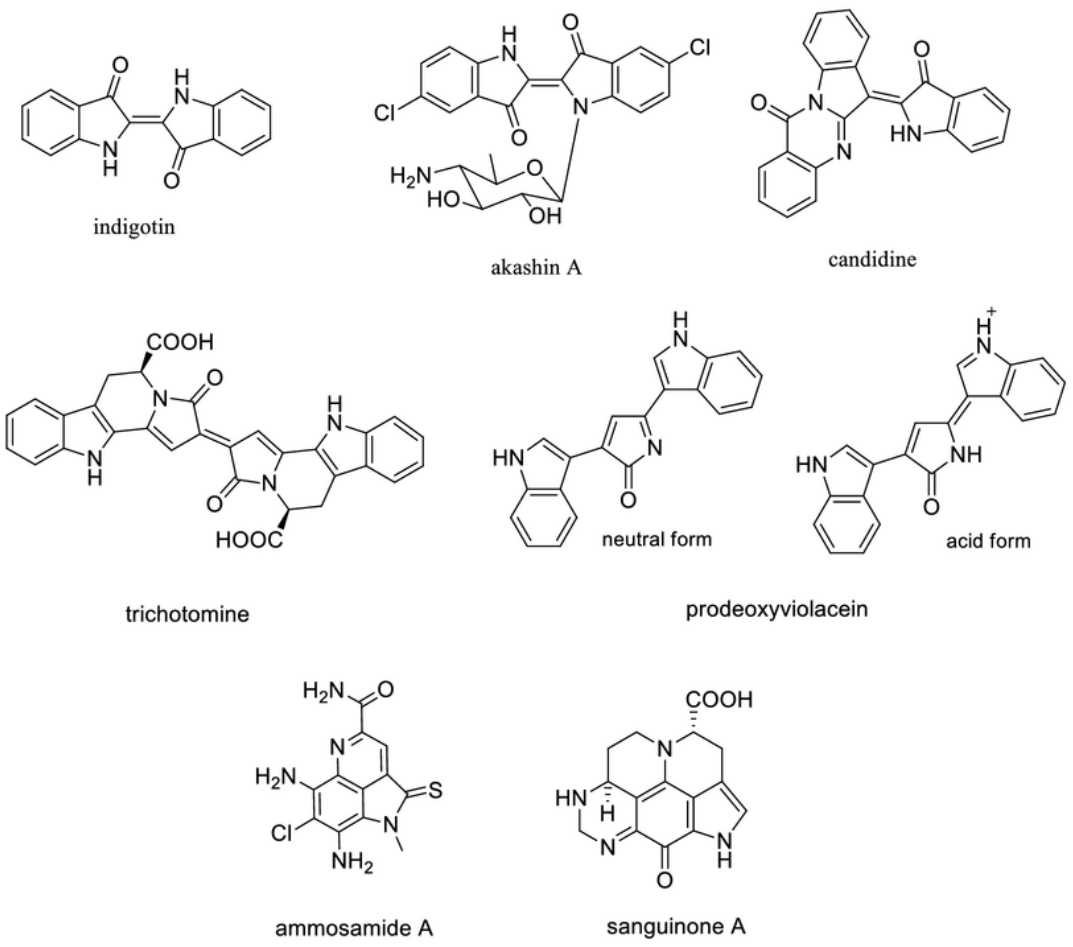

Figure 8. Chemical structures of indole-derived blue colored natural products.

1.4.6 Pyridine Alkaloids

Blue pigments containing 3-3'-bipyridyl chromophores (Figure 9) have been isolated from a variety of microbial sources. Indigoidine and indochrome A (also known as amylocyanin) were isolated in the 1960's as part of studies on the structurally related blue pigments of *Arthrobacter* sp., *Erwinia* sp.,

and *Corynebacterium* sp. (105-107). An unnamed blue pigment, a 3-3'-bipyridyl uncatalyzed oxidation product of 2,3,6-trihydroxypyridine, was identified as a side product of 2-hydroxypyridine metabolism in *Nocardia* sp. (*108,109*). The unnamed blue pigment of Figure 9 was shown to be identical to the acidic hydrolysis product of indigoidine (110). Similar but unidentified blue pigment byproducts such as "nicotine blue" (111) have been observed during the metabolism of various pyridine compounds by *Arthrobacter* sp. (110-112), *Pseudomonas* sp. (107), *Corynebacterium* sp. (113), and *Bacillus* sp. (114). More recently, an *N,N*-dialkylated indigoidine analog was isolated and characterized from the deep sea marine microorganism *Shewanella violacea* DSS12 (115). Lemonnierin, a blue metabolite produced by *Pseudomonas lemonnieri,* contains a similar 3-3' bipyridal blue chromophore (116,117). Glaukothalin, isolated from the marine microorganism *Rheinheimera* sp. HP1 (118,119), contains a rare bis-oxazepinone chromophore reminiscent of the 3-3'-bipyridyl chromophores. Glaukothalin has a LD_{100} of 0.1 mg mL^{-1} against brine shrimp. Little information is available concerning the stabilities and biological activities of most of the 3-3'-bipyridyl pigments.

Gardenia blue and huito juice are iridoid-derived mixtures with limited approval as food colorants. Colorless iridoids from *Genipa americana* and *Gardenia jasminoides* extracts can be converted to blue colorants by reacting the aglycones with a primary amine in the presence of oxygen (1,120-122). The resulting mixture of polymeric pigments is not well defined, but characterization of some brown-red intermediates (123,124) and of a blue dimer product genipocyanin G_1 (Figure 9) (125) have been reported. The reaction converts the iridoid scaffold into an aromatic 2-pyrindine [5+6] scaffold that has visible absorbance properties distinct from the indole ring (126). Structures of these pyridine-derived compounds are shown in Figure 9.

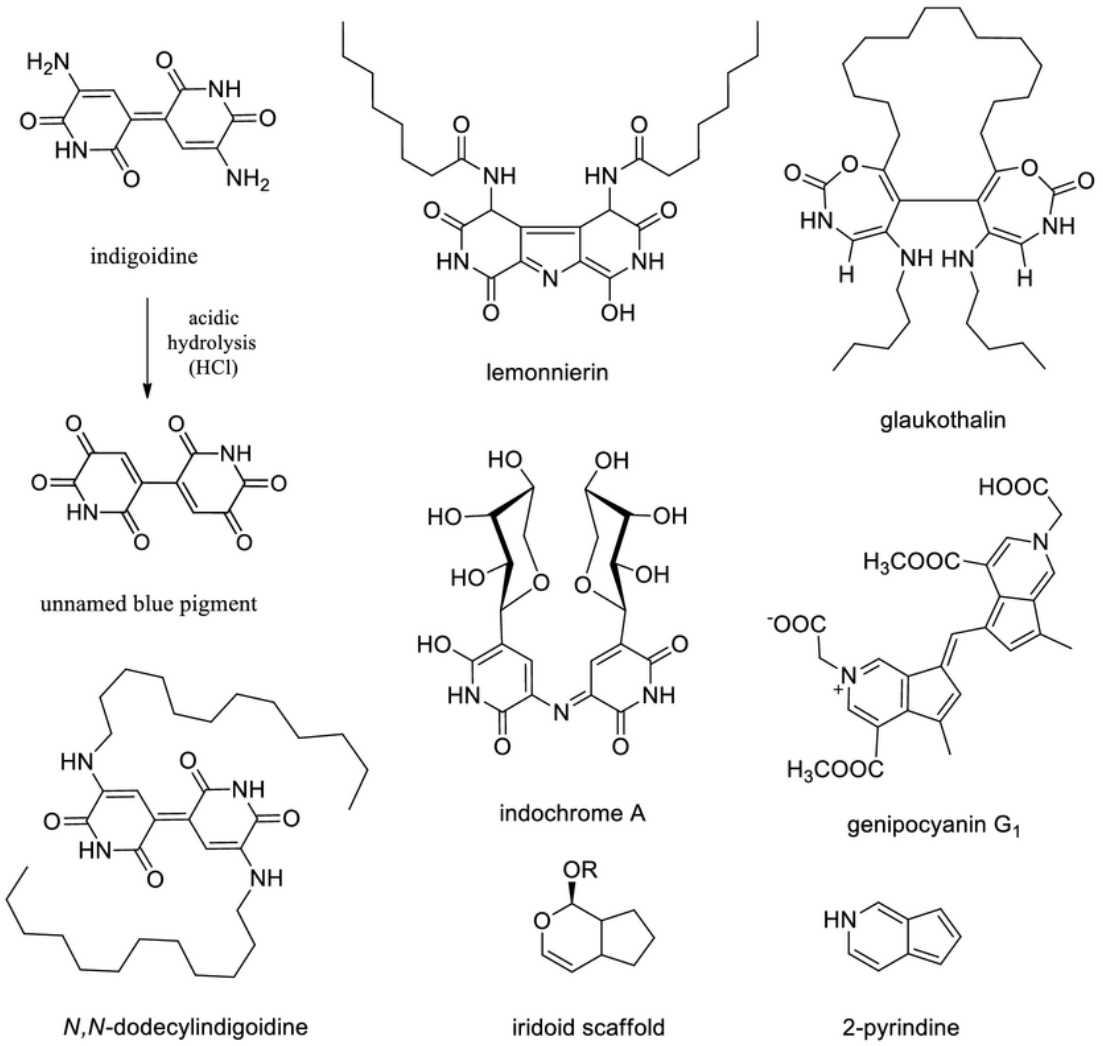

Figure 9. Chemical structures of blue pyridine-derived natural products.

1.4.7 Azulenes

The azulene [5+7] ring system (Figure 10) is the only reported blue organic chromophore found in nature that does not contain heteroatoms. Guaiazulene and related blue sesquiterpenes such as lactarazulene, and guaiazuleneone have been isolated from various fungi (*Lactarius* sp.) and plant

essential oils (*Matricaria* sp., *Artemisia* sp.) (127-129). Blue chlorinated and brominated analogs of guaiazulene and dimeric guaiazulene derivatives (anthogorgienes A-O) have been isolated from marine Gorgonian species (130,131). Most dimeric azulene derivatives are not blue but purple or green. The 2,12'-bis-hamazulenyl dimer isolated from *Ajania fruticulosa* (132) is blue because the saturated ethyl linkage does not significantly alter the azulene chromophore. Azulene and its derivatives tend to be lipophilic, have low molar absorptivities and poor stabilities (127,131,134,135). Guaiazulene is approved for use in cosmetics by the US FDA (136). Structures of some blue azulene natural products are shown in Figure 10.

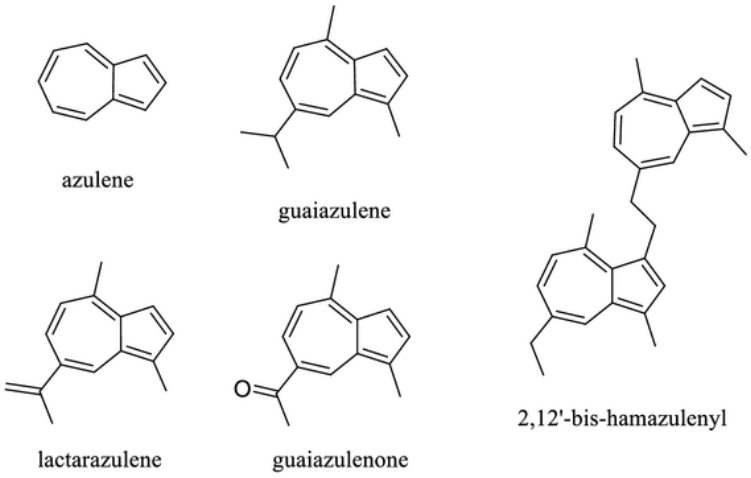

Figure 10. Chemical structures of some natural blue azulenes.

1.4.8 Organometallics and Metalloproteins

Blue metalloproteins and organometallic complexes have been identified in natural sources. A ferric ceratenolone complex is thought to be responsible for the blue color of the pine rot fungus

Ceratocystis minor (137) and a pale blue colored vanadium V^{4+} complex, amavadin, (Figure 11) has been isolated from *Amanita muscaria* which is known to accumulate vanadium (48,138). Crustaceans and arthropods have blue blood due to the respiratory protein hemocyanin instead of iron-based hemoglobin (139). The hemocyanin chromophore contains a binuclear copper active site that reversibly binds O_2 molecules (Figure 11). Each copper is coordinated by three histadyl residues. Other blue copper proteins occur in some plants and bacteria where they usually serve biosynthetic functions involving electron transfer (140). Stellacyanin (141) and plastocyanin (142,143) are Type I copper binding proteins (cupredoxins) common to vascular plants. The blue cupredoxin chromophore found in stellacyanin contains a cupric ion coordinated by one cysteine and two histidines (Figure 11) (141). Other Type I copper binding proteins include cuscacyanin and phytocyaninin from cucumber (144,145), umecyanin from horseradish root (146) and allergen Ra3 from ragweed (147).

Bacterial Type I copper binding proteins include amicyanin from *Thiobacillus versutus* (148) and *Paracoccus denitrificans* (149) as well as halocyanin from the halophilic archaea *Natronomonas pharaonis* (150). Halocyanin is one of the few pigmented compounds known from the Archaea. The blue arsenate reductase enzyme azurin (14 kDa) found in some *Pseudomonas* sp. and *Alcaligenes* sp. also contains the blue cupredoxin chromophore (Figure 11) (151,152). Auracyanin (12.8 kDa) from *Chloroflexus aurantiacus* is similar in structure to azurin but serves a role in photosynthesis (153). Rusticyanin (16.5 kDa) from *Thiobacillus ferrooxidans* has the highest redox potential and best acid stability among the cupredoxin proteins (154,155). Nevertheless, rusticyanin showed a color loss of 50% after two weeks at pH 2.0 and 4 °C (154). Consequently, none of these copper proteins has sufficient stability for use as a food colorant.

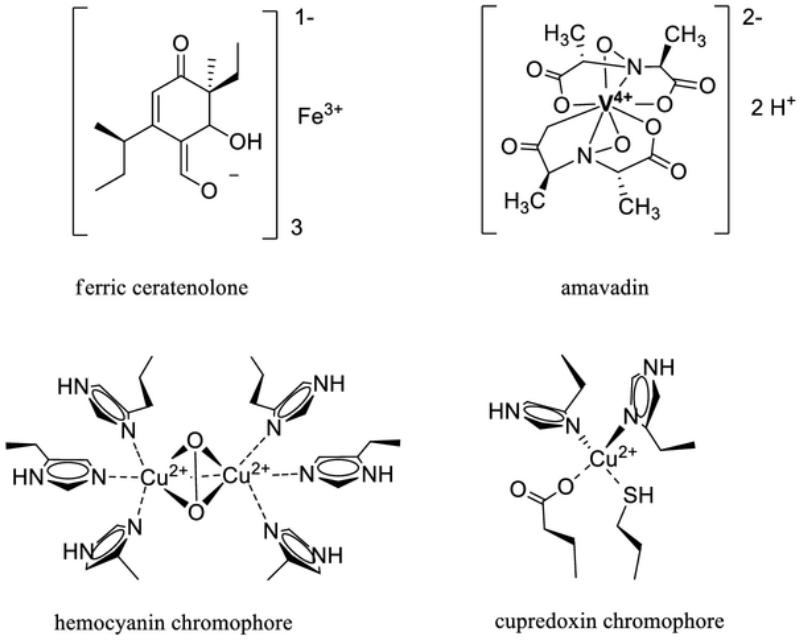

Figure 11. Chemical structures of some natural blue organimetallic complexes.

1.5 Unidentified Blue Pigments

The source of blue coloration of many marine animals remains underexplored. A novel class of blue chromoprotein was recently isolated from the barrel jellyfish *Rhizostoma pulmo*, but the structure of the chromophore has not been determined (156). Studies of the blue pigmentation of *Pollicopora* sp. and *Acropora* sp. corals led to the isolation of still unidentified chromoproteins (157). An investigation of abalone shells in Japan has resulted in the partial characterization of a novel blue compound (electrospray MS *m/z* 581.8, $[M-H]^-$), but the structure remains unknown (158). Investigations of the consumer preferred greening of cultured oyster (159) led to the isolation and partial characterization of a blue polyphenolic substance, marennine (λ_{max} water pH 8, 672 nm, ε = 7,200) from an associated marine

diatom, *Haslea ostrearia* (160,161). Although its structure has not yet been determined, marennine (~10 kDa) is not composed of peptide, flavanoid, anthocyanin, or hydrolyzable tannin units and is not a metal complex.

Blue pigments observed in some fungi such as *Penicillin sp.* and *Hypocrea sp.* have been investigated but remain unidentified (162,163) due to challenges in isolating sufficient material for analysis. Some *Psilocybe* sp. fungi bruise blue when the tissue is broken and exposed to air, and the pigment structure is unknown but thought to be a psilocybin-related or indole oxidation product (164). An unidentified water soluble and unstable pigment reported from a soil strain of *Pantoea agglomerans* remains uncharacterized (165). *Bacillus subtilis var. aterrimus A*TCC 6461 excretes an unidentified blue-black substance that is believed to be melanin related (166). An attempted characterization of this substance in the present study found the pigment too unstable for isolation. The unidentified purple pigment of acidophilic *Zygogonium sp.* algae was characterized in this research (Chapter 3) and the color was found to arise from the complexation of ferric iron with gallic acid moieties. Future work to isolate and characterize blue compounds from natural sources will certainly continue to reveal novel blue chromophores.

1.6 Conclusion

Sections 1.2 through 1.5 stated the problem and the approach to be used in the present work, established a definition for a blue pigment, and reviewed the literature relating to known and unknown natural blue pigments. Table I summarizes published data on the reviewed blue pigments. Table 2 provides information on the biological sources of these natural blue pigments. The reviewed compounds fall into seven structural classes and are derived from a broad range of sources.

Blue compounds would need to meet stringent criteria before being considered for use in foods. Ideally, the natural blue pigment should have a shade and brilliance similar to FD&C Blue No. 1. Visible λ_{max} and ε_{max} data are provided in Table I for comparison. New color additives must be safe, stable, and effective in the target application. Commercial production requires an abundant supply of the raw material and high pigment concentrations for economical extraction. Most of the reviewed pigments have not been investigated as potential colorants and so specific data on human safety, application stability, and commercial production are not available. Nonetheless, it is apparent from published data that none of the blue pigments reviewed here are likely to meet all these criteria. Very few of the compounds listed in Table I have extinction coefficients approaching that of FD&C Blue No. 1, so higher concentrations would be required to achieve the same appearance in food applications.

In general terms for the structure classes, the phenazines are toxic, the azulenes and tetrapyrroles lack robust stability, and many of the quinoids and flavanoids are not blue in acid. The indole alkaloids are blue in acidic conditions but tend to have bioactivity or toxicity. Scarce data exists for the bipyridal pigments. Fungal and microbial secondary metabolites show great structural diversity and are good candidates for production on an industrial scale (167, 168). Unfortunately, compounds from these sources are often produced as part of a defense mechanism and have biological activities that render them unsuitable for food use.

Table 3 lists the more promising candidates of those reviewed. The portisins come close to providing the desired color, but additional information about their stabilities and solubilities is required. Furthermore, portisins are found at only very low levels in wine, so an alternate pathway for commercial production will be required. Trichotomine, the focus of a later chapter in the present work, is among the few pigments considered a good match in for FD&C Blue No. 1 in terms of shade and intensity in acidic solutions. Trichotomine has limited water solubility and stability, but its glycosylated derivatives are far

more soluble and may be more stable. Anthocyanin and trichotomine derivatives are among the best candidates for new blue colorants.

The challenges of developing a new blue colorant cannot be overstated. The colorant must meet targets for hue, color intensity and solubility. Ideally, it should be stable to heat, acid, light and oxygen. The pigment should not contribute flavor or interact with other ingredients. Raw materials and processes must be in place for commercial production. Even if all of these criteria are met, the new colorant must be safe and go through the petitioning process for new color additives to get regulatory approval for use. This may require extensive safety and toxicity testing. Petitioning must be repeated in every region with a separate regulatory process.

Food and beverage producers continue to look for a naturally derived alternative to FD&C Blue No. 1. Anthocyanins are the primary source of blue in fruits, vegetables and flowers, but as their color is pH dependent, they appear pink in most foods and beverages. Fungi and microorganisms produce a diverse array of blue compounds, often in response to environmental stress or predators. The associated biological activities of these compounds so far have rendered them unsuitable for food use. The best existing candidates for new blue color additives, anthocyanin and trichotomine derivatives, will require significant investment for development and regulatory approval. The review of natural blue pigments from nature was previously published as part of this dissertation (172).

TABLE I. SELECTED DATA FOR NATURAL BLUE PIGMENTS

compound name	formula	m.w. (Da)	λ_{max} (nm)[a]	ε (M^{-1} cm^{-1})[a]	sol. (mg L^{-1})[b]	citations[c]	refs[d]
synthetic							
FD&C Blue No. 1	$C_{37}H_{36}N_2O_9S_3Na_2$	792.9	629 (w)	134,000	n.a.[e]	1447	***8***
FD&C Blue No. 2	$C_{16}H_{10}N_2O_8S_2Na_2$	466.4	607 (w)	7,920	n.a.[e]	2530	***9***
flavanoid							
portisin A	$C_{42}H_{39}O_{18}^+$	831.8	587 (m)(B)	82,900	n.a.[e]	4	*21*, ***24***, *25,26*
oenin	$C_{23}H_{25}O_{12}^+$	493.4	538 (m)(A)	16,000	n.a.[e]	1571	*21*, ***24***, *25,26*
quinoid							
daunorubicin	$C_{27}H_{29}N_1O_{10}$	527.5	530 (dmf)	6,000	20,000	9848	*32,33*, ***169***
actinorhodin	$C_{32}H_{26}O_{14}$	634.5	640 (w)(B)	25,300	0.025	419	*34*, ***35***, *36*
granaticin B	$C_{28}H_{30}O_{12}$	558.5	630 (et)(B)	8,910	6.7	18	*37*, ***38***, *39*
diosindigo A	$C_{24}H_{20}O_6$	404.4	697 (dcm)	28,180	0.5	27	***40***, *41*
anthracyclinone-blue B	$C_{24}H_{21}N_1O_8$	451.4	608 (m)	28,890	0.014	1	***42***, *43*
ventilein A	$C_{30}H_{24}O_8$	512.5	645 (m)	n.a.	0.004	2	***44***, *45*
oxyblepharismin A	$C_{39}H_{24}O_{11}$	668.6	592 (et)	n.a.	4×10^{-10}	2	***46***, *47*
variegatic acid anion	$C_{18}H_{12}O_9$	372.3	605 (w)(B)	n.a.	63,000	19	*48*, ***50***
albatrellin	$C_{44}H_{56}O_6$	680.9	535 (m)	3,162	0.001	2	***53***
corticin A	$C_{21}H_{16}O_8$	396.4	565 (et)	6,900	0.062	1	***54***
scleroderris blue	$C_{38}H_{33}N_1O_{10}$	663.7	612 (dcm)	50,000	0.2	8	***55***, *56,57*
popolohuanone B	$C_{42}H_{57}N_1O_3$	623.9	512 (hex)	2,290	0.0004	1	***58***
tetrapyrrole							
phycocyanobilin	$C_{33}H_{38}N_4O_6$	586.7	604 (m)	17,100	6	395	*62,63*, ***170***
biliverdin-IX_a	$C_{33}H_{34}N_4O_6$	582.7	674 (w)(B)	12,200	200	1281	***60***, *61*
bactobilin	$C_{39}H_{38}N_4O_{18}$	850.7	633 (chl)	n.a.	73,000	5	***64***, *65,66*
prodigiosin tetrapyrrole	$C_{19}H_{18}N_4O_2$	334.4	588 (et)(A)	n.a.	87	8	***67***, *68-72*
phenazine							
pyocyanin	$C_{13}H_{10}N_2O$	210.2	746 (m)	5,800	150	758	*74-77*, ***78***
phenazinomycin	$C_{27}H_{32}N_2O$	400.6	745 (m)	6,600	0.06	17	***78***, *79*
lavanducyanin	$C_{22}H_{24}N_2O$	332.4	705 (m)	1,700	1.2	14	***80***, *81*
benthocyanin A	$C_{31}H_{28}N_2O_4$	492.6	638 (m)(A)	16,200	0.026	6	***82***, *83*

[a] (A) = acidic conditions; (B) = alkaline conditions; (w) = water; (m) = methanol; (et) = ethanol; (chl) = chloroform; (dcm) = dichloromethane; (hex) = hexane; (dmf) = dimethylformamide; (acn) = acetonitrile

[b] Solubility in water, pH 3, 25 °C. Calculated using ACD/Labs Software V11.02 or ACD/Percepta Build 2254

[c] Number of citations currently associated with the compound in CAS SciFinder scholar.

[d] The source of the λ_{max} and ε value is given in bold.

[e] Species is ionic or charged. Solubility cannot be calculated.

[f] For trichotomine dimethyl ester

[g] Authors' unpublished research

TABLE I. SELECTED DATA FOR NATURAL BLUE PIGMENTS (continued)

compound name	formula	m.w. (Da)	λ_{max} (nm)[a]	ε (M^{-1} cm^{-1})[a]	sol. (mg L^{-1})[b]	citations[c]	refs[d]
indole							
indigotin	$C_{16}H_{10}N_2O_2$	262.3	610 (dmf)	22,140	0.55	2574	*30,84,* ***85***
akashin A	$C_{22}H_{19}Cl_2N_3O_5$	476.3	619 (m)	10,232	210	2	*86,* ***87***
candidine	$C_{23}H_{13}N_3O_2$	363.4	573 (chl)	12,880	13	13	*88,* ***89****,90*
trichotomine	$C_{30}H_{20}N_4O_6$	532.5	658[f] (chl)	70,000	24,000	15	*91-94,* ***95****,96*
prodeoxyviolacein	$C_{20}H_{13}N_3O$	311.3	609 (et)(A)	25,000	1.5	9	*97-100,* ***101***
ammosamide A	$C_{12}H_{10}Cl_1N_5O_1S_1$	307.8	584[g] (m)	5,200	160	6	*103*
sanguinone A	$C_{15}H_{14}N_4O_3$	298.3	578 (w)	437	330	1	***104***
pyridyl							
indigoidine	$C_{10}H_8N_4O_4$	248.2	602 (dmf)	23,400	4,500	35	*105,106****,107***
indochrome A	$C_{20}H_{23}N_3O_{12}$	497.4	570 (w)(A)	38,100	15,000	3	*105-107****,171***
N,*N*-dodecylindigoidine	$C_{36}H_{56}N_4O_4$	584.8	636 (chl)	n.a.	0.00042	1	***115***
blue pigment (unnamed)	$C_{10}H_4N_2O_6$	248.2	648 (dmf)	17,380	14,000	2	***107,*** *108-112*
lemonnierin	$C_{26}H_{37}N_5O_6$	515.6	625 (dmf)	56,230	2.6	2	***116****,117*
glaukothalin	$C_{34}H_{56}N_4O_4$	584.8	636 (chl)	32,360	0.59	1	***118****,119*
genipocyanin G_1	$C_{27}H_{24}N_2O_8$	504.2	595 (w)	43,700	n.a.[e]	3	*120-124,* ***125***
azulene							
azulene	$C_{10}H_8$	128.2	576 (et)	362	140	3588	*127,* ***133****,134*
guaiazulene	$C_{15}H_{18}$	198.3	648 (acn)	407	0.12	995	*127-129,* ***135***
lactarazulene	$C_{15}H_{16}$	196.3	604 (m)	871	0.27	20	*127-129,* ***134***
2,12'-bis-hamazulenyl	$C_{28}H_{30}$	366.5	657 (chl)	132	0.00016	1	***132***

[a] (A) = acidic conditions; (B) = alkaline conditions; (w) = water; (m) = methanol; (et) = ethanol; (chl) = chloroform; (dcm) = dichloromethane; (hex) = hexane; (dmf) = dimethylformamide; (acn) = acetonitrile

[b] Solubility in water, pH 3, 25 °C. Calculated using ACD/Labs Software V11.02 or ACD/Percepta Build 2254

[c] Number of citations currently associated with the compound in CAS SciFinder scholar.

[d] The source of the λ_{max} and ε value is given in bold.

[e] Species is ionic or charged. Solubility cannot be calculated.

[f] For trichotomine dimethyl ester

[g] Authors' unpublished research

TABLE II. NATURAL BLUE PIGMENTS ACCORDING TO BIOLOGICAL SOURCE.

compound name (no.)	compound class	biological source(s)
synthetic		
FD&C Blue No. 1	triphenylaryl	none
FD&C Blue No. 2	*bis*-indole	derivative of natural indigo dye
animal		
biliverdin-Ixa	linear tetrapyrrole	*Aves* (egg shell); mammal bile pigment
oxyblepharismin A	naphthodianthrone	*Blepharisma japonicum* (protist)
popolohuanone B	diterpene azaquinone	*Dysidea* sp. (marine sponge)
plant		
oenin	anthocyanin	*Vitis vinifera* skin, aged wine
portisin A	pyranoanthocyanin	*Vitis vinifera*; aged wine
diosindigo A	benzoisochromaquinone	*Diospyros sp.* (tree; heartwood)
ventilein A	naphthodianthrone	*Ventilago goughii* (root bark)
indigotin	*bis*-indole	*Indigofera tinctoria* (Indigo plant)
trichotomine	*bis*-indoloid	*Clerodendron trichotomum* (fruit callus)
genipocyanin G_1	2-pyrindine	*Gardenia jasminoides, Genipa americana*
azulene	azulene	*Artemisia* sp. (oil), *Lactarius* sp. (fungi)
guaiazulene	sesquiterpene	*Matricaria chamomilla* (oil), various fungi
lactarazulene	sesquiterpene	*Artemisia* sp. (oil), *Lactarius* sp. (fungi)
2,12'-bis-hamazulenyl	*bis*-azulene	*Ajania fruticulosa* (essential oil)
fungal		
variegatic acid anion	benzofuranoquinone	Basidiomycete fungi
albatrellin	meroterpenoid quinone	*Alabtrellus flettii* (Basidiomycete)
corticin A	*bis*-benzofuranone	*Corticium caeruleum* (fungi)
candidine	*bis*-indoloid	*Candida lipolytica* (yeast)
sanguinone A	indoloquinone	*Mycena sanguinolenta* (fungi)
scleroderris blue	azobisquinone	*Gremmeniella abietina* (fungi)

TABLE II. NATURAL BLUE PIGMENTS ACCORDING TO BIOLOGICAL SOURCE (continued).

compound name (no.)	compound class	biological source(s)
microbial		
daunorubicin	anthraquinone	*Streptomyces peucetius*
actinorhodin	benzoisochromaquinone	*Streptomyces coelicolor*
granaticin B	benzoisochromaquinone	*Streptomyces violaceoruber*
anthracyclinone-blue B	tetracyclic quinone	*Streptomyces galilaeus* mutant
phycocyanobilin	linear tetrapyrrole	*Spirulina* sp., common among cyanobacteria
bactobilin	linear tetrapyrrole	*Clostridium tetanomorphum*
prodigiosin tetrapyrrole	linear tetrapyrrole	*Serratia marcescens*, *Hahella* sp. (marine)
pyocyanin	phenazine	*Pseudomonas aeruginosa*
phenazinomycin	phenazine	*Streptomyces sp.* WK-2057 mycelia
lavanducyanin	phenazine	*Streptomyces aeriouvifer*
benthocyanin A	phenazine	*Streptomyces prunicolor*
akashin A	*bis*-indole	*Streptomyces* sp. GW48/1497 (marine)
prodeoxyviolacein	*bis*-indoloid	*Chromobacterium violaceum*
ammosamide A	thiopyrroloquinoline	*Streptomyces* CNR-698 (marine)
indigoidine	3-3'-bipyridoid	*Corynebacterium insidiosum*
indochrome A	3-3'-bipyridoid	*Arthrobacter polychromogenes*
N,*N*-dodecylindigoidine	3-3'-bipyridoid	*Shewanella violacea* DSS12 (marine)
blue pigment (unnamed)	3-3'-bipyridoid	*Arthrobacter* sp., *Nocardia* sp.
lemonnierin	3-3'-bipyridoid	*Pseudomonas lemonnieri*
glaukothalin	*bis*-oxazepinone	*Rheinheimera* sp. HP1 (marine)

TABLE III. LEADING BLUE COLORANTS AND NATURAL COLORANT CANDIDATES.

compound name	compound class	λ_{max} (nm)[a]	ε (M^{-1} cm^{-1})[a]	acid color	commercial colorant applications
synthetic					
FD&C Blue No. 1	triphenylaryl	629 (w)	134,000	blue	widespread commercial use in beverages and food.
FD&C Blue No. 2	*bis*-indole	607 (w)	7,920	blue	commercial textile dye; limited food applications
natural					
trichotomine	*bis*-indoloid	658[b] (chl)	70,000	blue	textile dye and natural ink (ethnographic use; Japan).
guaiazulene	azulene	648 (acn)	407	blue	cosmetics
phycocyanobilin	tetrapyrrole	604 (m)	17,100	blue	solid packaged food formulations.
gardenia blue	2-pyrindine	595[c] (w)	43,700	blue	limited use in food (Asia); skin and hair dye (South America).
portisin A	pyranoanthocyanin	587 (m)(A)	82,900	purple	none.
actinorhodin	benzoisochromaquinone	640 (w)(B)	25,300	red	none.

a. (A) = acidic condition; (B) = alkaline condition; (w) = water; (m) = methanol; (chl) = chloroform; (acn) = acetonitrile.

b. For trichotomine dimethyl ester. c. For the genipocyanin G_1 dimer

CHAPTER 2: LEAD GENERATION AND DEREPLICATION OF NATURAL BLUE PIGMENTS

(Contains sections previously published as Newsome AG, Murphy BT, van Breemen RB. Isolation and Characterization of Natural Blue Pigments from Underexplored Sources. In *Physical Methods in Food Analysis*. *ACS Symposium Series*, Vol. 1138. Chapter 8, pp 105–125, 2013.)

2.1 INTRODUCTION

As established in Chapter 1, the search for natural colorant alternatives for blue shades has been ongoing for decades but has not produced a natural alternative for FD&C Blue No. 1 (173,174). The majority of the global search effort has focused on blue pigment molecules sourced from flowers and fruits of plants. Most pigmentation in flower and fruit bodies is due to molecules of the anthocyanin class, but anthocyanins are problematic as colorant alternatives particularly in the context of acidic beverages because they are generally not stable to acid, heat, or light and few if any maintain a blue shade below pH 5. Continued exploration of plant anthocyanins for new blue colorant alternatives is very likely to result in the dereplication of known anthocyanins or the discovery of new ones with similar acid shade and stability shortcomings as the more than 500 anthocyanins that have been described (175,176).

Therefore, the present work focused on pigmented material derived from less scientifically explored or less accessible biological organisms and environments such as underexplored plants and the marine environment. The rationale was that natural pigments derived from such environments or organisms are more likely to contain novel structure classes or yield a new blue chromophore. Less accessible or underexplored biological sources of pigments include organisms living in extremophilic environments (acidophiles and thermophiles), organisms derived from aquatic (freshwater or marine) environments, and non-plant organisms (microbes, cyanobacteria, algae, and fungi) in general. Pigments from organisms living in more extreme environments (acidophiles and thermophiles) are of particular interest since acid and heat stability is a critical prerequisite for the success of a candidate colorant molecule.

This chapter covers general experimental approaches used in the cultivation, isolation, and the dereplication of known pigments in the pursuit of novel ones. A pilot study exploration of marine biomass material for marine-derived microbial pigments and exploration of miscellaneous literature or collaborative leads is described. Data and results for the spectroscopic dereplication (usually by HPLC-PDA-HRMS^2) of previously known pigments obtained from marine and other sources as well as work with miscellaneous leads that were ruled out early as colorant candidates are presented. The marine pigment dereplication aspect of this work was published as an ACS Symposium series book chapter (177).

2.2 General experimental overview

The following section covers general experimental approaches and techniques that were applied in this work and that are applicable to any pigment dereplication analysis. This chapter is largely focused on pigment discovery from marine-derived microbes since this line of investigation led to the dereplication of many previously known pigment compounds. The overall research scheme for the discovery of natural blue pigments used in this work is summarized in Figure 12 (177).

2.2.1 Blue pigment leads

For the purposes of pigment detection, the human eye serves as a suitable qualitative spectrophotometer and so simple visual inspection was used as the primary means of lead detection for this work. This is a distinct advantage over typical lead detection in drug discovery which requires bioactivity screening assays. Since the eye cannot discern a blue pigment within a complex mixture, HPLC-UV/Vis data of natural product extracts or fractions was also mined for visible absorbance in the 550-700 nm (red light absorbance) region for the detection of blue pigments in this work.

While the ability to visually detect and follow a molecule having the desired candidate property is an advantage, there are also difficulties inherent in the pursuit of novel pigments. Pigmented compounds span the entire molecular weight range from less than 100 mass units to 100 MDa protein

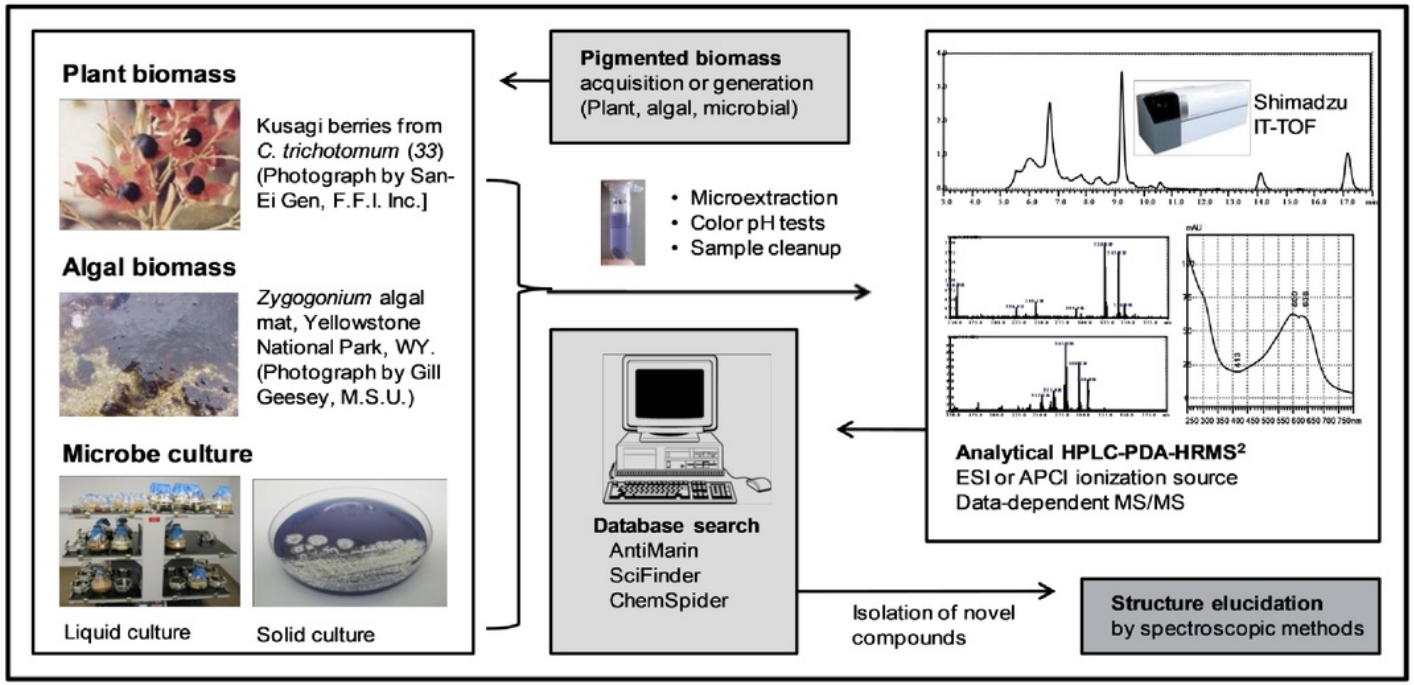

Figure 12. Flow diagram for the isolation and discovery of natural pigments. Pigmented biomass from plants and algae or microbial strains are isolated from environmental samples and extracted on a small scale for analysis by high performance liquid chromatography-photodiode array absorbance detection-high resolution tandem mass spectrometry (HPLC-PDA-HRMS^2). Known compounds are dereplicated by comparing their mass spectrometric and spectrophotometric data against compound databases while novel compounds proceed to scale-up for structure elucidation by NMR spectroscopy.

complexes, the entire polarity range from aqueous to extremely lipophilic, and may involve organic, inorganic, or organometallic complexes, nanoparticles, or molecular aggregates. Molar absorptivities (ε) span 5 orders of magnitude and pigments with high molar absorptivities may appear abundant even when present at trace levels. The absorbance of many pigments is dramatically dependent upon solvent and pH. Because an acid stable blue colorant was the ultimate goal of this work, many extracts, cultures, and fractions encountered in this work were routinely acidified to check for the appearance of blue pigmentation.

2.2.2 Pigment dereplication

In this research it was often the case that a single hyphenated HPLC-PDA-HRMS^2 analysis of microextracted pigments from lead biomaterial such as a single agar plate culture could provide sufficient data to rapidly dereplicate pigment metabolites (excluding finer structural details such as stereochemistry) and determine the presence of novel pigment analogs. Relative to colorless metabolites, the UV-Vis absorbance pattern of pigments adds an additional data point for compound dereplication. Microscale extraction, cleanup, and HPLC-PDA-HRMS^2 analysis of pigment compounds was often rapid and efficient aided in part by color serving as a visual guide to the location of the compounds during extraction and clean up steps. Examples of dereplicated pigments with experimental details are covered in section 2.4.

Pigments produced by microbes can be either intracellular or extracellular. In the case of intracellular pigments, the cells must be lysed to release their contents. Intracellular pigment extraction was achieved using typical cell extraction strategies such as hypotonic buffers, sonication cycles, lyophilization, and freeze-thaw cycles. Extracellular pigments must be separated from the high

concentration of salts in marine nutrient media. Pigments were typically extracted from the aqueous media through liquid-liquid extraction, precipitated by addition of a miscible organic solvent (typically, methanol or ethanol), or by solid-phase extraction using a resin such as Amberlite XAD16. Acidification of the media (0.1% formic acid) followed by liquid partitioning into ethyl acetate was a successful approach for extraction of most extracellular microbial pigments.

Highly polar pigments posed an additional analytical challenge since they are not amenable to liquid-liquid extraction and often showed little to no retention on reversed phase stationary phases. Silica gel separation is a mainstay for fractionation of crude natural product extracts but was unsuccessful for some highly polar pigments encountered in this work that adsorbed irreversibly to the silica. Instead, size-exclusion gel filtration materials such as Sephadex LH-20 or hydrophilic interaction liquid chromatography (HILIC) columns were used for fractionation of highly polar pigments. Conveniently, HILIC columns enable the separation of highly polar pigment metabolites using a standard acetonitrile-water gradient system.

Pigment compounds had some value as chemotaxonomic markers that were helpful and informative in terms of project prioritization, strain novelty, and dereplication of the metabolites in general by comparison to the literature. With microextraction of a single Petri culture followed by analysis using HPLC-PDA-HRMS^2 analysis, it was often possible to guess the microbial species based on the pigment metabolites and morphology For example, *Streptomyces* Strain D030 was predicted to be *S. coelicolor* and later confirmed by 16S rRNA sequencing.

The primary system used for dereplication was a Shimadzu (Columbia, MD) HPLC with a PDA detector connected to a Shimadzu (Kyoto, Japan) Ion Trap – Time of Flight (IT-TOF) mass spectrometer. The use of a PDA detector instead of a less expensive single or dual λ UV detector is a significant advantage for pigment analysis since a complete UV-Vis spectrum can be obtained for each

individual pigment. Electrospray was the usual ionization method, but atmospheric pressure chemical ionization (APCI) was used for more lipophilic pigments. Positive and negative ion mass spectra were typically collected in a single run using polarity switching. Tandem mass spectra were collected in a data-dependent mode by computerized selection of the most abundant ions for fragmentation during product ion tandem mass spectrometry.

In the final preparation of an extract or fraction for HPLC-PDA-HRMS^2 analysis, the sample was generally diluted to a concentration between 50 and 500 μg mL^{-1} in a solvent close to the starting mobile phase composition (*e.g.* MeCN:H_2O; 20:80, v/v) and centrifuged at 10,000 x *g* for 15 min to remove particulates prior to injection. After the analysis, accurate mass and mass fragmentation data were used to generate a short list of likely chemical formulas. The accurate masses or the chemical formulas were then searched using the chemical databases Antimarin, Scifinder Scholar, ChemSpider, Reaxys, and PubChem. The database matches were further refined by comparison with UV-Vis spectral data. Other secondary characteristics which were useful for consideration include the culture morphology, compound polarity, and chemical behavior such as acid-base tautomerization and solubility.

2.2.3 Structure elucidation considerations

In cases of compelling leads where milligram quantities of compound were desired, the amount of culture growth was scaled up. Obtaining pigment metabolites in amounts suitable for structure elucidation was often a challenge. Organisms can usually be grown on a larger scale to obtain milligram quantities of pure pigmented compounds for isolation and structure elucidation by NMR spectroscopy. Although up to 40 L of liquid culture of the microbial strain would typically be required, pigments observed in solid cultures were not always produced when transferred to liquid culture of the same media. In these cases, scaled-up agar culture was carried out using any large autoclave-compatible and

sealable glass containers (such as with strain D034). Some microbial strains were very slow growing (*Actinomycetes* are notorious for slow growth) and may take several months to mature for metabolite extraction. Since some pigments are light sensitive, microbial cultures were usually protected from light exposure during growth. Crude pigment extracts of large scale cultures were generally fractionated by open column chromatography facilitated by visual detection of the colored bands.

When the chromophore class of a novel pigment is known, the quantity of the culture needed to obtain milligram quantities of the pure compound can be estimated using molar absorptivity. In theory, using typical ε values for pigments of the same chromophore type from the literature, experimental HPLC-PDA data and Beer's law ($A = \varepsilon cl$) provide a guideline for the amount of scale-up culture required based on the back-calculated estimate for the amount of pigment present in microculture (*i.e.*, μg compound per mL of culture). Although this estimate approach was used for a scale-up of *Streptomyces sp.* strain D034 (section 2.4.5), much less pigment was produced in large scale culture than in petri dish culture.

For isolation and structure elucidation of novel compounds, purifications were generally performed by using semipreparative HPLC with UV-Vis detection. Reversed phase chromatography sufficed for most applications, but HILIC or other specialty columns were used for highly polar, macromolecular or ionic pigmented compounds. High resolution mass spectrometry with accurate mass measurement for elemental composition determination combined with two-dimensional (2D) NMR spectroscopy (using 600 MHz or higher magnet strength) was used for structure determination of novel compounds. A typical set of 2D NMR experiments for the elucidation of a novel pigment metabolite includes DEPT Q, COSY, HSQC, HMBC, and ROESY as for any organic natural product metabolite.

2.3 Marine-derived microbial cultures

A branch of the pigment discovery project involved working with marine-derived microbial cultures as a source of lead pigment compounds. The work with culturing marine microbes and dereplication of pigments from these organisms is covered in sections 2.3 and 2.4, respectively.

2.3.1 Culture considerations for marine-derived microbial pigments

A biodiversity study found that there are more than 10^5 microbial cells per 1 mL of ocean water (178). Access to marine microbe cultures and environmental sediments in this research was provided by Dr. Brian Murphy (UIC College of Pharmacy). In contrast to pigments of terrestrial organisms which often serve photosynthetic, UV protectant, or insect attractant roles, microorganisms dwelling in the darkness of the ocean have little or no use for visible light absorption. However, pigments do occur commonly in marine microbes. The unexplored marine microbial biodiversity makes natural drug discovery and also natural pigment discovery from the marine environment appealing due to the higher likelihood of discovering previously unidentified compounds. However, since marine pigment metabolites likely serve biological roles less benign than light absorption, a possible disadvantage of sourcing the marine environment for nontoxic consumable pigments is the occurrence of undesirable toxic biological activity.

The marine-derived microbial diversity that can be obtained under laboratory conditions from environmentally collected samples is dependent upon culture methods. Research groups typically use heat shock, limited nutrients, or other means (179,180) to kill the majority of Gram-negative microbes in marine samples prior to culture and then use culture conditions that select for *actinobacteria* (Gram-positive) since these are prolific secondary metabolite producers (181). Most solid and liquid marine nutrient media (e.g. A1, M1, ISP2, and TCG) used for solid and liquid culture are slightly alkaline (~ pH

8) to mimic the pH of the ocean. However, it is common for anthraquinone and phenolic pigments that are blue colored in alkaline conditions to tautomerize to a red form under acidic conditions. Owing to these various considerations, an effort to find pretreatment conditions for marine sediment samples such as the use of acid shock or acidic media were explored through a marine culture pilot study.

2.3.2 Marine-derived pigment pilot project

An exploratory pilot project was conducted with the goal of culturing marine-derived microbes from marine sediment samples using a variety of sample pretreatments and growth media to generate both pigment producing microbial strain leads and to determine what conditions, if any, tended to produce more pigmented strains. Ten environmental marine sediment samples that were collected from the coastal waters of Massachusetts (Back beach, Old Garden beach, Urell beach, Duxbury beach, and Boston harbor) were selected for the study of different pretreatment conditions. The original solutions were diluted 1:5 in water, and aliquots were subjected to different pretreatments to kill the majority of microbes as follows: acid treatment (A_x) at pH 2 with H_3PO_4 for 30 min, base treatment (B_x) at pH 10 with NH_3 for 30 min, heat shock treatment (H_x) with a water bath at 80 °C for 30 min, and cold shock treatment (C_x) at -78 °C with an isopropanol/CO_2 bath for 30 min. A solution of each sediment sample was inoculated onto agar plates of each of four marine nutrient media (A1, M1, ISP2, and TCG). To observe the effect of dilution and of sample pretreatment, undiluted sediment solution (N) as well of as untreated 1:5 diluted sediment solution (N_d) of each of the 10 environmental samples was inoculated on each of the four marine nutrient media. All of the agar cultures contained 5 μM cycloheximide to inhibit fungal growth except for one set ($ISP2_x$) of plates inoculated with 1:5 diluted sediment solution to screen for pigmented fungi.

The culture plates (300 total) were allowed to mature for 6 weeks. The untreated diversity cultures were overrun with colorless slime within the first week. Of the four types of marine nutrient media, the least nutrient-rich marine media (M1) resulted in the least populated and therefore most selective plates. Of the four treatments, the heat shock (A_x) and acid shock treatments (H_x) appeared to produce the most selective and interesting cultures. Some pigmented colonies were produced, but none produced and excreted distinctly blue or purple pigment. One culture, environmental sample DB045 grown on A1 media and subjected to acid pretreatment, produced a morphologically apparent *Bacillus sp.* which excreted a black-brown pigment when isolated in pure culture. Investigation of this pigment resulted in comparison with the bluish-black pigment excreted by *Bacillus subtilis* ATCC 6461 as described in section 2.5.1. Representative of the pilot project, petri cultures of one of ten environmental sediment samples (sample DB045) after 3 weeks of growth are shown in Figure 13.

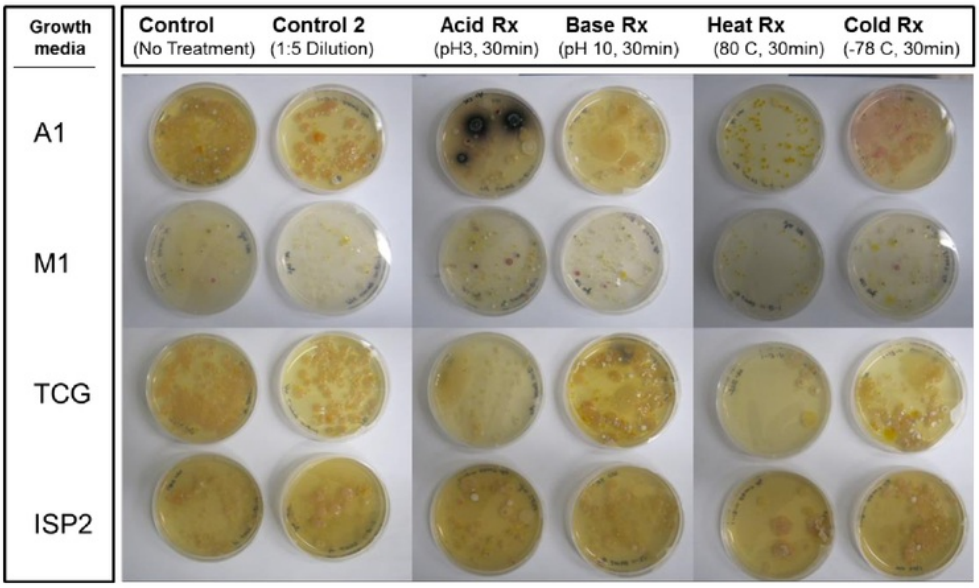

Figure 13. Representative marine pigment pilot project results of petri cultures of one of ten environmental sediment samples (sample DB045) a set of petri cultures marine pigment pilot project after 3 weeks of growth.

2.4 Marine-derived dereplicated pigments

A variety of blue and purple pigmented compounds were dereplicated from marine-derived strains using microextraction and the HPLC-PDA-HRMS^2 analysis procedures discussed in section 2.3. Agar plate cultures, extracts, and fractions that were observed to have compelling pigmentation were pursued. Analysis of the absorbance data, mass spectrometric data and culture morphology in comparison to the literature provide a strong set of chemical identifiers for dereplication. Some of these strains and structures of blue or purple pigments are shown in Figure 14, and dereplicated pigments are summarized in Table IV.

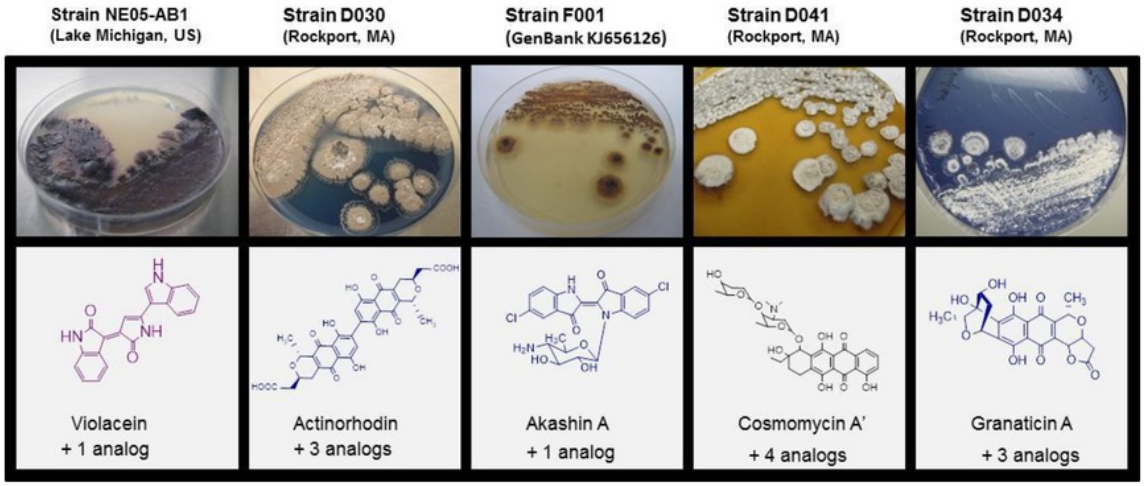

Figure 14. Blue or purple pigment compounds found during the pilot study cultures of marine-derived microbial strains. The compounds were identified by using high resolution accurate mass measurement, mass fragmentation and UV/Vis spectra. The strain source or collection location is given in parenthesis.

2.4.1 Violacein from Strain NE05-AB1

Strong purple pigmentation was observed when the cells of marine strain NE05-AB1 were cultured on freshwater media (sterilized Lake Michigan water). The compound violacein was identified as the primary pigmented agent as follows. The intracellular violet pigment produced by cells from a 4 cm^2 area of Petri dish culture of strain NE05-AB1 (Lake Michigan, USA) was scraped from the surface. The purple pigment extracted readily by sonication in 2 mL of methanol. The extract was centrifuged at 10,000 x *g* for 15 min, and the supernatant was evaporated to dryness under a stream of nitrogen. The residue was reconstituted in 50 µL of methanol/water (50:50, v/v), centrifuged again and filtered through a 0.2 µm Nylon membrane.

Following several HPLC test injections of the residue using an analytical C_{18} column, two peaks were collected after a single injection onto a semi-preparative C_{18} column (300 x 10 mm, 5 µm) using a methanol gradient from 10% to 95% over 20 min and detection at 580 nm. The collected peaks were analyzed by HRMS-PDA-$HRMS^n$. Because the compounds were highly lipophilic, APCI was chosen instead of electrospray.

For the two major compounds, abundant $[M+H]^+$ and $[M-H]^-$ ions were observed which were consistent ($\Delta M < 5$ ppm) with the formulas $C_{20}H_{13}N_3O_3$ (major peak) and $C_{20}H_{13}N_3O_2$ (minor peak). The chemical formulas, UV-Vis spectra, and tandem mass spectra of these unknown pigments (Figure 15) were consistent only with the compounds violacein and deoxyviolacein (182) found in chemical databases SciFinder and Antimarin.

TABLE IV: DEREPLICATED PIGMENT-PRODUCING MICROBIAL STRAINS

microbial strain	source information	compound example	formula	HRMS observed (error)
Strain NE05-AB1	Lake Michigan, USA	violacein	$C_{20}H_{13}N_3O_4$	$[M+H]^+$ 344.103 (-1.5 ppm)
Streptomyces Strain D030	Rockport, MA	γ-actinorhodin	$C_{32}H_{22}O_{14}$	$[M+H]^+$ 631.111 (+3.5 ppm)
Streptomyces Strain F001	GenBank KJ656126	akashin A	$C_{22}H_{19}Cl_2N_3O_5$	$[M+H]^+$ 476.0778 (-0.4 ppm)
Streptomyces Strain D041	Rockport, MA	kesarirhodin B	$C_{40}H_{53}NO_{13}$	$[M+H]^+$ 756.3704 (+14.4 ppm)
Streptomyces Strain D034	Rockport, MA	granatomycin E	$C_{22}H_{22}O_{11}$	$[M-H]^-$ 461.1027 (-12.3 ppm)
Nostoc punctiforme 7179 zyz*	Orjala laboratory (UIC)	phycocyanobilin	$C_{33}H_{38}N_4O_6$	Protein-bound chromophore
Extracts 1270t, 1341t, 1386	Montana Polysaccharides	prodigiosin	$C_{20}H_{25}N_3O$	$[M+H]^+$ 324.210 (+7.4 ppm)

*Cyanobacteria. Phycocyanobilin chromophore dereplicated via UV/Vis spectrum match.

2.4.2 Actinorhodins from *Streptomyces* Strain D030

Marine-derived Strain D030 produced an extracellular blue pigment in agar cultures (Figure 14). The pigment extracted readily into water directly from chopped culture agar. Acidification of the blue aqueous extract with 0.1% formic acid tautomerized the pigments into a red (uncharged) form which readily extracted into ethyl acetate. Actinorhodin, γ-actinorhodin, and related analogs were identified from the agar microextract by HPLC-PDA-HRMS^2 analysis and dereplication (Figure 16)(183). The 16S rRNA sequence of the strain later showed a 100% match with the terrestrial species *Streptomyces coelicolor* (183). No compelling novel analogs were detected worth further pursuit.

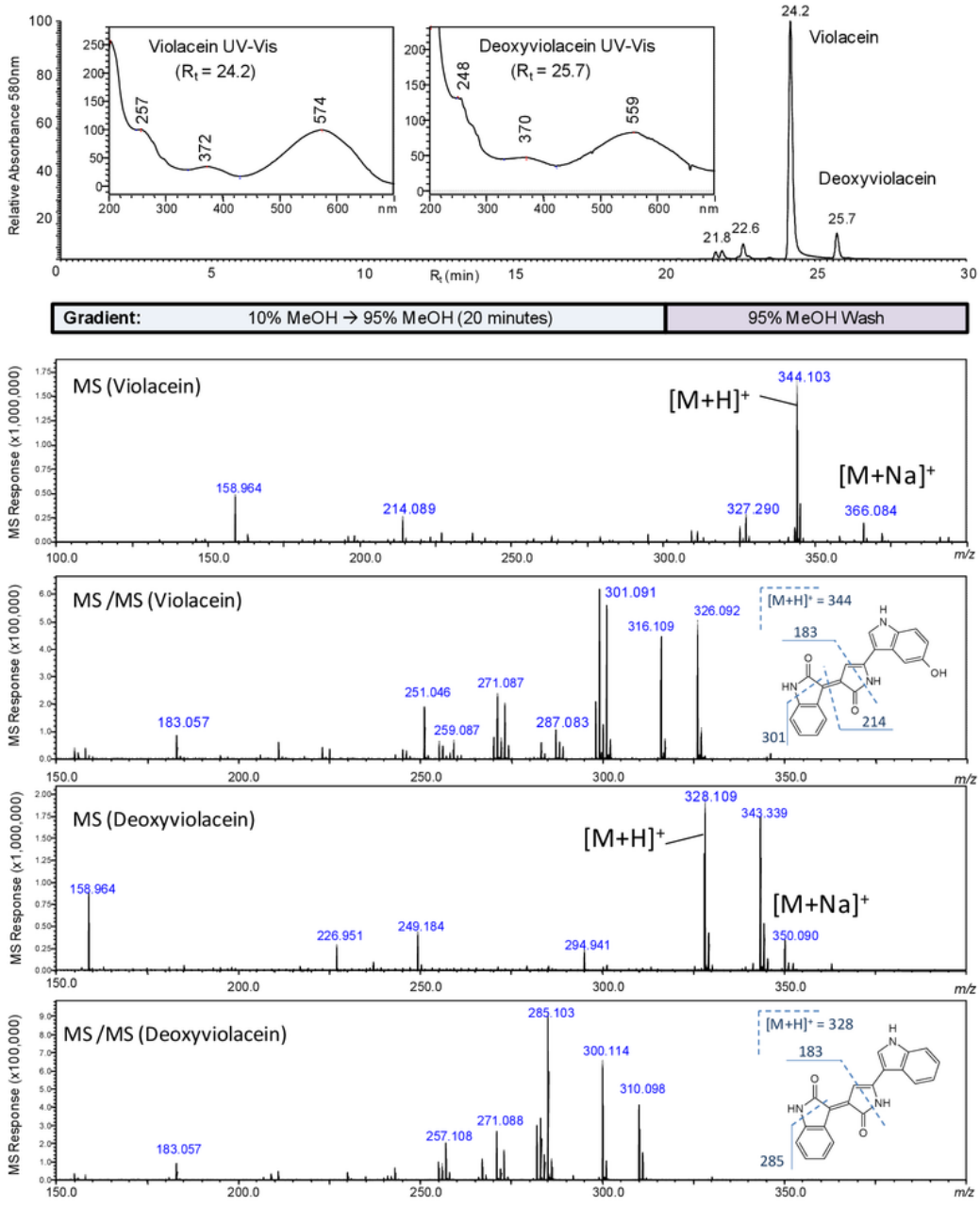

Figure 15. Semi-preparative HPLC chromatogram, UV/Vis spectra, high resolution MS spectra, and tandem MS spectra with fragmentation assignments for two violet pigment compounds identified as violacein and deoxyviolacein. The pigments were, obtained from strain NE05-AB1 which was cultured from sediment collected from Lake Michigan (USA).

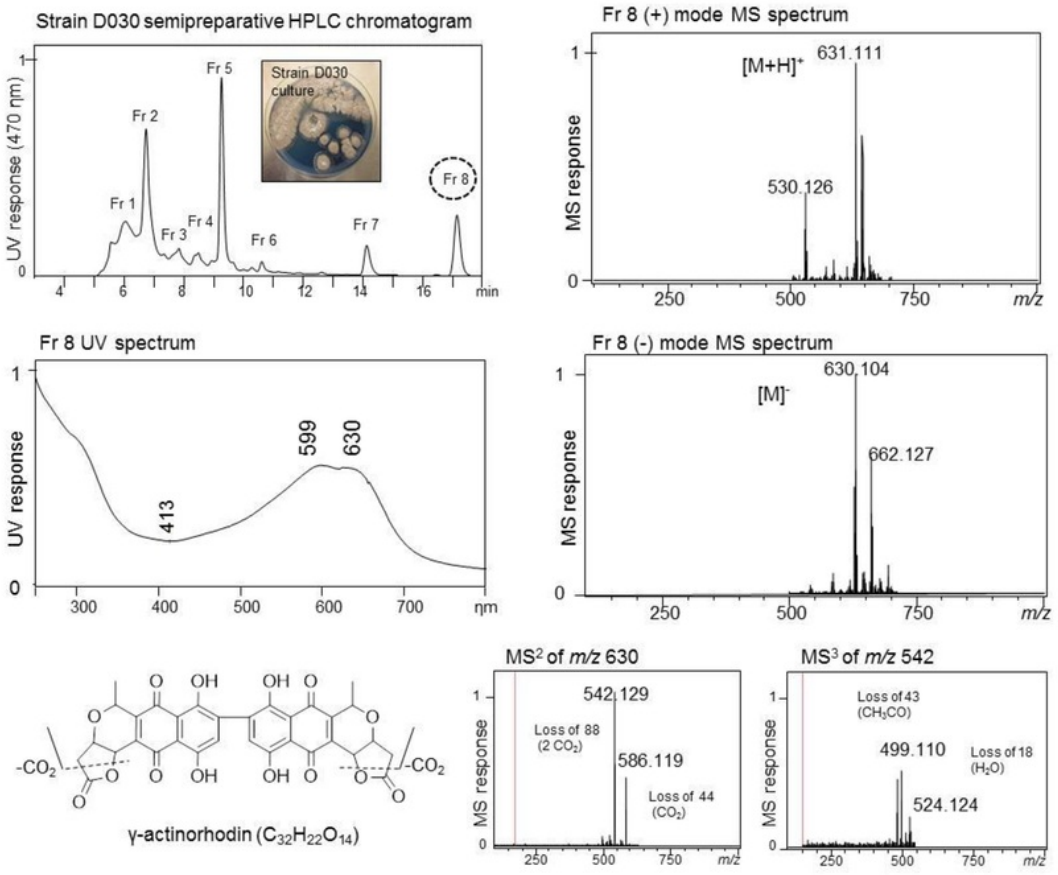

Figure 16. Semipreparative HPLC chromatogram for blue pigments from *Streptomyces* strain D030. Representative dereplication data (UV/Vis spectra, high resolution MS spectra, and tandem MS spectra using APCI) with fragmentation assignments is shown for fraction 8, γ-actinorhodin.

2.4.3 Akashin A from marine-derived *Streptomyces sp.* Strain F001

Metabolites from a 5 L batch of *Streptomyces sp.* Strain F001 (ISP2 media) was extracted with Amberlite XAD-16 resin and fractionated using a 5 g silica solid phase extraction (SPE) cartridge. The 50:50 DCM:Hexane layer (Fr 1) was purified by semipreparative C_{18} HPLC (isocratic 85:15 MeCN/water 0.1% formic acid) to obtain a deep blue solid. The blue fraction was dissolved in methanol

and analyzed using HPLC-PDA-HRMS^2 using a C_{18} 50 x 2.1 mm 5 µm column using a gradient of 30% to 60% ACN over 10 minutes with water containing 0.1% formic acid. The chlorinated indigo-*N*-glycoside pigment, Akashin A, was identified by using accurate mass and UV-Vis data (Figure 17). The tandem mass spectra showed a loss of the *N*-glycosaminoglycan sugar to give the aglycone at *m/z* 331. The chlorinated indigo derived akashin pigments (akashin A, B, and C) were reported previously from a terrestrial *Streptomyces sp.* (184,185). Although the blue akashins were previously reported, subsequent structure elucidation studies on orange diazoquinomycin pigments from *Streptomyces* Strain F001 and marine-derived *Streptomyces* sp. Strain B026 led to the identification of novel orange pigmented diazoquinomycin analogs (186).

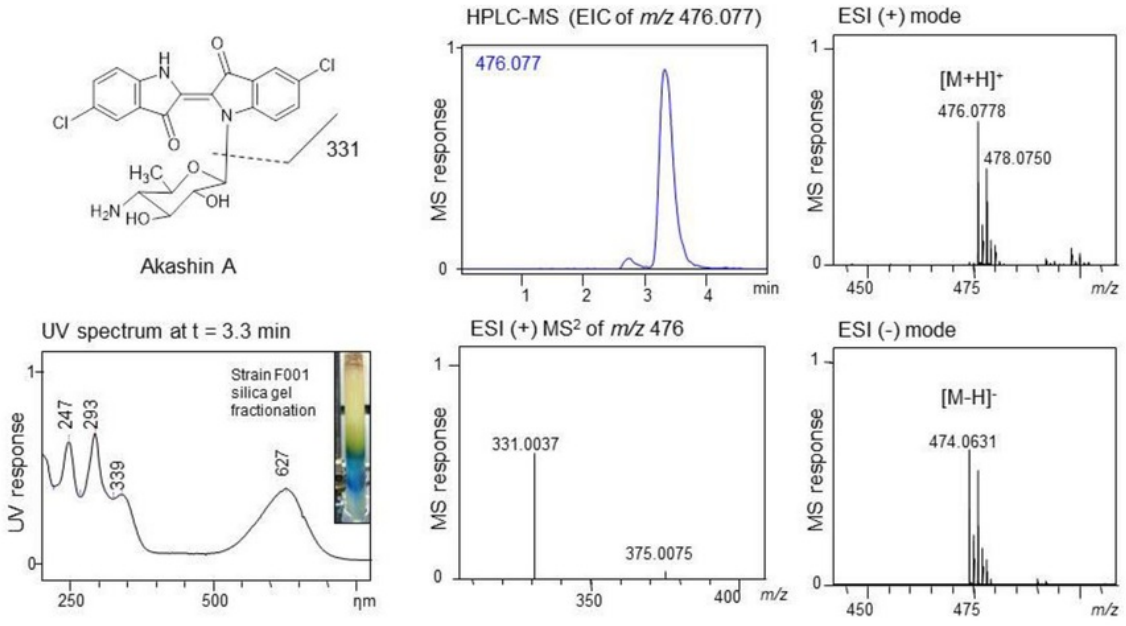

Figure 17. HPLC-MS^2 and UV dereplication data for the blue pigment akashin A from *Streptomyces* strain F001.

2.4.4 Cosmomycins from marine-derived *Streptomyces* Strain D041

Five pigmented doxorubicin-like analogs were identified in the Amberlite XAD16 resin extract of marine-derived *Streptomyces sp.* strain D041. An orange silica SPE fraction was analyzed by HPLC-PDA-HRMS^2 using a C_{18} 150 x 2.1 mm 5µm column with a gradient of 30% to 95% MeCN from 2 to 20 min with mobile phase A containing 0.1% formic acid. Retention times and UV-Vis spectra were similar to the standard doxorubicin. The HRMS^2 data matched accurate mass, UV-Vis, and fragmentation patterns for the previously identified anthraquinone antibiotics iremycin, cosmomycin A', cosmomycin B, cosmomyin B', and kesarirhodin B (Figure 18) from *Streptomyces cosmosus* (187).The pigments are cytotoxic, blue only in base (pH > 9) and red-orange at neutral or acidic pH.

2.4.5 Granaticins from marine-derived Strain D034

A series of blue anthraquinone pigments were identified in an Amberlite XAD16 resin extract of marine-derived strain D034 using HPLC-PDA-HRMS^2. The pigments were dereplicated by accurate mass, tandem mass spectra, and UV-Vis spectra as granatomycin E, metenaticin A, and granaticin B (188,189). Dereplication data for granaticin analogs from Strain D034 are provided in Figure 19.

Minor amounts of two potentially novel blue analogs were detected, a putative granaticin diglycoside ($C_{34}H_{40}O_2$, $[M-H]^-$ *m/z* 767.195) and an unknown analog ($C_{26}H_{28}O_{12}$, $[M-H]^-$ *m/z* 531.148). Normally, liquid media would be used to scale up a strain culture for purification of milligram amounts needed for structure elucidation. However, further study of the strain revealed that the novel compounds were only produced using solid agar culture, and the novel analogs were not present when cultured in liquid media. Therefore, the very slow-growing strain was cultured in bulk agar for 2 months in glass vessels. Unfortunately, the amount of novel analogs remained below what was necessary for structure elucidation.

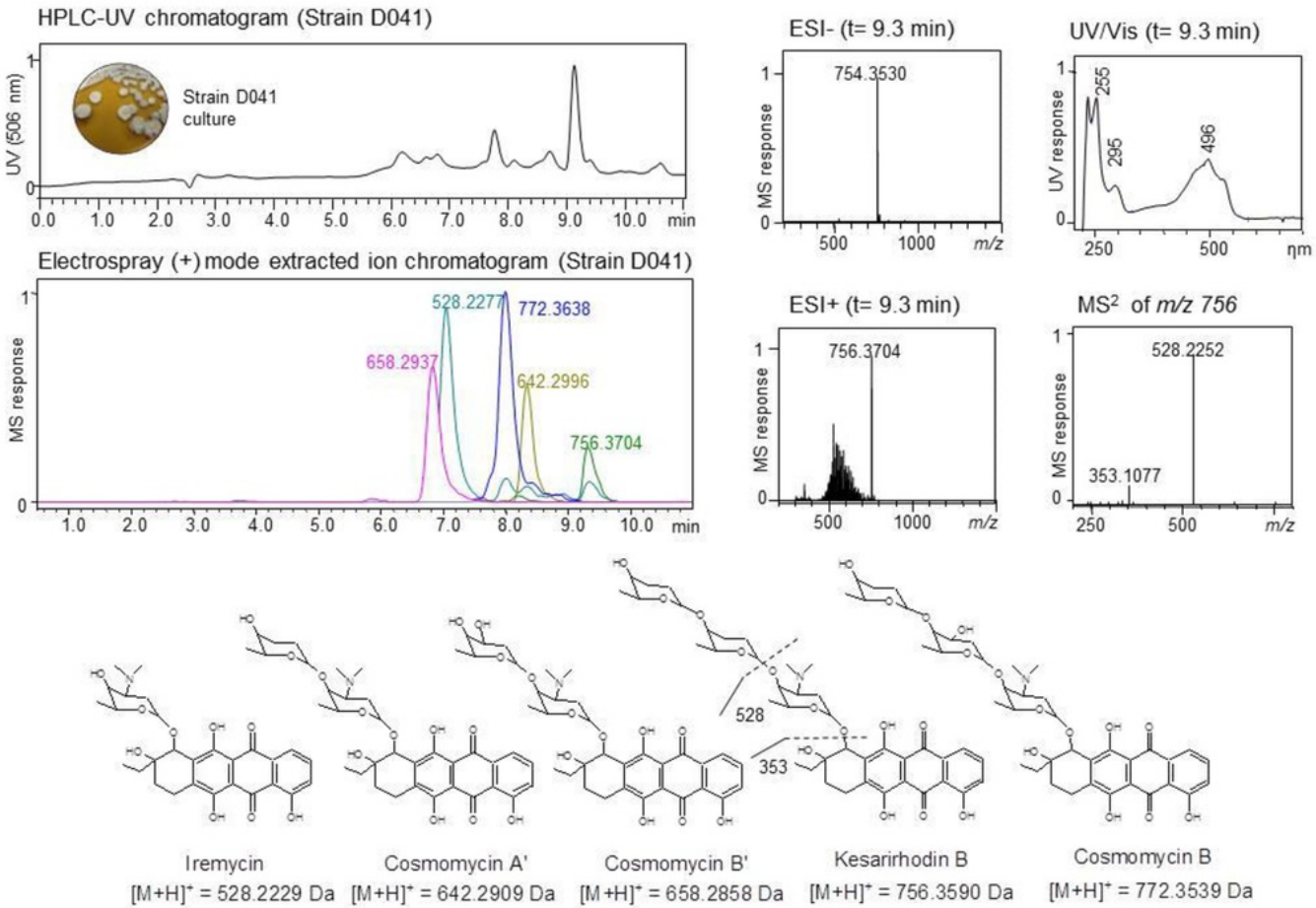

Figure 18. HPLC-UV-HRMS chromatogram for anthroquinone pigments from marine-derived *Streptomyces* strain D041. Representative dereplication data (UV/Vis spectra, high resolution MS spectra, and tandem MS spectra using APCI) with fragmentation assignments is shown for the *m/z* 756 proposed to be kesarirhodin B.

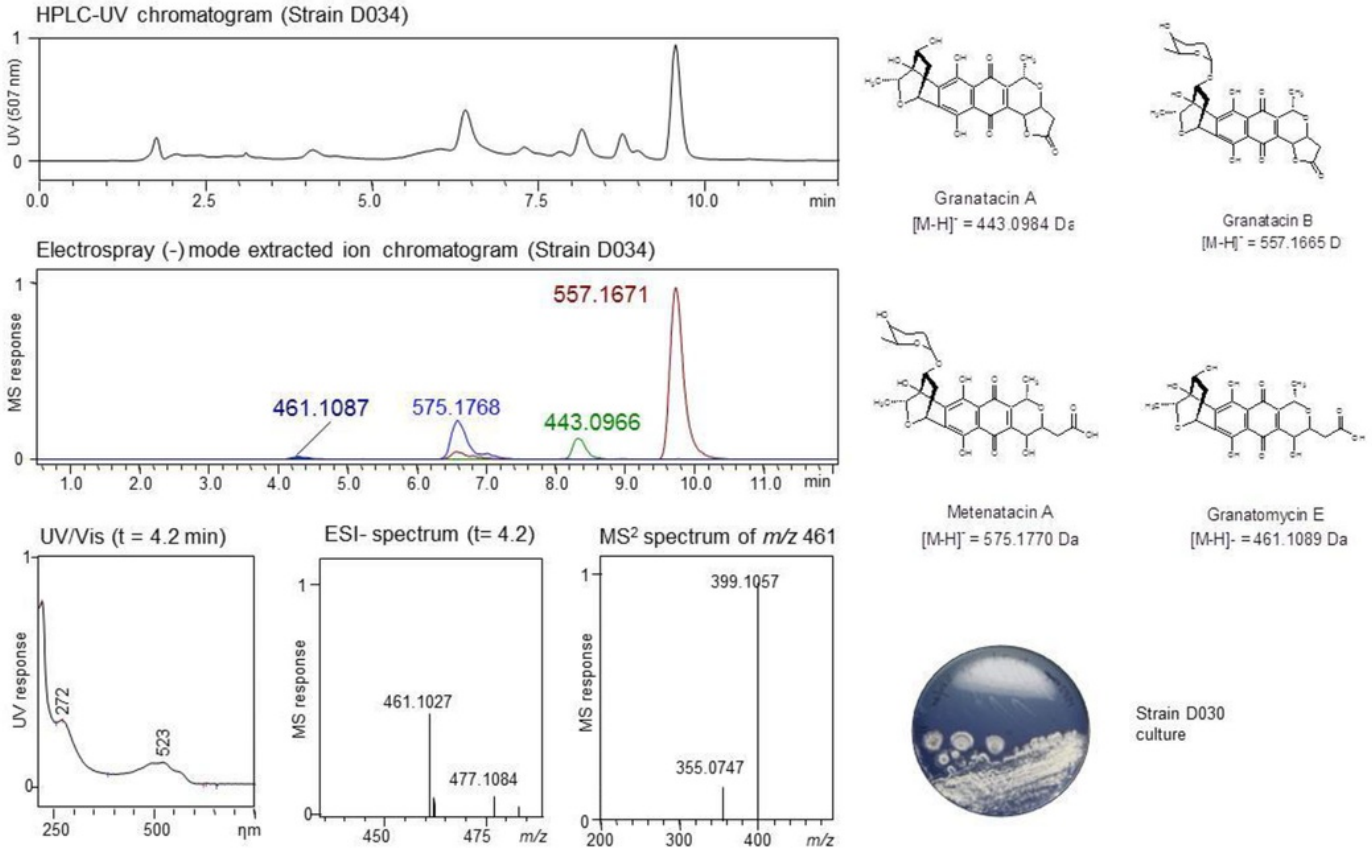

Figure 19. HPLC-UV-HRMS chromatogram for anthroquinoid pigments from marine-derived Streptomyces strain D034. Representative dereplication data (UV/Vis spectra, high resolution MS spectra, and tandem MS spectra using APCI) with fragmentation assignments is shown for the m/z 461 proposed as granatomycin E.

2.5 Additional pigment leads

Miscellaneous blue pigment leads from various sources which were investigated but abandoned or dereplicated are covered in this section. These include the blue-black pigment from *Bacillus subtilis* ATCC strain 6461**,** the investigation of ammosamide A from a marine *Streptomyces* CNR-698, and the dereplication of phycocyanin and prodigiosin from extracts of cyanobacteria and thermophilic microbes, respectively.

2.5.1 Blue-black pigment from Bacillus subtilis ATCC strain 6461

The dark black-brown pigment from the marine-derived *Bacillus sp*. found through the marine pilot pigment study led to the investigation of the bluish-black pigment reported (190) to be produced by *Bacillus subtilis* ATCC strain 6461.

2.5.1.1 Literature Background

Bacillus subtilis is fast growing, rod-shaped, aerobic, Gram-positive bacterium found in soil. *Bacillus subtilis* has become a model Gram-positive among in molecular and cell biology in terms of differentiation, gene regulation, and secondary metabolite production including complete genome sequencing (190) identifying 4,100 protein-coding genes. Nonetheless, the bluish-black pigments excreted by some strains of *Bacillus subtilis* are not understood at the genetic or chemical level. A taxonomic and genetic study of 40 pigment-producing *Bacillus subtilis* strains has provided some clarity with respect to *Bacillus* pigment production (191). Pigments excreted by various *Bacillus* species have been described as brown, black, brownish-black, and sometimes rarely as distinctly blue or

bluish-black. The *B. subtilis* strains that were found to produce a brown pigment or a distinctly bluish black pigment (depending on the growth media) were established as *B. subtilis var. aterrimus*. Partial characterization of the soluble brown, black, or brownish-black pigments has established these compounds as melanin-like polymeric substances (192-194). However, little investigation has been reported of the rare distinctly bluish-black pigment (as opposed to the typical brown-black pigment) excreted by *Bacillus subtilis var. aterrimus*.

2.5.1.2 Investigation of *Bacillus subtilis* ATCC strain 6461 pigment

The reported bluish-black pigment producing strain *Bacillus subtilis var. aterrimus* ATCC 6461 (191) was purchased from the American Type Culture Collection. The strain was initially cultured on a nutrient-rich Todd-Hewitt Yeast (THY) agar which is commonly used for cultivating *Bacillus subtilis*, but no pigment was produced. When the cells were grown on several glycerol-glutamate (G-G agar)(194) plates or in G-G liquid culture at 37 °C, gray pigmented colonies were observed with 24 h that excreted a bluish-black pigment into the agar (Figure 20). Since the agar darkened to a brown-black pigment that covered the plate within 72 h, the window of opportunity to study the blue pigment was brief. The mature liquid and agar plates displayed an intensely blue fluorescence under long wave (λ 365 nm) UV light (Figure 20).

Liquid 250 mL aliquots of 24-h bluish-black culture broth were centrifuged to remove cells and other insoluble material to obtain blue-black supernatants for study. After 24 h of growth, a bluish colored supernatant of the centrifuged culture broth of *B. subtilis* ATCC6461 was analyzed by UV spectrophotometry. The pH of the broth solution was 6.7. Aliquots of the solution were adjusted to pH values of 1, 3, 6, 9, 11, and 11.6 using acetic acid, HCl, or NH_3. The intensity of the blue color increased when the solution was adjusted with HCl to pH 1 and 3. The blue pigmentation in the pH 3 solution

(most relevant for colorant additive use) degraded within a few days. The UV spectra (Figure 20) confirmed that the absorbance giving the blue color (λ_{max} = 595 nm) intensified in acid and became red above pH 9.

Purification methods were explored for separating the water soluble blue pigment. The addition of methanol or ethanol (in excess of 30%, v/v) resulted in precipitation of black solids. Attempts at liquid-liquid extraction into EtOAc, hexane, chloroform, or DCM also formed a black precipitate. A black precipitate also sometimes formed spontaneously within 48 hours in solutions at room temperature. The black precipitates were removed by filtration. The FTIR spectrum of the precipitate (data not shown) was broad and featureless and was similar to FTIR spectra of bacterial melanins partially characterized in the literature (193). The water-insoluble black matter could sometimes not be redissolved completely in water or organic solvents even with heating, acid, or base. Due to serious concern with insoluble precipitate forming in an HPLC-MS system, an HPLC-MS analysis of the pigment solution was not attempted.

B. subtilis is known to produce polymeric black melanin-like compounds that are either water soluble or insoluble depending on molecular weight (192). The unstable blue pigment from *B. subtilis* ATCC6461 may contain a transitory novel blue chromophore that is blue in acidic conditions (as opposed to displaying an acid-red form as do many blue pigments). However, the lead was abandoned due to the poor stability and the tendency to precipitate black insoluble matter which could compromise instrumentation. The blue pigment is a putative unstable lower molecular weight precursor of the known brown or black bacterial melanin polymers consistent with a "bacterial melanin derivative" as the literature suggests (192-194).

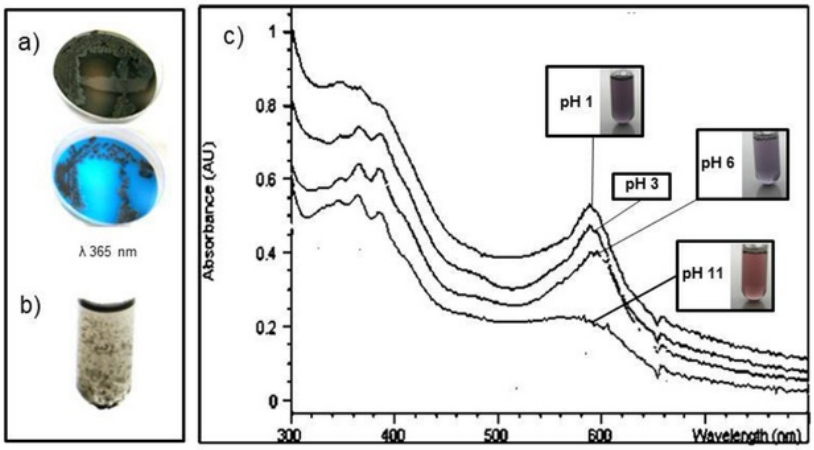

Figure 20. a) Petri cultures of *Bacillus subtilis* ATCC 6461 excreting pigment under normal and longwave ultraviolet light. b) Water soluble blue pigment forming insoluble black precipitate. c) UV/Vis spectra of excreted blue pigment in water at pH 1, 3, 6, and 11 (λ_{max} = 592, pH 3).

2.5.2 Ammosamide A from *Streptomyces* strain CNR-698

Ammosamide A is a novel blue microbial pigment isolated and identified from a marine sediment-derived *Streptomyces* CNR-698 collected near the Bahama Islands by collaborator Dr. William Fenical (University of California San Diego) (196). Ammosamides A and B have shown selective cytotoxic activity (IC_{50} values of 20 nM to 1 uM against several cancer cell lines (196). The two compounds differ at a single atom (ammosamide A contains a sulfur atom while ammosamide B contains an oxygen) and absorb light at opposite ends of the visible spectrum. Because of the novelty of the blue chromophore, the candidacy of the pigment as a color additive was investigated in this work.

Ammosamide A has low water solubility, is slightly soluble in methanol and is highly soluble in dimethylsulfoxide. The acid stability of ammosamide A was examined by preparing 16 μM solutions in methanol (containing 1-2% DMSO) at measured non-aqueous pH values of 1, 3, 5, and 7 (adjusted as follows: pH 1 with HCl, pH 3 with H_3PO_4, and pH 5 with acetic acid). Although standard glass

electrodes show different responses in nonaqueous solvents than in aqueous systems, the pH values measured for methanolic solutions as prepared should be comparable with aqueous solutions within 0.5 pH units (197). The solutions were stored at room temperature and protected from light for one year. As shown in Figure 21, ammosamide A in methanol was stable at pH 7, pH 5 and even at pH 3 for one year and degraded in methanol at pH 1. Ammosamide A also degraded in water at pH 7 within an hour and completely within 24 hrs.

The molar absorptivity of ammosamide A in methanol/DMSO (90:10, v/v) at the blue chromophore absorption maximum of 584 nm was determined to be 5,100 M^{-1} cm^{-1}. For comparison, the molar absorptivity of FD&C Blue 1 is 42,000 M^{-1} cm^{-1} (λ 630 nm). Since the color of ammosamide A is not particularly intense, the concentrations of ammosamide A required for obtaining desirable color intensities are significantly above the 20 nM to 1 μM levels showing cytoxicity toward human cells. Due to aqueous insolubility instability and toxicity, the pigment would be unsuitable for use as a color additive.

2.5.3 Phycocyanobilin from cyanobacteria

Spent (post metabolite extracted) blue cell mass of *Nostoc punctiforme 7179 zyz* (a mesophilic freshwater species) was obtained from collaborator Dr. Jimmy Orjala (UIC College of Pharmacy). The blue pigment was extracted into 100 mM phosphate butter (pH 7.0) using several freeze-thaw cycles, centrifuged, and analyzed by HPLC-PDA-HRMS. A single pigment peak (λ_{max} 641 nm) was observed, and the UV-Vis spectrum matched the presence of a phycocyanobilin chromophore ($C_{33}H_{40}N_4O_6$) bound to protein (Figure 22) which is ubiquitous in cyanobacteria (198). The mass of the phycocyanobilin chromophore was not detected probably due to being bound within the large phycocycanin protein. Since nearly all cyanobacteria use the same phycocyanobilin chromophore in

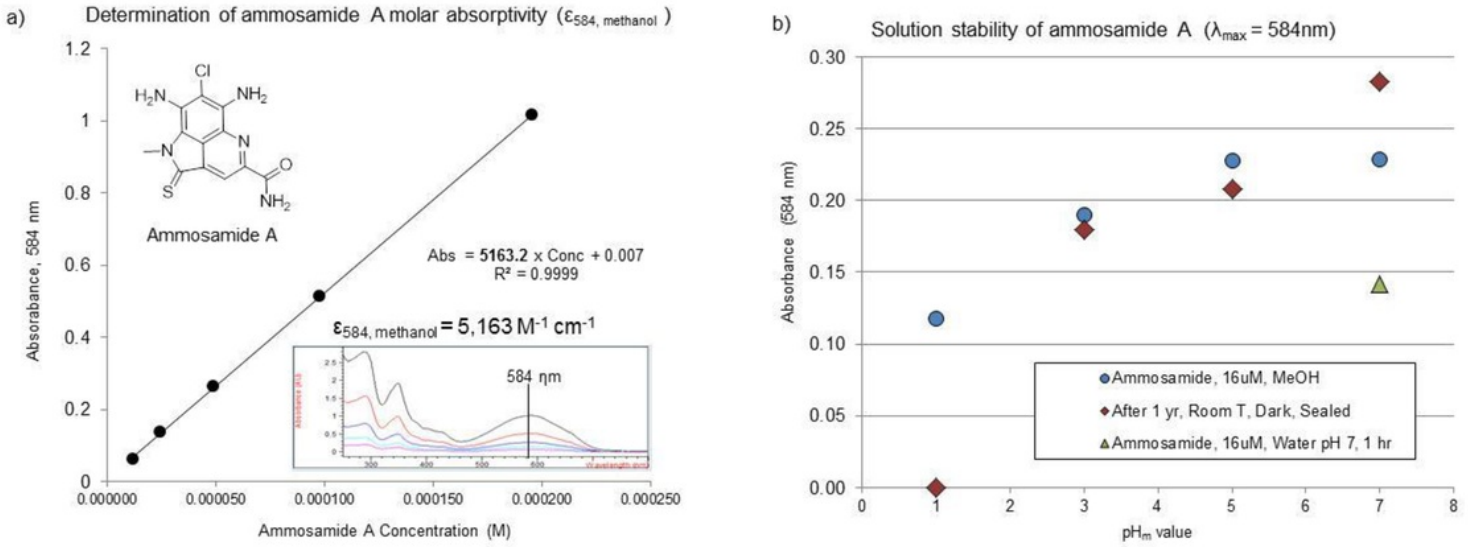

Figure 21. Investigation of ammosamide A as a colorant candidate. a) Determination of the molar extinction coefficient of ammosamide A in methanol. B) Preliminary data on the solution color stability of ammosamide A in methanol and water (%RSD <5).

their photosynthetic accessory phycocyanin pigment proteins, they are not likely to be fruitful for the pursuit of novel pigment chromophores. Nevertheless, cyanobacteria derived from extremophilic environments might contain more stable versions of phycocyanin that could be suitable as natural blue colorants (199).

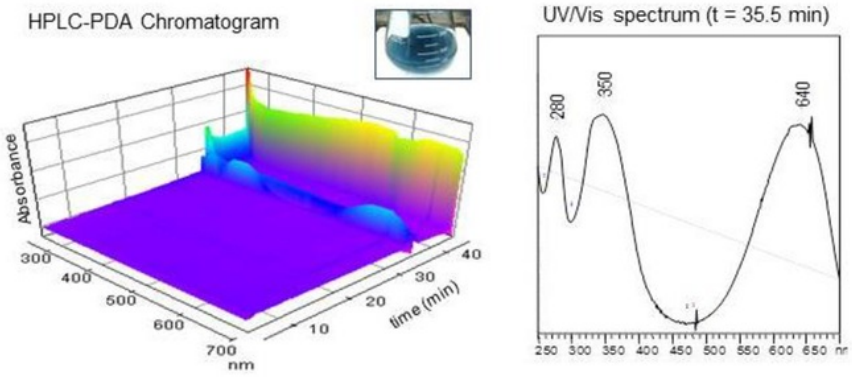

Figure 22. HPLC-UV chromatogram and UV spectrum of blue pigment phycocyanin extracted from *Nostoc punctiforme 7179 zyz* cyanobacterial cells.

2.5.4 Prodigiosin from thermophilic microbial extracts

Pigmented extracts of cultured thermophilic microbes from Yellowstone National Park, WY, were received for analysis from Dr. Joan Combie at Montana Polysaccharides Corp. (Winnsboro, SC) under 2010-NDA-03614. Thirteen of the sixteen extracts were yellow orange or pink and remained so when aliquots were treated with acid (pH < 4) and base (pH > 9) and so were not relevant for this project. Three purple-red colored extracts (1270t, 1341t, and 1386t) were selected for analysis. The extracts were diluted 1:10 in methanol, centrifuged, and analyzed by HPLC-PDA-HRMS^2 using an electrospray source and a Phenomenex 150 x 2 mm 5 µ C_{18} column with a 0.1% formic acid / MeCN gradient from

30:70 MeCN:H_2O to 95% MeCN:H_2O from 2 min to 16 min. All three extracts showed a single pigment peak with UV spectra and accurate mass measurements matching the common red cytotoxic microbial pigment prodigiosin ($C_{20}H_{25}N_3O$) within 5 ppm as shown in Figure 23 (200).

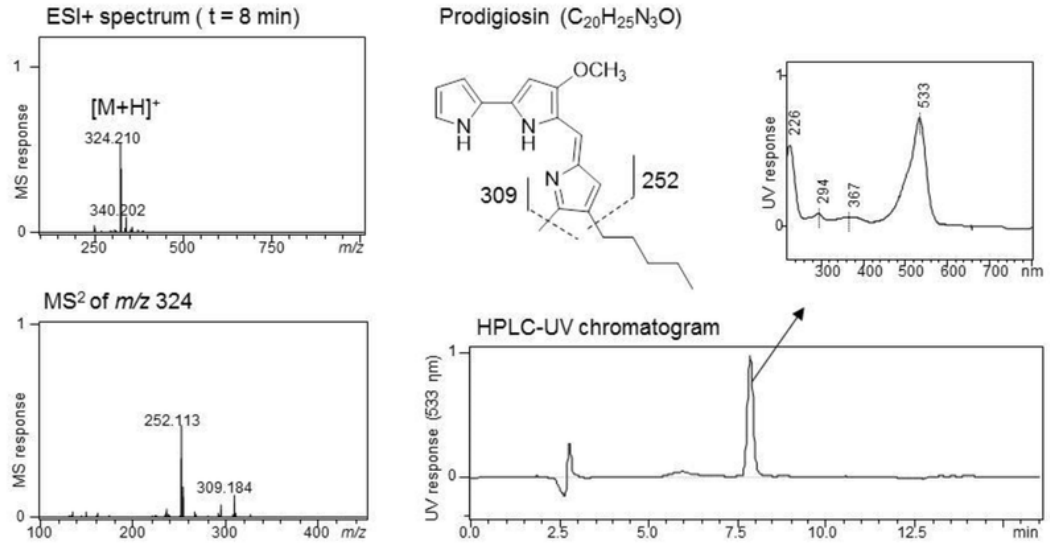

Figure 23. Representative dereplication data from the thermophilic microbial extract 1270t. The HPLC-UV chromatogram, UV and MS spectra are consistent with the microbial pigment prodigiosin.

2.6 Discussion

None of the blue pigments dereplicated in this work were suitable for the project objective due to toxicity and lack of stability. Pigments are often considered as "nuisance compounds" by many natural product chemists. Particularly with plants, there are pigments such as chlorophylls which occur ubiquitously. However, there are many less common or unknown pigments for which potential biological activities as well as dye and colorant applications of potential should be considered. Many of these dereplicated pigments have other potential applications related to their biological activity or as potential colorants in other applications. Some of the potential uses of individual dereplicated pigments were covered in Chapter 1. The pigments ammosamide A, the granaticins, cosmomycins, and violacein

dereplicated here all displayed substantial biological activity. The blue pigmented phycocyanin protein extracted from cyanobacteria does not have suitable aqueous stability for commercial beverage use but has proven to be a satisfactory colorant additive in solid food preparations. Applications of the pigment property of molecules may also include use as natural fabric dyes, tattoo inks, printer inks, pH indicators, chemotaxonomic markers, paper coatings, and a host of other possibilities.

2.6 Conclusion

An overview of general experimental techniques and considerations applicable for the pigment project for the extraction, isolation, and spectroscopic analysis of pigment molecules was provided. A large pilot study investigating culture treatment techniques led to the actinorhodines from *Streptomyces* Strain D030 and an unknown black putative bacterial melanin derivative from a *Bacillus sp.* too unstable to merit further investigation. Investigation of marine-derived microbial cultures, a cyanobacterial extract, and thermophilic microbial extracts led to the dereplication of over 20 previously reported blue pigment molecules. The pigment ammosamide A was investigated as a pigment candidate and found unsuitable due to aqueous insolubility, aqueous instability and cytotoxicity. This experimental approach and some of the dereplication applications reported here were published in a peer-reviewed book chapter (177).

CHAPTER 3: CHARACTERIZATION OF THE PURPLE PIGMENT OF *ZYGOGONIUM SP.* ALGA

(Contains sections previously published as Newsome AG, Murphy BT, van Breemen RB. Isolation and Characterization of Natural Blue Pigments from Underexplored Sources. In *Physical Methods in Food Analysis*. *ACS Symposium Series*, Vol. 1138. Chapter 8, pp 105–125, 2013.)

3.1 INTRODUCTION

The *Zygogonium* (Chlorophyta) genus has been of continued interest due to its remarkable ability to survive in diverse harsh environments. Members of *Zygogonium* are among the few photosynthetic organisms found dwelling in the cold, desiccated, and nutrient depleted conditions of high Alpine mountainous regions and glacial surfaces (201-205) and also thrive in warm acidic bog waters as low as pH 1 in Yellowstone National Park and other areas of North America (202).

The presence of purple pigments in the vacuoles of algae of the *Zygnemataceae* family has been documented for over a century (206-210). Intensely sunlight-exposed colonies of alga within this family have been observed to contain a dark purple pigment which has been suggested to serve a UV protective role. Purple *Zygnemataceae* pigments were first described and proposed to be "algal anthocyanins" in 1895 by Lagerheim (203). The purple pigment which accumulates in the vacuoles of sun exposed layers of *Zygogonium ericetorum* algae was studied and concluded to be an "iron tannin" complex (201). Gallotannins, which are common in plants, have been reported from related *Spirogyra* sp. algae (211,212).

None of the *Zygogonium* sp. vacuolar purple pigments have been chemical characterized until now. In this work, samples of *Zygogonium* sp. algae were collected from acid bogs in Yellowstone National Park, WY. The water-soluble intracellular purple pigment was isolated and characterized by NMR, mass, IR, UV, EPR, X-ray, and ^{57}Fe Mössbauer spectroscopy. Through extensive analysis the purple pigment was established as a macromolecular galloferric oligosaccharide complex containing Fe^{2+} and Fe^{3+} with purple chromophore centers ferric iron chelated to two gallic acid (**1**) moieties in a *bis* (L_2Fe^{3+}) configuration (**2**) (Figure 24). Purple pigments extracted and analyzed from *Zygogonium* sp. mats across multiple sites were found to consist of similar constituents.

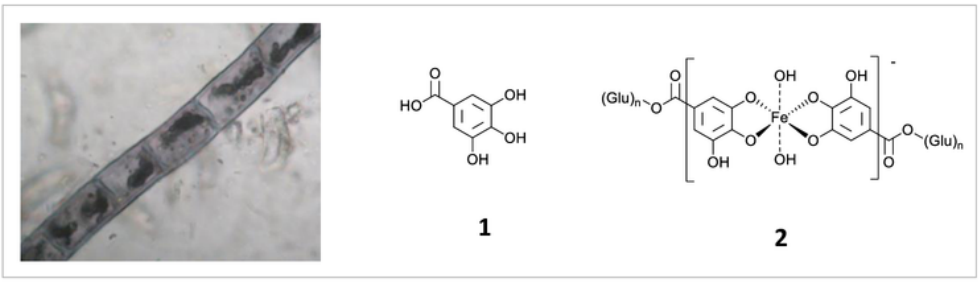

Figure 24. A light microscope image of a field collected purple pigmented *Zygogonium* sp. algal filament and the structure of gallic acid (**1**) and the ferric digallate (**2**) purple pigment chromophore characterized in this work.

3.2 Materials and Methods

3.2.1 *Zygogonium sp.* sample collection. Environmental samples of the *Zygogonium ericetorum* alga were collected from acidic bogs in Yellowstone National Park in September 2010 from Succession Mat and shipped overnight at ambient temperature. Still fresh filaments were examined via light microscopy. The biomass was sent to UIC through a material transfer agreement (Appendix D).

3.2.2 Pigment extraction and isolation. Solid purple algal biomass was separated from natural bog water by vacuum filtration. The bog water was saved, and the biomass was rinsed 2 x 30 mL with water. The biomass was resuspended in 30 mL water and subjected to five freeze-thaw cycles which released the water soluble purple pigment from the cells. Solid cell mass was removed by vacuum filtration and dark purple water was centrifuged at 4500 x *g* for 15 min. The purple water was filtered through a 0.2 μm Nylon filter disc and evaporated. The pigment was isolated by methanol precipitation followed by passage over Sephadex G_{25} size-exclusion gel as follows. The crude extract was dissolved in 50 mL of water and diluted to 500 mL with methanol and stored at 4 °C for 4 hrs. The purple precipitate was collected as a pellet by centrifugation. The supernatant remained faintly purple in color. The pellet was rinsed with water and dried for a yield of 346 mg. The pellet was redissolved in 10 mL of water, filtered

through a 0.2 μm Nylon filter disc, and passed over a Sephadex G_{25} gel with water as the mobile phase. The purple pigment band showed no retention and was collected and dried under N_2 gas giving 75 mg of purple powder.

3.2.3 Size exclusion chromatography (HP-SEC). Size exclusion chromatography was performed using a Phenomenex BioSep s2000 300 mm x 7.8 mm column with 50 mM ammonium acetate as the mobile phase and a flow rate of 0.5 mL / min.

3.2.4 Carbohydrate composition and linkage analysis. The molecular weight, glycosyl residue, and glycosyl linkage analysis of the polysaccharide component of the pigment was performed by the Complex Carbohydrate Research Center (CCRC) (Appendices A-C). Molecular weight determination of the purified pigment was performed by the CCRC using dextran MW standards.

3.2.5 General Experimental Procedures. UV spectra were recorded using either an HP Diode-Array 8452A spectrophotometer or by flow injection through a Shimadzu SPD-M20A photodiodearray detector. FTIR spectra were recorded using Shimadzu IRPrestige-21 spectrophotometer with an ATR crystal. NMR spectra were recorded on Bruker Avance NMR operating at 400 MHz for ^{1}H and 125 MHz for ^{13}C. High-resolution mass spectral data for characterization purposes such as for $^{57}Fe(TFA)$ and $^{57}Fe^{3+}$ model compounds were obtained with a Shimadzu IT-TOF mass spectrometer using electrospray ionization. Analytical and Preparative HPLC was performed on a Shimadzu HPLC system with an SPD-20A UV/Vis detector. Chromatography solvents were HPLC grade or better and were purchased from Thermo Fisher (Waltham, MA). Quantitative determinations were performed in

duplicate or triplicate. General reagents and standards were purchased from Fisher Scientific (Hampton, NH) or Sigma-Aldrich (St. Louis, MO) unless otherwise specified.

3.2.6 Scanning electron microscopy with X-ray elemental microanalysis. The SEM images were acquired using a Hitachi S-3000N SEM A minute amount of purified sample was attached to adhesive $C_{(s)}$ stub with an aluminum backing. The energy dispersive x-ray spectroscopy spectrum for elemental analysis was collected using an accelerating voltage of 15 keV, a spectral window of 20 keV, and an acquisition time of 100 s.

3.2.7 Electron Paramagnetic Resonance. The EPR spectrum of the pigment was collected on a Bruker X-band EMXPlus EPR spectrometer. The 0.1 mg mL^{-1} solution of the pigment in DMSO was frozen and read in liquid N_2 with a 90 s scan time.

3.2.8 MALDI-TOF Mass Spectrometry. A 1 µL aliquot of a 1 mg / mL aqueous solution of the purified pigment was mixed with 1 µL of 10 mg / mL trihydroxyacetophenone matrix (THAP) matrix in 50:50 ACN:water (v/v). Spectra were acquired using an Applied Biosystems Voyager-DE Pro MALDI-TOF MS in negative reflectron mode.

3.2.9 Determination of Iron Content. The iron in the sample was quantitated in duplicate using the colorimetric 1,10-phenanthroline method (213) with a calibration curve based upon the primary standard ferrous ammonium sulfate hexahydrate (Purity 99.999%, Alfa Aesar). Samples were analyzed after 72 hrs to allow for quantitative formation of the ferrous 1,10-phenanthroline complex before absorbance

measurements. Standards showed no loss of absorbance and were thus established as stable during the time period.

3.2.10 LC/MS Quantitation of Gallic acid. The gallic acid content of the pigment was determined using a modified acidic methanolysis procedure in which the gallic acid was quantitatively hydrolyzed and convert to methyl gallate according to the method covered in detail Chapter 4. The hydrosylate was then analyzed using a Shimazu 8040 triple quadrupole UPLC-MS system with MRM mode. 3-*O*-methyl-methyl gallate was used as an internal standard to correct for degradation during methanolysis.

3.2.11 Preparation of ^{57}Fe Gallate complexes. To first generate a source of labile $^{57}Fe^{3+}$ ions, a ferric trifluoroacetate salt was prepared from 44 mg of 95% enriched ^{57}Fe metal by heating the metal in concentrated TFA at 90 °C in a sealed glass tube for 100 hrs. Excess TFA was removed by co-evaporation with water, and the product was washed with hexane and filtered. To promote a complete ferric oxidation state, air was gently bubbled through the solution for 4 hrs. The solution was evaporated under N_2 gas to yield 220 mg of a rust-orange solid. The product was characterized by mass spectrometry to confirm the ferric oxidation state of the product. The total iron content was 7.6 ± 0.3 % wt/wt as determined in triplicate by 1,10-phenanthroline method.

Preparation of $^{57}Fe(GA)^{+}$: To a stirred solution containing 30 μmoles of gallic acid in 5 mL H_20 (pH = 3.4) there was added 14.5 mg of the $^{57}Fe(TFA)_3$ product at once. The solution became dark blue in color (pH = 2.4) and was frozen at -78 °C within 30 s and lyophilized to yield 15.0 mg of dark blue powder.

Preparation of $^{57}Fe(GA)_2^-$: A solution of 54 μmoles of gallic acid in 5 mL H_20 was adjusted to pH 6.5 with 1M NaOH. While keeping the pH above 4.5 using 1M NaOH, A total of 14.5 mg of the $^{57}Fe(TFA)_3$ product was added dropwise. The final dark purple colored solution (pH = 7.0) was lyophilized to yield 22.6 mg of dark purple powder.

Preparation of $^{57}Fe(GA)_3^{6-}$: A total of 9.0 mg of the $^{57}Fe(TFA)_3$ product was added dropwise to a well-stirred solution of 50 μmoles of gallic acid in 5 mL H_20 while keeping the pH between 4.5 and 6.5 using The pH was adjusted quickly to 10.1 with addition of 1M NaOH upon which it became a dark maroon color. The solution was frozen at -78 °C and lyophilized to yield 23.2 mg of maroon colored powder.

3.2.12 Mössbauer and Nuclear Resonance Vibrational Spectroscopy. Samples were analyzed in a 2 mm diameter copper disc with a 25 μm deep well covered with aluminized mylar filmed sealed with APIEZON N grease. The mounted sample was covered with a $Be_{(s)}$ cap and outfitted with liquid helium cooled cryostat stabilized at 18.5 K. Five scans for each sample from -20 to 100 meV. Mössbauer Spectra were obtained at 298 K using a ^{57}Co source with the assistance of Dr. Ercan Alp at Argonne National Laboratories.

3.2.13 HPLC-PDA-HRMS^2 analysis. The HPLC-PDA-HRMS^2 analysis of purified *Zygogonium* sp. pigment after removal of iron by EDTA was performed using a Shimadzu Prominence XR HPLC system equipped with an SPD-M20A photodiodearray detector interfaced with a Shimadzu IT-TOF mass spectrometer. The UV spectrum was scanned from 200- 800 nm with a 4 nm bandwidth and no reference correction. The HPLC gradient method was from 5% to 20% MeCN with 0.1% formic acid from 6 min to 20 min with water containing 0.1% formic acid as the aqueous phase using a Phenomenex

C_{18} 150 x 2.1 mm 5 µm column and a flow rate of 0.2 mL/min. Mass spectra and tandem mass spectra were acquired using negative ion electrospray ionization with polarity switching. The MS^2 data were collected in data-dependent MS^2 mode using two scan events (loop time 2 sec): Event 1, MS scan range of *m/z* 120-800 and *m/z* 100-800 for automatic MS^2; Event 2, MS scan range of *m/z* 800-1500 and *m/z* 500-1500 for automatic MS^2. The HRMS analysis parameters were as follows: Detector voltage of -3.5 kV, CDL and block temperature 200 °C, N_2 nebulizing gas, N_2 drying gas at 1.5 L/min. Argon was used as the collision cell gas at a CID collision energy of 90% and an automatic MS^2 ion selection trigger of 70% BPC.

3.3 Results and Discussion

Sections 3.3.1 through 3.3.3 address the environmental sourcing, extraction and isolation, and purification of the *Zygogonium* sp. algae purple pigment. Sections 3.3.4 presents the characterizations on the isolated pigment from Succession mat with a summary in section 3.3.4.9. Section 3.3.3 discusses data from pigments from multiple *Zygogonium* sp. collection sites and the possible ecological role of the pigment.

3.3.1 Environmental sampling

Purple and green pigmented *Zygogonium* sp. samples involved in this study were collected from multiple spring locations (Succession mat, Nymph creek, Dragon spring, Beowolf spring, and Gap runoff) within Yellowstone National Park, WY. The majority of the characterization work was performed on the sample collected from Succession mat. Characterizations where samples collected from other sites were involved are noted. Microscopic examination of fresh filaments of the *Zygogonium*

sp. alga from Succession mat upon arrival showed purple colored pigment within the vacuoles of the cells. The genus *Zygogonium* sp. was concluded based upon morphological characteristics and habitat. Of the only four species of *Zygogonium* known from North America (203-205), the species *Z. ericetorum* was most consistent with the morphological and environmental characteristics of this specimen. The identification at the species level is tentative.

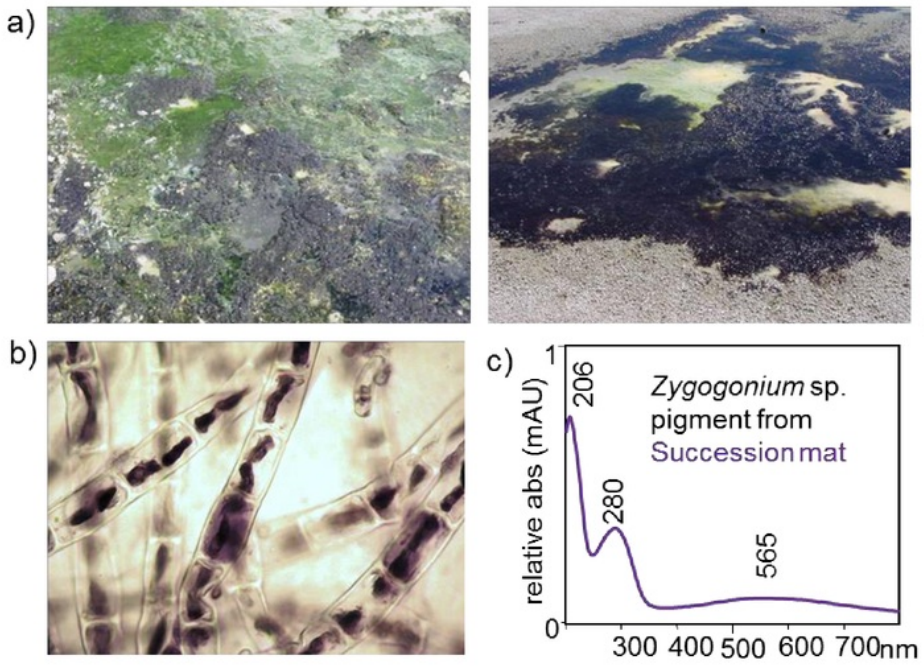

Figure 25. a) Photographs of environmental sample collection sites (Yellowstone National Park, WY) courtesy of Dr. Gill Geesey, MSU. b) Light microscopy of *Zygogonium* sp. filaments after one freeze-thaw cycle. c) UV/Vis spectrum (H_2O) of the purified *Zygogonium* sp. pigment (Succession mat).

3.3.2 Investigation of the crude pigment extract

The *Zygogonium* sp. purple pigment was previously reported as a likely iron gallate complex (201). The general properties of the extracted and purified macromolecular purple pigment were in

agreement with the hypothesized the pigment as "a sort of iron-tannin complex" (201) in terms of the UV/Vis absorbance and initial chemical wet testing. An HPLC-UV analysis of the environmental spring water (pH 2.8) of the Succession mat sample showed the presence showed gallic acid (**1**) as the major peak by comparison with a neat solution of gallic acid.

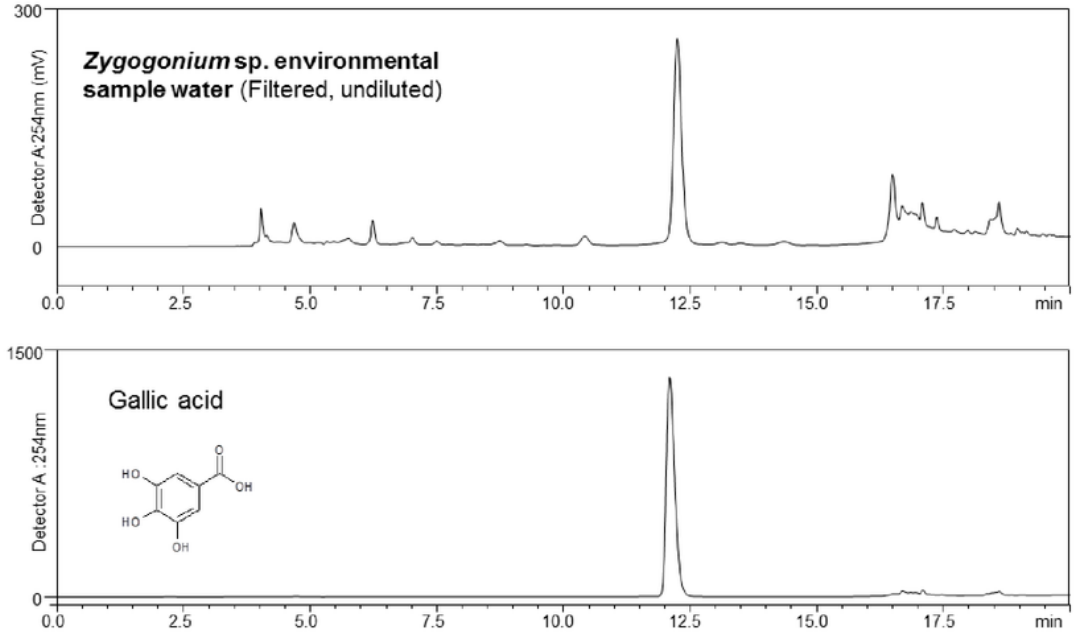

Figure 26: HPLC-UV chromatograms of the filtered environmental spring water (*Zygogonium* sp. (Succession mat sample) compared to neat gallic acid.

The pigment was extracted into the spring water readily with freeze-thaw cycles and was dried to obtain a crude pigment extract. The extract was first investigated for consistency with the "iron-tannin" hypothesis using wet chemistry tests. The purple pigment was stable to heat and survived boiling in water for one hour without any significant loss of intensity. The pigment was however decolorized at low pH and turned orange in alkaline pH with formation of an orange precipitate. The purple pigment was insoluble in ethanol, ether, chloroform, ethyl acetate, and hexane, and soluble only in water and

dimethyl sulfoxide. Solutions of purple pigment were completely decolorized by EDTA and $NaBH_4$ with gentle heating. The addition of excess sodium borohydride also resulted in precipitation of black ferromagnetic particles of $Fe_{(s)}$ which strongly suggested a visible purple chromophore directly involving iron.

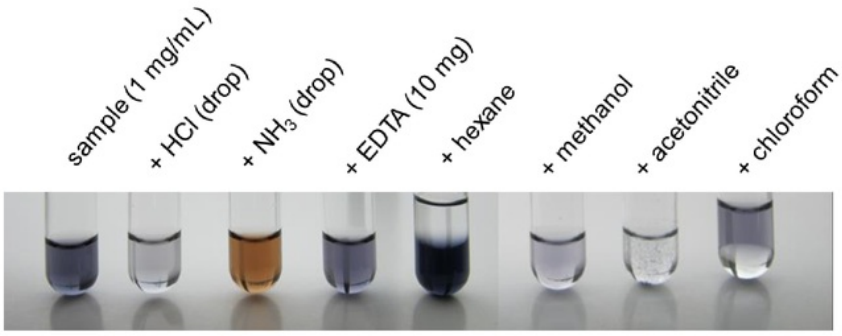

Figure 27. Photographs of some initial wet chemical and solvent tests performed on the *Zygogonium* sp. crude aqueous pigment extract (Succession mat).

3.3.3 Pigment purification

The formation of a precipitate in methanol by the pigment was employed for purification. Further investigation of the pigment precipitate using a variety of purification materials (C_{18}, HILIC, and size-exclusion gels) revealed the purple pigment to be a high molecular weight species. The purple pigment eluted with the void volume using the size-exclusion material Sephadex G_{25} (exclusion limit = 5000 Da) with pure water as the mobile phase. The purple pigment similarly extracted and precipitated from the Nymph creek *Zygogonium* sp. samples was similarly purified using Sephadex G_{25}. The purple pigment from the Nymph creek site fell within the fractionation range of the Sephadex G_{25} (1000 to 5000 Da) and fractions were collected as shown in Figure 29. The HPLC-SEC-UV_{560} analysis of the purified Succession mat and Nymph creek pigments is shown in Figure 30.

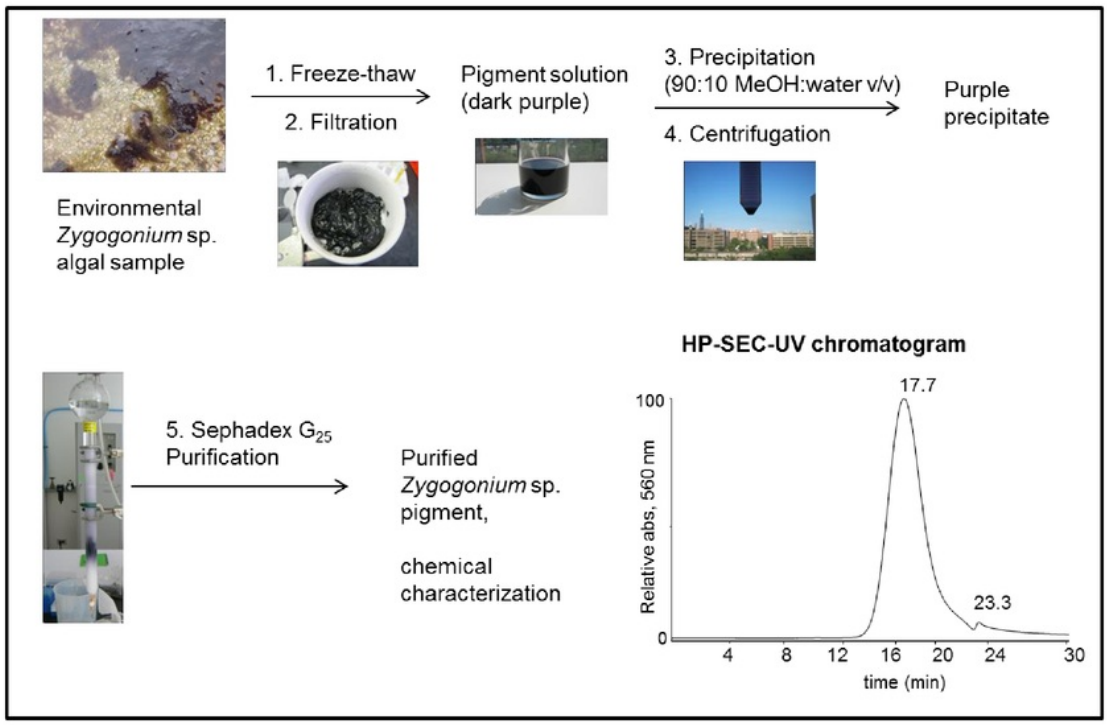

Figure 28. Schematic for the purification process used for the Zygogonium sp. purple pigment (Succession mat).

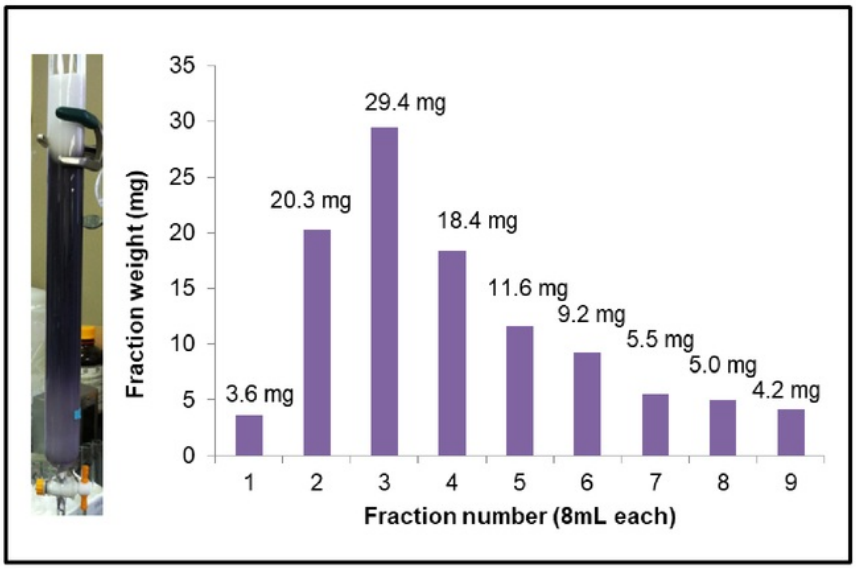

Figure 29. Sephadex G_{25} fractionation of *Zygogonium* sp. pigment extracted from the Nymph creek site environmental samples.

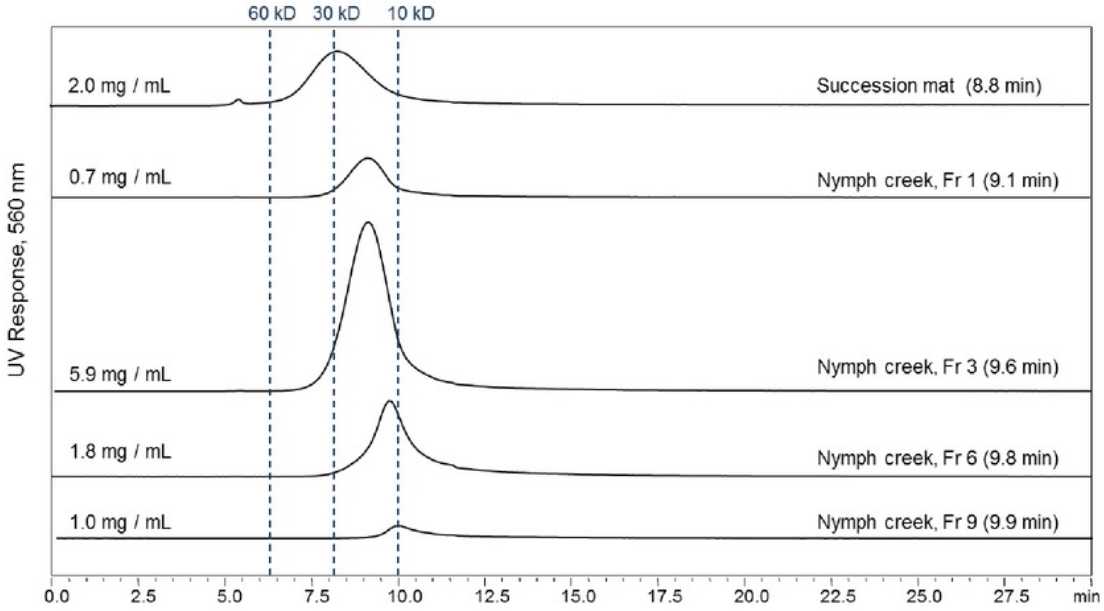

Figure 30. HPSEC-UV chromatograms of Sephadex G_{25} purified *Zygogonium* sp. pigment from Succession mat and Nymph creek. The injection concentration for each sample is shown. The molecular weight markers are based on the high and low M.W. range established for the purified pigment from Succession mat in Section 3.3.4.2.

3.3.4 Characterization of the purified Succession mat site pigment

The purified intact Succession mat purple pigment was analyzed using a variety of analytical and spectroscopic techniques: HPLC-UV-HRMS, ^{1}H and ^{13}C NMR, FT-IR, SEM with X-ray microanalysis, UV/Vis spectroscopy with time-course kinetics, MALDI-TOF MS, electron paramagnetic resonance (EPR) spectroscopy, Mössbauer spectroscopy, and Nuclear resonance vibrational spectroscopy (NRVS). These analyses established that the Succession mat purple pigment consisted of a majority of glucose chains by weight with purple chromophores arising from ferric iron atoms coordinated to gallic acid moieties in a 1:2 ratio ("bis" ferric gallate, $Fe^{3+}(galloyl)_2$. The results of these individual analyses are discussed in sections 3.2.4.1 through 3.3.4.9.

3.3.4.1 MS, NMR, and FT-IR analysis

Various HPLC-PDA-HRMS analyses of the purified Succession mat pigment showed the elution of a single broad purple pigment peak with no clear corresponding MS signals using either an electrospray or an APCI source. This was indicative of good purity and a lack of ionization of the intact high molecular weight Succession mat pigment. The pigment showed no retention with C_{18} columns (retention time $= V_o$) and eluted as a single broad peak using HILIC columns.

A 400 MHz ^{1}H and ^{13}C NMR analysis of the purified pigment (in D_2O) showed broadened signals consistent with hexose sugars such as glucose (Figure 31). The presence of ferromagnetic species in a sample is known to interfere with NMR signals. The FT-IR spectrum of the pigment was also characteristic of a substance which was primarily carbohydrate in composition (Figure 32). The positive mode MALDI-TOF spectrum (Figure 33) displayed an *m/z* series separated by 162 D characteristic of a hexose polysaccharide. Since MALDI-MS of even very large polysaccharides

commonly produce MALDI ions no larger than a few thousand *m/z* (214), the spectrum provides no indication of the MW of the intact pigment.

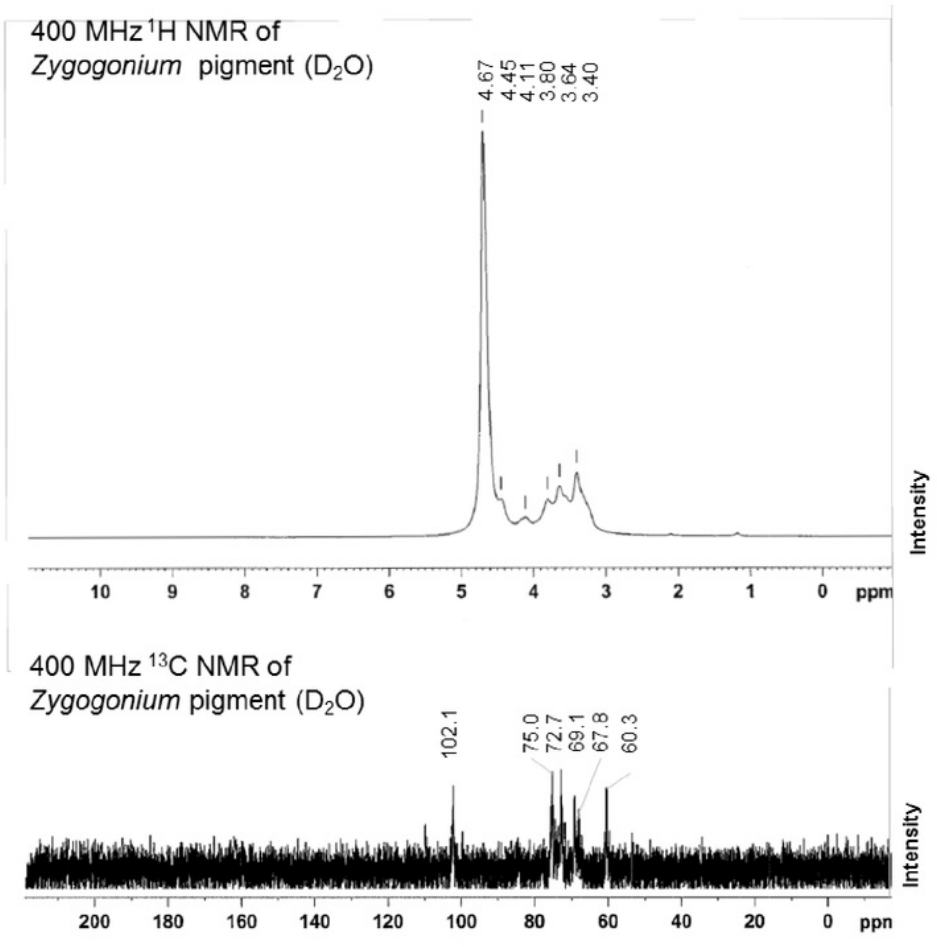

Figure 31. 400 MHz ^{1}H and ^{13}C NMR spectra of the *Zygogonium sp.* pigment from Succession mat after purification by size-exclusion chromatography.

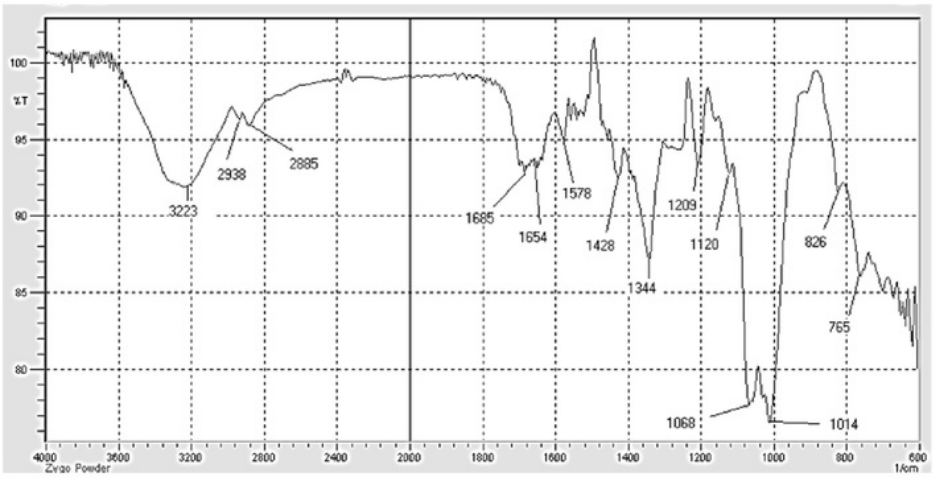

Figure 32. FTIR spectrum of *Zygogonium sp*. pigment from Succession mat after purification by size-exclusion chromatography.

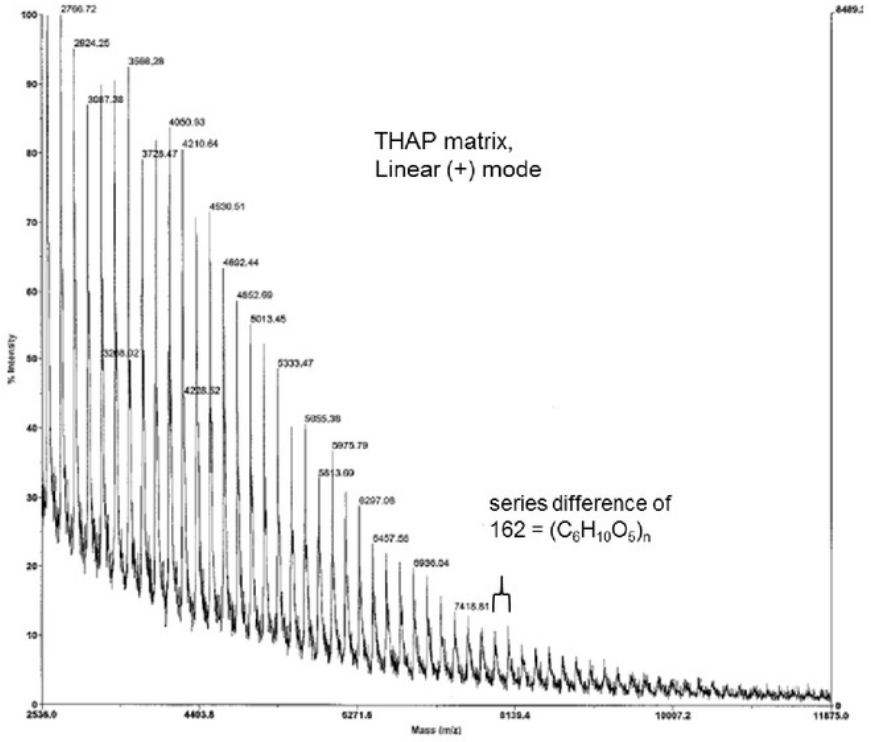

Figure 33: Linear positive ion mode MALDI-TOF mass spectrum of the purified *Zygogonium* sp. pigment (Succession mat).

3.3.4.2 Carbohydrate and molecular weight characterization results

The purified Succession mat pigment was sent to carbohydrate specialists (Complex Carbohydrate Research Center) for molecular weight determination and analysis the glycosyl residue, glycosyl composition. The HP-SEC chromatogram showed a single broad peak and the average molecular weight of the pigment was determined to be 30 kDa with a broad distribution from 10 to 60 kDa and an estimated carbohydrate content of 85% ± 10% wt/wt. The glycosyl composition and linkage analysis showed a highly and variably branched polymer composed of D-glucose (99.7 %) with major glucopyranosyl linkages of 1,6-Glc (22.6 %), 1,3-Glc (27.7 %), 1,4,6-Glc (10.0 %) and 1,4-Glc (9.0%) and a high proportion of terminal glucose (24.6 %).

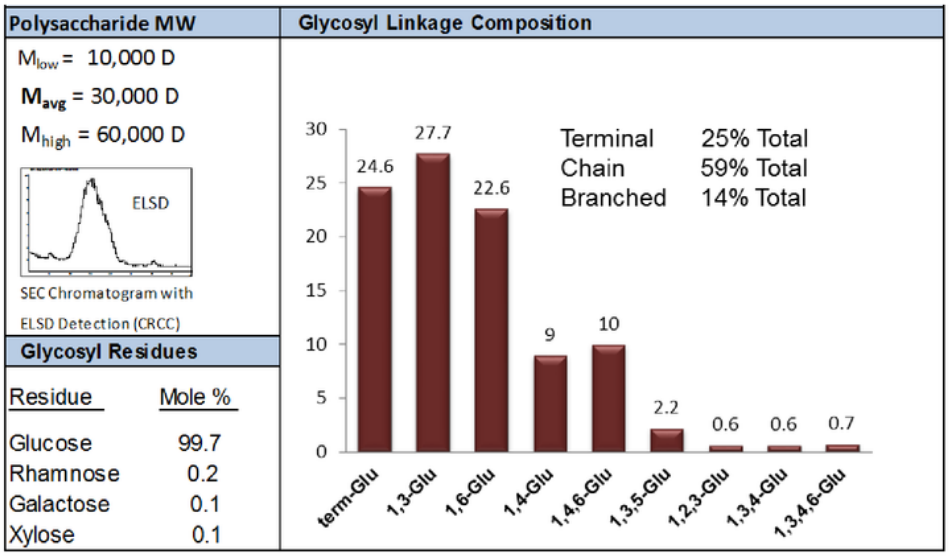

Figure 34. A summary of the carbohydrate analysis data provided by the CCRC on the purified purple pigment from Succession mat.

3.3.4.3 Determination of free and bound gallic acid

Gallic acid tends to degrade during both acidic and alkaline hydrolysis and the accurate determination the bound gallic acid content was further complicated by the presence of iron and excess polysaccharide content of the pigment. The accurate determination of bound gallic acid in the pigment was achieved using an acidic methanolysis followed by UHPLC-MS/MS quantitation using the method described in Chapter 4. The bound gallic acid content of the *Zygogonium* sp. pigment (Succession mat) was determined to be 109.7 ± 7.4 µg/mg with <4 µg/mg of free gallic acid.

3.3.4.4 SEM and electron paramagnetic resonance analysis

A scanning electron microscopy (SEM) with x-ray microanalysis performed on the pigment precipitate before and after Sephadex G_{25} purification (Figure 35) confirmed the removal of trace elemental impurities (Ca, K, S) and the presence of iron in the purified pigment (K transition lines of 6.4 and 7.0 keV) (Figure 35).

The electron paramagnetic resonance (EPR) spectra obtained for the purple pigment showed a dominant signal corresponding to a g-value of 4.3 common for biological high spin ($S = 5/2$, d^5) ferric iron in sites of low symmetry (215). A weak inflection corresponding to a g-value of 2.03 indicated the possible presence of ferrous iron. The raw spectra are shown in Figure 36.

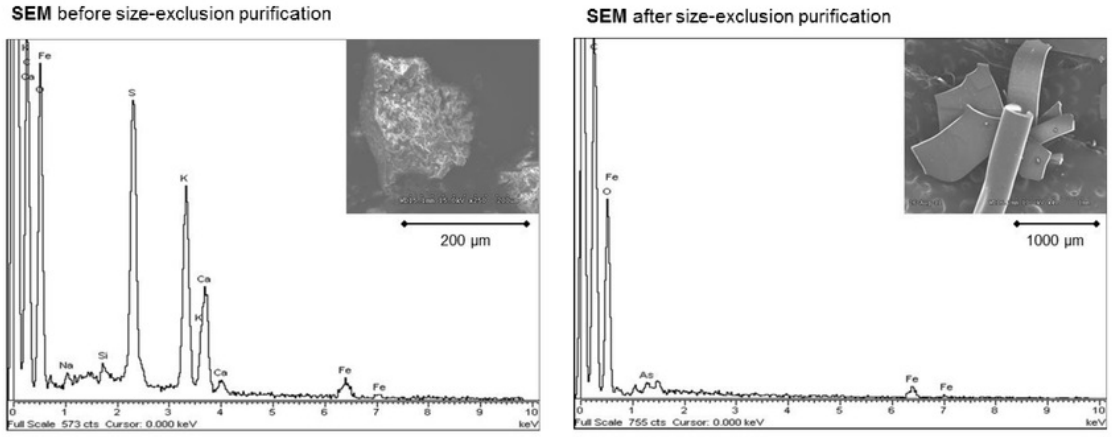

Figure 35. Scanning electron microscopy with elemental x-ray microanalysis of the *Zygogonium sp.* pigment (Succession mat) before and after purification by size-exclusion chromatography.

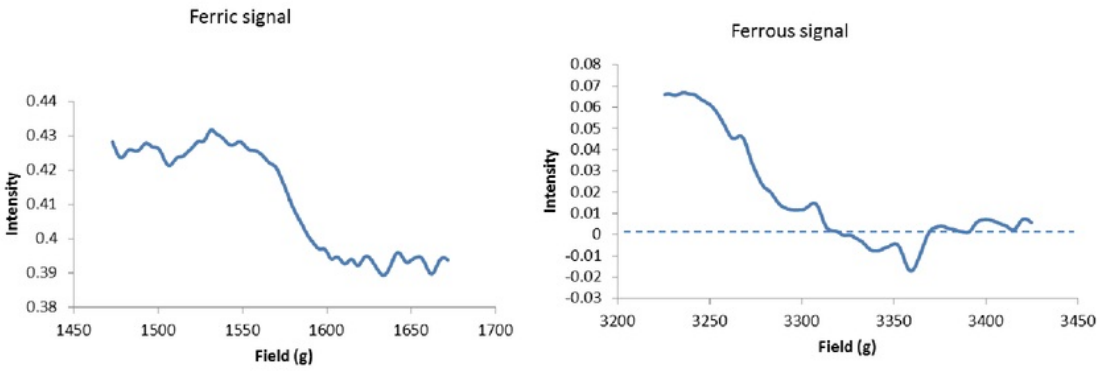

Figure 36: The EPR spectral signals of purified *Zygogonium* sp. pigment from Succession mat.

3.3.4.5 Determination of total iron by 1,10-phenanthroline

The 1,10-phenanthroline reagent is commonly used for the colorimetric determination of total (ferric and ferrous) iron by the formation of an orange colored complex, ferrous (1,10-phenanthroline)$_3$

(213). The conversion of the iron in the *Zygogonium sp.* purple pigment to the orange colored complex was slow. Figure 37 shows the monitoring the UV/Vis spectrum of a solution of the purified pigment for 24 hrs after addition of the iron chelating reagent 1,10-phenanthroline. The gradual disappearance of purple pigment chromophore (λ_{max} = 564 nm, monitored at λ 650nm) proportional to the appearance of the orange 1,10-phenanthroline complex (λ_{max} = 508 nm) confirmed the purple pigmentation of the natural product is directly attributed to an iron chromophore.

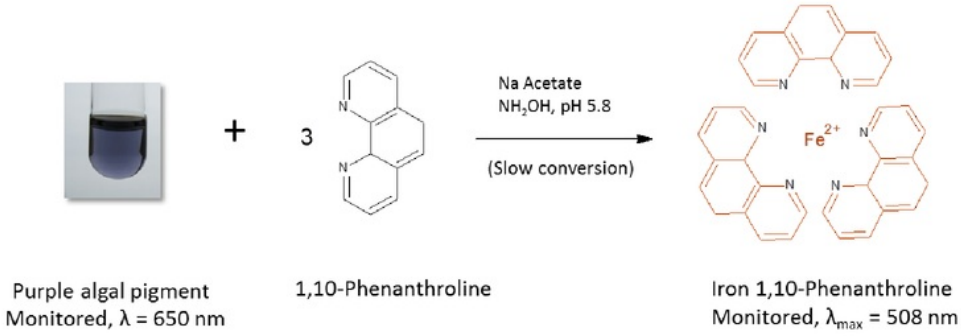

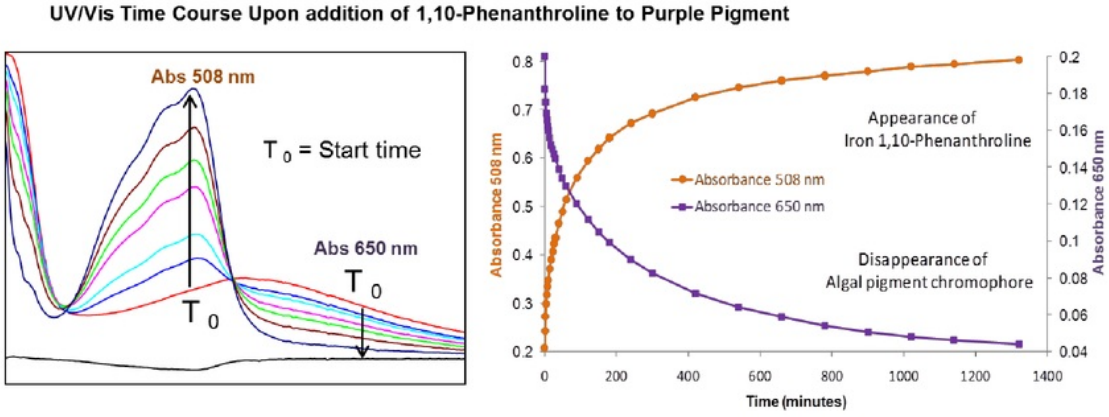

Figure 37: The colorimetric 1,10-phenanthroline reaction and the subsequent UV/Vis time course monitoring of the of the purple pigment showing the slow disappearance (over 24 hrs) of the natural purple pigment as ferrous 1,10-phenanthroline complex is formed.

The total iron content of the pigment was determined using the 1,10-phenanthroline method in triplicate to be 37.2 ± 4.9 µg/mg. The reaction was allowed to proceed for 48 hrs to ensure the full

conversion of the iron in the pigment to the colorimetric complex. The stability of the ferrous 1,10-phenanthroline complex over 48 hrs was verified by measurement of the standard curve solutions fresh and after 48 hours (Figure 38).

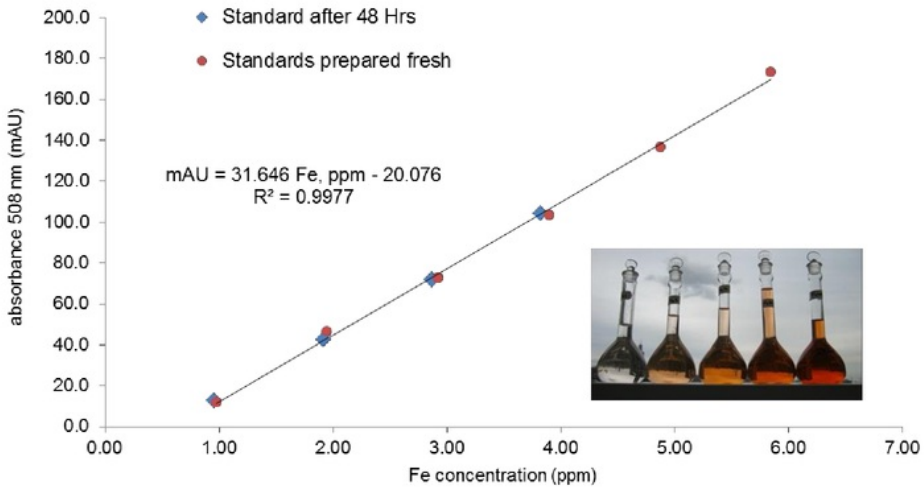

Figure 38: Standard curve for the determination of total iron by 1,10-phenanthroline used for the determination of iron in the *Zygogonium* sp. purple pigment (Succession mat).

3.3.5 Iron-catechol bonding chemistry

The catechol function, which is present in all tannins, is known to chelate ferric iron in 1:1, 1:2, and 1:3 ratios dependent upon pH. Ferric gallate complexes have a large stability constants (log K_1 = 11.2, log K_2 = 8.5, log K_3 = 4.4, for one, two and three gallate groups respectively)(216) and form spontaneously in aqueous solution (217-220). Initially at a pH below 3.5, ferric ions in form a blue 1:1 complex $[Fe^{3+}(gallate)]^+$ which tends to spontaneously reduce to $[Fe^{2+}(gallate)]^+$ at lower pH. From approximately pH 3.5 to 8, the catechol groups chelates ferric ion in a 2:1 ratio giving a purple colored

charge-transfer complex $[Fe^{3+}(gallate)_2]^{+}$. Above pH 8 and above, ferric iron chelates catecholate functions in a 1:3 ratio to form a maroon complex $[Fe^{3+}(gallate)_3]^{6-}$. The chemistry of iron gallate complexes was studied through preparation of the complexes using a pure system of ferric iron and gallic acid (**1**) as shown in Figure 39.

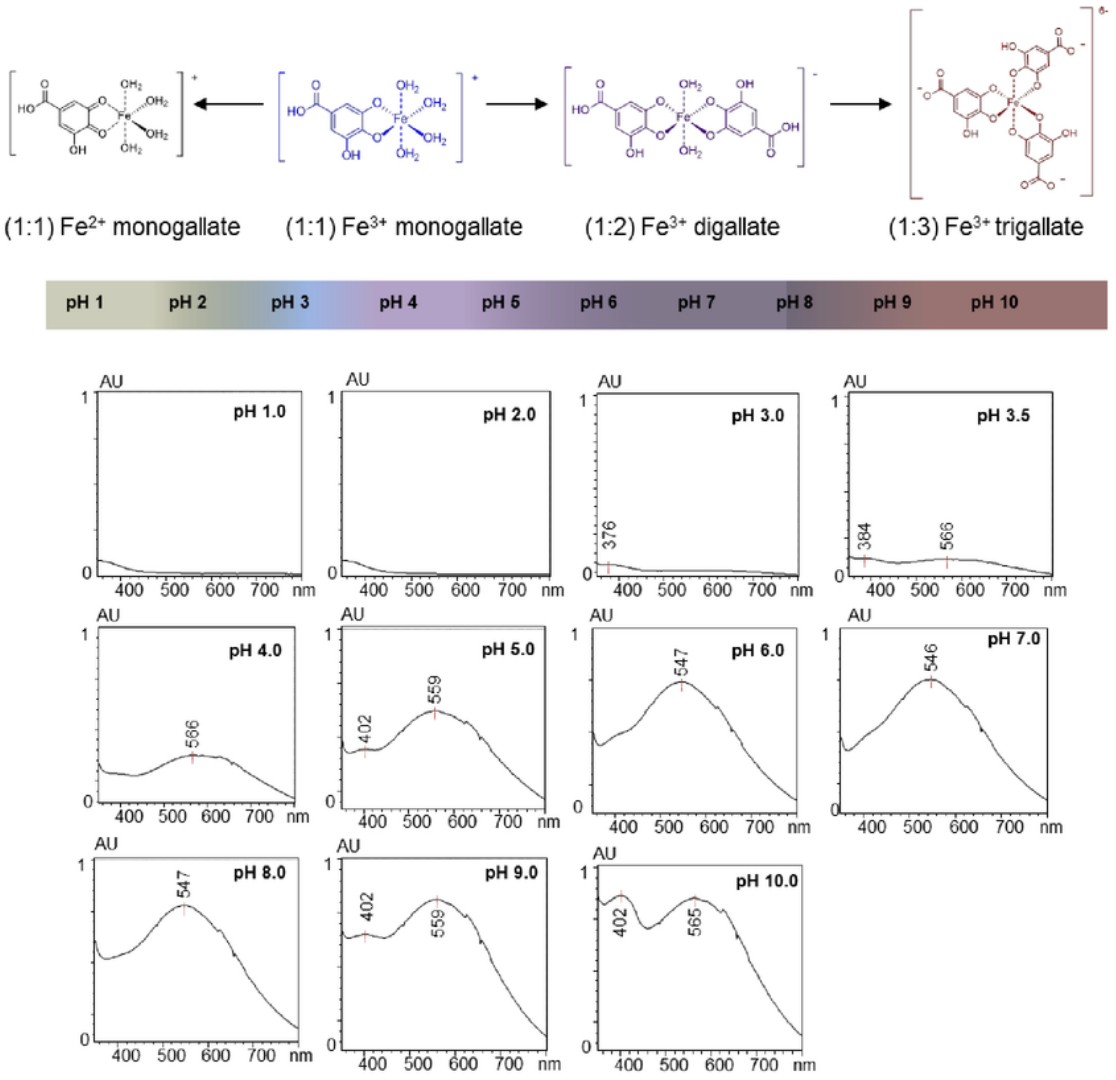

Figure 39: The progressive formation of ferrous monogallate (pH <2), ferric monogallate (blue, pH 2-3.5), ferric digallate (violet, pH 3.5-8) and ferric trigallate (maroon, pH 8-10) complexes as pH is increased from 1 to 10. The experimental UV/Vis spectra of the titrated solution at each pH are shown.

3.3.4.7 Mössbauer spectroscopy

Mössbauer spectroscopy offers atomic selectivity for probing the environment around ^{57}Fe (stable isotope, natural abundance 2.12%) nucleus. The advantage of the technique enabled centers of the iron chromophore centers of the pigment could be probed directly without alteration of the intact macromolecular pigment. Mössbauer spectroscopy mainly provides empirical hyperfine parameters on two types of nuclear interactions, isomeric shift (I.S.) and quadrupole splitting (Q.S.), that occur when an ^{57}Fe nuclei are bombarded with gamma (γ) radiation. The parameters vary depending on the charge state and immediate bonding environment of the iron. Previously published Mössbauer parameters of ^{57}ferric gallate and ^{57}ferrous gallate and related catechol complexes are available for comparison (221-223).

With the assistance of Dr. Ercan Alp at Argonne National Labs, a ^{57}Fe Mössbauer spectrum was acquired for the intact purified *Zygogonium* sp. pigment (Succession mat). The results are shown in Figure 40. In comparison with published I.S. and Q.S. values for relevant iron complexes such as (1:1) and (1:2) ferric catechol complexes, the values for the pigment (Q.S. 1.08, I.S. 0.31) were closest to those of the $Fe^{3+}(gallate)_2$ *bis* complex (Q.S. 1.07, I.S. 0.31). As discussed by Gust et. al, the signal for ferrous iron complexes are typically weaker and may be buried under the signals for the ferric iron.

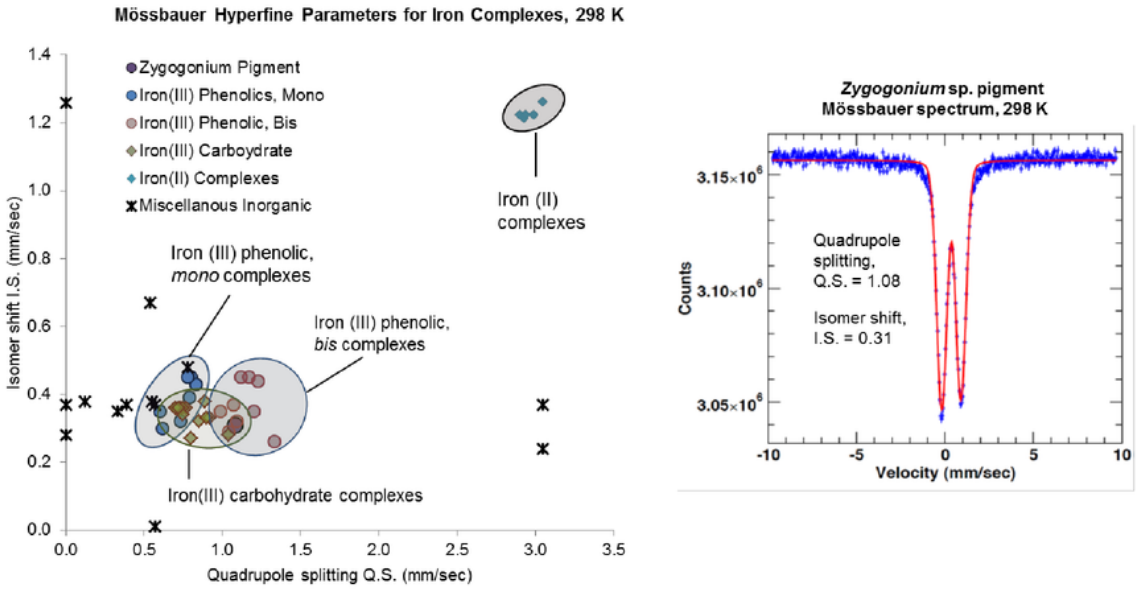

Figure 40: Mössbauer spectrum (289K) of *Zygogonium sp.* pigment (Succession mat) with a comparison of the hyperfine parameters (Quadrupole splitting and isomer shft) for the pigment to published values for other relevant ferric and ferrous complexes.

3.3.4.8 Nuclear resonance vibrational spectroscopy

Nuclear resonance vibrational spectroscopy (NRVS) is a relatively new synchrotron beamline technique which provides a complete vibrational spectrum of the ^{57}Fe nucleus (224). Like Mössbauer spectroscopy, NRVS offers atomic selectivity as the ^{57}ferric centers of the chromophore of the pigment could be probed directly without modification of the intact macromolecular pigment. In simple terms, NRVS can be considered as providing a complete map of the vibrational modes of an atomic nucleus which is inclusive of the vibrational modes of the FT-IR and a Raman spectrum. An NRVS analysis also provides a variety of thermoelastic parameters useful in condensed matter physics. In this work, the NRVS spectra of the purified Succession mat purple pigment was obtained with the assistance of Dr. Ercan Alp at Argonne National Laboratories (ANL).

For comparison to the natural pigment, ^{57}ferric gallate model compounds (*mono*, *bis*, and *tris)* were prepared from ^{57}Fe(s) and analyzed using NRVS. Ferric trifluoroacetate (TFA) product prepared from ^{57}Fe(s) metal was used because the common $^{57}FeCl_3$ reagent typically used as a $^{57}Fe^{3+}$ source (prepared from $^{57}Fe_{(s)}$ and HCl) in NRVS studies did not generate the expected blue, purple, or maroon colored iron gallate complexes in combination with gallic acid. The ^{57}ferric trifluoroacetic acid complex was analyzed by (ESI+)-HRMS via flow injection analysis to confirm the production of ferric trifluoroacetate species (Figure 41). The *mono*, *bis*, and *tris* model compounds were prepared using the pH titration with gallic acid as shown in Section 3.3.4.6 and were also analyzed by HRMS using flow injection analysis. The HRMS and MS^2 spectra of the ^{57}ferric digallate complex is shown in Figure 42.

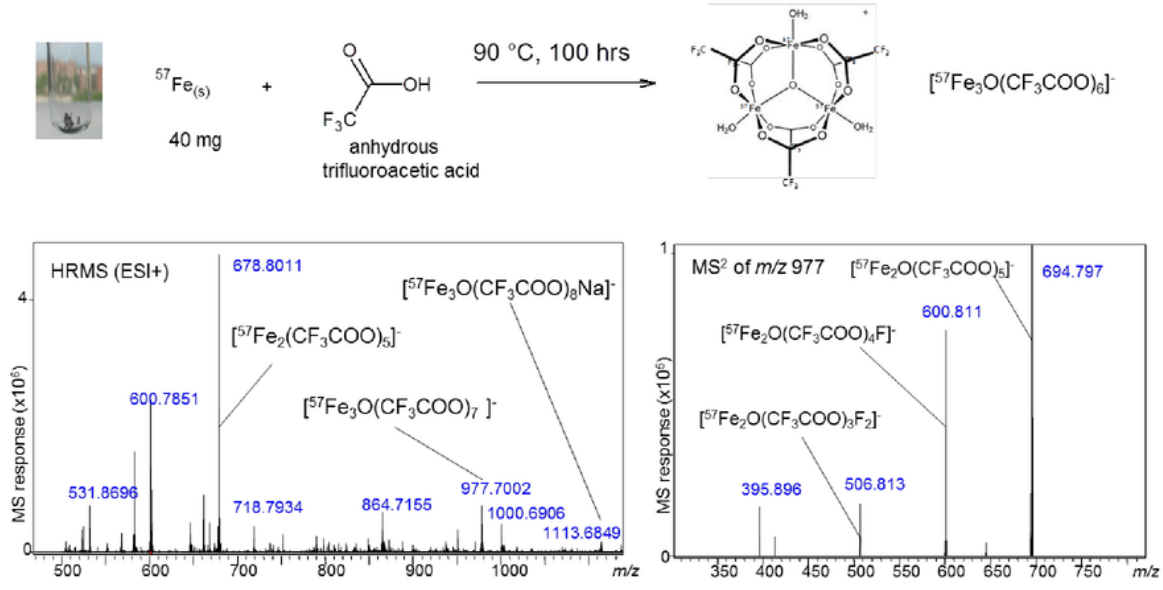

Figure 41: Preparation and HRMS and tandem MS/MS spectra confirmation of synthesized ^{57}ferric trifluoroacetic acid complex from $^{57}Fe_{(s)}$ metal.

The prepared ferric gallate (*mono, bis*, and *tris* gallate) model compounds were analyzed by FIA-PDA-HRMS. The ESI(+)-HRMS and MS/MS spectrum of the prepared $^{57}Fe(GA)_2$ complex is shown in Figure 42. High resolution mass spectra of these intact iron gallate ion species have not been reported previously (225-227). The NRVS spectra of the three model compounds (Figure 43) was acquired along with the spectra of the purified Succession mat pigment (Figure 44). The NRVS spectrum of the natural pigment was most comparable to the purple *bis* $^{57}Fe^{3+}(GA)_2$ complex. Various thermoelastic parameters are derived from the NRVS data using algorithms. The thermoelastic parameters for the three model compounds are shown in Figure 45 relative to those of the natural pigment. The mean force constant (229.8 N/m for the natural pigment) is perhaps most directly relevant to the bonding environment of the iron. Of the three model compounds, the mean force constant was closest to that of the $^{57}Fe^{3+}(GA)_2$ *bis* complex. The overall parameters for the natural pigment were most similar to those of purple colored $^{57}Fe^{3+}(GA)_2$ *bis* complex. The NRVS study is consistent with the hypothesis that the purple chromophore of the natural pigment arises from ferric iron complexed by two galloyl groups.

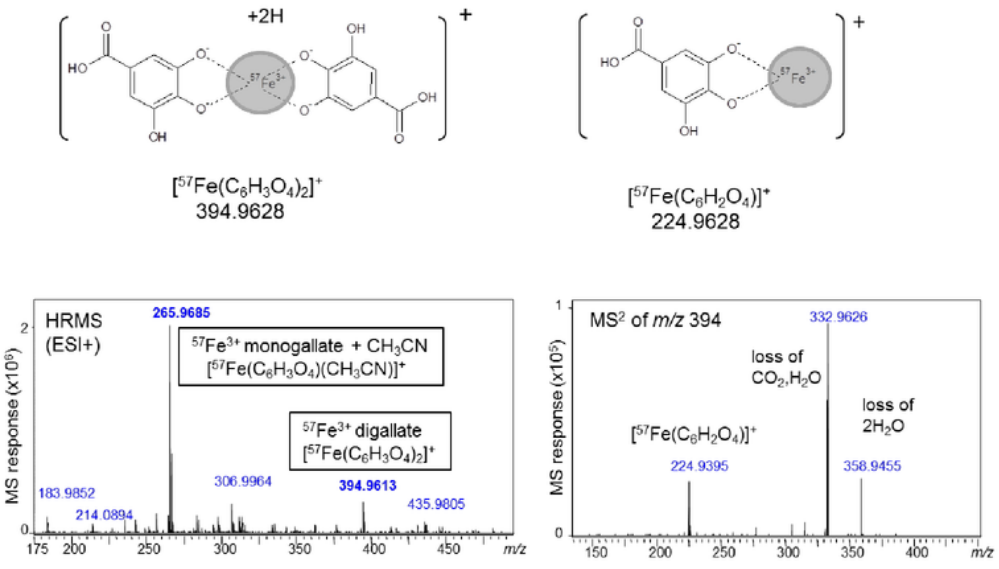

Figure 42: HRMS and tandem MS/MS spectra of synthesized 57-ferric digallic acid complex.

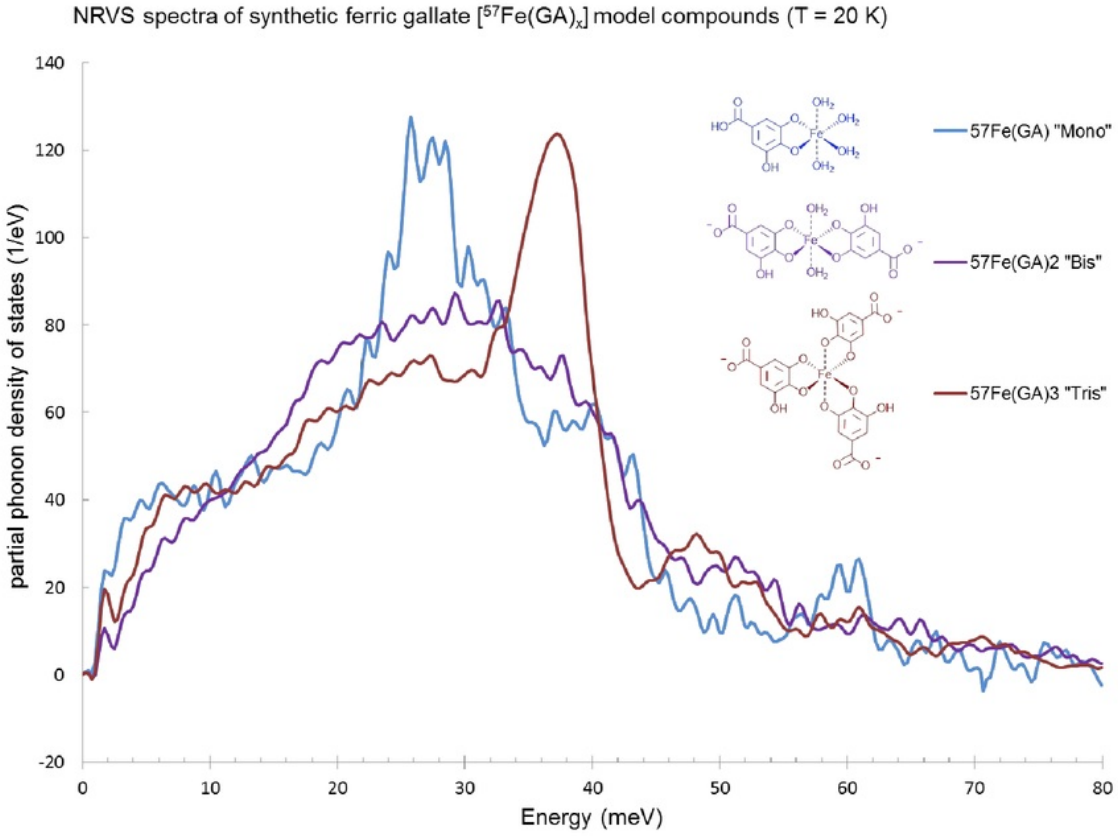

Figure 43: Nuclear resonance vibrational spectra (temperature = 20 K) of synthetic ferric monogallate ($^{57}FeGal_1$) , ferric digallate ($^{57}FeGal_2$), and ferric trigallate ($^{57}FeGal_3$) complexes.

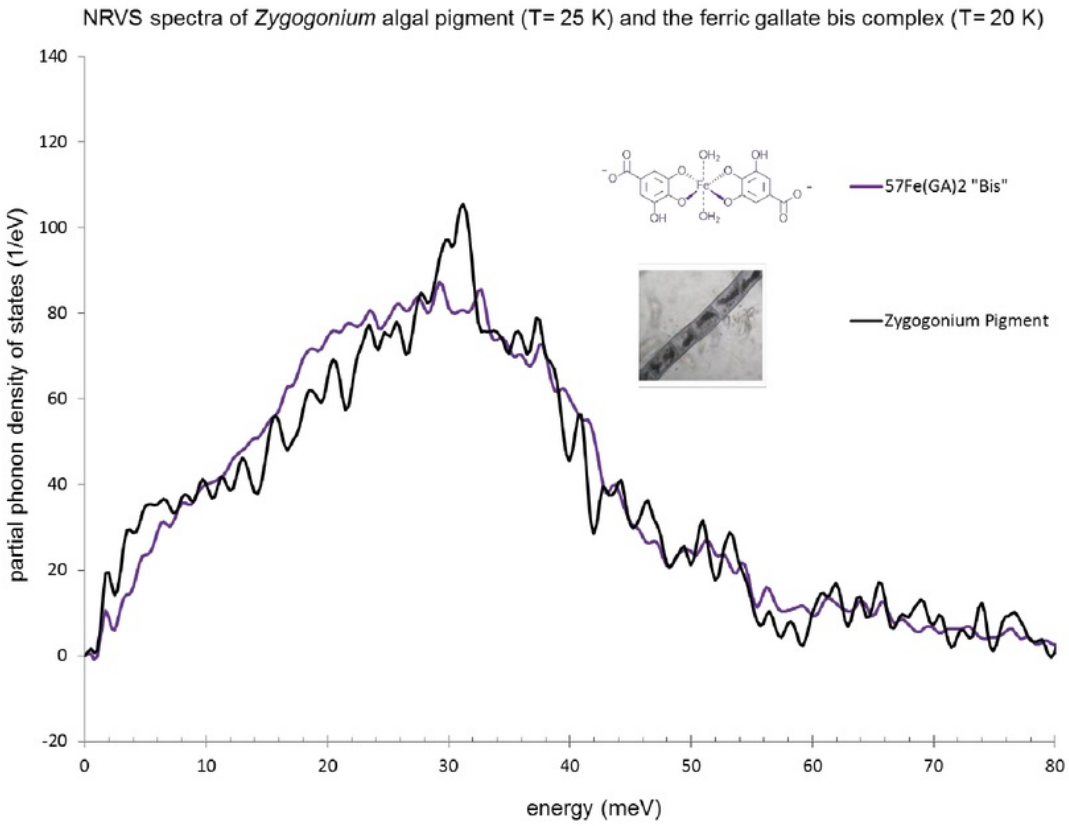

Figure 44: Nuclear resonance vibrational spectra (temperature = 20 K) of synthetic ^{57}ferric digallate ($^{57}FeGal_2$) and purified *Zygogonium* sp. pigment (Succession mat).

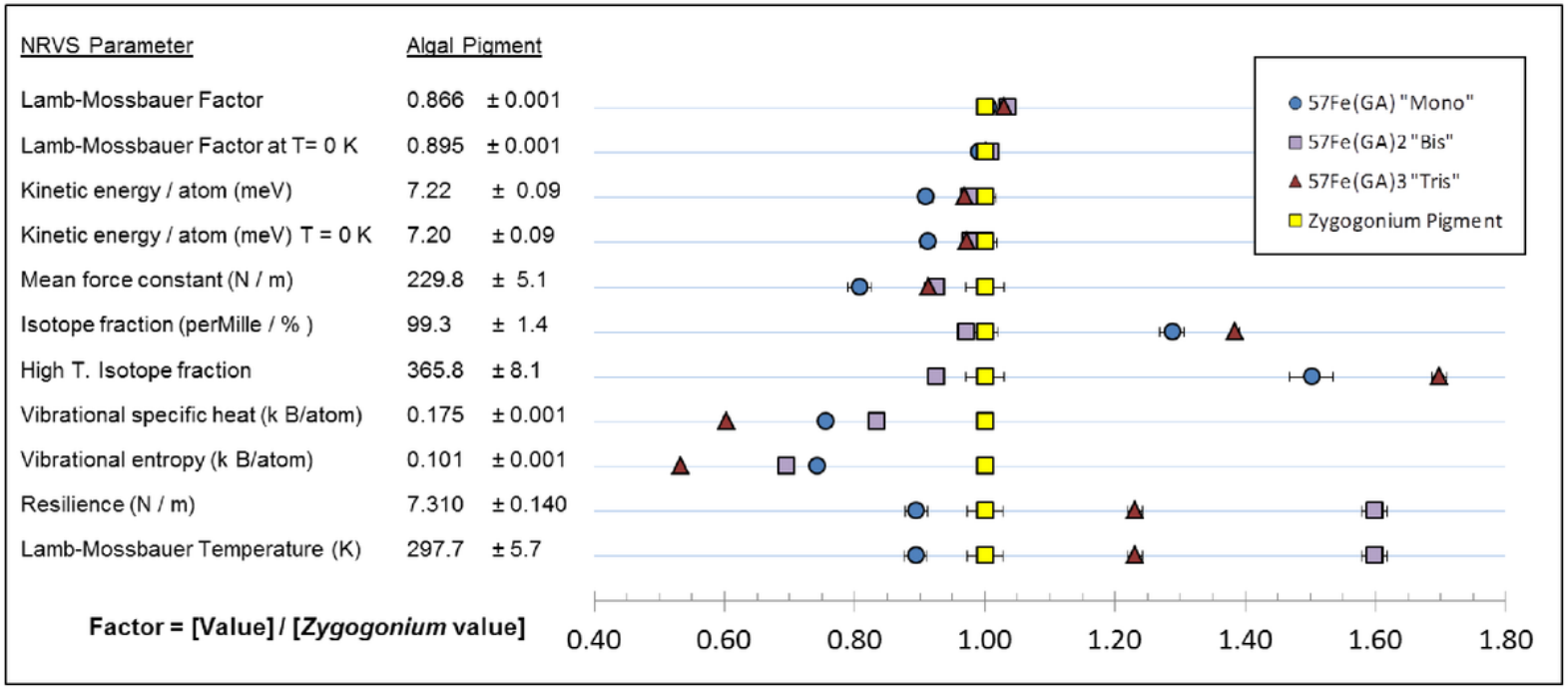

Figure 45: Thermoelastic parameters derived from the nuclear resonance vibrational spectra (T = 20 K) for synthetic ^{57}ferric monogallate ($^{57}FeGal_1$), ferric digallate ($^{57}FeGal_2$), and ferric trigallate ($^{57}FeGal_3$) relative to those of the natural *Zygogonium* sp. algal pigment.

3.3.4.9 HPLC-PDA-HRMS analysis of the EDTA deconstructed pigment

The intact purified macromolecular pigment complex from Succession creek showed no ionization signals with HPLC-HRMS using either electrospray or APCI sources. Acidic hydrolysis of the pigment followed by HPLC-PDA-HRMS analysis was destructive to the natural pigment constituents and only revealed a complex mixture of unidentified products with a dominant presence of gallic acid (*m/z* 169, ESI). Since the purple pigment is a macromolecular structure held together by the chelation of ferric iron to galloyl groups, successful HPLC-PDA-HRMS analysis of the individual native constituents of the purple pigment was achieved by removal of the iron by treated with an excess of EDTA. This resulted in loss of color and dissociation of the polymeric complex by sequestration of the ferric ions as $Fe^{3+}(EDTA)^{3-}$.

These negative mode HRMS data for the Succession mat side are summarized in Table V. The analysis revealed ions corresponding to gallic acid (**1**), ellagic acid. A series of galloylhexoses were detected ranging from 1 sugar (Gal_1Hex_1, monogalloylglucose) to 14 sugars (Gal_1Hex_{14}). Across all five sample sites, the major component of the pigment was digalloyl diglucose (Gal_2Hex_2). According to the carbohydrate analysis of the Succession mat pigment (Section 3.3.4.2), the hexose portion of these constituents is overwhelmingly composed of D-glucose (99.7% composition). The oligosaccharide gallate constituents are distinct from the common hydrolysable tannin has one central sugar with two or more gallic acid groups attached (Chapter 4). To the author's best knowledge, these detected oligosaccharides gallates represent a novel subclass of natural products.

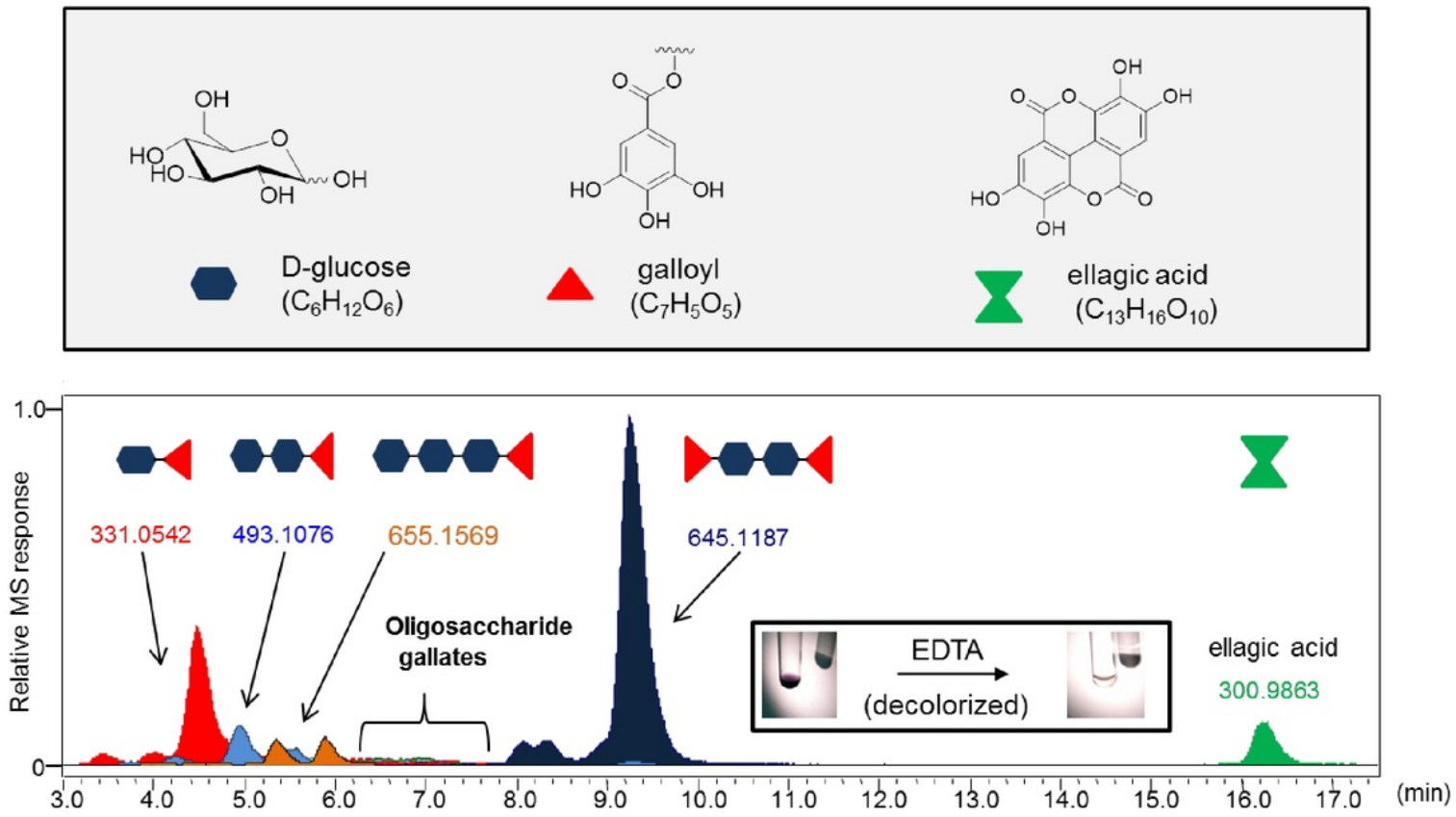

Figure 46: Computer reconstructed HPLC-(ESI⁻)-HRMS mass chromatogram of the purified *Zygogonium* sp. pigment (Succession mat) after treatment with EDTA to remove the iron. The major ions detected were monogalloylglucose (m/z *331*) and digalloyldiglucose (*m/z* 645). Oligosaccharide gallates ionized poorly due to their large mass and predominant carbohydrate content.

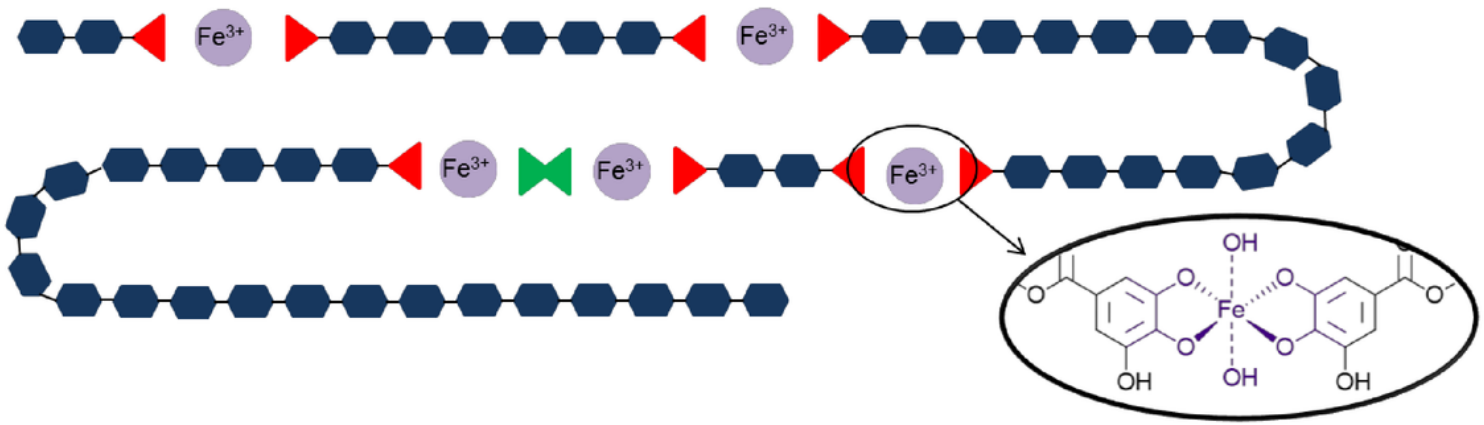

Figure 47: An illustration depicting a possible segment of *Zygogonium* sp. pigment macromolecular complex primary structure. Ferric iron atoms chelate catechols such as ellagic acid, gallic acid, and various oligosaccharide gallate constituents of the purple pigment to form a polar water soluble macromolecular complex.

TABLE V: ELECTROSPRAY NEGATIVE MODE HPLC-HRMS DATA FOR *ZYGOGONIUM* SP. PURPLE PIGMENT (SUCCESSION MAT) AFTER REMOVAL OF IRON WITH EDTA

retention time (min)	HRMS obsvd	ion species	formula	HRMS calcd	error (ppm)	MS^2 ions	proposed identity
2.8	343.9889	$[EDTA^{4-} + Fe(III)]^-$	$C_{10}H_{12}N_2O_8Fe$	343.9943	-15.7	300, 256, 212	ferric EDTA complex
4.5	331.0621	$[Gal_1Hex_1 - H]^-$	$C_{13}H_{16}O_{10}$	331.0665	-13.4	271, 211, 169, 125	galloylglucose
5.0	493.1205	$[Gal_1Hex_2 - H]^-$	$C_{19}H_{26}O_{15}$	493.1194	2.3	443, 373, 331, 271, 211, 169	galloyldiglucose
5.5, 6.0	655.1714	$[Gal_1Hex_3 - H]^-$	$C_{25}H_{36}O_{20}$	655.1722	-1.2	595, 535, 493, 373, 331, 313, 271, 211	galloyltriglucose
3.6, 4.1, 4.6, 5.4, 5.7, 6.1, 6.4	817.2143	$[Gal_1Hex_4 - H]^-$	$C_{31}H_{46}O_{25}$	817.2250	-13.1		galloyltetraglucose
5.2, 5.6, 5.8, 6.2, 6.5	979.2669	$[Gal_1Hex_5 - H]^-$	$C_{37}H_{56}O_{30}$	979.2778	-11.2	809, 707, 697, 545	galloylpentaglucose
5.1, 5.7, 6.0, 6.3, 6.7	1141.3196	$[Gal_1Hex_6 - H]^-$	$C_{43}H_{66}O_{35}$	1141.3307	-9.7	971, 809, 707, 545	galloylhexaglucose
6.1, 6.7	1303.371	$[Gal_1Hex_7 - H]^-$	$C_{49}H_{76}O_{40}$	1303.3835	-9.6	1133, 971, 869, 809, 545	galloylheptaglucose
6.1, 6.7	1465.4246	$[Gal_1Hex_8 - H]^-$	$C_{55}H_{86}O_{45}$	1465.4363	-8.0		galloyloctaglucose
6.8	813.2306	$[Gal_1Hex_9 - 2H]^{2-}$	$C_{61}H_{96}O_{50}$	813.2407	-12.4		galloylnonaglucose
6.5, 6.8	894.2546	$[Gal_1Hex_{10} - 2H]^{2-}$	$C_{67}H_{106}O_{55}$	894.2671	-13.9		galloyldecaglucose
6.5, 6.8	975.2788	$[Gal_1Hex_{11} - 2H]^{2-}$	$C_{73}H_{116}O_{60}$	975.2935	-15.1		galloylhendecaglucose
6.5, 6.8	1056.3011	$[Gal_1Hex_{12} - 2H]^{2-}$	$C_{79}H_{126}O_{65}$	1056.3199	-17.8		galloylundecaglucose
6.8	1137.3252	$[Gal_1Hex_{13} - 2H]^{2-}$	$C_{85}H_{136}O_{70}$	1137.3463	-18.6		galloyltridecaglucose
6.8	1218.3450	$[Gal_1Hex_{14} - 2H]^{2-}$	$C_{91}H_{146}O_{75}$	1218.3727	-22.7		galloyltetradecaglucose
8.2, 8.4, 9.4	645.1311	$[Gal_2Hex_2 - H]^-$	$C_{26}H_{30}O_{19}$	645.1303	1.2	493, 433, 373, 331, 271	digalloyldiglucose
8.5. 9.7	807.1714	$[Gal_2Hex_3 - H]^-$	$C_{32}H_{40}O_{24}$	807.1831	-14.5	655, 637, 595, 577, 535	digalloyltriglucose
8.6, 9.2	969.2257	$[Gal_2Hex_4 - H]^-$	$C_{38}H_{50}O_{29}$	969.2360	-10.6	799, 757, 697, 655, 595	digalloyltetraglucose
9.0	1131.2734	$[Gal_2Hex_5 - H]^-$	$C_{44}H_{60}O_{34}$	1131.2888	-13.6	961, 817	digalloylpentaglucose
9.0	1293.3252	$[Gal_2Hex_6 - H]^-$	$C_{50}H_{70}O_{39}$	1293.3416	-12.7	1123, 979	digalloylhexaglucose
16.3	300.9934	$[Ellagic\ acid - H]^-$	$C_{14}H_6O_8$	300.9984	-16.8	284, 257, 229, 201, 185	ellagic acid

3.3.4.9 Compositional summary of the purple pigment

The characterization summary of the purified *Zygogonium* sp. purple pigment from Succession mat is given in Table VI. The data indicate that the pigment is a highly polar heterogeneous macromolecular complex of gallic acid, galloylglucose, and oligosaccharide gallates containing both Fe^{2+} and Fe^{3+} and bound together by purple chromophoric organimetallic $Fe^{3+}(galloyl)_2$ linkages.

3.3.5 *Zygogonium* sp. pigments from multiple environmental locations

To investigate the individual constituents of the macromolecular pigment complex across *Zygogonium* sp. algal populations, pigments from *Zygogonium* sp. mats from additional YNP collection sites (Nymph creek, Dragon spring, Beowolf, and Gap runoff) were purified (according to Figure 28), treated with EDTA to remove iron, and analyzed by HPLC-PDA-HRMS analysis along with the Succession mat pigment. The major constituents of the pigment from Nymph creek, major fraction 3 (Figure 29) were very similar to those of the Succession mat pigment: galloyldiglucose (*m/z* 493), digalloyldigluclose (*m/z* 645), monogalloyl triglucose (m/z 655), ellagic acid (*m/z* 301). A later analysis of additional sites (Dragon spring, Beowolf, and Gap runoff) in comparison to the Succession mat pigment showed common major constituents of monogalloylglucose (*m/z* 331), digalloyldigluclose (*m/z* 645) along with the presence of oligosaccharide gallates. The HPLC-HRMS extracted ion chromatograms of the additional pigments are provided in Appendix E.

TABLE VI: SUMMARY OF DATA FOR *ZYGOGONIUM* SP. PURPLE PIGMENT (SUCCESSION MAT)

Analytical technique	**Data summary**	**Interpretation**
Wet chemical and solubility tests	Soluble in water and DMSO; $Fe_{(s)}$ with $NaBH_4$; decolorized with EDTA; Stable to boiling (Figure 27)	highly polar, contains iron
UV spectroscopy	λ_{max} (water) = 564 nm, broad; ε_{water} = 55,200 cm^{-1} mol^{-1} (based upon M_{avg} = 30 kD)	broad absorbance typical of a charge-transfer complex
400 MHz ^{1}H NMR	3.40, 3.64, 3.80, 4.11, 4.45 ppm, all broad	glucose
400 MHz ^{13}C NMR	60.3, 67.8, 69.1, 72.5, 75.0, 102.1 ppm (Figure 31)	glucose
MALDI-TOF MS	*m/z* series, Δ162 D (hexose units) (Figure 33)	hexose polymer
Fourier transform IR	3223, 2885, 1685, 1344, 1068, 1914 cm-1	sugar
SEM with xray microanalysis	6.4 and 7.0 keV transition lines (Figure 35)	Iron, Fe
EPR spectroscopy	g values of 4.3 and 2.0 (Figure 36)	High-spin Fe^{3+}, Fe^{2+}
UV/Vis with 1,10-phenanthroline	Chromophore loss proportional to formation of $Fe(1,10\text{-phen})_3$ complex (Figure 37)	iron chromophore
Determination of iron	37.2 ± 4.9 µg/mg by 1,10-phenanthroline method	3.7% Iron by weight
Determination of bound gallic acid	109.7 ± 7.4 µg/mg by UHPLC-MS/MS (Chapter 4)	11% bound galloyl groups by weight
Molecular weight analysis (CCRC)	M_{avg} = 30 kD, range 10 kDa to 60 kD (Figure 34)	heterogeneous macromolecule
Carbohydrate analysis (CCRC)	85% ± 10 % carbohydrate by wt; Composition of 99.7% D-glucose; Major linkages 1,3-Glu (0.28) and 1,6-Glu (0.23)	75% to 95% D-glucose by weight
Mössbauer spectroscopy, 298 K	Q.S. = 1.08, I.S. = 0.31 (Figure 40)	ferric digallate
NRVS with ^{57}Fe model compounds	Closest match with ferric gallate (Figure 106-108)	ferric digallate
HPLC-PDA-HRMS after EDTA	gallic acid, ellagic acid, monogalloylglucose, oligosaccharide gallates (Figure 46)	mixed galloyl components

3.3.3.2 Ecological role of the pigment as a UV sunscreen

The alga is remarkable for its acid tolerance and exposure to prolonged desiccation and solar irradiation, the molecular details of which are unknown. The water soluble polysaccharide contents of the algae have remained unknown. The presence and intensity of the purple pigmentation in *Zygogonium* sp. mats has been observed in the field to correlate with exposure to solar radiation across multiple locations (202,207-209). The purple pigment of the algae is most abundant in the uppermost surface layers of a mat.

In this work, the sun exposed top layers of the *Zygogonium* sp. mats produce far more bound gallic acid than the underlayer which is far less exposed to the sun. To examine the gallic acid on the ultraviolet light exposure, Dr. Gill Geesey collected biomass samples from the top sun exposed side and the underneath side of a *Zygogonium* sp. algal mats at four unspecified locations in Yellowstone National Park. A sample of green algal mat containing no visible purple pigment was also analyzed. The total and bound gallic acid in these samples were determined using the UHPLC-LCMS method discussed in Chapter 4. The results (Table VII) show significant quantities of bound gallic acid only in the in the algal biomass samples taken from the top of a purple *Zygogonium* sp. mats. This suggests the production of the gallic acid containing species critical to the formation of the pigment are an adaptational response to UV light exposure.

TABLE VII: DETERMINATION OF FREE AND BOUND GALLIC ACID IN UPPER AND LOWER SURFACES OF *ZYGOGONIUM* SP. MATS

environmental biomass sample	**total galloyl groups by UHPLC-MS/MS[1]**	**gallic acid, free by UHPLC-MS/MS[1]**	**Galloyl, bound calculated[1,2]**
Top of *Zygogonium* sp. mat 1	12.6 ± 6.1	2.0 ± 0.1	10.6 ± 6.2
Top of *Zygogonium* sp. mat 2	15.6 ± 5.8	0.7 ± 0.1	14.9 ± 5.9
Top of *Zygogonium* sp. mat 3	2.7 ± 1.2	0.8 ± 0.0	1.9 ± 1.2
Top of *Zygogonium* sp. mat 4	14.3 ± 1.0	1.4 ± 0.0	12.9 ± 1.0
Bottom of *Zygogonium* sp. mat 1	< 0.2	< 0.2	< 0.2
Bottom of *Zygogonium* sp. mat 2	< 0.2	< 0.2	< 0.2
Bottom of *Zygogonium* sp. mat 3	< 0.2	< 0.2	< 0.2
Zygogonium sp. green mat sample	0.4 ± 0.1	0.2 ± 0.0	0.2 ± 0.1

1. Results in µg/mg of raw biomass sample

2. galloyl (bound) = total gallate - gallic acid (free)

The types of secondary metabolites which have been clearly established to function as ultraviolet sunscreens are all organic are relatively few: melanins, microsporins, carotenoids, and scytonemin (228-232). Gallic acid moieties absorb UV energy in the range of (about 250-300 nm) of UVB/UVC rays which DNA damage. It is not yet clear if there is an added biological advantage with the formation of large water soluble complexes by the chelation of gallic acid groups by ferric ions in the alga. The purpose of the iron may influence the localization of the pigment within the cytoarchitecture of the *Zygogonium* sp. cells or to simple enhancement of the sunscreen capacity of gallic acid. The comparison of the UV spectra of gallic acid to that of the *Zygogonium* sp. purple pigment (Succession mat) shows an enhancement and a broadening of the UV absorbing shoulder (λ 280 nm, br) relative to gallic acid alone

(λ 269 nm) suggesting that *bis* ferric gallate bonding centers afford more UV protection than galloyl groups alone (Figure 48).

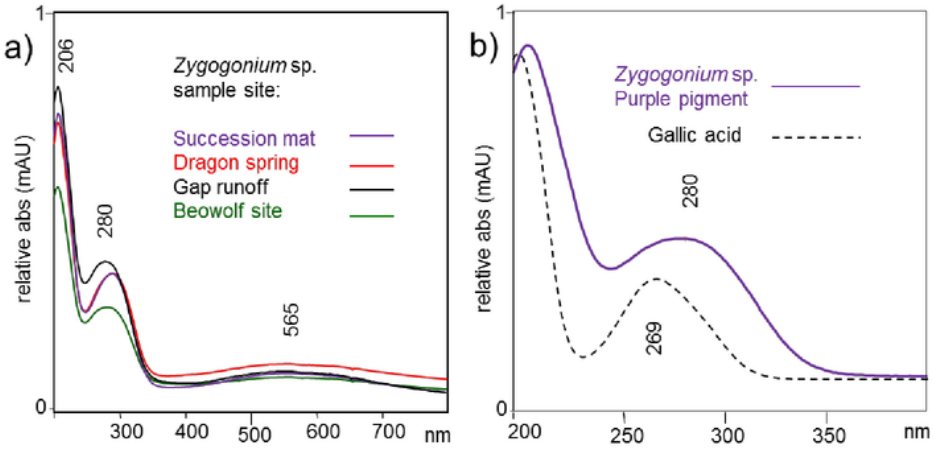

Figure 48. a) Overlaid UV/Vis spectra of purified Zygogonium sp. purple pigments from 4 different collection sites (YNP, WY) and b) an overlay of the UV/Vis spectra of the pigment (Succession mat) with gallic acid showing an increased absorbance shoulder in the UVB/UVC range for the pigment relative to that of gallic acid alone.

The potential for ferric oxides to function as ultraviolet sunscreens has been established through *in vitro* culture studies with microorganisms (229). Ferric sunscreens have been proposed as a possible adaptational mechanism for ancient microorganisms and for potential life forms on Mars (229). However, no ferric ultraviolet sunscreens have been demonstrated from living organisms to date. The evolutionary role of the production of the oligosaccharide gallates in this organism may relate to the increased water solubility of the resulting ferric gallate pigment complex. It is possible that the *bis*-type galloferric chromophore serves an ecological sunscreen, and future studies are in progress to investigate that role.

3.4 Conclusion

Zygogonium sp. is an acid and desiccation tolerant filamentous green algae that thrives in extreme habitats. A purple pigment which accumulates in the vacuoles of sun exposed layers of *Z. ericetorum* algae has remained unidentified for over fifty years. In this work, samples of the algae were collected from acid bogs in Yellowstone National Park, WY. The purple pigment was isolated and characterized by NMR, mass, IR, UV, EPR, X-ray, and ^{57}Fe Mössbauer spectroscopy. The purple pigment was found to contain highly branched polymers of glucose containing traces of ester linked gallic acid (**1**). The purple color of the polysaccharide is due to complexation of the polyphenolic groups by ferric iron in a *bis* (L_2Fe^{3+}) configuration (**2**). A new subclass of biological molecule, oligosaccharide gallates, was discovered. The possible role of the ferric oligosachharide complex characterized here as a novel iron containing biological UV sunscreen was discussed.

CHAPTER 4: ACCURATE QUANTIFICATION OF BOUND GALLIC ACID BY UHPLC-MS/MS

(Previously published as Newsome, A. G.; Li, Y.; Van Breemen, R. V. B. Improved Quantification of Free and Ester-Bound Gallic Acid in Foods and Beverages by UHPLC-MS/MS. *J. Agric. Food Chem.* **2016**, 64, 1326-1334.)

4 INTRODUCTION

The results for the quantitative determination of bound gallic acid in the *Zygogonium sp.* purple pigment complex was presented previously (Section 3.3.4.3). The measurement was accomplished using an improved UHPLC-MS/MS method for the determination of bound gallic acid described here. While the measurement was useful for the *Zygogonium sp.* pigment characterization, the utility of the improved method extends to applications involving free and bound gallate groups. Developed as part of this dissertation, this new UPHLC-MS/MS method has been published (233).

The most common application for the measurement of bound gallic acid is in the determination of hydrolysable tannin content. Hydrolysable tannins are measured routinely during the characterization of food and beverage samples. Most methods for the determination of hydrolysable tannins use hydrolysis or methanolysis to convert complex tannins to small molecules (gallic acid, methyl gallate and ellagic acid) for quantification by HPLC-UV. Often unrecognized, analytical limitations and variability inherent in these approaches to the measurement of hydrolysable tannins include the variable mass fraction (0 to 0.90) that is released as analyte, contributions of sources other than tannins to hydrolysable gallate (can exceed >10% wt/wt), the measurement of both free and total analyte, and lack of controls to account for degradation. An accurate, specific, sensitive, and higher-throughput approach for the determination of hydrolysable gallate based on UHPLC-MS/MS was developed which overcomes these limitations.

4.1 Hydrolysable tannins

Tannins (hydrolysable and condensed) are complex polyphenolic metabolites that are abundant in the wood, bark, herbage, roots, fruits, and seeds of diverse higher plants (234). In the human diet, tannins have significant impact on color and flavor of foods and exhibit a host of biological activities

(235) including digestive inhibition, biological iron complexation (236), antioxidation (237), and protein complexation (238). These compounds probably serve adaptive or biochemical roles including chemical defense agents (239), predation deterrents (240), nutrient cycling (241), and as redox participants (242,243). The analytical measurement of tannins is of considerable interest because of their prevalence in nature and in the human diet. Several reviews have addressed their quantitative and qualitative measurement (244-247).

Hydrolysable tannins can be subcategorized into simple tannins, gallotannins and ellagitannins (Figure 49 and Figure 50) (245,248). Simple tannins consist of a carbohydrate core with one or more ester-linked gallate groups, while gallotannins contain additional gallate groups linked through depside bonds (i.e. decagalloylglucose, a large molecular weight gallotannin component of tannic acid). Ellagitannins are more structurally variable and complex than gallotannins as they involve a variety of additional biaryl couplings between galloyl groups.

The determination of hydrolysable tannins is routine during the characterization of food and beverage samples. In this context, estimation of total hydrolysable tannins is usually sufficient rather than a quantitative analysis of individual constituents. Popular methods for estimation of hydrolysable tannins include colorimetric, gravimetric (249), and protein precipitation (250) all of which have shortcomings (245). More modern methods employ heated hydrolysis or methanolysis to convert hydrolysable tannins into their common constitutive units, usually gallate and sometimes ellagic acid, for quantitation typically using HPLC-UV. The most popular lysis methods are the rhodanine assay (251), the potassium iodate method (252), and the methanolic-HCl method (253). These methods provide reasonable estimations, but it is unclear which of these methods produces the most accurate determination of hydrolysable tannins.

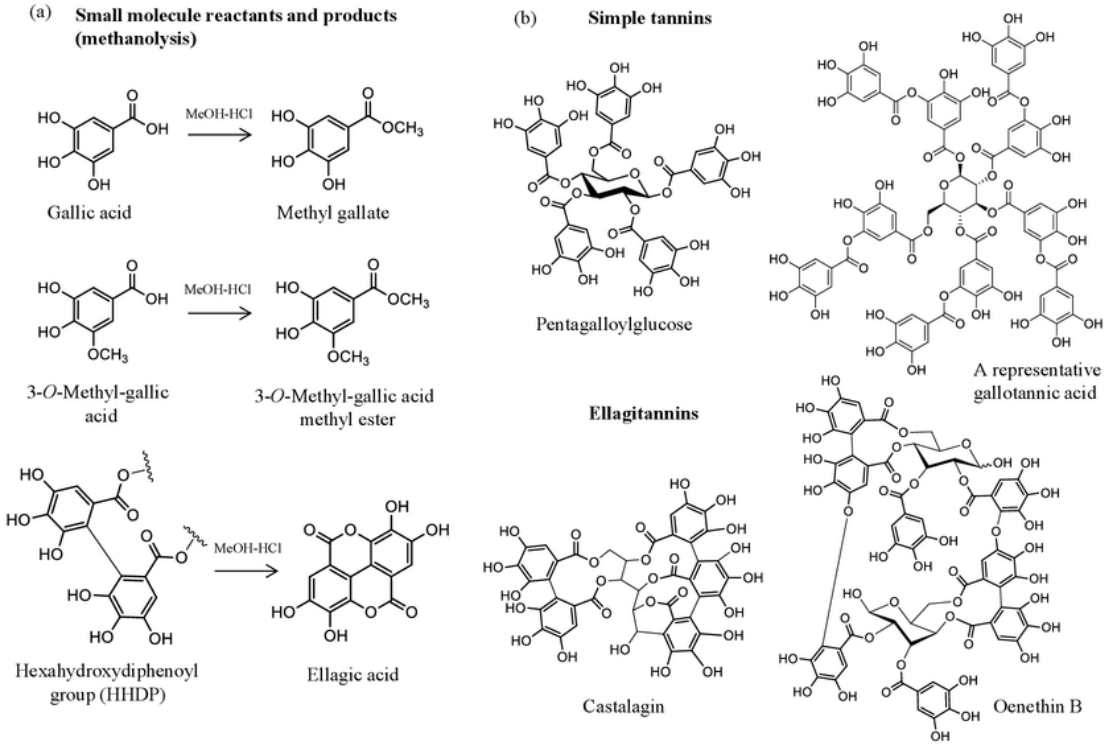

Figure 49. (a) Chemical structures, names and abbreviations of small molecule reactants and products involved in the methanolysis of hydrolysable tannins, and (b) selected simple tannins and ellagitannins.

Since there are hundreds of unique hydrolysable tannin structures but few reference standards, the estimation of total hydrolysable tannins through determination of many individual species requires the laborious isolation of many reference materials. As a result, the measurement of all these different species is impractical for routine analysis. Nevertheless, simultaneous quantitative analyses of many constituents of hydrolysable tannins in food and beverage samples have been reported (254-257).

Given the biological, medical, economic, ecological, historical, microbiological, and industrial relevance of hydrolysable tannins and their constituent ester-bound (esterified) gallic acid, a determination of total hydrolysable tannins and/or esterified and free gallic acid is desirable that is both accurate and practical. However, a method for the accurate determination of hydrolysable tannins in food and beverages has not been established. Therefore in this chapter, (a) the major factors responsible

for limiting the accuracy of hydrolysable tannins, particularly via degradative lysis approaches, are identified and discussed; and (b) a practical UHPLC-MS/MS approach is described for the measurement of total hydrolysable tannins and esterified gallic acid with improved accuracy, sensitivity, and selectivity.

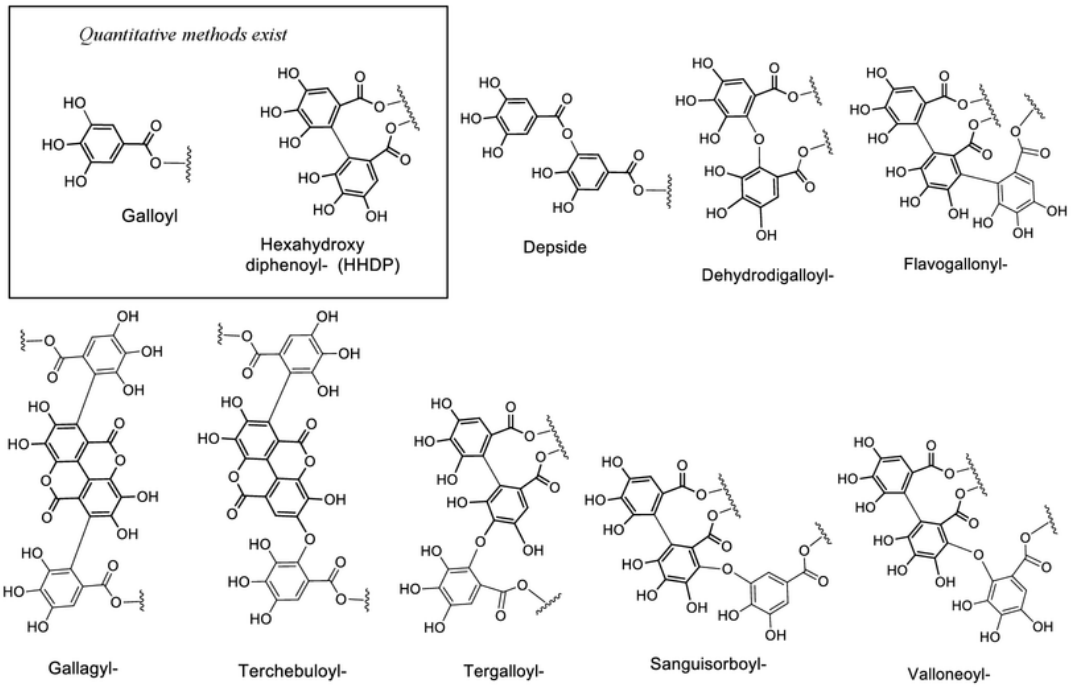

Figure 50. Varieties of galloyl-galloyl couplings found in hydrolysable tannins. Quantitative methods typically measure only ester-bound and HHDP-bound galloyl groups.

4.2 Materials and Methods

4.2.1 Reagents

The internal standards 3-*O*-methyl-gallic acid and 3-*O*-methyl-gallic acid methyl ester were purchased from Chromadex (Irvine, CA) and JPM^2 Pharmaceuticals (Wayland, MA), respectively. Anhydrous methanol (99.8%), gallic acid (>99.0%), ellagic acid (>95%), tannic acid (>95%), gallic acid

methyl ester (methyl gallate), and acetyl chloride were purchased from Sigma-Aldrich (St. Louis, MO). All chromatography solvents were HPLC grade or better and were purchased from Thermo Fisher (Waltham, MA). Commercially available food samples ('Van Gogh' mango, Grade A maple syrup, pure pomegranate juice from concentrate, bourbon whiskey, organic cocoa powder, loose green tea leaves, whole raspberries, and carob powder) were obtained from local markets (Chicago, IL).

4.2.2 Standard and sample preparation

Methanolic-HCl was prepared by slow addition of 190 µL of acetyl chloride per 1 mL of well-stirred anhydrous methanol at 0 °C (253). Stock solutions containing gallic acid, methyl gallate and ellagic acid were prepared in anhydrous methanol at 1.00 mg/mL of each compound, and from these, diluted standard solutions (100 µg/mL of each compound) were prepared in anhydrous methanol. Standard samples were prepared in acetonitrile/water (30:70; v/v) by dilution of evaporated aliquots of standard solutions. Thermo Fisher rubber-lined screw top glass test tubes (100 x 13 mm) were used for all methanolysis reactions. Flushing the test tubes with nitrogen gas before capping them for methanolysis improved reaction yields slightly (<10%).

Standards were prepared for methanolysis by transfer of aliquots of stock or diluted standard solutions into reaction test tubes followed by evaporation under a stream of nitrogen gas. For samples and standards, the reaction test tubes were spiked with 20 µg (20 µL of 1 mg/mL) internal standard (either 3*O*Me-G or 3*O*Me-MG) and dried under a stream of nitrogen gas. Solid food samples were dried, ground into a powder using a mortar and pestle, and then lyophilized to remove moisture. For analysis, 10 mg to 20 mg of each sample was accurately weighed into test tubes in triplicate. For liquid samples (whiskey and pomegranate juice), 1.00 mL of neat liquid was evaporated under nitrogen gas overnight in methanolysis reaction test tubes.

For determination of free gallic acid, 10 to 20 mg of prepared food sample was accurately weighed into test tubes in duplicate. Samples were heated in 1.00 mL of acetonitrile or methanol/water (50:50; v/v) at 70 °C for 1 h with periodic shaking, and then 500 µL was withdrawn and centrifuged at 12,000 x *g* for 15 min. The supernatant (100 µL) was removed, dried under a stream of dry nitrogen gas, reconstituted in acetonitrile/water (30:70; v/v), and transferred to autosampler vials for UHPLC-UV-MS/MS analysis.

4.2.3 Methanolysis reaction

For methanolysis, 1.00 mL of methanolic-HCl was added to each sample. Test tubes were capped tightly, inserted into an aluminum heating block, and heated at 85 ± 3 °C for 6 h. After cooling to room temperature, the caps were loosened and the test tubes sonicated for 5 min to remove dissolved gases. Samples were vortex mixed, and then 50 µL aliquots were transferred to 1.5 mL Eppendorf tubes, evaporated to dryness under a stream of nitrogen gas, and then reconstituted in 1.00 mL of acetonitrile/water (30:70; v/v). Samples were centrifuged at 12,000 x *g* for 15 min, and 100 µL aliquots of each supernatant were transferred to autosampler vials for analysis using UHPLC-MS/MS.

4.2.4 UHPLC-MS/MS analysis

Samples were analyzed using a Shimadzu (Kyoto, Japan) Nexera UHPLC system interfaced with a Shimadzu LCMS-8040 triple quadrupole mass spectrometer. For measurement of free gallic acid and for comparison with MS/MS analysis of methanolyzed samples, a Shimadzu SPD-20A dual wavelength UV detector (280 nm and 330 nm) was used in tandem between the UHPLC column and the mass spectrometer. Separations were carried out using an Agilent (Santa Clara, CA) Zorbax RRHD SB-C_{18}

UHPLC column (2.1 x 50 mm, 1.6 μm) with a linear gradient from water to acetonitrile as follows: 10% to 40% acetonitrile from 0.3 to 3 min; and 40% to 55% acetonitrile from 3 to 5.7 min. The eluent was diverted to waste for the first 0.5 min of each analysis, and the column was reconditioned at 10% acetonitrile for 0.8 min prior to the next injection. The flow rate was 0.4 mL/min, and the injection volume was 3 μL, except for the measurement of free gallic acid, for which the injection volume was 10 μL.

Negative ion electrospray was used with an ionization voltage of -3500 V, a desolvation line temperature of 250 °C, a heating block temperature of 400 °C, a nebulizing gas flow of 3 L/min, and a drying gas flow of 15 L/min. Selected reaction monitoring (SRM) was used with collision-induced dissociation, and pairs of SRM transitions (quantifier and qualifier, respectively) were used for each analyte as follows: gallic acid (retention time 0.83 min) *m/z* 169.1 to 125.2 and *m/z* 169.1 to 79.3; methyl gallate (retention time 2.40 min) *m/z* 183.0 to 124.1 and *m/z* 183.0 to 78.3; 3-*O*-galloyl-gallic acid methyl ester (retention time 2.76 min) *m/z* 334.9 to 183.1 and *m/z* 334.9 to 124.2; 3-*O*-methyl-gallic acid methyl ester (retention time 3.80 min) *m/z* 197.1 to 182.2 and *m/z* 197.1 to 123.2; and ellagic acid (retention time 4.02 min) *m/z* 301.0 to 284.1 and 301.0 to 145.2. The dwell time for each SRM transition was 20 ms with a total duty cycle of 0.23 s. Collision energies were optimized for each SRM transition and ranged from 14 V for gallic acid to 45 V for 3-*O*-galloyl-gallic acid methyl ester. Selected ion monitoring (SIM) of *m/z* 183 and *m/z* 331 was used during negative ion electrospray for the reaction time study involving the release of the dimer 3-*O*-galloyl-gallic acid methyl ester from gallotannins in tannic acid during methanolysis. A dwell time of 20 ms/ion was used during SIM. Quantitation was carried out by calculating analyte concentrations from SRM MS/MS (or MS SIM) peak areas based on peak area calibration curves ($r^2 > 0.998$).

4.3 Results and Discussion

During the structure elucidation of a macromolecular *Zygogonium sp.* pigment (Chapter 3) it had become apparent that literature methods for the measurement of hydrolysable tannin (designed for the measurement of esterified galloyl groups) were insufficient for determination of ester-bound galloyl groups of the pigment accurately. To develop a more accurate method, factors that impact the accuracy of hydrolysable tannin measurement by degradative lysis were carefully investigated. As explained below, these factors included the types of galloyl couplings present, depside bond resistance to acidic hydrolysis, chemical degradation of analytes during reaction, and contributions from free gallic acid. Based upon these considerations, a UHPLC-MS/MS approach was developed and validated for the measurement of ester-bound gallate (and therefore hydrolysable tannin) that addresses these factors for improved accuracy, speed, and specificity. The method is also qualitative for the detection of ellagic acid released from ellagitannins containing hexahydroxydiphenoyl (HHDP) groups.

4.3.1 Measurable hydrolysable tannin mass fraction

Most routine analytical methods for hydrolysable tannin determination by lysis are based upon the determination of free gallic acid (or methyl gallate) released from ester-bound galloyl groups by aqueous hydrolysis (or methanolysis). Sometimes, the determination of free ellagic acid released from ellagitannins containing HHDP groups (with lysis under anhydrous methanolysis conditions) is also included. At least 16 different biaryl and phenolic couplings occur in hydrolysable tannins. Because lysis products of only one or two of these are typically measured, the determination of total hydrolysable tannins by lysis is an approximation where accuracy is dependent on the tannin structures present in the sample. The variety of the galloyl coupling patterns found in gallotannins and ellagitannins has been described previously (Figure 50) (245,258,259). Table VIII shows the theoretical amounts of methyl gallate and ellagic acid that would be released by methanolysis from ester-bound gallate and from

HHDP groups. The fraction of hydrolysable tannin measurable as lysed gallic acid and ellagic acid varies substantially depending on the tannin species.

For simple tannins and gallotannins, the mass of methyl gallate released by methanolysis usually approximates the mass of the tannin (for example, see decagalloylglucose in Table VIII) since ester-bound gallate composes the majority of the gallotannin mass (252) and only the carbohydrate mass is neglected. However, for ellagitannins and other complex hydrolysable tannins, the mass fraction released as methyl gallate and ellagic acid is highly variable and can even be zero such as with castalin (Table VIII). Therefore, a lysis measurement approach for ellagitannin or complex tannin-containing species will usually underestimate the true tannin content (260). Well known ellagitannin-producing plants include raspberry, blackberry, pomegranate fruits, and various wood samples such as oak and chestnut (253).

TABLE VIII. THEORETICAL MASS FRACTIONS OF SOME HYDROLYSABLE TANNINS RELEASED THROUGH METHANOLYSIS AS METHYL GALLATE AND ELLAGIC ACID.

Compound	Formula	MW	Methyl gallate[a]	Ellagic acid [a]	Mass fraction released[b]
Simple tannins					
glucogallin	$C_{13}H_{16}O_{10}$	332	1	0	0.55
digalloylglucose	$C_{20}H_{20}O_{14}$	484	2	0	0.76
trigalloylglucose	$C_{27}H_{24}O_{18}$	636	3	0	0.87
tetragalloylglucose	$C_{34}H_{28}O_{22}$	788	4	0	0.93
pentagalloylglucose	$C_{41}H_{32}O_{26}$	940	5	0	0.98
decagalloylglucose	$C_{76}H_{52}O_{46}$	1700	10	0	1.08
Ellagitannins					
castalin	$C_{27}H_{20}O_{18}$	632	0	0	0
roburin A	$C_{82}H_{50}O_{50}$	1835	0	1	0.16
oenothein B	$C_{68}H_{48}O_{44}$	1569	2	0	0.22
puniculagin	$C_{48}H_{28}O_{30}$	1085	0	1	0.28
grandinin	$C_{46}H_{34}O_{30}$	1067	0	1	0.28
castalagin	$C_{41}H_{26}O_{26}$	934	0	1	0.32
sanguiin H-6	$C_{82}H_{54}O_{52}$	1871	1	3	0.58
HHDP-β-D-glucose	$C_{20}H_{18}O_{14}$	482	0	1	0.63
pedunculagin	$C_{34}H_{24}O_{22}$	784	0	2	0.77
tellimagrandin II	$C_{41}H_{30}O_{26}$	938	3	1	0.86

[a]Moles released per mole of hydrolysable tannin

[b]Mass fraction released = (moles methyl gallate released x $MW_{methyl\ gallate}$) + (moles ellagic acid released x $MW_{ellagic\ acid}$)/$MW_{hydrolysable\ tannin}$

4.3.2 Tannic acid and depside bonds

Tannic acid and many other hydrolysable tannins contain gallate groups linked through depside bonds. Depside-bound galloyl groups (Figure 51a) are resistant to lysis in acidified methanol (pH <3) (261). The theoretical yield of methyl gallate released from 1 μg of from tannic acid is 1.08 μg (assuming decagalloylglucose as the structure for tannic acid). However, the methanolysis of tannic acid (6 h at 85 °C) was found to release no more than 0.50 μg of methyl gallate per 1 μg of tannic acid. If only ester bonds but not depside bonds were cleaved during acidic methanolysis, then tannic acid would release 3-*O*-galloyl-gallic acid methyl ester (Figure 51a). Analysis of methanolyzed tannic acid using UHPLC-MS and tandem mass spectrometry with negative ion electrospray (Figure 51b) showed an intense peak for 3-*O*-galloyl-gallic acid methyl ester (*m/z* 335), and the product ion tandem mass spectrum of this ion was consistent with this dimer (Figure 51b insert).

Monitoring the levels of 3-*O*-galloyl-gallic acid methyl ester and methyl gallate during acidic methanolysis of tannic acid over 10 h (Figure 51c), the amount of dimer fell to less than half (0.25 at 10 h) while methyl gallate more than doubled (2.36 at 10 h). This suggests a slow lysis of the depside bond to release methyl gallate. Since methanolysis inadequately cleaves depside bonds, methanolysis of molecules containing depside-bound gallate will underestimate gallate content. Future work might investigate lysis conditions capable of efficient lysis of both ester and depside bound gallate groups.

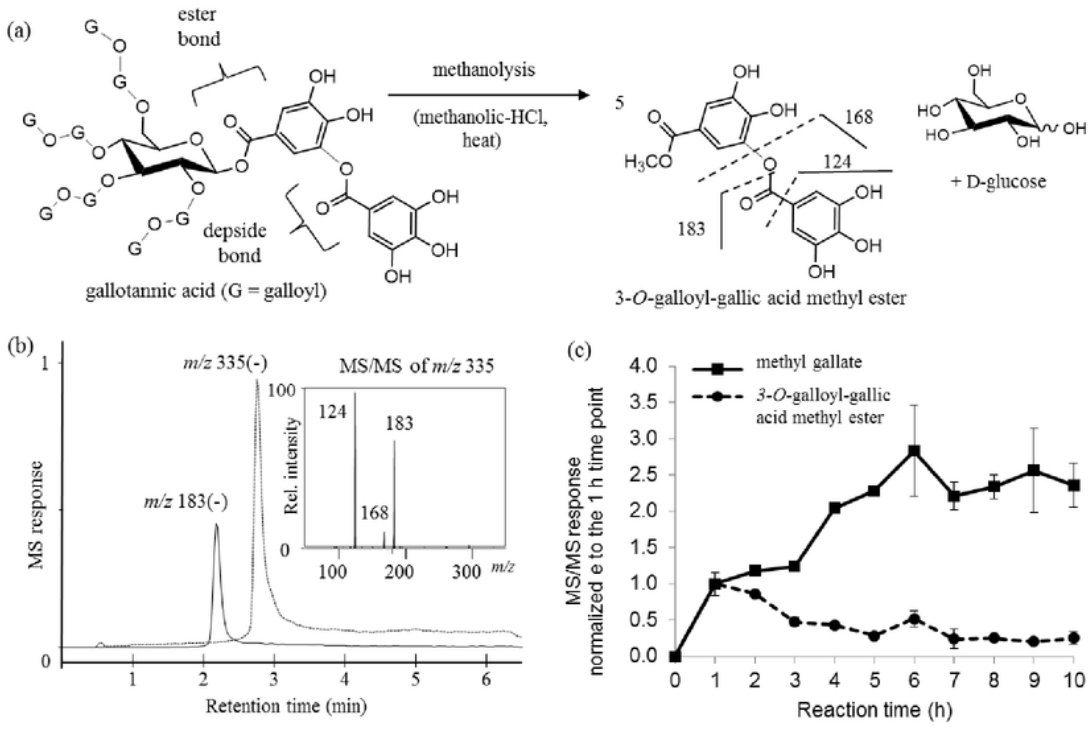

Figure 51. (a) Acidic methanolysis of decagalloylglucose (as a gallotannin example) containing a depside-bound galloyl group to form 3-*O*-galloyl-gallic acid methyl ester. The MS/MS fragmentation pattern for the dimer product is indicated. (b) Negative ion electrospray UHPLC-MS selected ion monitoring chromatograms showing the detection of methyl gallate (*m/z* 183) and the dimer (*m/z* 335) for tannic acid after 1 h of methanolysis at 85 °C. Inset: product ion tandem spectrum of the dimer. (c) The relative amounts of methyl gallate (*m/z* 183) and the dimer 3-*O*-galloyl-gallic acid methyl ester (*m/z* 335) formed over time during methanolysis of tannic acid at 85 °C in 2 M HCl (measured using negative ion electrospray UHPLC-MS/MS).

4.3.3 Other sources of hydrolysable gallate

Hydrolysable tannins are the most abundant sources of ester-linked galloyl groups in the plant kingdom. However, some plants produce secondary metabolites containing ester-bound galloyl groups that may contribute to the amount of gallic acid or methyl gallate released by degradative lysis. Among these, flavanoid gallates are relatively common and may be significant sources of hydrolysable galloyl groups. For example, epigallocatechin gallate may constitute over 10% wt/wt of green tea (*Camellia*

sinensis)(262).Other secondary metabolites with hydrolysable galloyl groups include condensed tannin gallate esters, theaflavin gallates (263), theanaphthoquinone gallates, theasinensin gallates (264), galloylquinates (265), anthraquinone and stilbene gallate esters (266), and steroidal gallate esters (267). Alkyl gallate esters such as propyl, butyl and lauryl gallate are also common in plants and microbes (268,269).

4.3.4 Analyte degradation

The analysis of hydrolysable tannins usually relies on determination of gallic acid, methyl gallate, and ellagic acid which are all susceptible to chemical, oxidative and thermal degradation (270,271). For example, gallic acid, methyl gallate and ellagic acid degrade significantly during typical methanolysis conditions, with 50% or more being lost during the first hour (Figure 52a). To illustrate how a control is critical for accurate measurement of hydrolysable tannins, a standard curve prepared using neat methyl gallate (that does not account for degradation) and a methyl gallate standard curve subjected to methanolysis following the same procedure are shown in Figure 52b. A neat standard curve will overestimate gallate levels because it does not control for the significant analyte degradation that occurs during the reaction. Therefore in our new approach, a methanolyzed standard curve and an internal standard were used to control for degradation.

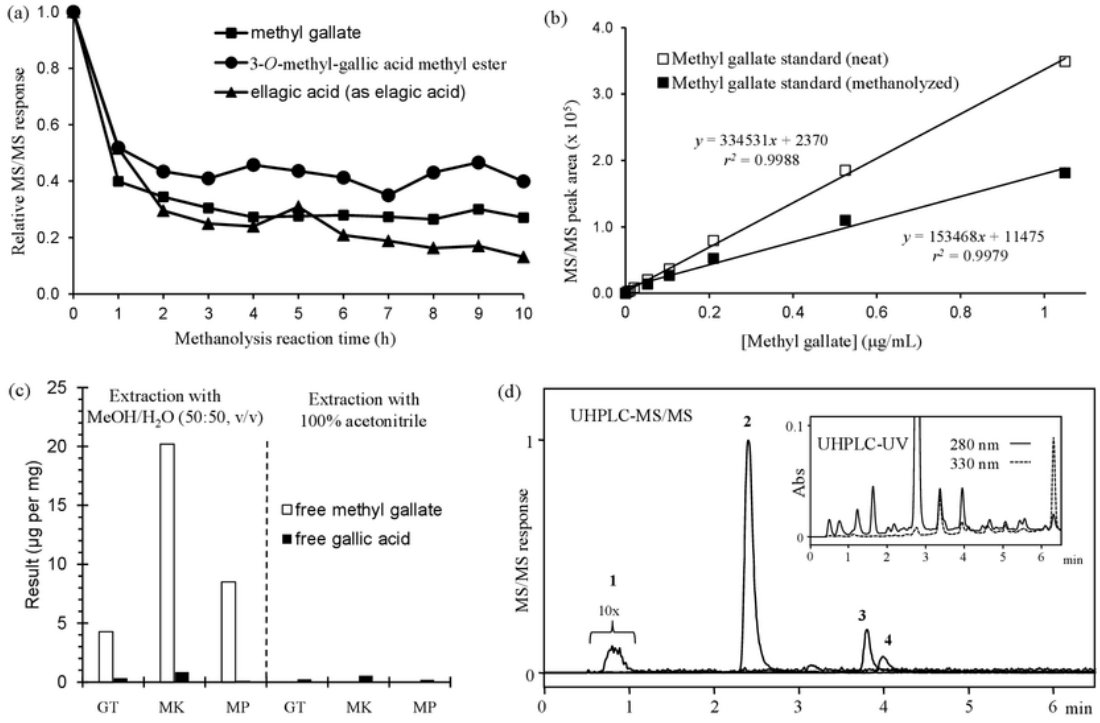

Figure 52. (a) Reaction curves showing the loss of standard methyl gallate, 3-*O*-methyl-gallic acid methyl ester, and ellagic acid during methanolysis for 10 h at 85 °C. The MS/MS peak area response at each time point was normalized to the peak area response of the initial ($t = 0$) time point of the respective analyte. (b) MS/MS peak area standard curves for neat methyl gallate or methanolyzed (85 °C for 5 h) methyl gallate. (c) The amount of apparent free gallic acid and methyl gallate in green tea (GT), mango kernel (MK) and mango peel (MP) measured by using UHPLC-MS/MS after extraction with methanol/water (50:50; v/v) or 100% acetonitrile at 70 °C for 1 h. Values of methyl gallate with acetonitrile extraction were <0.1 μg/mg. (d) UHPLC-MS/MS chromatogram for pomegranate juice methanolyzed at 85 °C for 5 h. Inset: corresponding UHPLC-UV chromatograms (280 nm and 330 nm). 1. Gallic acid (signal 10x); 2. Methyl gallate; 3. Internal standard, 3-*O*-methyl-gallic acid methyl ester; 4. Ellagic acid.

4.3.5 Free gallic acid, methyl gallate and ellagic acid

Plants may contain gallic acid, ellagic acid, and even methyl gallate in the free form (Figure 53)(255,272,273). For the specific measurement of only bound analyte, free gallic acid and/or ellagic acid should be extracted with an aprotic solvent such as acetonitrile and measured separately without

hydrolysis. Because both free and esterified galloyl are converted to methyl gallate during methanolysis, the esterified galloyl content determined by lysis methods is actually a measure of total gallate content. As free gallic acid, ellagic acid and methyl gallate levels are usually low compared with hydrolysable tannins, their contributions are typically neglected. An alternate approach is pre-extraction of samples with organic solvents to remove the free gallic acid, methyl gallate and ellagic acid prior to lysis (253,274). However, soluble hydrolysable tannins can be lost during pre-extraction resulting in underestimation of the levels of these molecules.

Extraction of free gallic acid from food and beverages includes extraction with ethanol/water at 70 °C (275), extraction with methanol at 65 °C (274), or extraction with methanol/water containing HCl (277). A problem with these extraction protocols is that the combination of alcohol, heat and acidic conditions will result in at least partial Fisher esterification of ester-bound gallate to methyl (or ethyl) gallate. For example, the amounts of free methyl gallate and free gallic acid measured in various food samples after extraction with methanol/water (50:50; v/v) or with pure acetonitrile are shown in Figure 52c. Significant quantities of methyl gallate were detected after methanol/water extraction but not after extraction using acetonitrile, and considerable ester-bound gallate was released as methyl gallate during the methanol extraction procedure. This caused the sum of free methyl gallate and gallic acid to appear erroneously high. Therefore, in the measurement of small free phenolic acids and especially those that also occur as ester-bound moieties, an aprotic extraction solvent such as acetonitrile should be used instead of alcohols.

Species [Common name] (part)

3-*O*-methylgallic acid (ester -bound)

Camellia sinensis L. [Green tea] (leaves)
Mangifera indica L. [Mango] (leaves)
Acer rubrum L. [Red maple] (bark)
Diospyros sanza -minika (bark)
Polygonum bistorta L. (rhizome)
Limonium sinense (aerial parts)
Parapiptadenia rigida (Benth .) Brenan (bark)
Glochidion sumatranum
Corylopsis willmottiae
Astilbe chinesis

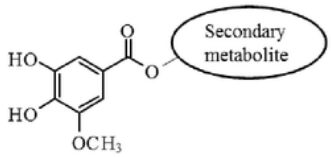

3-*O*-methyl gallic acid (ester bound)

3-*O*-methyl -gallic acid (free)

Smilax glabra Roxb . (rhizome)
Rhodiola crenulata L. (root)
Rhododendron dauricum L. (leaves)
Frankenia laevis L. (foliage)
Atraphaxis frutescens
Geranium collinum
Phycomyces blakesleeanus strain NRRL1555 [microbe]

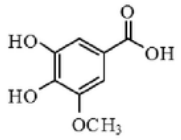

3-*O*-methyl gallic acid

3-O-methyl -gallic acid methyl ester (free)

Acer rubrum L. [Red maple](bark)
Cotoneaster racemiflora Desf . (whole plant)
Acacia arabica Lamk . (stems)
Crinodendron patagua
Myricaria alopecuroides
Crinodendron hookerianum

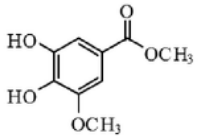

3-*O*-methyl gallic acid methyl ester

Figure 53. Natural occurrences of free or ester-bound 3-*O*-methylgalloyl moieties. The list was compiled using Reaxys (www.reaxys.com) and CAS SciFinder scholar (scifinder.cas.org).

4.3.6 Methanolysis and hydrolysis parameters for HT determination

The reaction conditions that have been used for the determination of hydrolysable tannins are highly variable. Reaction times have ranged from 1 h (252) to 26 h (251), reaction temperatures from 85 °C (252) to 100 °C (253), and acid lysis has used such different conditions as 2 M sulfuric acid in water (251), 1.6 M sulfuric acid in methanol (252), and 2 M methanolic-HCl (253). In the present investigation, the methanolysis reagent was prepared by the addition of acetyl chloride to anhydrous methanol (253) due to its rapid and quantitative yield of carboxylic acid methyl esters (278) and the ability to release HHDP groups from tannins as ellagic acid.

While neat solutions of gallic acid and 3-*O*-methyl-gallic acid yielded maximum levels of methyl gallate after 1 h at 85 °C, tannin-containing food samples and tannic acid required up to 6 h to reach maximum levels of released methyl gallate (Figure 52c). Therefore, a reaction time of 6 h at 85 °C was chosen for subsequent samples to ensure both maximum yield of methyl gallate and conversion of HHDP groups to ellagic acid. A reaction temperature of 85 °C instead of 100 °C also excluded potential vial leakage and sample loss that can occur at ≥100 °C (253).

4.3.7 Internal standard

Since the samples must undergo reaction and preparation steps prior to quantitation, addition of the internal standard 3-*O*-methyl-gallic acid to samples in this method served as an indicator of esterification efficiency and also for detecting and correcting for sample loss during reaction or sample preparation, sample concentration through evaporation, or excessive degradation. For practicality and affordability, the 3-*O*-methyl analogs of gallic acid and methyl gallate, both commercially available and inexpensive, were investigated as internal standards in this work. Since 3-*O*-methyl-gallic acid is converted to 3-*O*-methyl-gallic acid methyl ester during methanolysis (Figure 49), either compound may be added as an internal standard. However, 3-*O*-methyl-gallic acid is preferred because it also serves to verify that esterification is quantitative.

A disadvantage of the use of an internal standard with a different retention time than the analyte is the risk of possible matrix effects (signal suppression or enhancement due to co-eluting compounds) during UHPLC-MS/MS. Since matrix suppression was observed for the internal standard due to interference from some food samples as shown in Figure 54, an internal standard peak area correction was not used. Instead, the internal standard in this method serves as an indicator of esterification efficiency, major sample loss, or analytical system problems. Even without correction of analyte peak areas using an internal standard, the coefficients of variation for replicate samples were typically <5%.

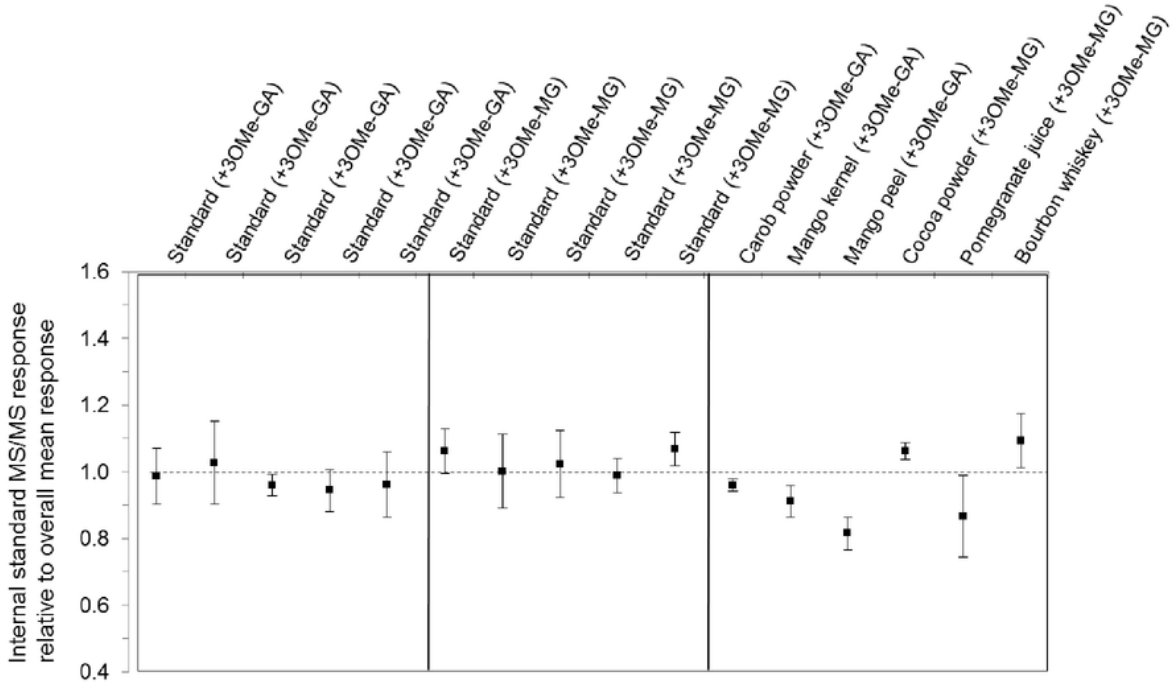

Figure 54. The effect of the sample matrix on the internal standard response. Each data point represents the mean ± SD response of three replicate injections of methanolyzed standards or food samples relative to the overall mean response of all methanolyzed methyl gallate standards (0.05 to 20 µg per mL). All samples were spiked with 20 µg of internal standard prior to methanolysis. The internal standard 3-*O*-methyl-gallic acid (3*O*Me-GA) is converted to and measured as 3-*O*-methyl-gallic acid methyl ester (3*O*Me-MG) during methanolysis.

A minor caveat with the use of the 3-*O*-methylated internal standard is that the 3-*O*-methylated gallic acid moiety is known to occur sparingly in nature, such as minor 3-*O*-methylgalloylated catechin constituents in *Camellia sinensis*. However, these rare natural occurrences of 3-*O*-methylgalloyl moieties usually involve only trace amounts. A list of species reported to contain 3-*O*-methylgalloyl moieties (free and esterified) is provided in Figure 53. Since three of the food samples analyzed in this work were among these species (mango, maple and green tea), one sample of each was prepared and reacted without internal standard to check for background levels of any natural 3-*O*-methylgalloyl moieties. Only the methanolyzed *Camellia sinensis* samples contained a detectable quantity of 3-*O*-

methyl-gallic acid methyl ester, and this amount was less than 5% of the peak area of the internal standard.

4.3.8 UHPLC-MS/MS determination

UHPLC-MS/MS chromatograms (Figure 52d) for a methanolyzed sample of pomegranate juice showed peaks for gallic acid (trace), methyl gallate, internal standard, and ellagic acid. Methyl gallate standard curves for methanolyzed standards were linear over the range 0.05 to 20.00 µg/mL ($r^2 > 0.999$) with a limit of quantitation (LOQ) of 0.05 µg/mL and a limit of detection (LOD) of 0.01 µg/mL. Calibration curves for gallic acid showed good linearity ($r^2>0.993$) over the range 1 to 100 µg/mL with a LOQ of 0.1 µg/mL and a LOD of 0.02 µg/mL.

Quantitative measurements of free gallic acid, total gallic acid and ester-bound gallic acid in methanolyzed food and beverage samples were obtained using UHPLC-MS/MS and are summarized in Table IX. Free methyl gallate was not detected in any of the samples extracted using acetonitrile for the measurement of free methyl gallate and gallic acid (no hydrolysis), but trace amounts of gallic acid were often detected in samples and standards after methanolysis. It is possible that the methanolysis reaction is quantitative, but small amounts of methyl gallate convert to gallic acid post-reaction when water is present.

Although the focus of this method was the determination of free and ester-bound galloyl groups in hydrolysable tannins, the feasibility of quantitation of ellagic acid was also investigated. Methanolyzed ellagic acid standards produced calibration curves with good linearity from 1 to 75 µg/mL ($r^2 > 0.999$) using UHPLC-MS/MS with negative ion electrospray, but the quantitative measurements of ellagic acid in standards as well as in food and beverage samples showed unacceptably high intraassay and interassay coefficients of variation (>15%). Ellagic acid was detected in the three methanolyzed samples known to contain ellagitannins, raspberry, blackberry, and pomegranate, at nominal

concentrations of 6.1 µg/mg, 2.2 µg/mg, and 626 µg/mL, respectively. Without further development and validation, this UHPLC-MS/MS approach for the analysis of ellagic acid should be considered as qualitative. Ellagic acid may be measured quantitatively using HPLC-MS/MS using an atmospheric pressure chemical ionization instead of electrospray (279). The use of UHPLC-MS/MS with atmospheric pressure chemical ionization for the measurement of gallic acid, methyl gallate and ellagic acid was investigated, and while ellagic acid measurement was acceptable, the sensitivity for the measurement of methyl gallate and gallic acid was significantly decreased relative to electrospray. Therefore, further development of the atmospheric pressure chemical ionization approach was not pursued. Representative standard curves for gallic acid and ellagic acid for both MS/MS and UV detection are provided in Figure 55.

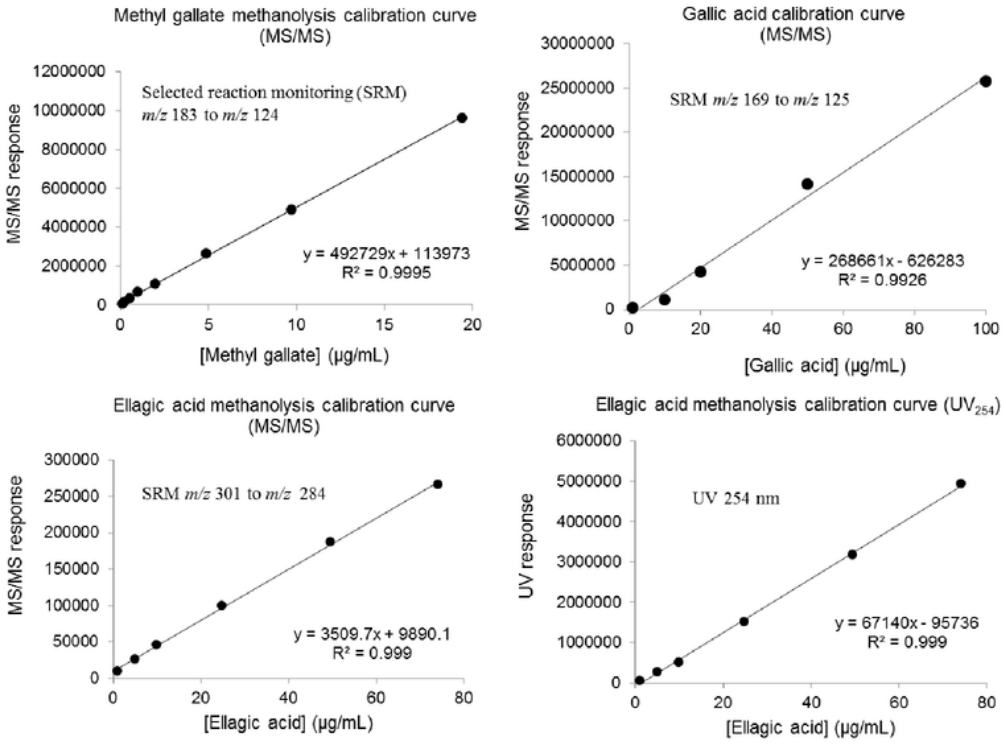

Figure 55. Calibration curves for gallic acid, methyl gallate, and ellagic acid

The advantages of this new UHPLC-MS/MS approach for the determination of hydrolysable tannins in food and beverage samples with previous methods are shown in Table X. Our UHPLC-MS/MS approach requires 10 to 20 mg of solid sample or 1.0 mL of liquid sample instead of 100 to 200 mg of solid sample (251,253) or 20.0 mL of liquid sample (253). The chromatographic analysis time per sample is 7 min instead of 40 min[21] or 15 min (252). To control for degradation due to methanolysis, a methanolyzed control curve was used instead of a single point correction (252) or no control (251,253). Like Lei, *et al*. (253) methanolic-HCl was used, but the reaction temperature was lowered from 100 °C to 85 °C to avoid potential vial leakage or overpressure problems. Reproducible results were obtained

(typical triplicate sample $c_v < 0.05$) with simple equipment. Our 6-h reaction time was shorter than the 20-h reaction of Hartzfeld, *et al*. (252) or the 26 h reaction time used by Inouye and Hagerman (250). The use of tandem mass spectrometry with multiple SRM transitions improved the selectivity and specificity of measurement by reducing the incidence of potential interference from other constituents within complex food matrices. The use of an internal standard increased the overall robustness of the method, and the accuracy was significantly enhanced by the use of a control curve constructed from methanolyzed methyl gallate samples.

TABLE IX. UHPLC-MS/MS QUANTITATIVE ANALYSIS OF FREE, TOTAL AND BOUND GALLIC ACID IN SELECTED FOODS AND BEVERAGES.[A,B]

Sample	Free gallic acid (CH_3CN extract)[c]	Total gallic acid (methanolysis)[d]	Bound gallic acid (total - free)[d]
Cocoa (*Theobroma cacao*) powder	< LOQ	< LOQ	<LOQ
Maple (*Acer* sp.) syrup, Grade A	< LOQ	< LOQ	<LOQ
Bourbon whiskey (oak barrel aged)	3.48 ± 0.03	8.50 ± 0.55	5.02 ± 0.58
Green tea (*Camellia sinensis*)	0.24 ± 0.01	22.3 ± 3.3	22.1 ± 3.3
Carob (*Ceratonia siliqua*) pod	0.20 ± 0.01	5.53 ± 0.08	5.33 ± 0.09
Mango (*Mangifera indica*) kernel	0.55 ± 0.03	47.7 ± 3.2	47.1 ± 3.2
Mango (*Mangifera indica*) peel	0.21 ± 0.01	5.90 ± 0.50	5.69 ± 0.50
Pomegranate (*Punica granatum*) juice	5.63 ± 0.92	67.6 ± 1.3	62.0 ± 2.2
Raspberry (*Rubus idaeus*) fruit	< LOQ	0.34 ± 0.25	0.34 ± 0.25
Blackberry (*Rubus fruticosus*) fruit	< LOQ	0.31 ± 0.03	0.31 ± 0.03

[a] Triplicate (total gallic acid) or duplicate (free gallic acid) determinations (mean ± SD)

[b] µg per mg (solids) or mL (liquids)

[c] LOQ of 0.1 µg/mL

[d] LOQ of 0.05 µg/mL

TABLE X. COMPARISON OF PREVIOUS HYDROLYSIS AND METHANOLYSIS METHODS WITH NEW METHANOLYSIS METHOD FOR THE DETERMINATION OF HYDROLYSABLE TANNINS.

	Rhodanine method, UV & TLC[251]	**KIO_3 method, HPLC-UV** [252]
Year	1988	2002
Citations	192	158
Hydrolysis reagent	2M H_2SO_4	MeOH + 1.6 M H_2SO_4
Reaction time	100 °C for 26 h	85 °C for 20 h
Sample processing	10-12 steps	12-14 steps
Derivatization	Rhodanine (colorimetric)	KIO_3 Oxidation (colorimetric)
Methanolysis control	No	Single-point correction
Internal standard	No	No
Detection	UV	HPLC-UV
(U)HPLC run time	none	15 min
Gallotannins (galloyl)	Gallic acid-Rhodanine (UV)	Methyl gallate-KIO_3 product (UV)
Ellagitannins (HHDP)	Ellagic acid (qualitative; TLC)	None
Advantages (+) and disadvantages (-)	(+) Simple instrumentation (+) Limited stability investigation (-) Complex procedure (-) Colorimetric derivatization	(+) Some control for methanolysis loss (-) Complex procedure (-) Colorimetric derivatization

	Methanolic-HCl, HPLC-UV[253]	**Methanolic-HCl, UHPLC-UV-MS/MS** (present work)
Year	2001	2015
Citations	59	new
Hydrolysis reagent	Methanolic-HCl	Methanolic-HCl
Reaction time	100 °C for 1 h	85 °C for 6 h
Sample processing	5 steps	6 steps
Derivatization	--	--
Methanolysis control	No	Methanolyzed methyl gallate standard curves
Internal standard	None	3-*O*-methyl-gallic acid or 3-*O*-methyl-gallic acid methyl ester
Detection	HPLC-UV	UHPLC-MS/MS
(U)HPLC run time	40 min	6.5 min
Gallotannins (galloyl)	as methyl gallate (UV)	as methyl gallate (MS/MS)
Ellagitannins (HHDP)	Ellagic acid (UV)	Ellagic acid (qualitative; MS/MS)
Advantages (+) and disadvantages (-)	(+) Simple procedure (+) Quantitative for HHDP (-) No internal standard control for reaction loss	(+) MS/MS specificity (methyl gallate) (+) Greater sensitivity (methyl gallate) (+) Methanolysis control curves (+) Internal standard control for reaction loss (+) UHPLC faster than HPLC methods

4.4 Potential applications

The determination of hydrolysable tannins has direct application to economically important consumables such as fruit, wine, green and black tea, barrel-aged spirits, herbs, spices, and botanical dietary supplements. Since gallic acid is a common phenolic acid found in both free and conjugated forms in many different classes of molecules within plants, fungi, microbes, and animal products, the practical applications for the accurate determination of ester-bound gallate go beyond the determination of hydrolysable tannins. This method provides faster and accurate determination of free, total, and ester-bound gallate groups in small amounts of almost any solid or liquid sample.

Flavanol gallates in green tea, for example, have been the subject of a great deal of research regarding probable health benefits. Because flavanol gallates are the only significant sources of esterified gallate within *Camellia sinensis*, determination of ester-bound gallate in these products might serve as alternative approach to the measurement of total catechin gallate content. Ester-bound small phenolic acids (such as protocatechuic acid, 4-hydroxybenzoic acid, vanillic acid, caffeic acid, cinnamic acid, ferulic acid, quinic acid, coumaric acids, sinapinic acid, and syringic acid) commonly occur as secondary metabolites in many plants (280). The framework of the approach used here – a controlled methanolysis reaction with internal standards followed by UHPLC-MS/MS determination of both free and methanolyzed amounts – could be adapted for the determination of other ester-bound small phenolic acids by addition of the appropriate SRM transitions and appropriate validation steps.

The determination of ester-bound (hydrolysable) galloyl groups following sample hydrolysis is a common approach used for the determination of hydrolysable tannins. Limitations and sources of error in these measurements were identified, examined and resolved in most cases. These include the excessive variation in hydrolysable mass fraction, undesirable esterification during the extraction of free analyte, other sources of bound gallate, degradative loss of analyte during reaction, and the resistance of

depside bonds to hydrolysis. An accurate, specific, sensitive, and fast UHPLC-MS/MS method for the determination of ester-bound galloyl groups (total – free) was developed that may be applied to either solid or liquid samples.

4.5 Conclusion

The determination of bound (hydrolysable) galloyl groups following sample hydrolysis is a common approach used for the determination of HT content. Limitations and sources of error in the measurement were identified, examined and resolved in most cases. These include the excessive variation in hydrolysable mass fraction, undesirable esterification during the extraction of free analyte, other sources of bound gallate, degradative loss of analyte during reaction, and the resistance of depside bonds to hydrolysis. An accurate, specific, sensitive, and fast UHPLC-MS/MS method for the determination of ester-bound galloyl groups (total – free) was developed that may be applied to either solid or liquid samples. In addition to providing an improved method for HT determination which was applied to measurement of bound gallate in the *Zygogonium sp.* pigment (Chapter 3), the method should be useful for applications requiring accurate determination of bound galloyl groups and might be extended to the determination of other small phenolic acids.

CHAPTER 5: STRUCTURE ELUCIDATION OF NOVEL TRICHOTOMINE MALONYLGLYCOSIDES FROM *CLERODENDRON TRICHOTOMUM*

5.1 INTRODUCTION

Clerodendron trichotomum Thunb. (Verbenaceae), also known as the Japanese kusagi berry, has been used historically as a textile dye. The intensely blue colored *bis*-indole alkaloid trichotomine and two trichotomine glycosides, trichotomine *N*-β-D-glucoside (trichotomine G_1) and trichotomine *N,N*-di-(β-D-glucoside) (trichotomine G_2) were previously reported from the fruits and structurally characterized using NMR spectroscopy, x-ray crystallography, and synthetic methods (281).

Trichotomine displays a rare set of properties which make it a leading candidate as a natural colorant alternative (16). Favorable properties include its high blue color intensity, trichotomine glycosides water solubility, and apparent lack of toxicity. In a 2002 study, dosing rats of up 3.2 g/kg of kusagi color extract daily did not display any toxicological effects (difference in survival rate, weight, food and water intake, organ weight, gross pathology, ophthalmology, histopathology, or blood biochemistry after one month (282).

In this dissertation, the structure elucidation of three new trichotomine 6-*O*-malonyl-β-*O*-glycosides, trichotomine G_3 (**2**), G_4 (**3**), and G_5 (**4**) (Figure 56) is reported using 2D NMR and high resolution tandem mass spectrometry ($HRMS^2$). In addition, $HRMS^2$ identification of three additional analogs (trichotomine G_6, G_7, and G_8) is described. Preliminary investigation of analog color stability of the purified trichotomines under various temperature (0, 25, 45 °C) and pH (1, 4, 7, 10) conditions is also reported in this work.

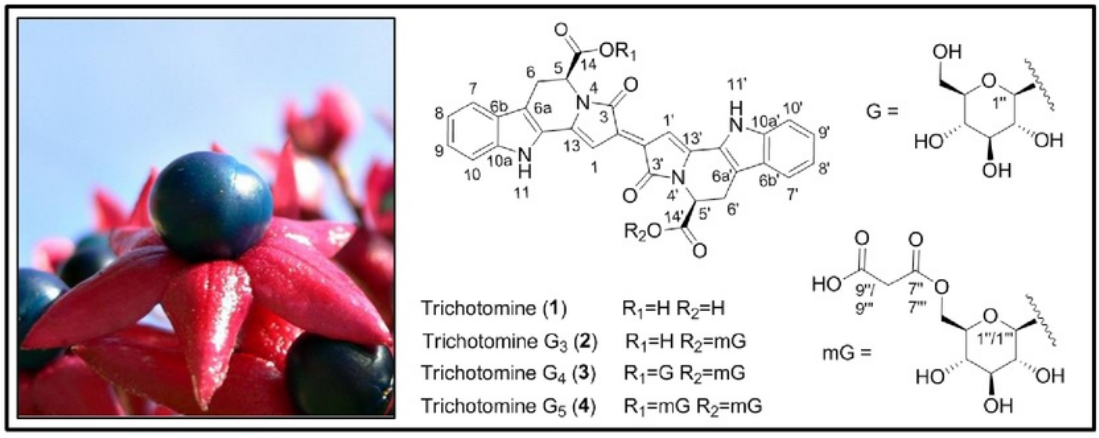

Figure 56. Photograph of the kusagi berry and numbered chemical structures of the new analogs characterized in this work: trichotomine (**1**), trichotomine G_3 (14-*O*-(6-*O*-malonyl-β-D-glucupyranosyl)-trichotomine) (**2**), Trichotomine G_4 (14-O-(6-*O*-malonyl-β-D-glucupyranosyl)-14'-*O*-(β-D-glucupyranosyl)-trichotomine) (**3**), and trichotomine G_5 (14,14'-*O*-(6-*O*-malonyl-β-D-diglucupyranosyl)-trichotomine) (**4**). mG = malonylglycoside.

5.2 Materials and Methods

5.2.1 Materials

High-performance liquid chromatography (HPLC) grade or better solvents were purchased from Fisher Scientific (Hanover Park, IL). All water was prepared using an Elga Purelab water purification system. Ammonium formate, ammonium acetate, acetic acid, hydrochloric acid, ammonium bicarbonate, and other common buffers and reagents were ACS grade or better and were also obtained from Fisher Scientific. High-purity (99.95%+) deuterated NMR solvents were purchased from Cambridge Isotope Laboratories (Andover, MA). Trichotomine (**1**) (250 mg) was obtained from San Ei Gen F.F.I. (Osaka, Japan) where it was chemical synthesized according to a previously published method (4) and purified (HPLC, 98.0%+) prior to use by semipreparative chromatography (Appendix F). One metric ton of whole fruits of *C. trichotomum* were collected in Japan (GPS Long. 107° 40' E, Lat. 33° 39' N) in September 2009 by China Agricultural University. The species was taxonomically

identified by comparison of the morphological characteristics of the field population with published descriptions of taxonomically verified specimens of *C. trichotomum* and also through the verification of the presence of trichotomine as a chemotaxonomically specific metabolite.

5.2.2 Kusagi berry pigment extraction

For the initial extraction performed by San Ei Gen F.F.I., 500 kg of kusagi fruits were immersed in ethanol/water (48:52, v/v) for 24 hours, filtered (7 mesh sieve), and adjusted to pH 4.0 using concentrated sulfuric acid. A second extraction was performed on two different 250 kg portions of separated kusagi fruits as follows. The fruits (250 kg) were immersed in 500 kg of ethanol/water (48:52, v/v) overnight. The extract was filtered using a 5 μm polypropylene wound cartridge filter (250 mm), and then adjusted to pH 4.0 using concentrated sulfuric acid. The three extracts were combined and adsorbed onto 20 L of Diaion HP-20 resin (Mitsubishi Chemical, space volume 2), the resin was washed with 60 L of ethanol/water (48:52, v/v), and then eluted with 80 L of ethanol/water (95:5, v/v). The eluate (80 L) was diluted with 80 L of water. The Diaion HP-20 resin extraction process was with another 20 L of resin. The 80 L of eluate was evaporated under vacuum for a final yield of 1.8 kg of extract. The extract was reconstituted in ethanol/water (65:35, v/v).

The extract was shipped to UIC for further purification and characterization. Individual analogs were purified from the extract as follows. A 100 mL portion of the extract was defatted with hexane (400 mL x 4). A 10 mL aliquot of the defatted extract was evaporated to yield 752 mg blue solids which were dissolved in 14 mL methanol (54 mg/mL) and filtered (0.2 μm). This material was used for HPLC-UV-HRMS analysis and HPLC purification.

For analysis of the trichotomine crude extract prior to semi-preparative purification, a 1 mL aliquot of the extract was centrifuged at 12,000 x *g* for 15 min. Then, a 20 μL aliquot of the supernatant was diluted to 100 μL with water and used for development of the chromatographic method and for HPLC-

PDA-HRMS^2 analysis. Fractions from the semi-preparative purification were diluted, centrifuged at 12,000 x *g* for 15 min, and analyzed by flow injection analysis for HRMS^2 characterization (Section 5.3.1).

5.2.3 Semi-preparative purification

Trichotomine constituents were purified by repeated injections onto a C_{18} YMC-Pak Semi-preparative column (300 x 10 mm 5μm) using a Shimadzu Prominence XR HPLC system with a Shimadzu SPD-20A dual wavelength UV detector (360 nm, 650 nm). The method parameters were as follows: flow rate, 5 mL/min; mobile phase A (MPA), water containing 0.1% formic acid; mobile phase B (MPB), acetonitrile containing 0.1% formic acid. A 50-min gradient (0.4% MPB/min) was used from 30% to 100% MPB. The synthetic trichotomine standard was found to be significantly degraded and was purified using semipreparative HPLC with the same mobile phase above with a 20 min gradient program from 40% MPB to 100% MPB.

5.2.3 2D-NMR analysis

Individual purified trichotomine analogs were analyzed by using ^{1}H, DEPT-Q, COSY, HSQC, and HMBC data sets obtained on a Bruker Avance 900 MHz NMR spectrometer. All purified material was dried thoroughly under high vacuum or under a stream of N_2 gas overnight and reconstituted in 150 μL of 99.9%+ DMSO-d_6 prior to analysis. Sample amounts ranged from 0.5 to 1.5 mg. Data processing was performed using MestReNova v. 6.0 software.

5.2.4 HPLC-UV-HRMS^2 analysis

HPLC-UV-HRMS^2 analysis was performed using a Shimadzu Prominence XR HPLC system equipped with an SPD-M20A photodiodearray detector and interfaced with a Shimadzu ion trap – time of flight (IT-TOF) mass spectrometer. The UV spectrum was scanned from 200 to 800 nm with a 4 nm bandwidth and no reference correction. Mass spectra and tandem mass spectra were acquired using positive and negative ion electrospray ionization with polarity switching. Most MS and MS^2 data were collected in data-dependent MS^2 mode with a positive and negative mode MS scan range of *m/z* 400-1000 and *m/z* 100-1000 for automatic MS^2. To avoid long MS loop times, separate experiments for analyzing higher MW (1000-1500 Da) analogs were performed using an MS scan range of *m/z* 1000-1500 and an MS^2 scan range of *m/z* 500-1500. In the case of trichotomine analog minor isomers, the tandem MS spectra were collected for the major isomer only unless otherwise noted. The HRMS analysis parameters were as follows: Detector voltage of 4.2 kV for positive mode and -3.5 kV negative mode, CDL and block temperature 200 °C, N_2 nebulizing gas, N_2 drying gas at 1.5 L/min. Argon was used as the collision cell gas at a CID collision energy of 70% and an automatic MS^2 ion selection trigger of 70% BPC. Some MS^n analyses were performed in manual mode using custom scan ranges such as the MS^3 analysis of trichotomine G_6 (*m/z* 1000-1200 MS, *m/z* 500-1200 MS^2, *m/z* 200-600 MS^3, CID collision energy 80%, CID collision gas 80%).

5.2.5 Color stability

Buffer solutions were prepared at pH 1 (100 mM KCl), pH 3 (100 mM ammonium formate), pH 7 (100 mM ammonium acetate), and pH 10 (100 mM ammonium bicarbonate). Approximately 250 µg of each purified trichotomine analog was dissolved in 0.5 mL of methanol transferred to six Fisherbrand 4 mL screw cap glass vials. Each solution was diluted to 1 mL by addition of 0.5 mL of buffer for a final

solution concentration of approximately 0.25 mg/mL in methanol/buffer (pH 1, 3, 7, or 10) (50:50, v/v). Vials were protected from light and stored at 4 °C (pH 7), 22 °C (pH 1, 3, 7, 10) (50:50, v/v), or 45 °C (pH 7). Photographs were taken initially and then every seven days for six weeks. The pH of each solution was retested after six weeks and all were within ±0.5 unit of the initial buffered pH. The UV/Vis readings for molar extinction coefficients were acquired using a Hewlett Packard 8452A diode-array spectrophotometer with a 1 cm quartz cell.

5.3 Results and Discussion

5.3.1 High resolution mass spectrometry

During HPLC-HRMS analysis of the crude kusagi extract, trichotomine (retention time 17.8 min. $[M+H]^+$ *m/z* 533.1464) was identified by coelution and by identical HRMS and HRMS/MS with purified synthetic standard trichotomine. Seven more polar blue pigmented trichotomine analogs (G_1-G_7) were observed eluting earlier between 9.2 and 14.3 min (Figure 57). The (5S,5S') absolute configuration at the two -CO_2H attachment points of natural trichotomine from *C. trichotomum* was previously established by x-ray crystallography (281). The coelution of natural trichotomine with the (5S,5S')-synthetic trichotomine standard used in this work stereospecifically synthesized using L-tryptophan (283) confirmed the (5S,5S') natural trichotomine. The (5S,5S') stereoconfiguration was assumed for all other trichotomine analogs in this work. No further confirmation of these stereocenters was performed. The HRMS and HRMS/MS analyses of these pigments are shown in Figure 61-68 and summarized in Table XI and XII. The corresponding semi-preparative HPLC-UV chromatogram for the purification of trichotomine G_1-G_7 is shown in Figure 58.

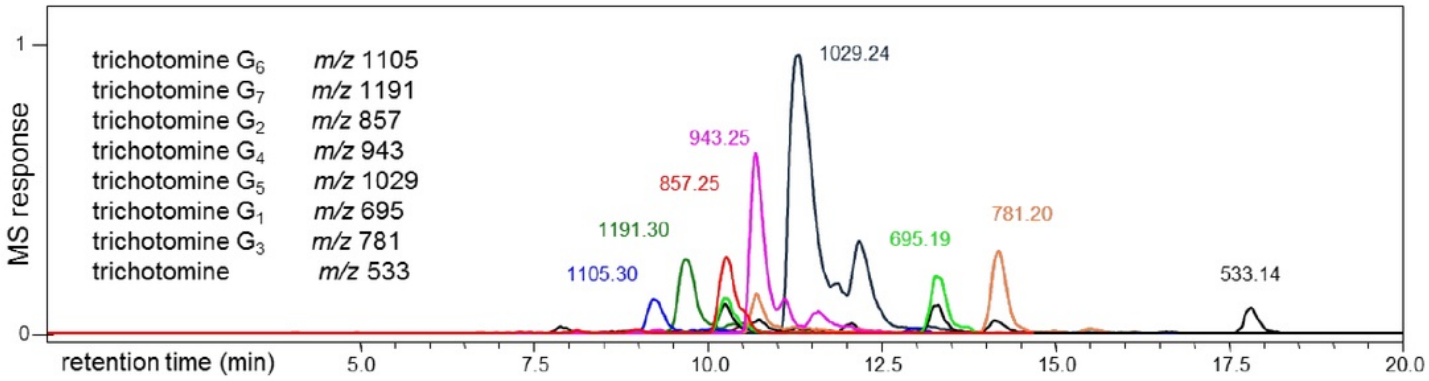

Figure 57. Computer-reconstructed positive ion electrospray HPLC-HRMS chromatograms of protonated trichotomine and analogs from kusagi berry extract. The trichotomine analog corresponding to each extracted *m/z* value is indicated.

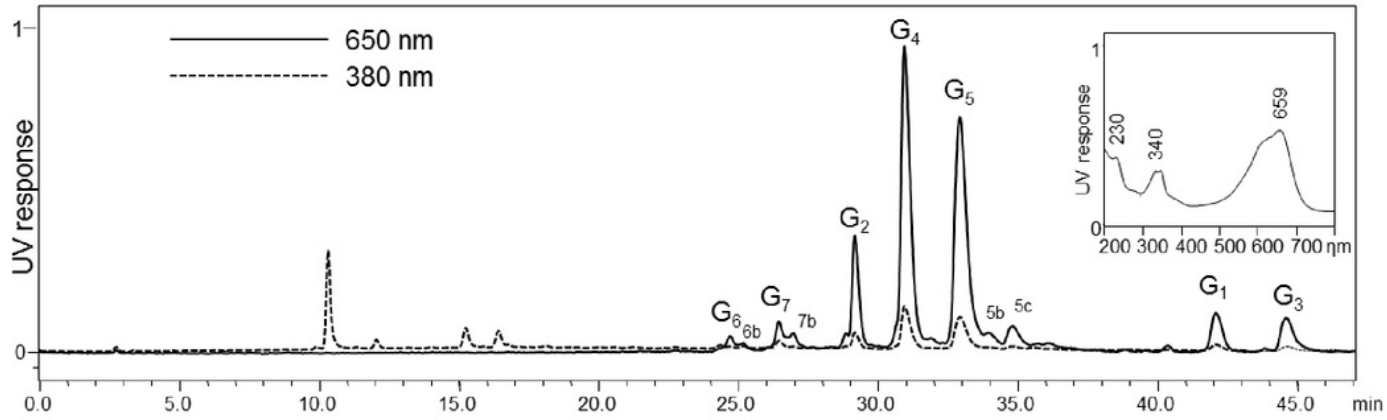

Figure 58. Semipreparative HPLC-UV chromatogram of kusagi berry extract. The UV spectrum of trichotomine G_4 is shown in the inset. The trichotomine aglycone (not shown) eluted later at approximately 54 min during the 100% acetonitrile wash phase.

5.3.1.1 Trichotomine MS/MS

No high resolution tandem mass spectra of trichotomine have been previously published. In this work, the MS/MS data for trichotomine (Figure 61) showed a positive mode fragment ion of *m/z* 487.14 ($-CO_2H$) and a small signal of 444.1632 ($-2CO_2H$) corresponding to losses of the carboxylic acid groups. The major positive mode ion of *m/z* 415.15 ($-2\ C_2H_3O_2$) is possibly due to loss of the CO_2H groups with successive rearrangement while the *m/z* 223.09 ion arises from the loss of a CO_2H group along with central cleavage. The negative mode MS/MS fragmentation of trichotomine also showed ions corresponding to the loss of one and two CO_2 groups (*m/z* 487.13 and 443.14), while the negative mode ions of m/z 223.08 and 267.07 are likely central cleavage products. Possible ion structures for some of these product ions are shown in Figure 59.

5.3.1.2 Trichotomine G_1-G_5 MS/MS

The lowest molecular weight trichotomine analog ($[M+H]^+$ *m/z* 695.2007, $C_{36}H_{30}N_4O_{11}$, 2.6 ppm) showed a positive mode MS/MS neutral loss of 162 ($C_6H_{10}O_5$) typical of a hexose residue (286 to give the product ion corresponding to protonated trichotomine (*m/z* 533) (Figure 62). A more polar trichotomine analog ($[M+H]^+$ *m/z* 857.2587, $C_{42}H_{40}N_4O_{16}$, 8 ppm) showed two positive mode MS/MS losses of 162 to give the product ions *m/z* 695 (protonated trichotomine monoglucoside) and *m/z* 533 (protonated trichotomine). The negative ion mode HRMS spectrum of trichotomine G_1 ($[M-H]^-$ *m/z* 693.1773) showed in-source fragment ions consistent with the loss of CH_2OH from glucose (*m/z* 663), the loss of CO_2 from trichotomine (*m/z* 649) and the neutral loss of glucose ($C_6H_{10}O_5$) to give *m/z* 531. The trichotomine G_2 negative ion mode mass spectrum (Figure 63) showed the expected major ion of *m/z* 693 due to in-source loss of 162 (glucose). The single ion of *m/z* 503 observed using negative mode MS^2 matched no reasonable formula and was probably noise. These data suggest the dereplication of two

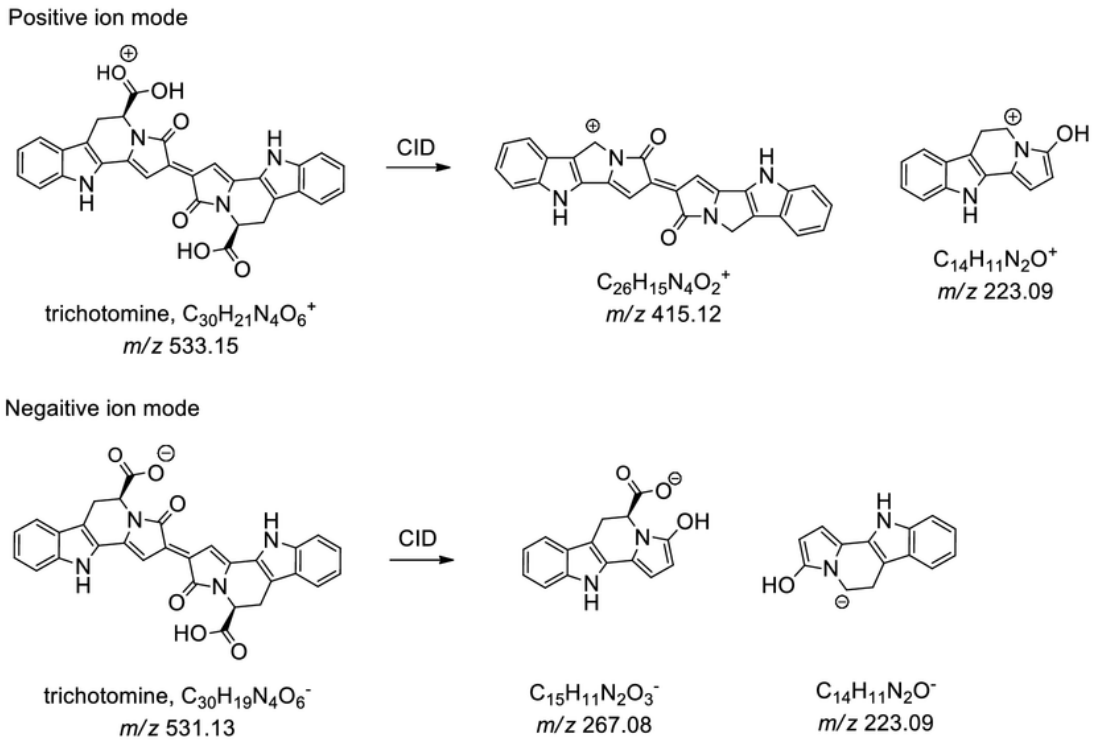

Figure 59. Possible product ion structures for ions observed in the electrospray positive and negative ion tandem mass spectra of trichotomine.

previously published trichotomine analogs, trichotomine β-D-glucose (trichotomine G_1, MW 694) (281) and trichotomine di-β-D-glucose (trichotomine G_2, MW 856) (284).

The next highest MW trichotomine analog ($[M+H]^+$ *m/z* 781.1997, $C_{39}H_{32}N_4O_{14}$, 0.1 ppm), named trichotomine G_3 (**2**), showed MS/MS neutral losses of 248 in both positive and negative ion mode to give trichotomine product ions (Figure 64). A loss of 86 in positive mode MS/MS to give the product ion corresponding to trichotomine glycoside (*m/z* 695) along with loss of 248 suggests trichotomine with a malonylglycoside ($C_3H_2O_3$, malonyl = m, 86 + $C_6H_{10}O_5$, glucose = Glu, 162) attachment. The negative mode tandem mass spectrum also showed a loss of 44 (CO_2) and a loss of 88 ($2CO_2$).

The exact mass of the trichotomine G_4 (**3**) analog ($[M+H]^+$ *m/z* 943.2546, $C_{45}H_{42}N_4O_{19}$, 2.5 ppm, major isomer) eluting after trichotomine G_2 (Glu_2) was consistent with trichotomine with two glycosides and one malonyl group attached (m_1Glu_2, 410). The MS/MS spectra showed losses of 248 (m_1Glu_1) and 410 (m_1Glu_2) in positive mode with losses of 248 and 206 ($Glu_1 + CO_2$) in negative mode (Figure 65). As established later by NMR (Section 5.3.2), the attachment points of the glycosides are to the trichotomine carboxylic acid groups. Whether the attachments for trichotomine G_4 are split (COO-Glu_1, COO-m_1Glu_1) or monosubstituted (H, m_1Glu_2) is not conclusive from the tandem mass spectra alone. The negative mode loss of 206 (CO_2Glu_1) along with a negative mode in-source fragment ion of *m/z* 649.1865 ($C_{35}H_{29}N_4O_9$, -10.8 ppm) corresponding to the loss of 292 ($m_1Glu_1CO_2$) supports a (COO-Glu_1, COO-m_1Glu_1) attachment pattern with substituents on both carboxylic acids for trichotomine G_4. This substitution pattern is further supported over a (COO-H, COO-m_1Glu_2) attachment pattern by the lack of a major negative mode MS/MS loss of 44 (CO_2) as was observed for trichotomine G_1 and G_3 which both have free carboxylic acid groups. The two minor isomers observed in the HRMS chromatogram of trichotomine G_4 were not purified or analyzed separately by MS/MS in this work.

The exact mass of the most abundant trichotomine analog, trichotomine G_5 (**4**) ($[M+H]^+$ *m/z* 1029.2520, $C_{48}H_{44}N_4O_{22}$, -0.6 ppm, major isomer) was consistent with trichotomine having two malonyl and two glycosides attached (m_2Glu_2, 496). The positive mode tandem mass spectrum showed two major ions (*m/z* 781 and *m/z* 533) corresponding to one and two losses of 248 (m_1Glu_1), respectively. The negative ion MS/MS ions of *m/z* 983 and 735 correspond to losses of CO_2 and $m_1Glu_1+CO_2$, respectively (Figure 66). The NMR analysis (Section 5.3.2) later confirmed a symmetric attachment of one malonylglycoside group to each carboxyl group of trichotomine G_5 (COO-m_1Glu_1, COO-m_1Glu_1). Trichotomine G_5 shows a minor negative ion MS^2 loss of CO_2 from a malonyl group whereas the disubstituted analog trichotomine G_4 (COO-m_1Glu_1, COO-Glu_1) does not. This is likely due to trichotomine G_5 having twice the abundance of malonyl groups and the apparent greater lability of the

(CO_2Glu_1) loss compared with trichotomine G_4. The positive and negative mode MS fragmentation losses of trichotomine G_4 and G_5 are shown in Figure 60. The second most abundant isomer observed in the HRMS chromatogram (trichotomine G_{5c} in Figure 58) was isolated for separate MS/MS analysis and also showed positive mode tandem MS/MS ions of *m/z* 781 and *m/z* 533 of similar abundance (data not shown) corresponding to two losses of 248 (m_1Glu_1). No negative mode ions were observed.

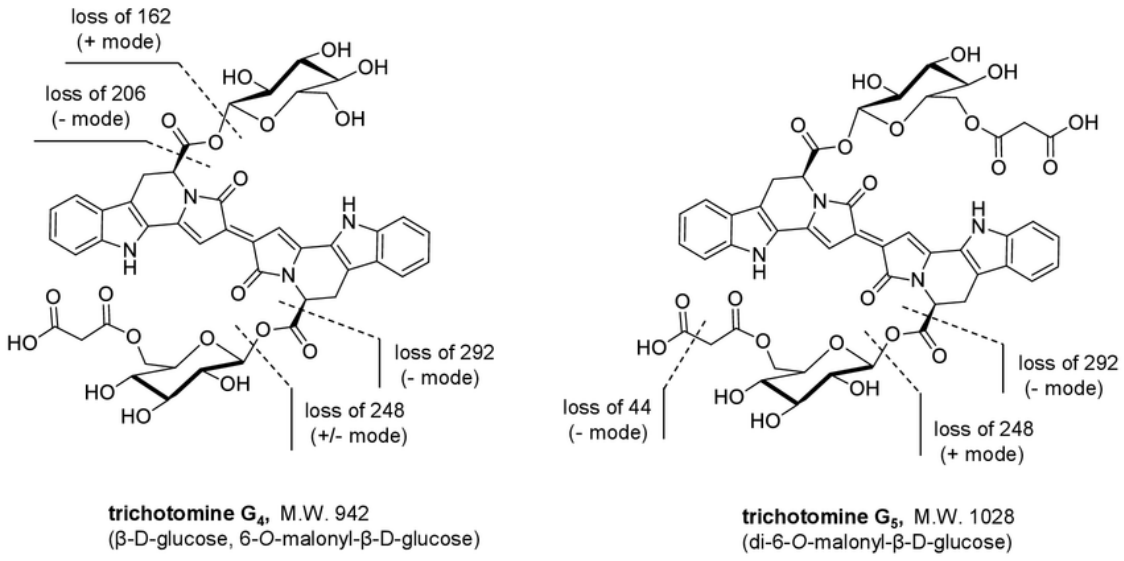

Figure 60. Neutral fragmentation losses observed in the positive and negative mode tandem mass spectra of trichotomine G_4 and trichotomine G_5.

5.3.1.3 Trichotomine G_6 and G_7 MS/MS

The higher molecular weight analogs trichotomine G_6 ($[M+H]^+$ *m/z* 1105.2977, $C_{51}H_{52}N_4O_{24}$, -6.6 ppm, major isomer) and G_7 ($[M+H]^+$ *m/z* 1191.3045, $C_{54}H_{54}N_4O_{27}$,, -0.8 ppm, major isomer) were isolated and analyzed by tandem mass spectrometry but were not structurally characterized further in this work. Trichotomine G_6 showed a positive mode MS^2 loss of 162 (Glu) and to give the product ion of *m/z* 943 which lost 410 (m_1Glu_2) during MS^3 to give the protonated trichotomine ion of *m/z* 533

(Figure 67). The ions of *m/z* 855 and 693 in the negative mode tandem mass spectrum of trichotomine G_6 correspond to losses of 248 (m_1Glu_1) and 410 (m_1Glu_2). Trichotomine G_7 showed a loss of 658 (m_2Glu_3) to give protonated trichotomine *m/z* 533 and also a loss of 410 (m_1Glu_2) in positive mode tandem mass spectrometry (Figure 68). Negative mode MS/MS showed an unknown ion of *m/z* 1007, a loss of 248 (m_1Glu_1) and a loss of 454 ($m_1Glu_2 + CO_2$). From these data, the trichotomine G_6 and G_7 analogs have m_1Glu_3 and m_2Glu_3 attachment compositions, respectively. A loss such as $m_1Glu_2 + CO_2$ for trichotomine G_7 suggests cleavage at the carboxylic acid group of one side of the trichotomine molecule. This along with the loss of m_1Glu_1 (248) suggests a m_1Glu_2, m_1Glu_1 attachment pattern for trichotomine G_7.

The more extensively glycosylated analogs trichotomine G_6 and G_7 appeared as two resolved peaks during HPLC-HRMS analysis of the crude extract (Figure 57) but eluted as two split peaks during semi-preparative HPLC purification (Figure 58). The minor semipreparative fraction trichotomine G_{7b} was collected and analyzed separately by MS/MS and showed the same positive (*m/z* 781, 533) and negative (*m/z* 1007, 941, 735) product ions with no significant differences in their relative abundances compared with those of trichotomine G_7. Trichotomine G_1 (Glu_1) also initially eluted as single peak but developed into a split peak during the course of HPLC purification. This peak splitting was possibly caused by α/β anomerization in solution commonly observed during the isolation of glycosides. A possible explanation for trichotomines G_3 and G_5 not displaying the same peak splitting behavior is that the malonyl group attached to the glycoside inhibits α/β anomerization. From these data, it is unclear whether the minor isomers represent α/β anomers or Glu and mGlu substituent attachment pattern variations. The structural details of the minor trichotomine isomers (G_{6b}, G_{7b}, G_{5b}, G_{5c}) will be addressed in future work.

TABLE XI. POSITIVE ION ELECTROSPRAY ACCURATE MASS AND TANDEM MASS SPECTROMETRIC DATA FOR TRICHOTOMINE AND TRICHOTOMINE GLYCOSIDES FROM KUSAGI FRUIT EXTRACT

compound	substituents	formula	$[M+H]^+$ calcd	$[M+H]^+$ obsvd	error (ppm)	MS^n ions
trichotomine (**1**)	aglycone	$C_{30}H_{20}N_4O_6$	533.1461	533.1464	+0.5	MS^2 487, 415, 223
trichotomine G_1	G	$C_{36}H_{30}N_4O_{11}$	695.1989	695.2007	+2.6	MS^2 533
trichotomine G_2	G,G	$C_{42}H_{40}N_4O_{16}$	857.2518	857.2587	+8.0	MS^2 695, 533
trichotomine G_3 (**2**)	mG	$C_{39}H_{32}N_4O_{14}$	781.1993	781.1997	+0.1	MS^2 763, 695, 533
trichotomine G_4 (**3**)	mG, G	$C_{45}H_{42}N_4O_{19}$	943.2522	943.2546	+2.5	MS^2 781, 695, 533
trichotomine G_5 (**4**)	mG, mG	$C_{48}H_{44}N_4O_{22}$	1029.2526	1029.2520	-0.6	MS^2 781, 533
trichotomine G_6	mG, G, G	$C_{51}H_{52}N_4O_{24}$	1105.3050	1105.2977	-6.6	MS^2 943; MS^3 533
trichotomine G_7	mG, mG, G	$C_{54}H_{54}N_4O_{27}$	1191.3054	1191.3045	-0.8	MS^2 781, 533

G, β-D-glucose
mG, (6-*O*-malonyl)-β-D-glucose

TABLE XII. NEGATIVE ION ELECTROSPRAY ACCURATE MASS AND TANDEM MASS SPECTROMETRIC DATA FOR TRICHOTOMINE AND TRICHOTOMINE GLYCOSIDES FROM KUSAGI FRUIT EXTRACT

compound	substituents	formula	$[M-H]^-$ calcd	$[M-H]^-$ obsvd	error (ppm)	MS^2 ions
trichotomine (**1**)	aglycone	$C_{30}H_{20}N_4O_6$	531.1305	531.1253	-9.8	487, 443, 223
trichotomine G_1	G	$C_{36}H_{30}N_4O_{11}$	693.1833	693.1773	-8.6	663*, 649*, 531*
trichotomine G_2	G,G	$C_{42}H_{40}N_4O_{16}$	855.2362	855.2208	-17.9	693*, 503
trichotomine G_3 (**2**)	mG	$C_{39}H_{32}N_4O_{14}$	779.1837	779.1764	-9.3	735, 691, 531
trichotomine G_4 (**3**)	mG, G	$C_{45}H_{42}N_4O_{19}$	941.2366	941.2268	-10.4	735, 693, 649*
trichotomine G_5 (**4**)	mG, mG	$C_{48}H_{44}N_4O_{22}$	1027.2370	1027.2301	-6.7	983, 735
trichotomine G_6	mG, G, G	$C_{51}H_{52}N_4O_{24}$	1103.2894	1103.2763	-11.8	855, 693
trichotomine G_7	mG, mG, G	$C_{54}H_{54}N_4O_{27}$	1189.2898	1189.2769	-10.8	1007, 941, 735

G, β-D-glucose
mG, (6-*O*-malonyl)-β-D-glucose
* In-source fragment ion

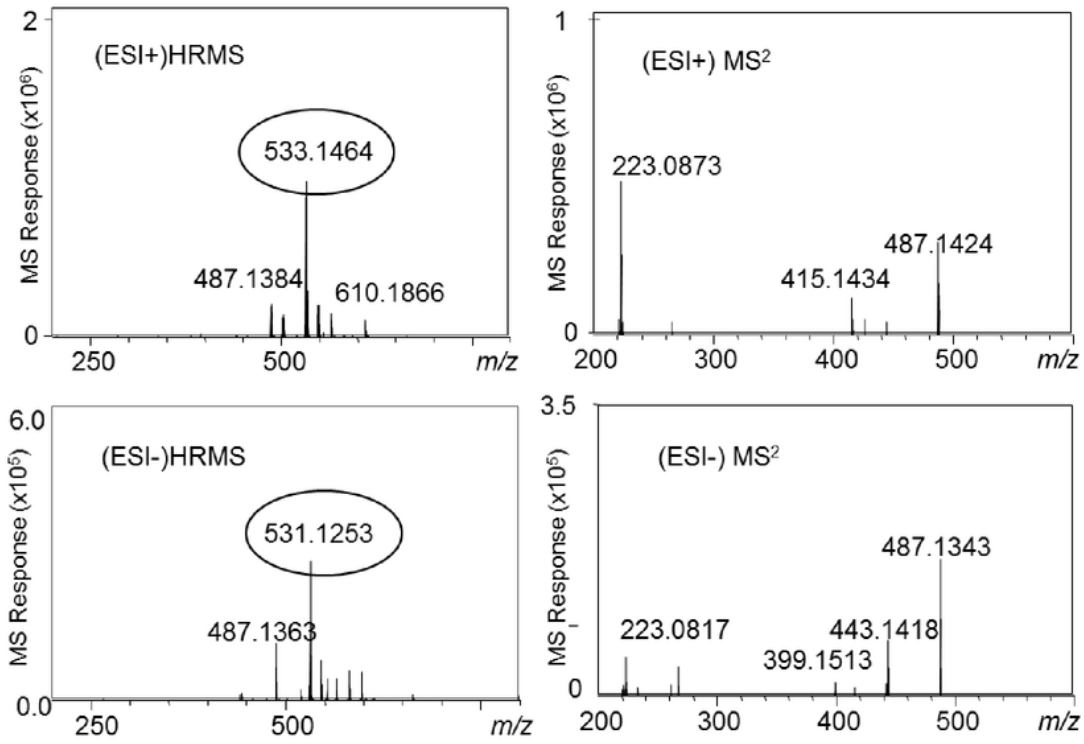

Figure 61. Positive ion and negative ion electrospray (ESI) high resolution mass spectra (HRMS) and product ion $HRMS^2$ of purified trichotomine (**1**).

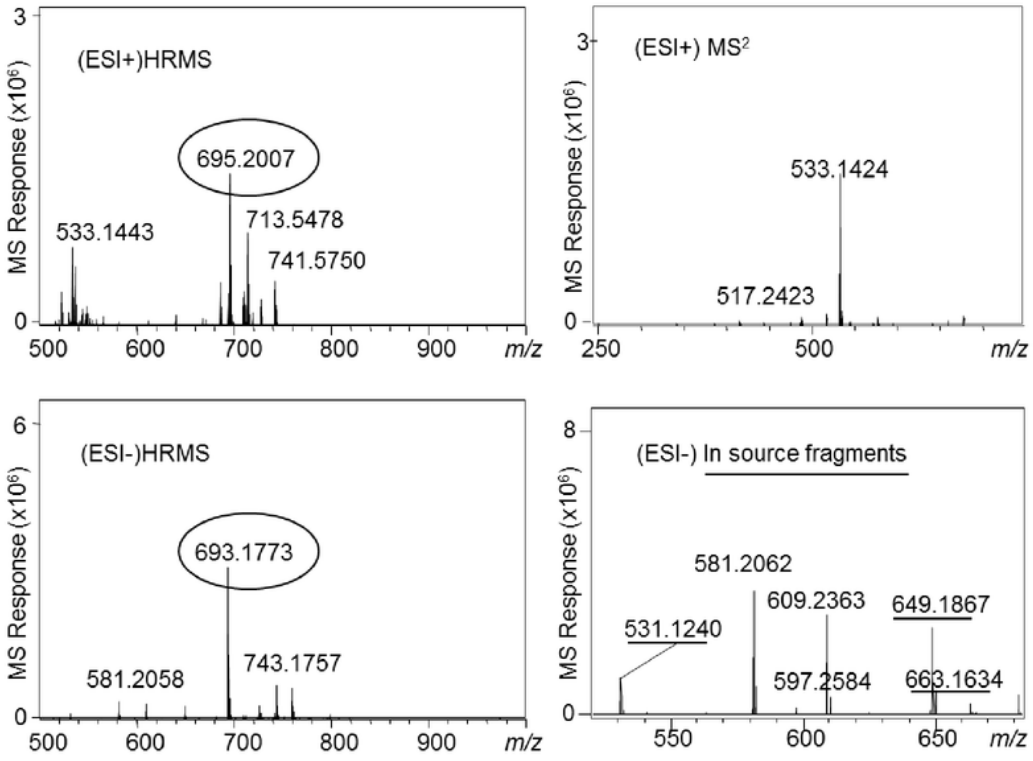

Figure 62. Positive and negative ion high resolution mass spectra and product ion tandem mass spectra of purified trichotomine G_1.

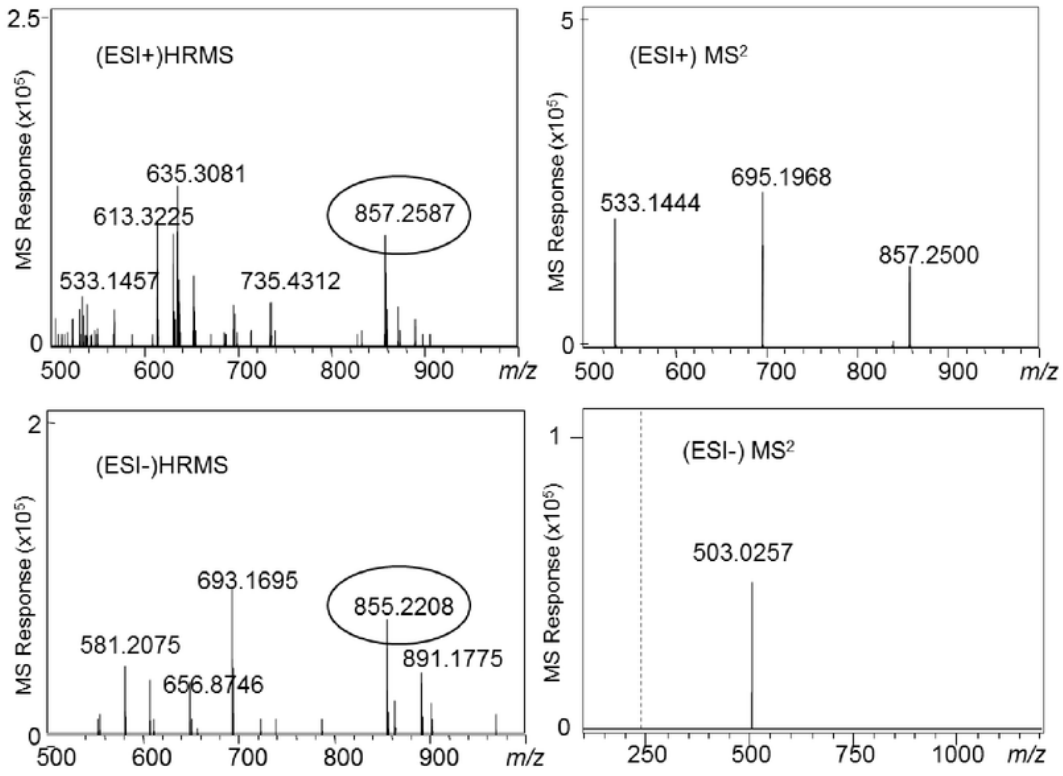

Figure 63. Positive and negative ion electrospray high resolution mass spectra and product ion tandem mass spectra of purified trichotomine G_2.

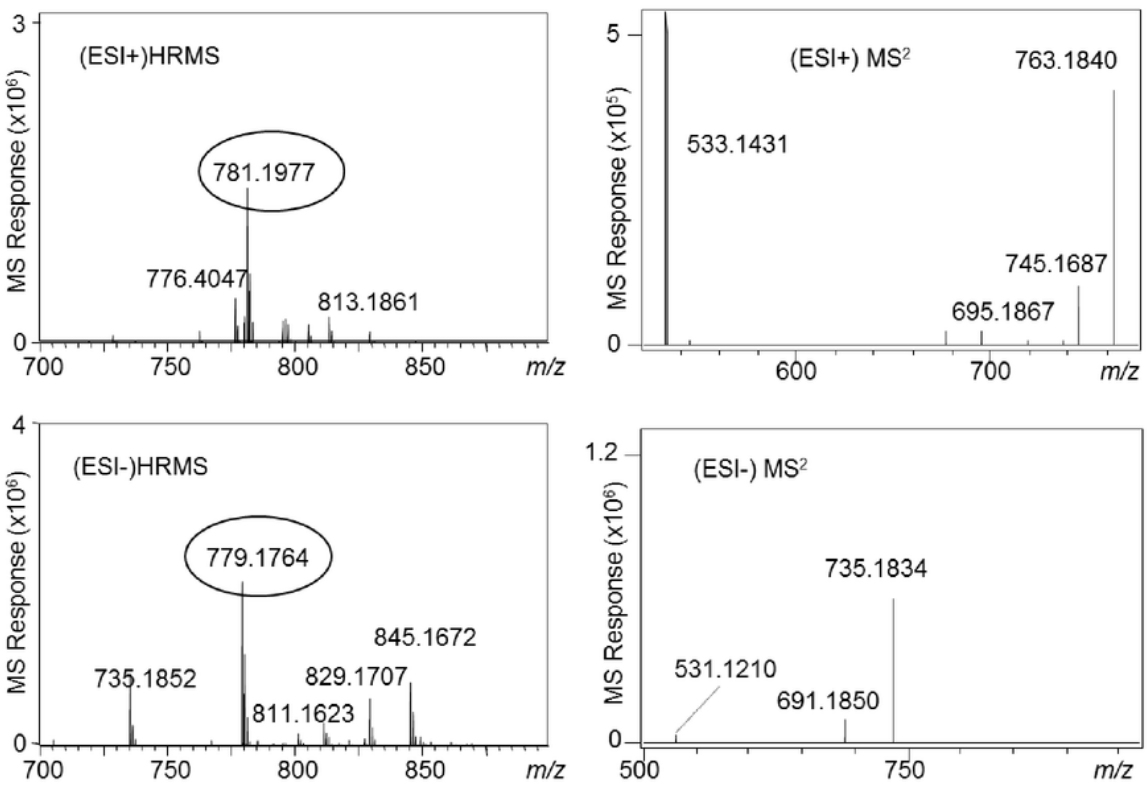

Figure 64. Positive and negative ion electrospray high resolution mass spectra and product ion tandem mass spectra of purified trichotomine G_3 (**2**).

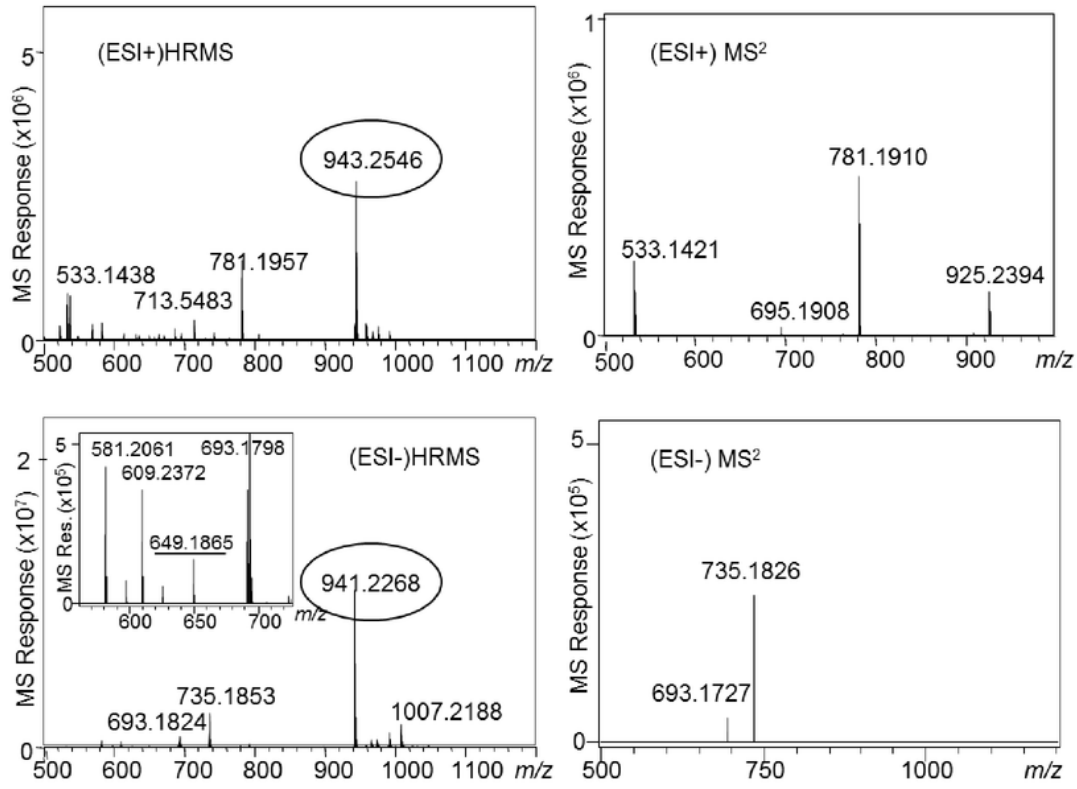

Figure 65. Positive and negative ion electrospray high resolution mass spectra and product ion tandem mass spectra of purified trichotomine G_4 (**3**).

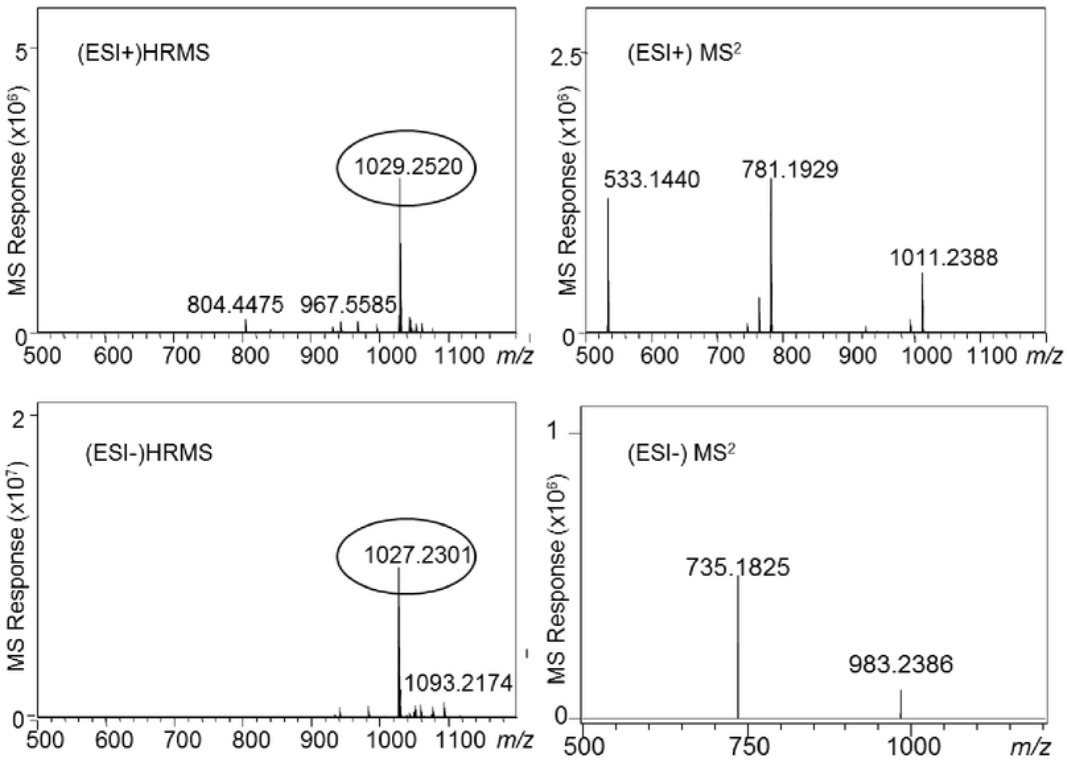

Figure 66. Positive and negative ion electrospray high resolution mass spectra and production tandem mass spectra of purified trichotomine G_5 (**4**).

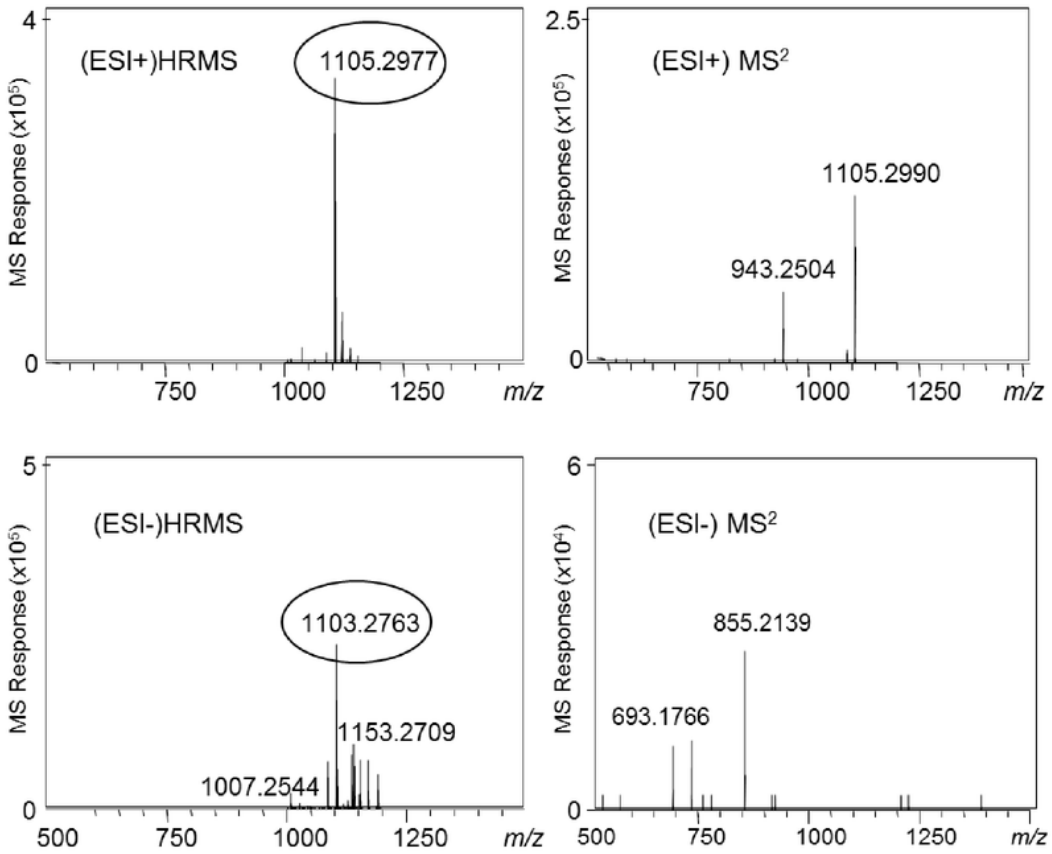

Figure 67. Positive and negative ion electrospray high resolution mass spectra and product ion tandem mass spectra of purified trichotomine G_6. The MS^3 spectrum of *m/z* 943 showed the product ion of *m/z* 533 (data not shown).

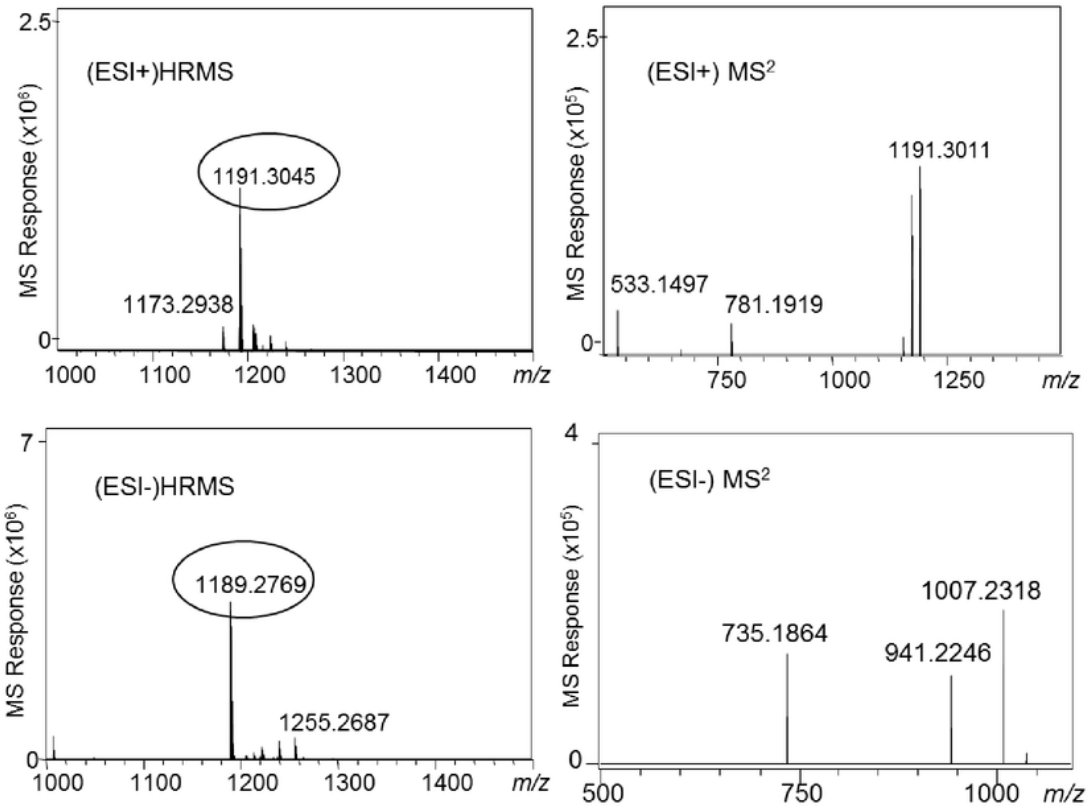

Figure 68. Positive and negative ion electrospray high resolution mass spectra and product ion tandem mass spectra of purified trichotomine G_7.

5.3.2 NMR analysis

The structures and numbering scheme for trichotomine and the novel analogs trichotomine G_3 (**2**), G_4 (**3**), and G_5 (**4**) are provided in Figure 56. The structures of the purified trichotomine analogs were elucidated using ^{1}H, DEPT-Q, COSY, HSQC, and HMBC data sets shown in Figures 70-92 obtained on a Bruker Avance 900 MHz NMR spectrometer.

5.3.2.1 NMR analysis of trichotomine standard

Low frequency (60-100 MHz) ^{1}H NMR data for trichotomine in $(CD_3)_2CO$ was previously published (281). The ^{1}H NMR resonances for aromatic (H-1, H-1'; H7 – H10; H7' – H10';) and aliphatic (H-5, H-6; H-5', H-6') hydrogens and their associated ^{13}C correlations from an HMBC NMR experiment suggested that each indole was fused to a neighboring substituted hydroindolizine at the shared double bond across C-6a–C-12 and C-6a'–C-12'. The HMBC experiment additionally supported the assignment of a methylene at C-6; C-6', a carboxyl group at C-5; C-5', a carbonyl at C-3; C-3', and an exocyclic double bond at the α-position, C-2; C-2'. Correlations between H-1 and H-2; H-2' and H-1' and H-3; H-3' indicated that the double bond across positions C-2–C-2' served as the bridge that formed the dimer of trichotomine. Structural assignments of trichotomine from ^{1}H, ^{13}C (DEPT-Q), COSY, HSQC, HMBC, and ROESY experiments in DMSO-d_6 are shown in Table XIII.

5.3.2.2 NMR analysis of trichotomine G_5

NMR signals for trichotomine G_5 (R = mGlu, mGlu) were symmetric due to the overall C_2 rotational symmetry at the central double bond (H1/H1', 7.27 (s), etc.) and exhibited an expected slight chemical shift relative to the NMR signals for the trichotomine standard due to the attachment of the (malonyl)glucose substituents. Structural assignments for trichotomine G_5 in DMSO-d_6 from ^{1}H, ^{13}C, (DEPT-Q), COSY, HSQC, HMBC, and ROESY experiments are shown in Table XIV.

The structures of trichotomine G_1 and G_2 were previously published with the β-D-glucose substituents attached to the indole nitrogen atoms (281) and were reported as the first indolic *N*-glucoside known from plants. Conversely, our data indicated that the (malonyl)glucose groups were O-linked at the carboxylic acid groups (C14,14', 171.86), evidenced by a three-bond ($^3J_{CH}$) HMBC correlation of the anomeric (H1''/H1''', 5.30 (d)) glucose protons to the trichotomine carbonyl carbons (C14,14', 171.86). The anomeric proton *J*-coupling constant of 8.0 Hz established a β-configuration for the glucose attachments.

5.3.2.3 NMR analysis of trichotomine G_3

The trichtomine G_3 **(2)** (R = mGlu, H) structure includes one (malonyl)glycoside group, as established by high resolution MS^2 analysis (Section 5.3.1), which is supported by a divergence of its aromatic ^1H chemical shifts from those of the trichotomine standard near the C14/14' attachment point. In the 90-100 ppm region of the DEPT-Q (^{13}C) NMR data (Figure 69), trichotomine G_3 chemical shifts appear as a combination of two sets of slightly offset signals: one set for the trichotomine standard (R=H) and one set for trichotomine G_5 (R=mGlu, mGlu). For example: trichotomine, C1/1', 96.83 (CH); trichotomine G_5, C1/1', 96.90; trichotomine G_3, C1/1', 96.70/96.98. Aside from the chemical shift at the attachment point, the signals and correlations for the trichotomine core of trichotomine G_3 (**2**) were indistinguishable from those of trichotomine G_5 (**4**).

5.3.2.4 NMR analysis of trichotomine G_4 (3) (R = mGlu, Glu)

The NMR data set for trichotomine G_4 (**3**) includes ^1H, COSY, and DEPTQ experiments. The signals and correlations corresponding to ^1H and ^{13}C of the trichotomine core were not distinguishable from those of trichotomine G_5 (**4**). TOCSY experiments of irradiation at both H-6''' of the

(malonyl)glycoside (3.99 and 4.13 ppm) and at H-6'' of the glycoside (4.43 ppm) were used to deconvolute signals for the β-D-glucose and 6-O-malonyl-β-D-glucose groups.

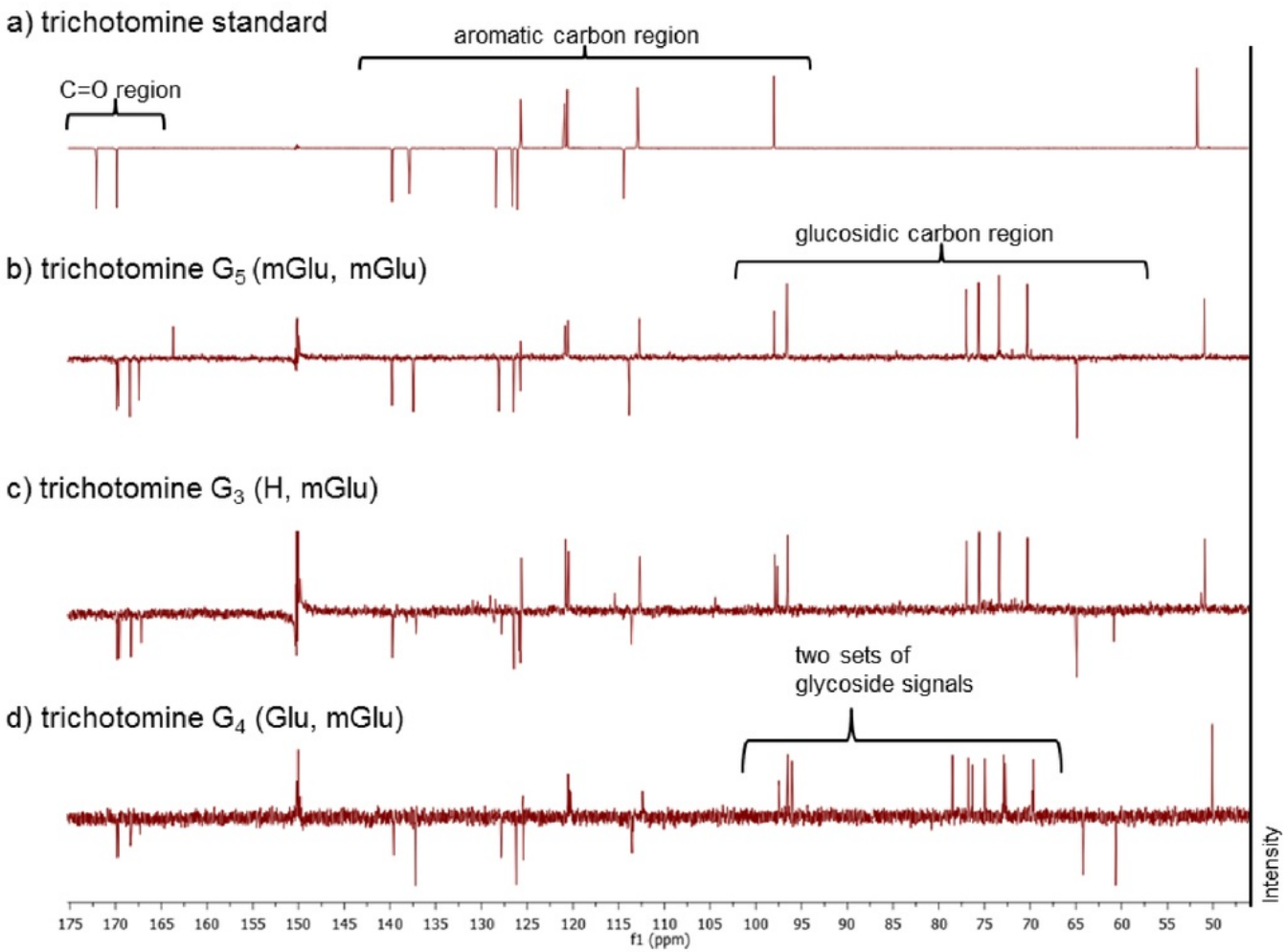

Figure 69. Overlay of 900 MHz DEPTQ NMR spectra of (a) trichotomine (b) trichotomine G_5 (c) trichotomine G_3 and (d) trichotomine G_4. Positive signals = CH_3/CH, negative signals = CH_2/C.

TABLE XIII. $^{1}H^{a}$, $^{13}C^{b}$, HMBC^{a}, COSY^{a}, AND ROESY^{a} NMR SPECTROSCOPIC DATA OF TRICHOTOMINE (**1**) IN DMSO-d_6.

Position	δ_C	δ_H (J in Hz)	HMBC	COSY	ROESY
1	96.83	7.24 s	2, 3, 5, 13		11
2	127.61				
3	169.59				
4					
5	49.99	5.11 d (7.3)	5a, 6, 6a, 13	6 (3.37 ppm), 6 (3.64 ppm)	6 (3.37 ppm), 6 (3.64 ppm)
5a	171.86				
6	23.63	3.64 d (16.3)	5, 5a, 6a, 12, 13	5, 6 (3.37 ppm)	6 (3.64 ppm)
		3.37 dd (7.5, 16.5)	5, 5a, 6a, 12, 13	5, 6 (3.64 ppm)	6 (3.37 ppm)
6a	113.46				
6b	125.81				
7	119.72	7.63 d (7.9)	6a, 9, 10a	8	8
8	120.05	7.08 t (7.4)	6b, 7, 10, 10a	7, 9	7, 9
9	124.86	7.25 t (7.4)	7, 10, 10a	8, 10	8, 10
10	111.91	7.41 d (8.1)	6b, 8	9	9, 11
10a	139.09				
11		11.97 s	6a , 10a, 12		9, 10
12	125.24				
13	137.19				
14	171.86				

[a] Measured at 900 MHz. [b] Measured at 226.2 MHz.

TABLE XIV. $^{1}H^{a}$, $^{13}C^{b}$, HMBC^{a}, AND COSY^{a} NMR SPECTROSCOPIC DATA OF TRICHOTOMINE-DI-*O*-(6-*O*-MALONYL-β-D-GLUCOSIDE) (**2**) IN DMSO-d_6.

position	δ_C	δ_H (*J* in Hz)	^{1}H-^{1}H COSY	HMBC
1	96.90	7.27 s		2, 3, 13
2	127.37			
3	169.23			
4				
5	48.69	5.32 d (8.4)	6 (3.47 ppm), 6 (3.63 ppm)	5a, 6, 6a, 13
6	23.25	3.63 d (16.4)	5, 6 (3.47 ppm)	5, 5a, 6a, 12
		3.47 dd (7.7, 16.7)	5, 6 (3.63 ppm)	5, 5a, 6a, 12
6a	113.03			
6b	125.74			
7	119.78	7.62 d (7.9)	8	6a, 9, 10a, 12
8	120.08	7.06 t (7.4)	7, 9	6a, 6b, 10, 9
9	124.96	7.24 t (7.5)	8, 10	7, 8, 10a
10	111.89	7.40 d (8.1)	9	6b, 8
10a	139.13			
11		12.01 s		
12	124.98			
13	136.79			
14	169.46			
1"	95.38	5.30 d (8.0)	2"	5", 5a"
2"	72.09	3.18 m	1"	1", 3", 4"
3"	75.87	3.22 m (9.0)	4"	1", 2", 4"
4"	69.03	3.14 m	3"	3", 5", 6"
5"	74.09	3.39 m	4", 6" (3.98 ppm), 6" (4.11 ppm)	1", 3", 4", 6"
6"	63.53	4.11 d (10.5)	5", 6" (3.98 ppm)	4", 5", 7"
		3.98 dd (5.6, 11.7)	5", 6" (4.11 ppm)	5", 7"
7"	167.01			
8"	41.63	3.16 m		7", 9"
9"	168.01			

[a] 900 MHz. [b] 226.2 MHz

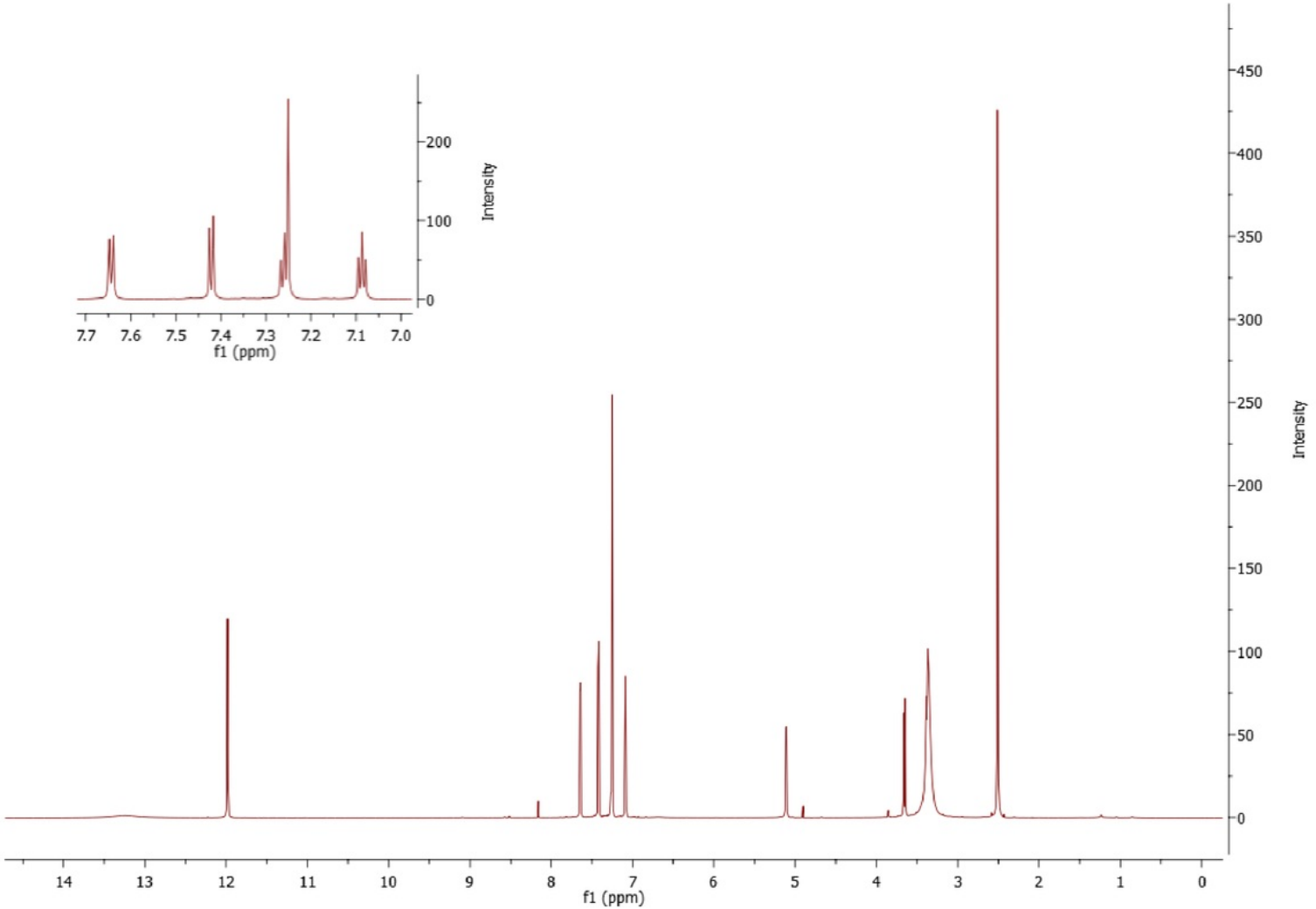

Figure 70: ^{1}H NMR spectrum (900 MHz, DMSO-d_6) of trichotomine (**1**) standard

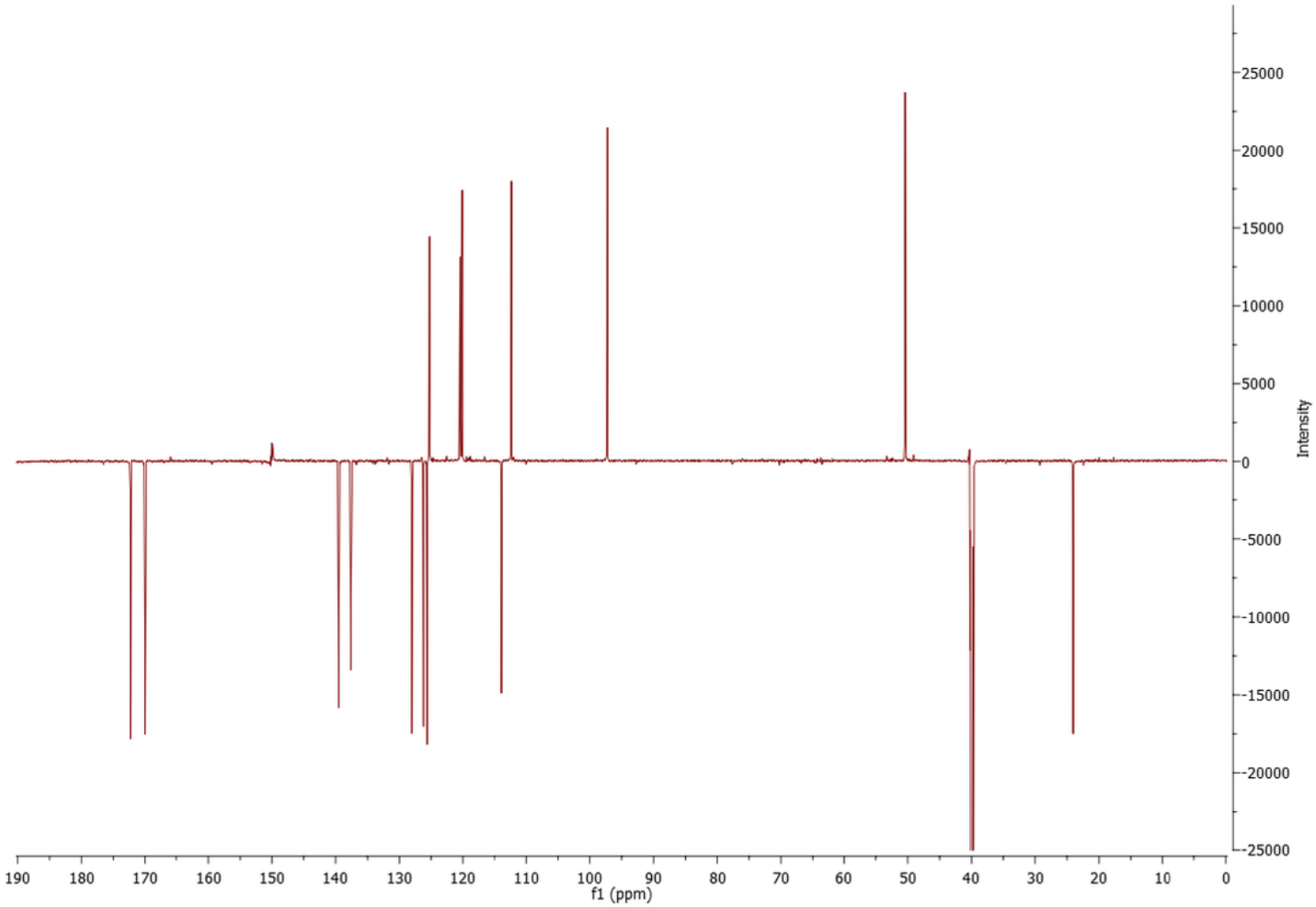

Figure 71: DEPTQ spectrum (900 MHz, DMSO-d_6) of trichotomine (**1**) standard

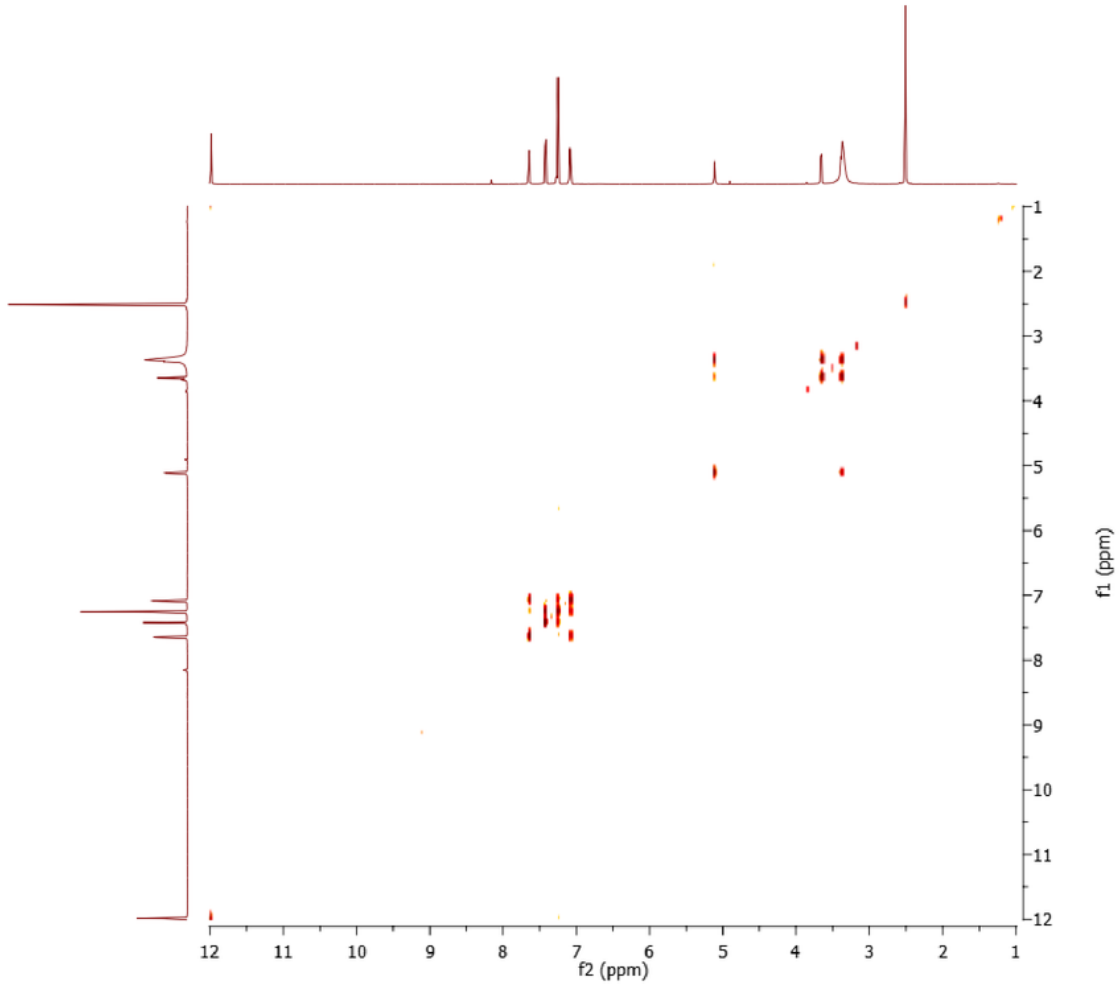

Figure 72: COSY spectrum (900 MHz, DMSO-d_6) of trichotomine (**1**) standard

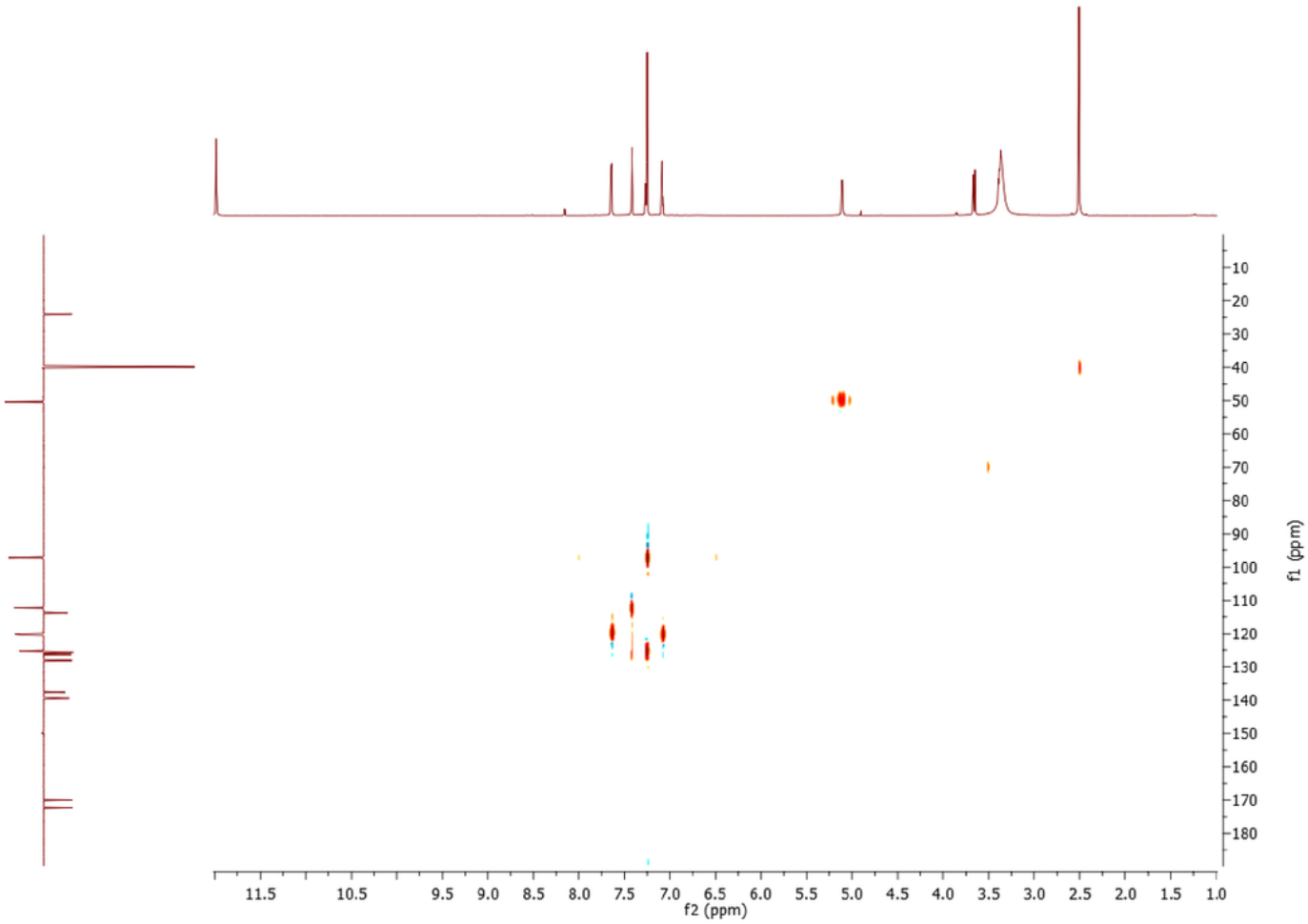

Figure 73: HSQC spectrum (900 MHz, DMSO-d_6) of trichotomine (**1**) standard

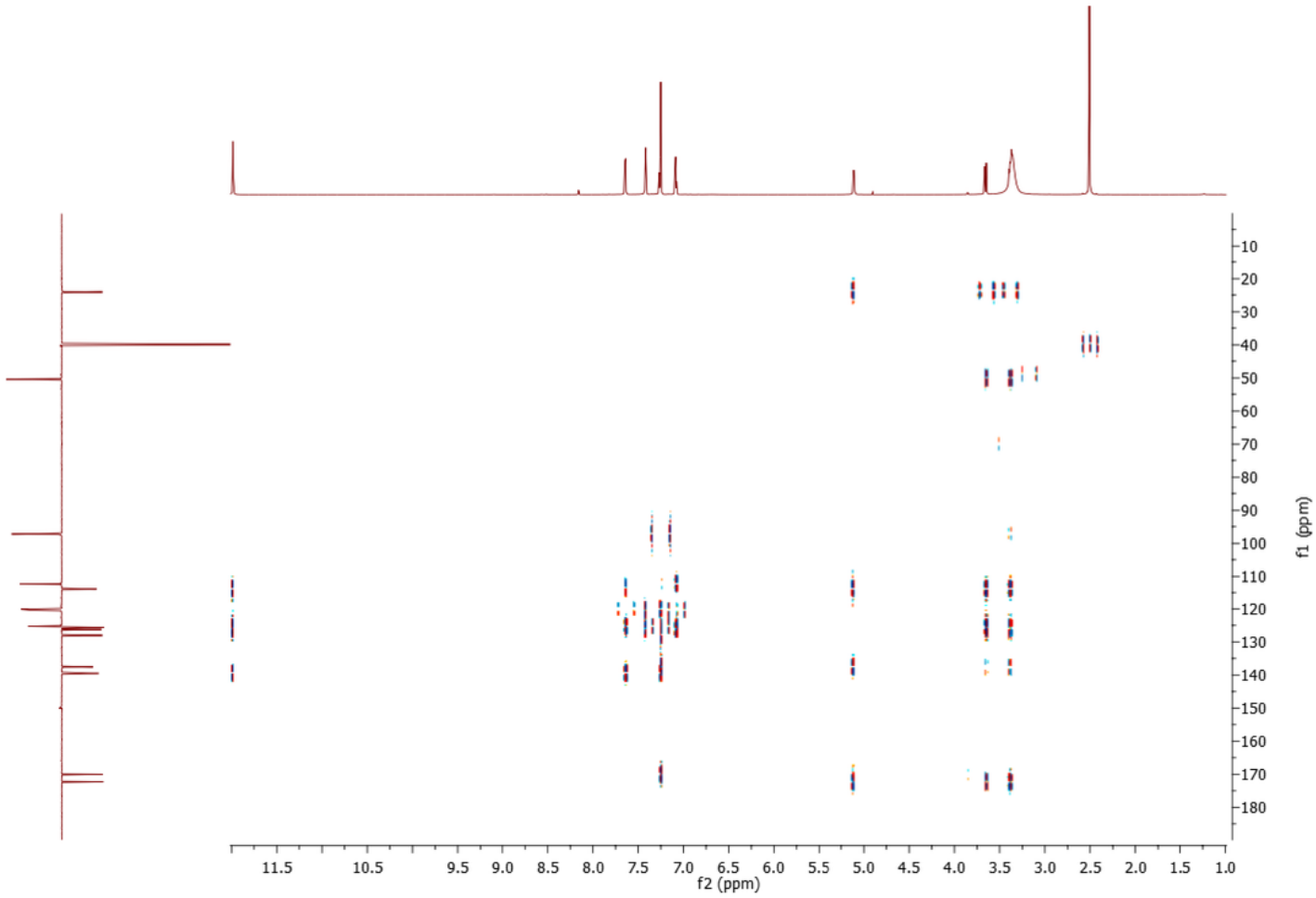

Figure 74: HMBC spectrum (900 MHz, DMSO-d_6) of trichotomine (**1**) standard

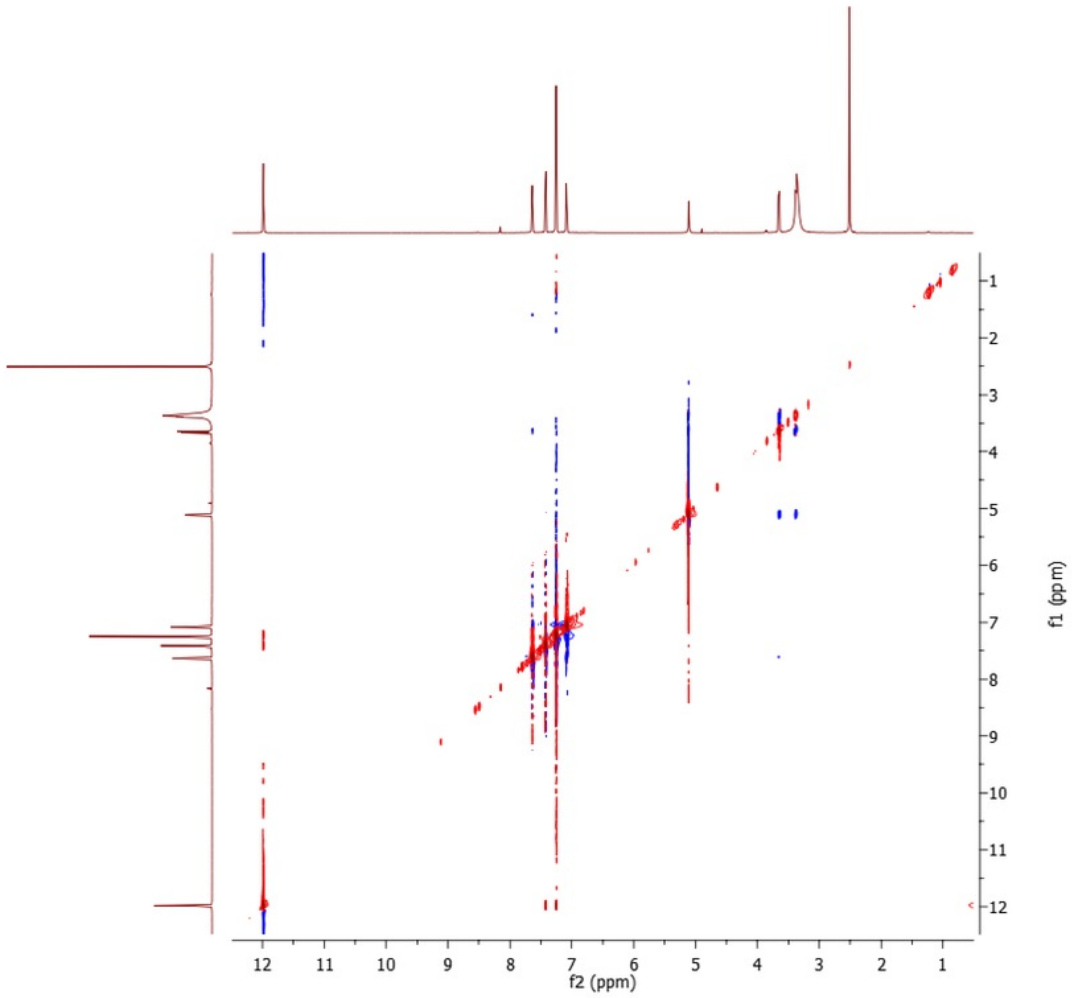

Figure 75: ROESY spectrum (900 MHz, DMSO-d_6) of trichotomine (**1**) standard

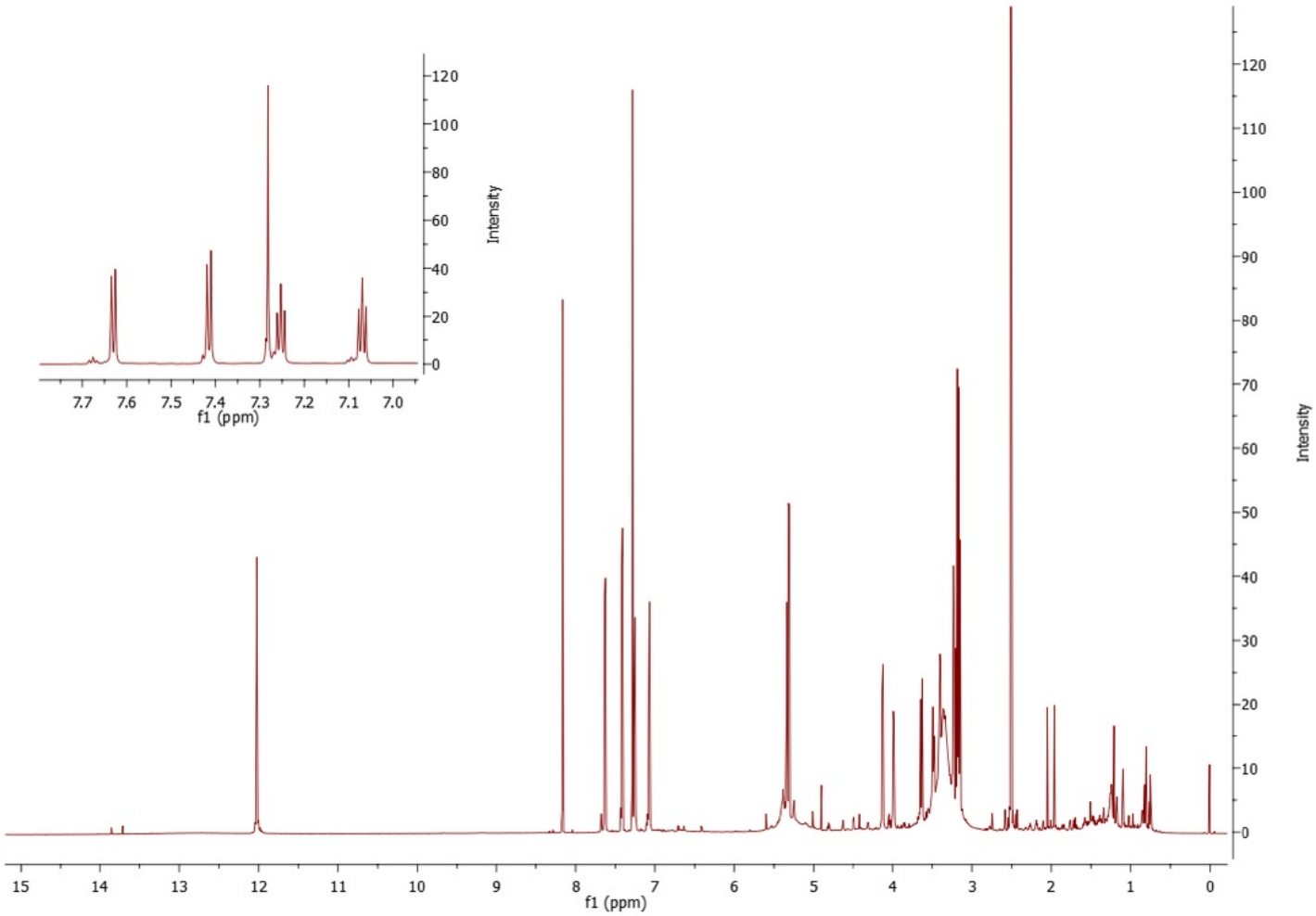

Figure 76: ^{1}H NMR spectrum (900 MHz, DMSO-d_6) of trichotomine G_5 (**4**)

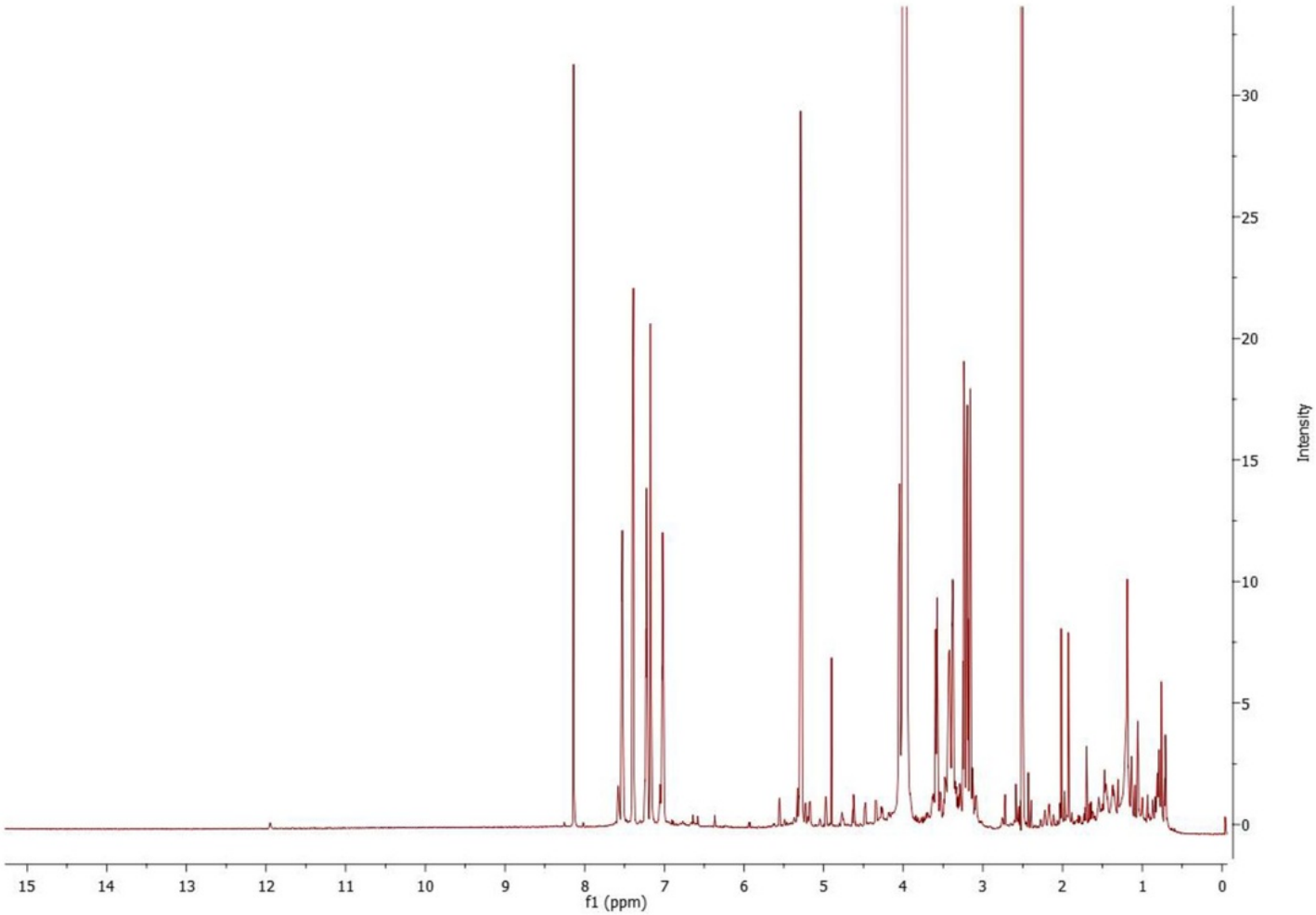

Figure 77: ^{1}H NMR spectrum after addition of one drop of D_2O (900 MHz, DMSO-d_6) of trichotomine G_5 (**4**)

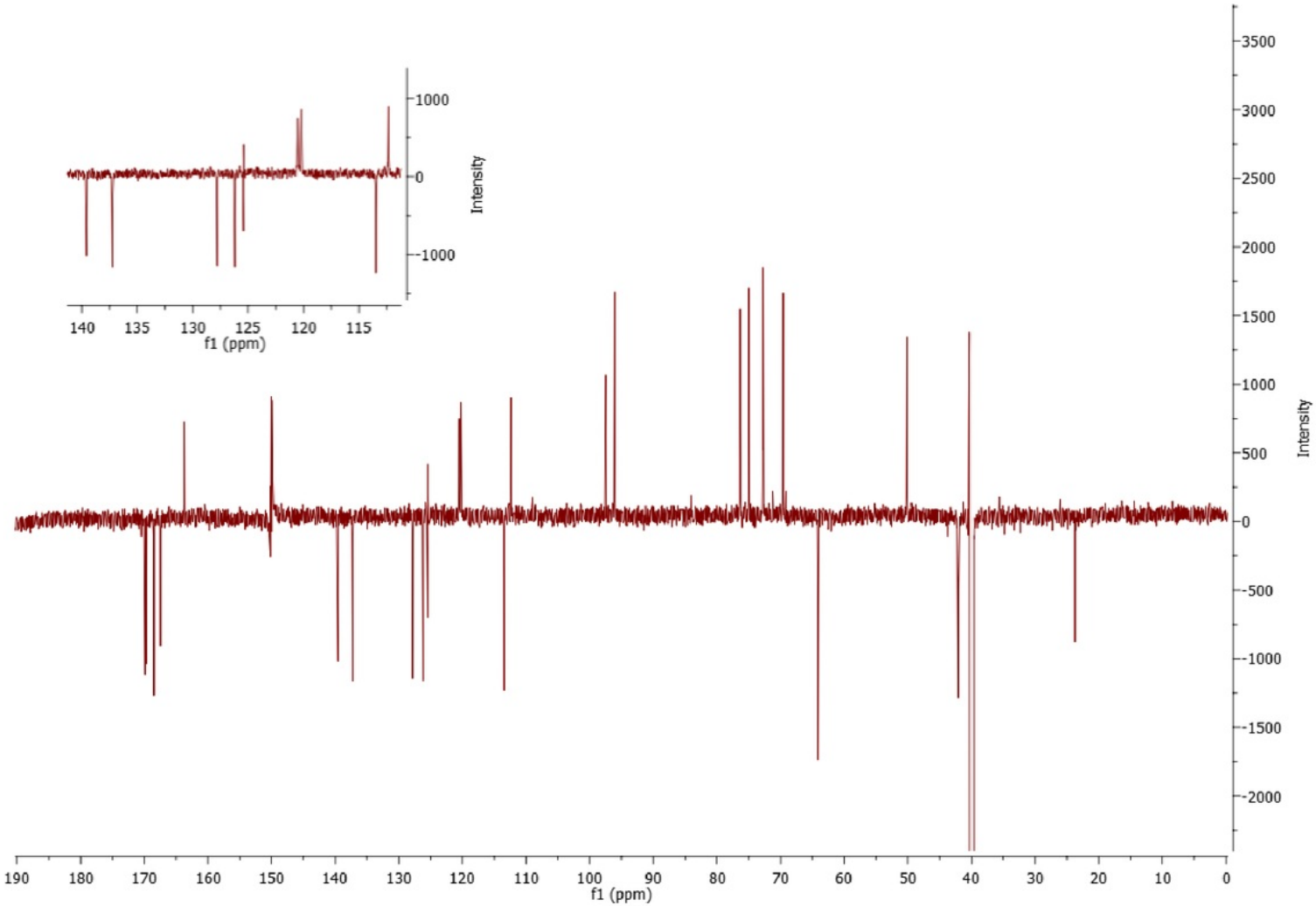

Figure 78: DEPTQ spectrum (900 MHz, DMSO-d_6) of trichotomine G_5 (**4**)

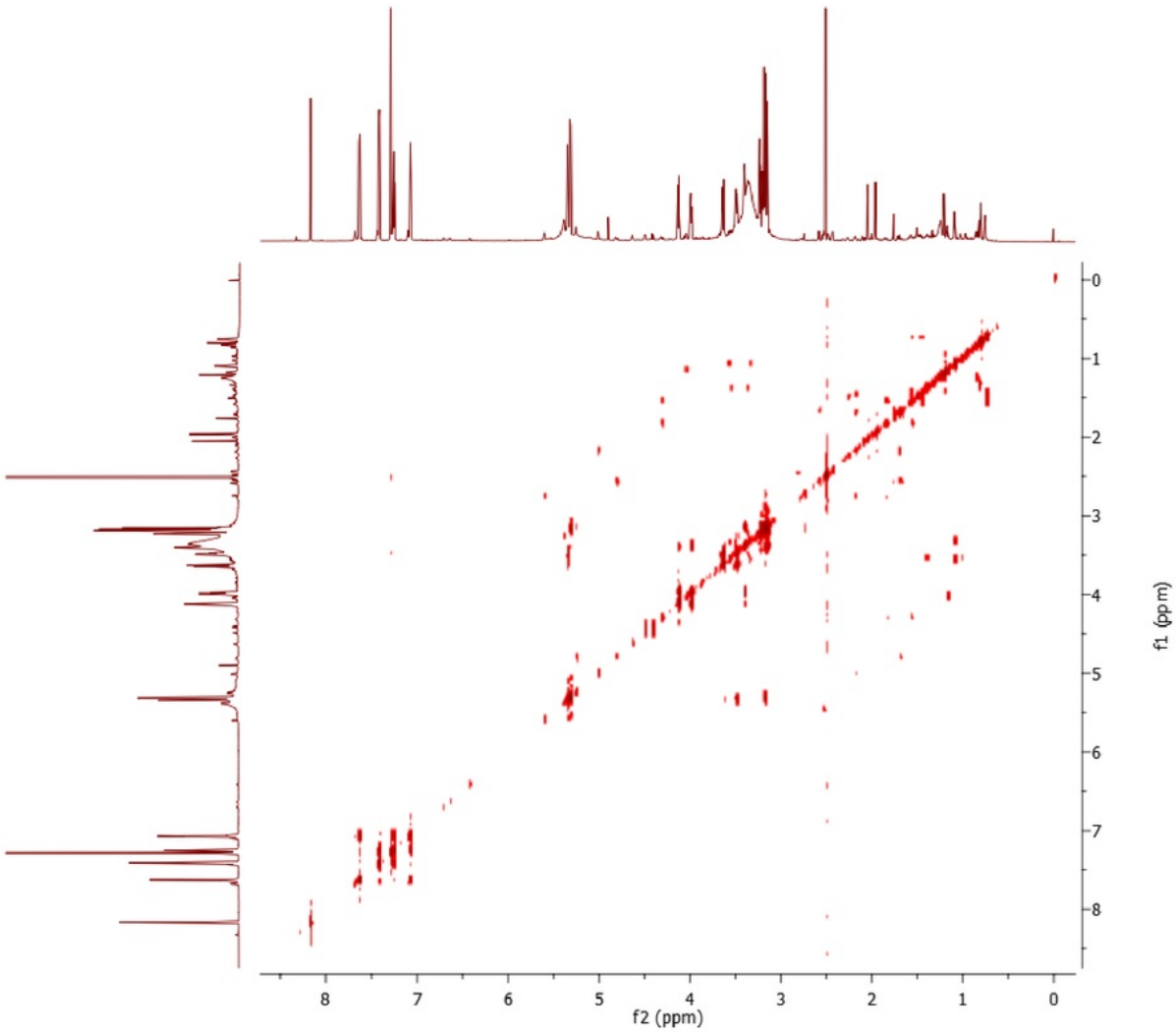

Figure 79: COSY spectrum (900 MHz, DMSO-d_6) of trichotomine G_5 (**4**)

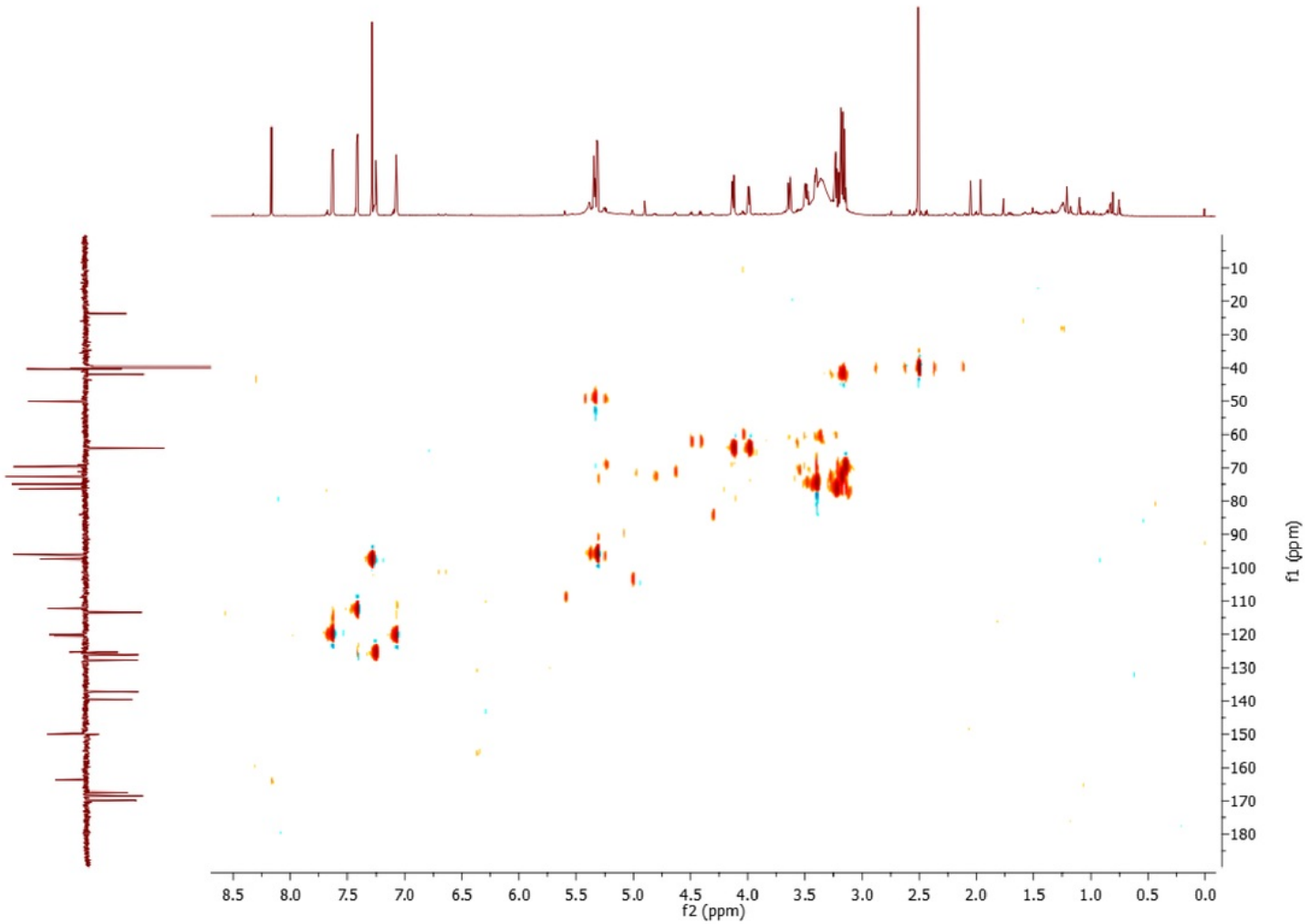

Figure 80: HSQC spectrum (900 MHz, DMSO-d_6) of trichotomine G_5 (**4**)

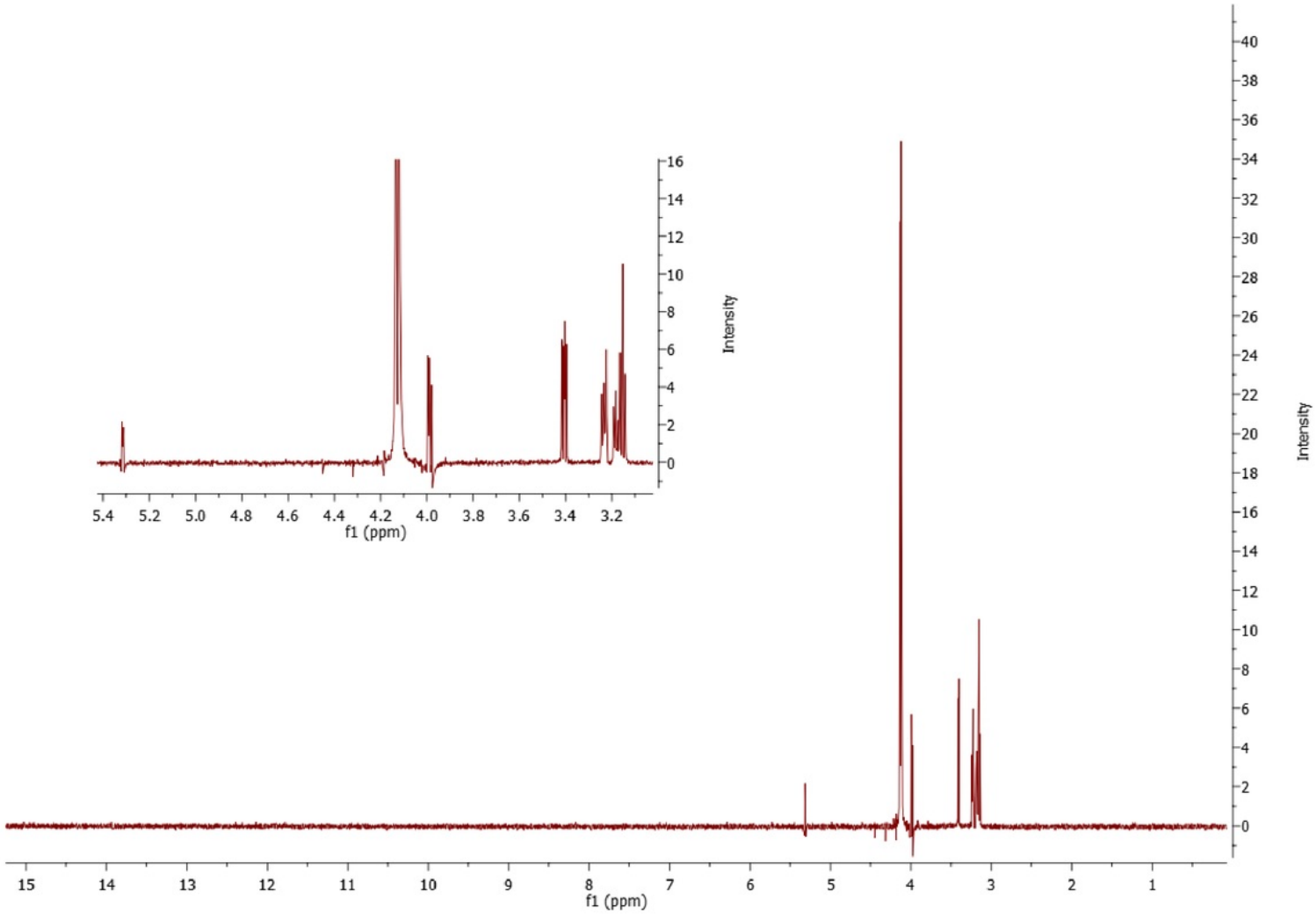

Figure 81: TOCSY spectrum of H-6''/H-6''' (900 MHz, DMSO-d_6, O1P = 4.12 ppm) of trichotomine G_5 (**4**)

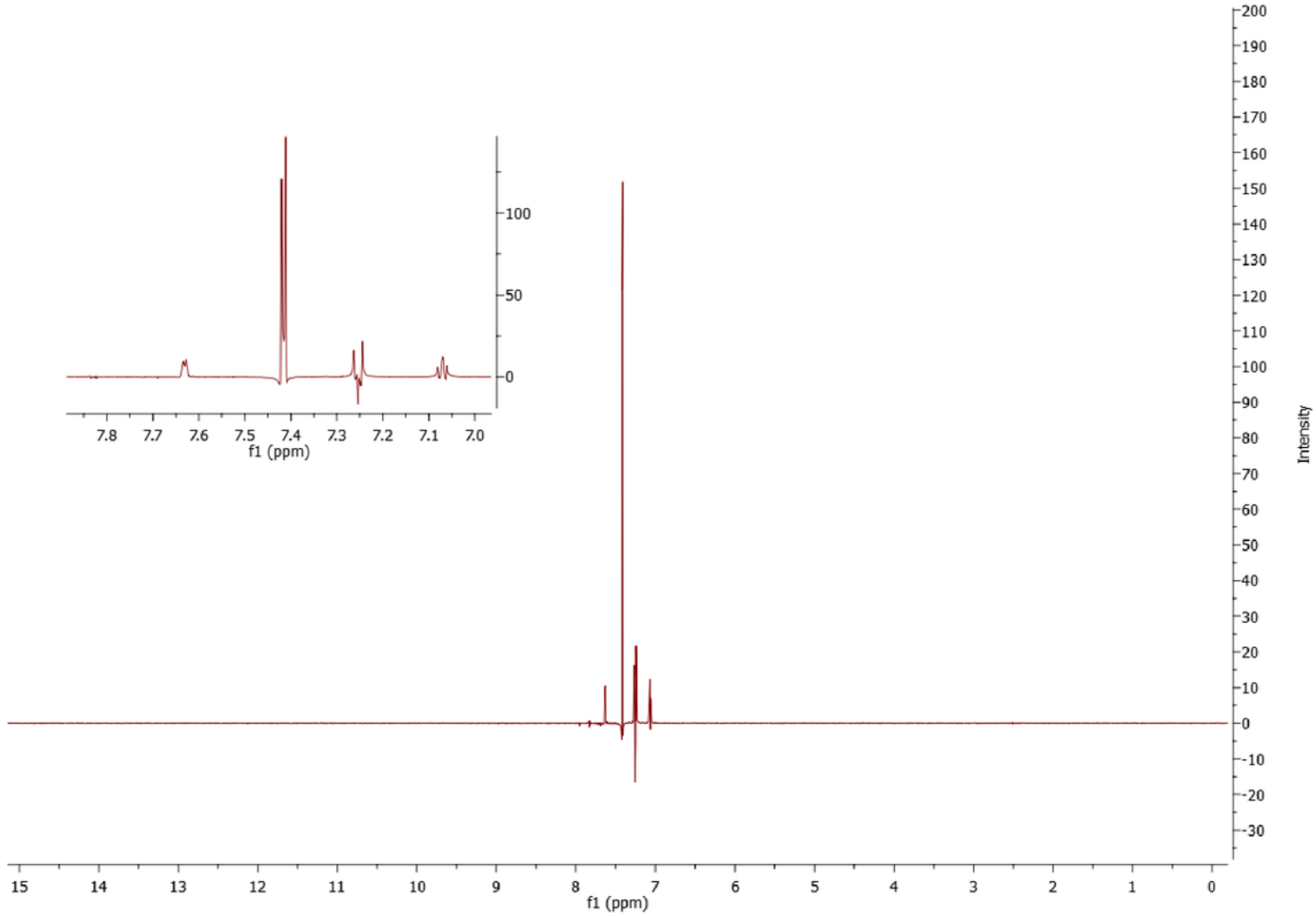

Figure 82: TOCSY spectrum of H-7 (900 MHz, DMSO-d_6, O1P = 7.62 ppm) of trichotomine G_5 (**4**)

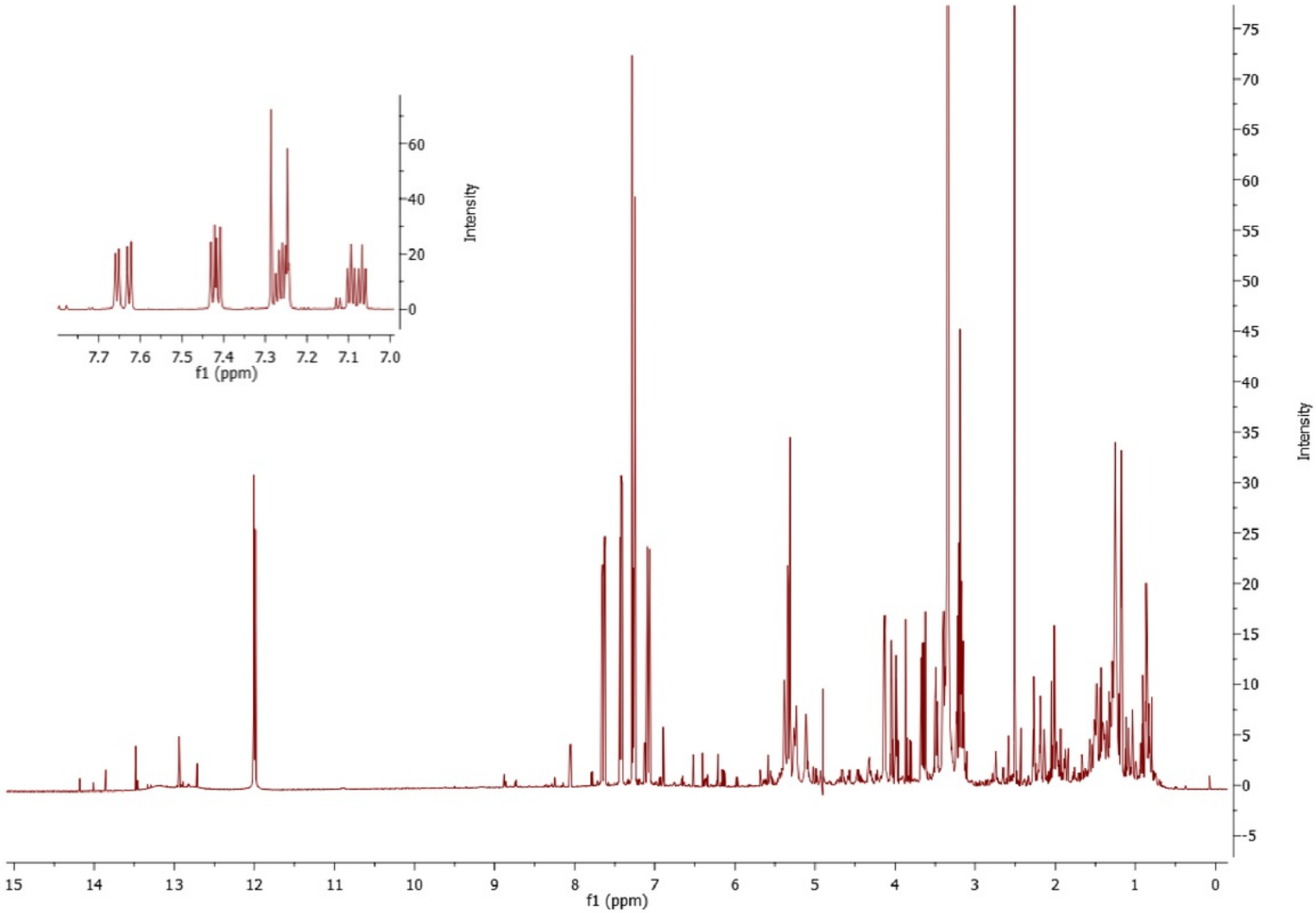

Figure 83: ^{1}H NMR spectrum (900 MHz, DMSO-d_6) of trichotomine G_3 (**2**)

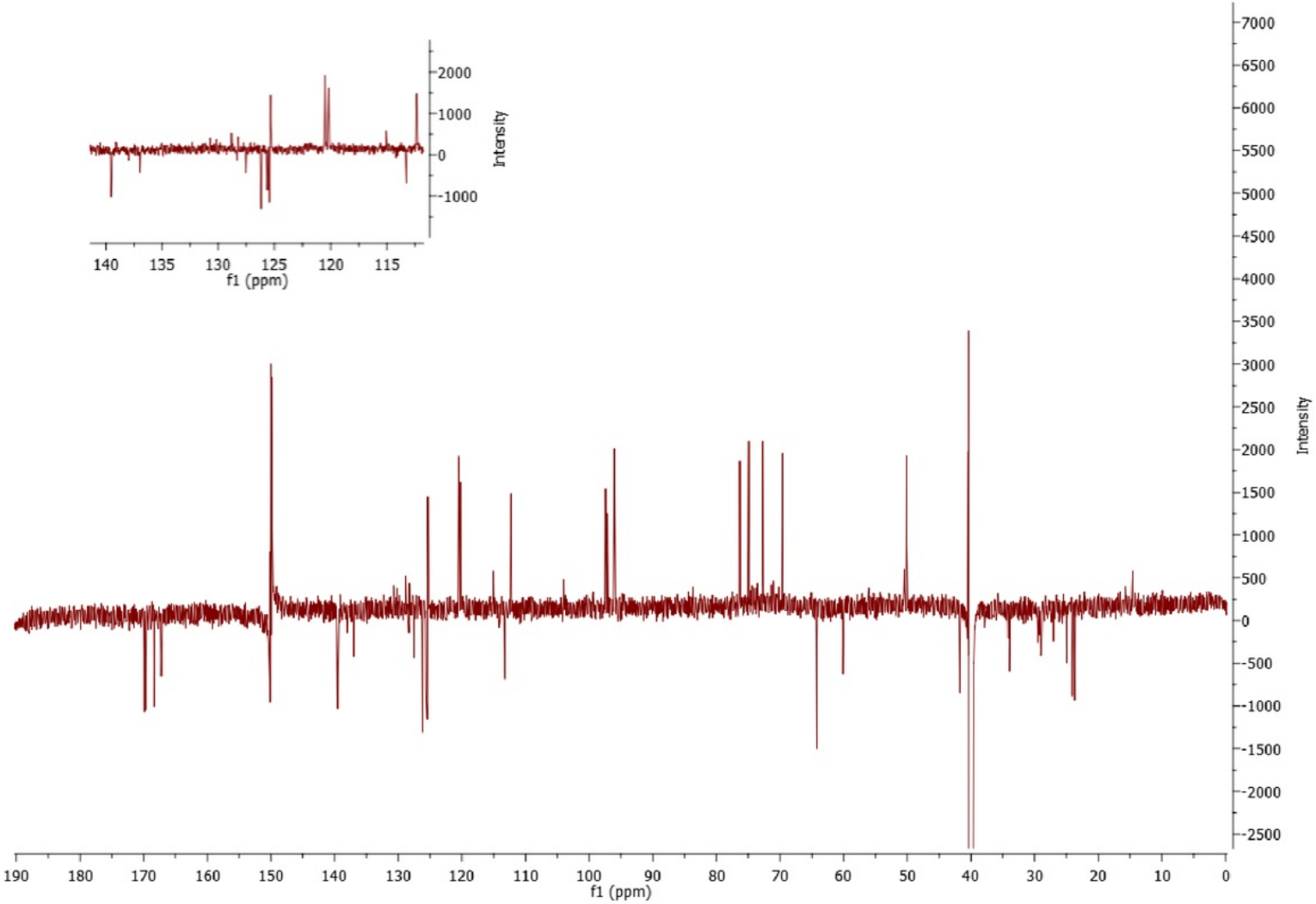

Figure 84: DEPTQ spectrum (900 MHz, DMSO-d_6) of trichotomine G_3 (**2**)

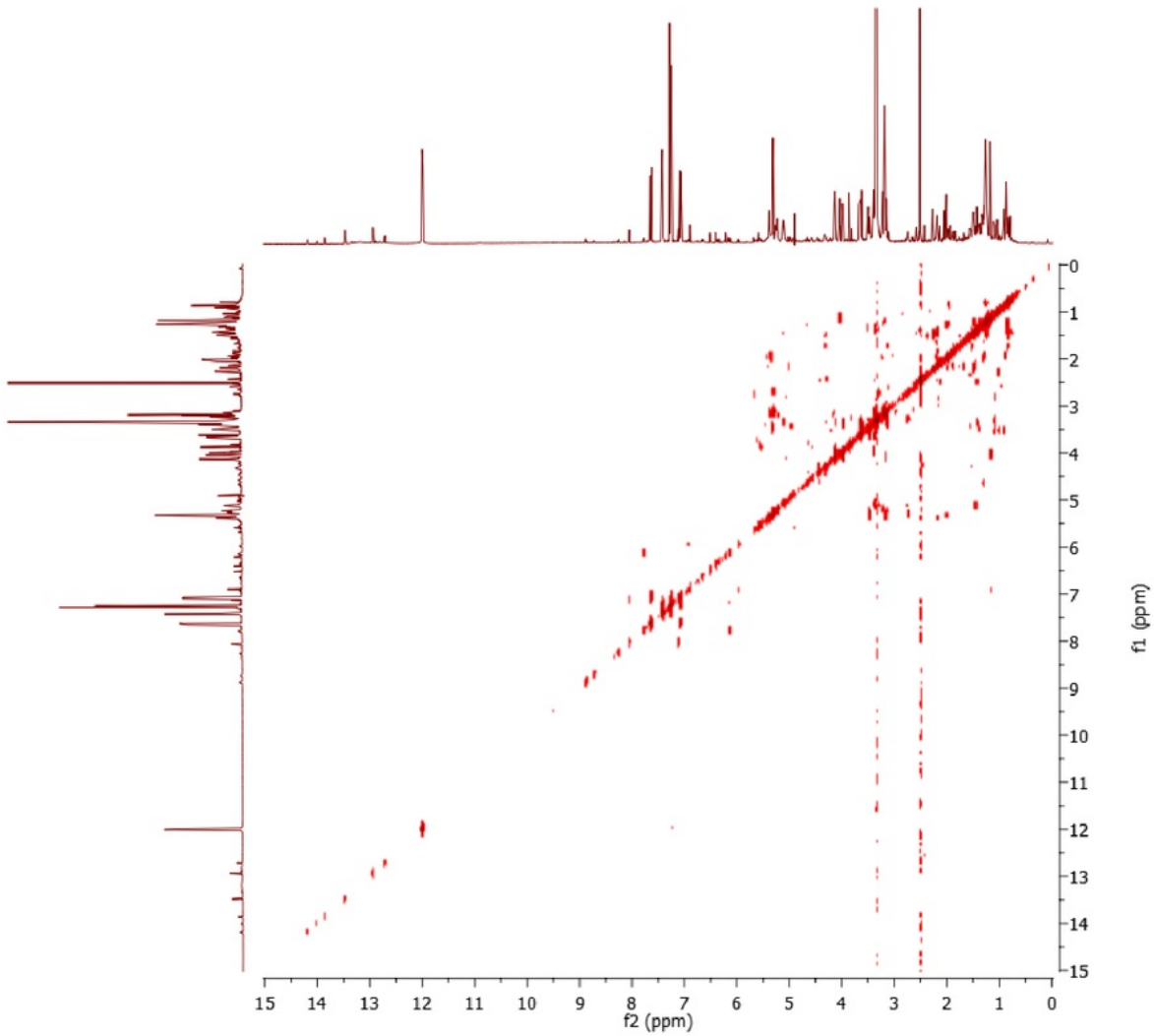

Figure 85: COSY spectrum (900 MHz, DMSO-d_6) of trichotomine G_3 (**2**)

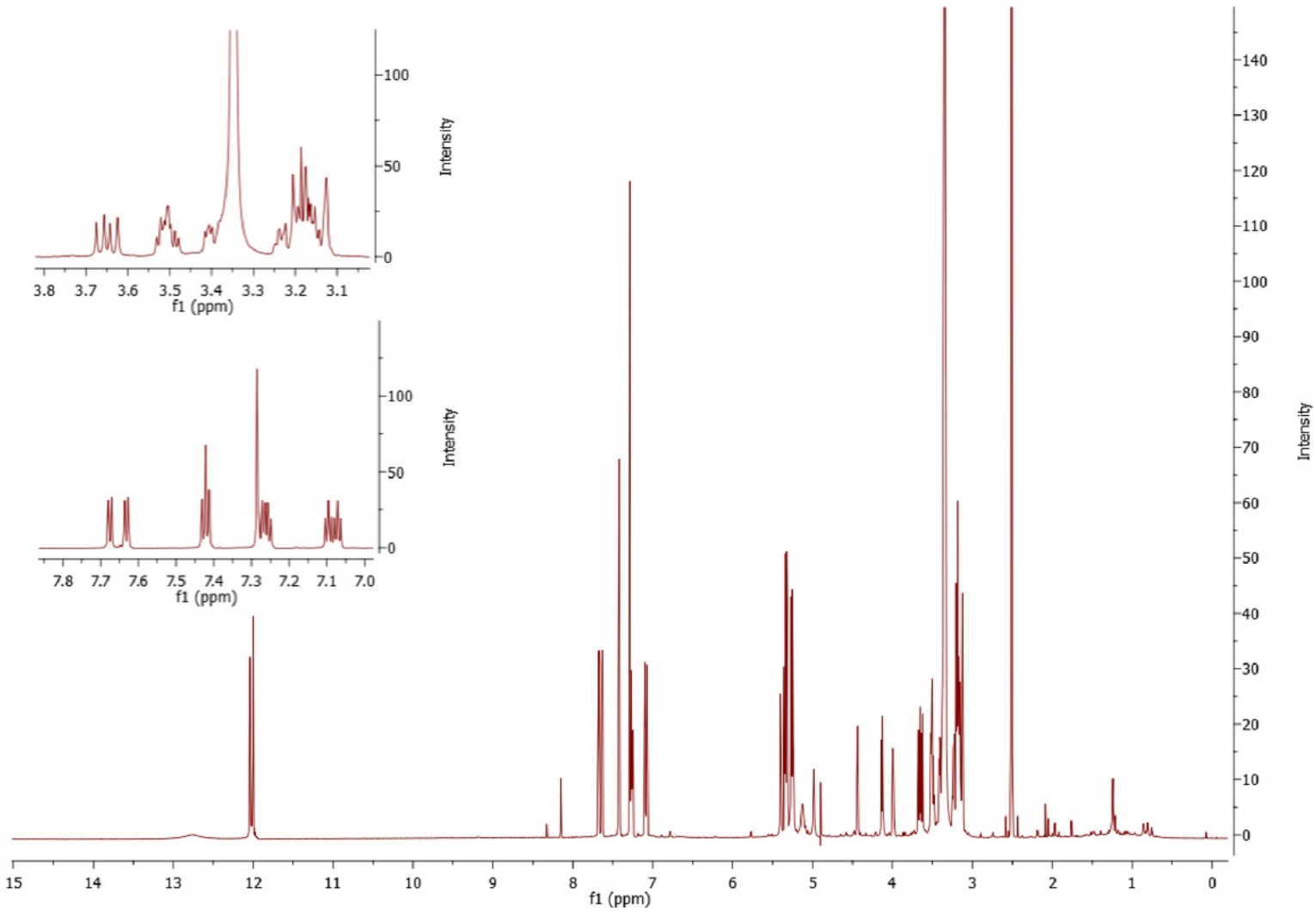

Figure 86: ^{1}H NMR spectrum (900 MHz, DMSO-d_6) of trichotomine G_3 (**2**)

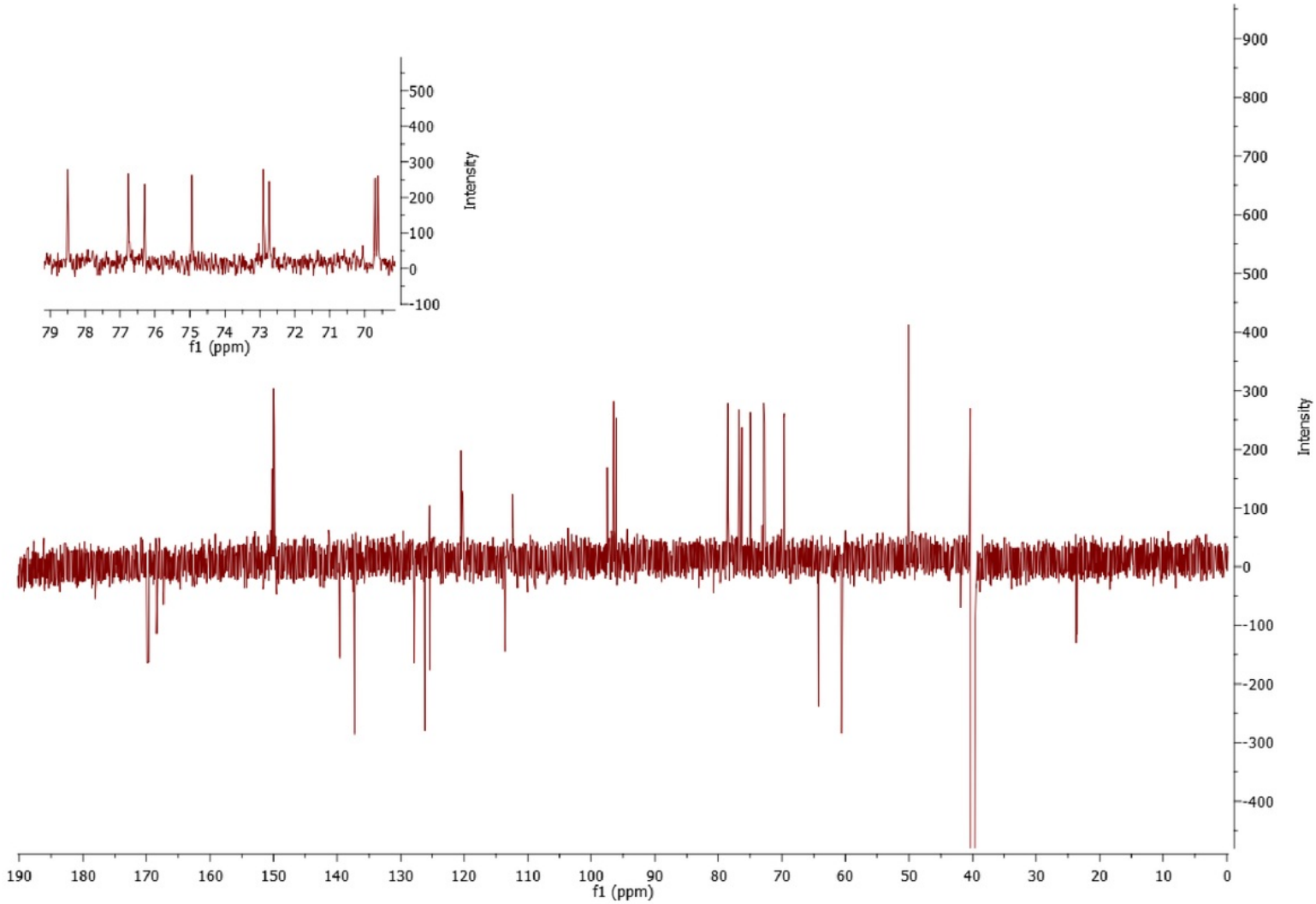

Figure 87: DEPTQ spectrum (900 MHz, DMSO-d_6) of trichotomine G_3 (**2**)

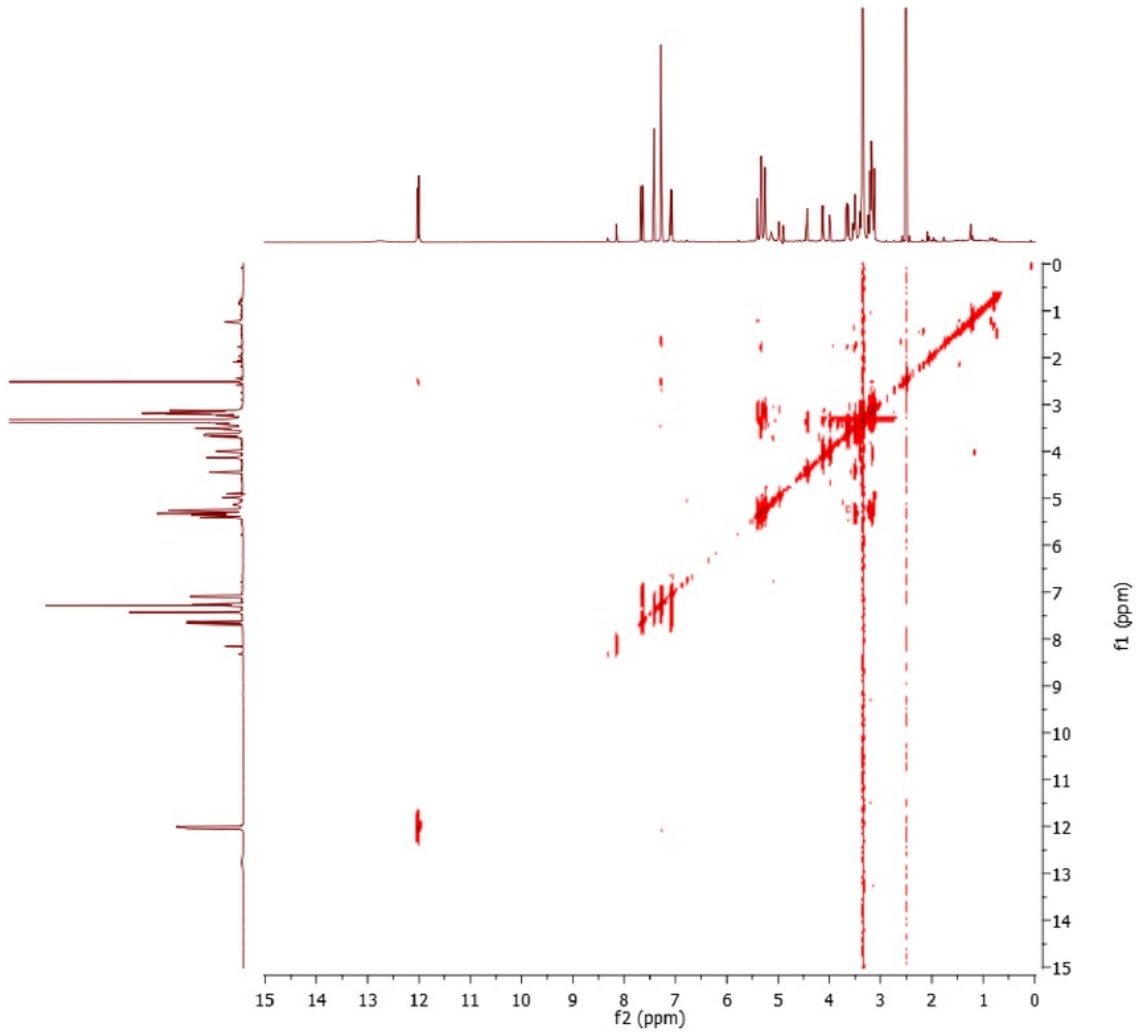

Figure 88: COSY spectrum (900 MHz, DMSO-d_6) of trichotomine G_3 (**2**)

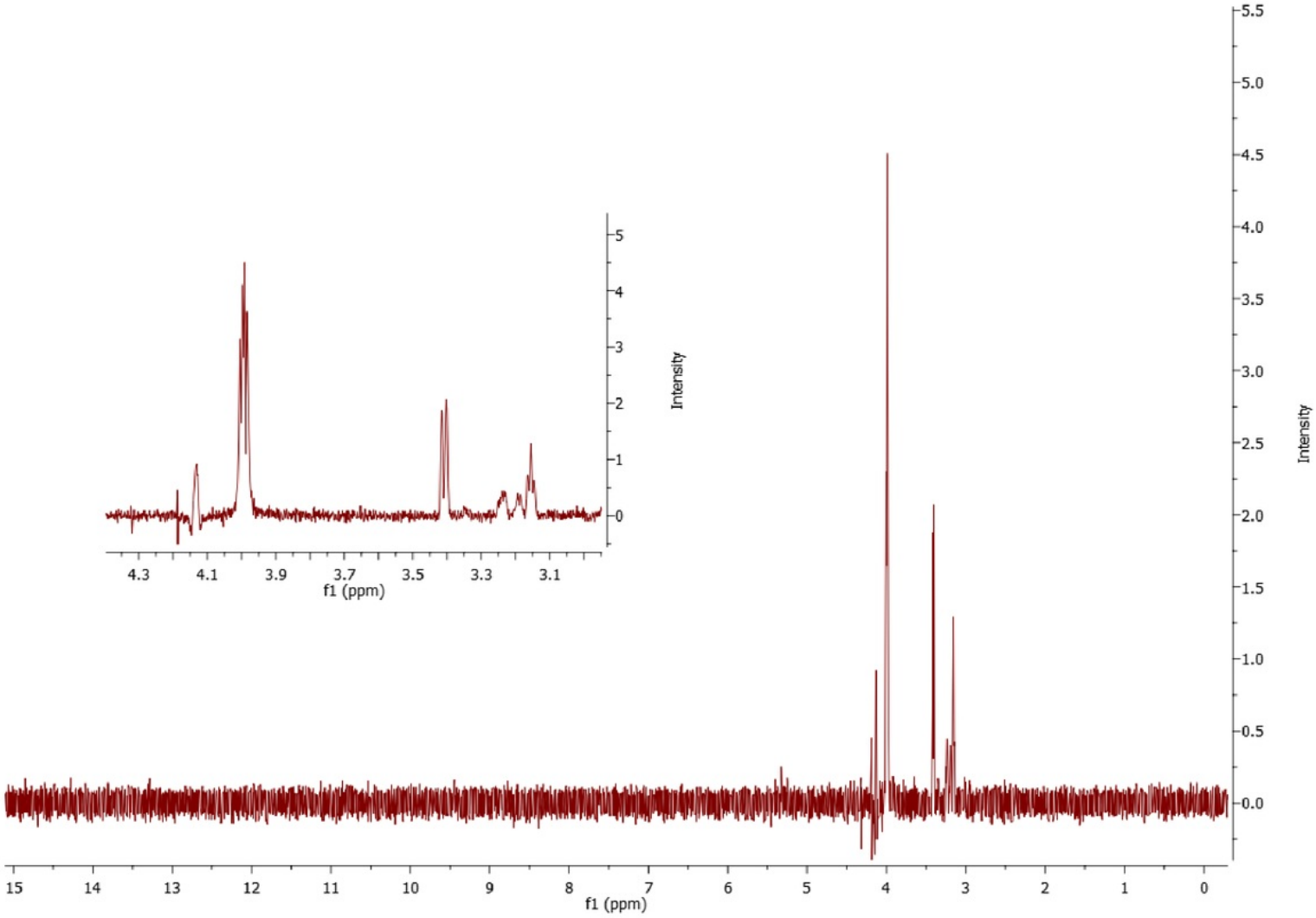

Figure 89: TOCSY spectrum of H-6''' (900 MHz, DMSO-d_6, O1P = 3.99 ppm) of trichotomine G_4 (**3**)

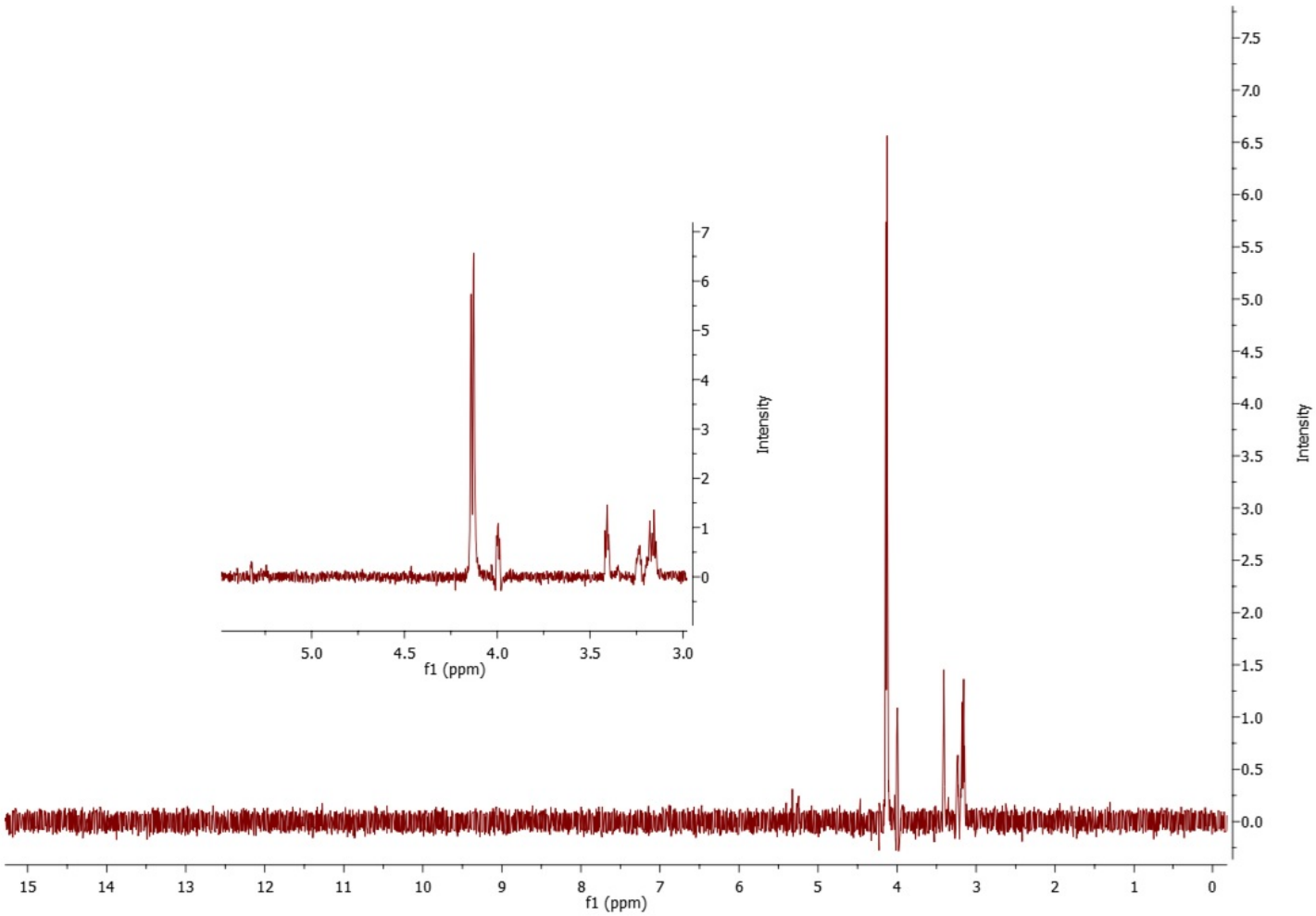

Figure 90: TOCSY spectrum of H-6''' (900 MHz, DMSO-d_6, O1P = 4.13 ppm) of trichotomine G_4 (**3**)

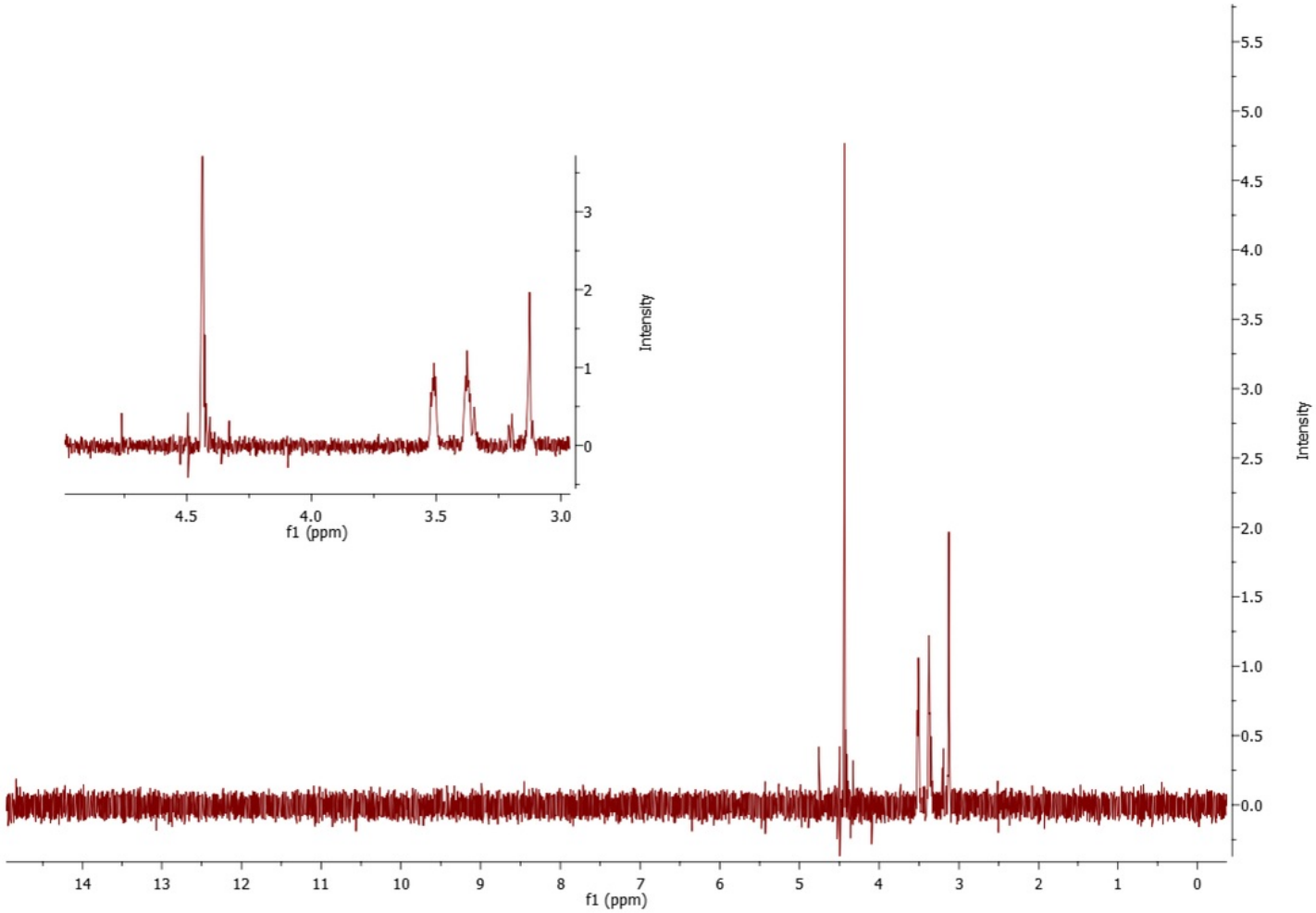

Figure 91: TOCSY spectrum of H-6'' (900 MHz, DMSO-d_6, O1P = 4.43 ppm) of trichotomine G_4 (**3**)

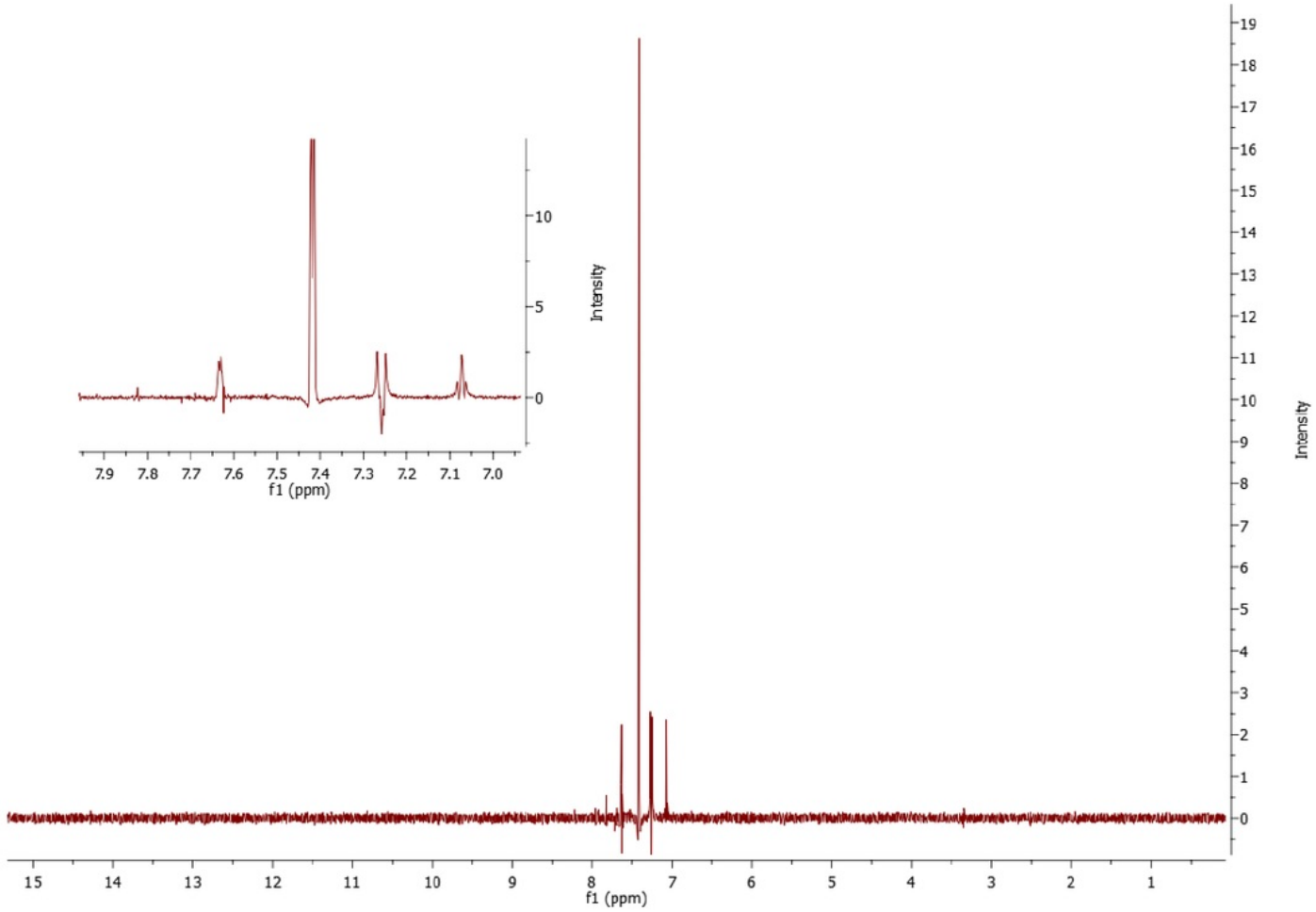

Figure 92: TOCSY spectrum of H-7 (900 MHz, DMSO-d_6, O1P = 7.62 ppm) of trichotomine G_4 (**3**)

5.3.3 Color Stability

Figure 93 shows the color stability over six weeks for solutions of trichotomine (**1**), trichotomine G_3 (**2**) and trichotomine G_5 (**4**). These preliminary qualitative results suggest that glycosylation stabilizes the trichotomine chromophore and protects against degradation. Surprisingly, the trichotomine standard was more stable at pH 1, pH 3, and pH 10 than at pH 7. For all analogs, the chromophore degraded more quickly at elevated temperature (45 °C) than at pH extremes. It was unclear from these preliminary data whether a malonylglycoside afforded more stability than a glycoside. The triglycosylated analogs G_6 and G_7 appeared to be slightly more stable than trichotomine G_1 but due to the more dilute concentration, it is unclear if they were more stable than the other diglycosylated analogs.

The molar extinction coefficients of trichotomine, trichotomine G_3, and trichotomine G_5 were measured at the blue chromophore maximum of λmax (659 nm, MeOH) and were as follows: ε 6.65 x 10^4 M^{-1} cm^{-1} (trichotomine), ε 5.12 x 10^4 M^{-1} cm^{-1} (trichotomine G_3), and ε 3.84 x 10^4 M^{-1} cm^{-1} (trichotomine G_5). Since the glycosidic attachments do not add to the blue color intensity of trichotomine, higher concentrations (on a gram/liter basis) will be needed to achieve the same blue color intensities as trichotomine becomes more extensively glycosylated. The blue color intensity of trichotomine is about half that of FD&C Blue No. 1 (ε_{629} = 1.34 x 10^5 M^{-1} cm^{-1}) but nearly four times that of the phycocyanobilin chromophore (ε_{604} = 1.71 x 10^4 M^{-1} cm^{-1}) (Chapter 1).

A future quantitative stability study might include the effect of light and investigate the mechanisms of degradation.

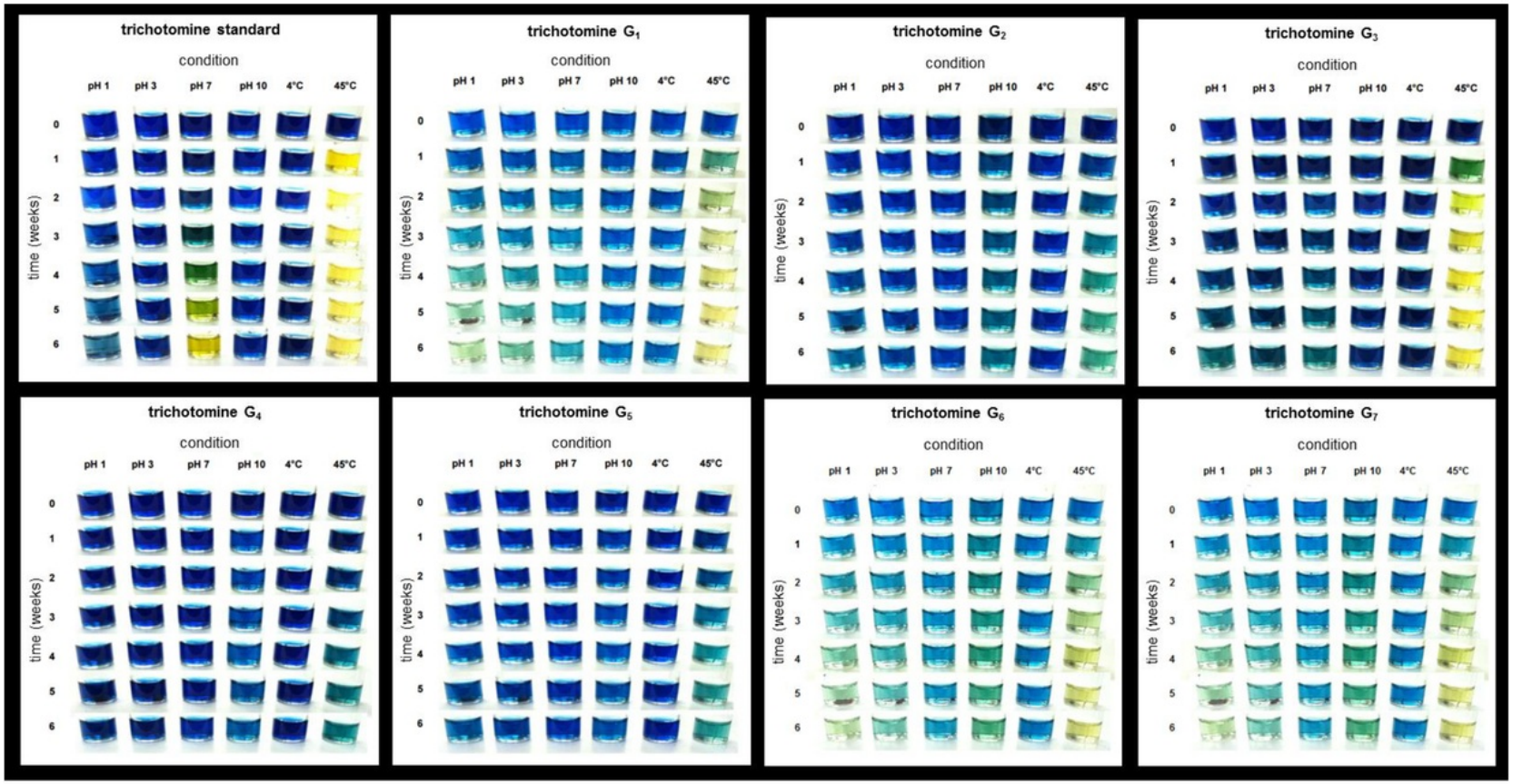

Figure 93. 6 week color stability study of trichotomine and trichotomine analogs G_1-G_7 in methanol/buffer 50mM (50:50, v/v) at 22 °C (for pH 1, 3, and 7), 4 °C (pH 7), and 45 °C (pH 7). All solutions were stored in the dark.

5.4 Conclusion

The 2D NMR assignments and MS and product ion MS/MS analyses are reported for trichotomine (aglycone), and the structure elucidation of three novel trichotomine 6-*O*-malonyl-β-*O*-glycosides including trichotomine G_3 (**2**), trichotomine G_4 (**3**), and trichotomine G_5 (**4**) are reported. The presence of more extensively glycosylated trichotomine analogs (trichotomine G_6, trichotomine G_7) was detected by HPLC-UV with high resolution MS^2 analysis. Trichotomine glycosides are *O*-(ester) linked rather than *N*- linked as was previously reported for trichotomine G_1 and G_2. Trichotomine glycosides have favorable properties as natural color candidates due to water solubility, color intensity, and apparent non-toxicity. However, a 6 week investigation of color stability of purified analogs revealed that the trichotomine chromophore stability is inadequate for viable commercial use in beverages and would need to be improved. While glycosylation significantly enhances the stability of the trichotomine chromophore, the pigment is particularly susceptible to heat (45 °C) degradation.

CHAPTER 6: INVESTIGATION OF "GARDENIA BLUE" AND GENIPIN-DERIVED PIGMENTS

6.1 INTRODUCTION

The iridoid genipin (Figure 94) is a plant constituent derived from the fruits of *Gardenia jasminoides* and *Genipa americana* used to produce the blue or violet colorant preparation "gardenia blue" upon reaction with an amino acid (286-290). The gardenia blue pigment is used for dying foods, fabrics, edible jet inks, and traditionally as a semi-permanent tattoo ink ("jagua ink") (291-295). The gardenia blue colorant is marketed as a natural colorant and consumed but is more correctly semi-natural or naturally derived. Geniposide, the major iridoid component of the mixture of iridoid glycosides in gardenia fruits, is first isolated and then hydrolyzed to genipin using β-glucosidase to yield genipin. Genipin is then heated with an amino acid or other primary amine which transforms genipin into a complex polymeric water-soluble dye mixture known as gardenia blue. Modification of the reaction conditions and selection of the primary amine substrate enable the production of red, blue, and violet colorants (296,297). A natural amino acid such as L-glycine or L-taurine is typically used for commercial gardenia blue dye preparations. The use of edible gardenia blue preparations by food and beverage companies is currently limited mainly to East Asian countries (such as Korea and Japan) due to the lack of regulatory approval elsewhere (298).

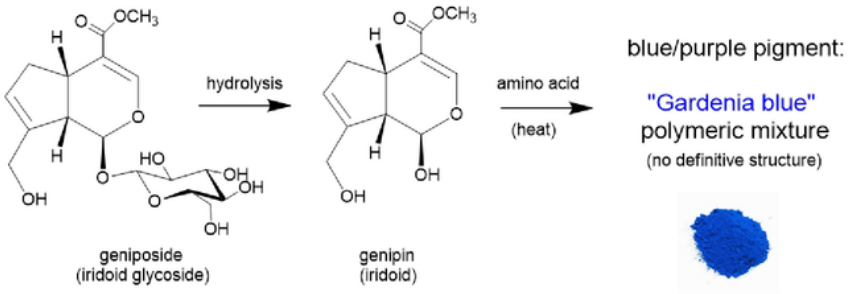

Figure 94. The process for the industrial production of gardenia blue colorant from geniposide.

Although the process to prepare the blue pigments from genipin with primary amines is simple, structural characterization of blue colorant product itself is lacking. Some published studies of the reaction of genipin with the simplest primary amine, methylamine, have elucidated the early stages of transformation of genipin to the 2-pyrindine skeleton as well as some brownish-red dimer and trimer intermediates (300,301). A more detailed scheme of the conversion of genipin to gardenia blue pigment with methylamine is shown in Figure 95. Putative mechanisms for the conversion of genipin to the major precursor GM5 and then to the apparent major 2-pyrindine monomer (BR1) have been proposed (286,299,300). The process of spontaneous polymerization of 2-pyrindine intermediates to the polymeric gardenia blue dye preparation is unknown. The number of monomer structure variants and the variety and frequency of the different linkages between monomer units in the gardenia blue product is also unknown.

In this study, the gardenia blue colorant was investigated with the aim of increase structural and chemical knowledge of the gardenia blue dye product with a focus on the blue chromophoric moieties. For spectroscopic study, gardenia blue pigment was generated by the simple reaction of genipin with methylamine. The reaction product was then analyzed by size-exclusion chromatography (SEC) and mass spectrometry. The UV spectra of the primary precursor monomer (BR1) and two dimers were predicted and compared using density functional theory (DFT) calculations. The first high resolution mass spectrum of a genipin-methylamine polymeric reaction product is reported. A commercial gardenia blue product provided by San Ei Gen F.F.I. was analyzed directly by 2D NMR spectroscopy. To study the effect of different primary amine sources on the resulting product color, gardenia blue pigment was generated by the reaction of genipin with various primary amines such as L-aspartame, L-glutathione, L-arginine, γ-aminobutyric acid, and L-glycine.

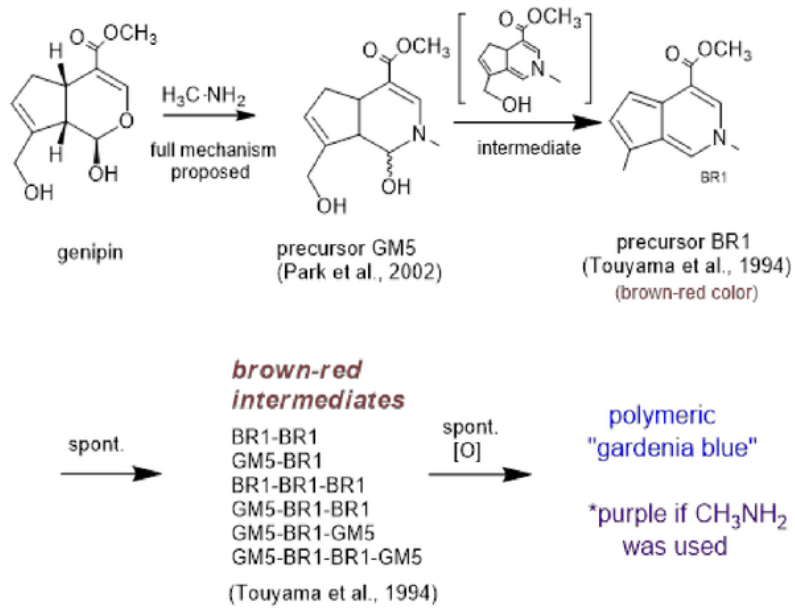

Figure 95. The reaction process for the formation of "gardenia blue" from genipin and methylamine

6.2 Materials and Methods

6.2.1 Materials. Genipin 98.0% was obtained from Santa-Cruz Biosciences. Other chemicals including methylamine were obtained from Sigma (Steinheim, Germany) and Aldrich (Milwaukee, WI). A commercial sample of gardenia blue pigment was obtained for analysis courtesy of San Ei Gen F.F.I. (Osaka, Japan) under a material transfer agreement.

6.2.2 Spectroscopic analysis. The UV-Vis spectra were obtained using a Shimadzu SPD-M20A photodiode array detector. The ^1H, DEPTQ, and 2D NMR spectra in D_2O were measured on a 900 MHz Bruker Avance NMR spectrometer using 4.0 mg of gardenia blue material dissolved in 500 µL of 99.9% D_2O in a 5 mm NMR tube. High resolution mass spectra were obtained with Shimadzu (Kyoto, Japan) IT-TOF mass spectrometer using an electrospray ionization source with polarity switching and a scan

range of *m/z* 100-1000 for most experiments. MALDI-TOF mass spectra were obtained using an Applied Biosystems MALDI Voyager DE Pro using α-cyano-4-hydroxycinnamic acid matrix in linear negative ion mode with pure matrix as the blank. The genipin-amine products (section 6.3.4) were prepared similarly to the reaction of genipin and methylamine (section 6.2.4), 0.2 μm filtered, and analyzed by flow injection through a Shimadzu SPD-M20A diode array detector.

6.2.3 Density Functional Theory calculations. Density functional theory (DFT) calculations were performed using Gaussian 03 (Gaussian, Inc., Wallingford, CT) software and uploaded to the UIC Argo supercomputer cluster for computation. Molecular geometries were optimized using the DFT model with B3LYP functional set and a 3-21G basis set with PCM solvent model (H_2O) with manual input parameters as follows: ofac=0.8, rmin = 0.5, nosymmcav, radii=uff. After optimization, the singlet state UV spectral absorptions were calculated using the TD-DFT using the same parameters, and the output results were plotted in Microsoft Excel.

6.2.4 Analysis of gardenia blue from genipin and methylamine. To 10 mg of genipin (44 μmol) suspended in 400 μL of 100 mM phosphate buffer (pH 7.0 at 25 °C), 55 μL (440 μmol methylamine) of a 33% solution of methylamine (8.03 M methylamine) was added in anhydrous ethanol. The solution (pH 9) was stirred at 70 °C for 5 h. The resulting dark blue-purple solution was diluted to 2 mL with water and centrifuged at 12,000 x *g* for 20 min. The supernatant was filtered through a 0.2 μm Nylon membrane and analyzed using a Phenomenex (Torrance, CA) BioSep s2000 300 x 7.8 mm size exclusion column (MW fractionation range 1-100 kDa) connected to a Shimadzu Prominence HPLC with a photodiode array (PDA) detector at a flow rate of 1.0 mL min^{-1} with water/acetonitrile (95:5; v/v) as the mobile phase. The purple pigmented peak (genipurin, t_R = 10.3 min) was collected, dried under N_2 gas (<10 μg), redissolved in 50 μL of methanol/water (75:25; v/v), and centrifuged at 12,000 x *g* for 20

min. The purple supernatant was analyzed by MALDI-TOF mass spectrometry and by flow injection analysis on a Shimadzu IT-TOF mass spectrometer.

6.3 Results and Discussion

Structural characterization of a heterogeneous polymeric mixture is inherently more difficult than that of a pure small molecule. Consistent with the aim of this project, a major goal of the present work was to increase structural understanding of the blue chromophore of the gardenia blue pigment. A discussion of the gardenia polymer composition and blue chromophoric moieties with support from DFT calculations is presented in Section 6.3.1. Results for the reaction, purification, and mass spectrometric analysis of gardenia blue pigment from genipin and methylamine are presented in Section 6.3.2. The NMR analysis of the commercial gardenia blue product provided by San Ei Gen F.F.I. is presented in Section 6.3.3, and the results for the generation of gardenia blue pigments from genipin and alternative primary amines are presented in Section 6.3.4.

6.3.1 Gardenia blue pigment chromophoric moieties

The gardenia blue pigment is likely a heterogeneous mixture and with a high degree of structural variation. The reaction of genipin with a primary amine is known to produce precursor monomers of the 2-pyrindine skeleton. The major precursor monomer to the formation of blue pigment appears to be the 2-pyrindine structure monomer BR1 (Figure 95). The blue pigmentation manifests when 2-pyrindine monomers such as BR1 and intermediates spontaneously polymerize to yield a poorly characterized heterogeneous mixture of high molecular weight blue products.

Investigation of the types of linkages between monomer units that result in a blue pigmentation (conjugated π electron systems, λ 500-700 nm) is informative towards understanding the blue pigmentation of the polymeric gardenia blue product. The intermediate dimers and trimer products of

the genipin-methylamine reaction characterized by Touyama et al., (14,15) were linked with a C_0 (direct), saturated C_1 (-CH_2-), unsaturated C_1 (=CH-), saturated C_2 (-CH_2CH_2-), or unsaturated C_2 (-CH=CH-) bridges. Polymerization linkages occur at the 6 and 8 position of the 2-pyrindine skeleton. Following these observations, there are at least 15 ways that two BR1 monomers can be linked as shown in Figure 96. However, BR1 is not the only monomer that may be involved in polymerization. At least 5 different variants of the BR1 monomer have been characterized (286,299). Therefore, the number of potentially reactive monomer intermediates involved in the formation of gardenia blue combined with the numerous possible linkages between the monomers suggests the possibility of hundreds of chemically distinct dimer species.

Although a defined structure of gardenia blue pigment may not exist, one aim of the present work was to increase structural understanding of the possible blue chromophoric units within the polymeric product. Two genipin derived 2-pyrindine dimers have been published that are reported to have blue pigmentation (Figure 97). All other previously reported monomers or higher intermediates were not blue (typically yellow red, or brown in color). The uncharged 8,8-linked dimer with a C_2 bridge was isolated as an unstable blue pigment (300). In separate research, the product genipocyanin G1 (derived from genipin and L-glycine) was isolated and characterized by NMR spectroscopy (301). Genipocyanin G1 displays a charged nitrogen and a (6,8)-linkage with a C_1 bridge. In this work, the UV spectrum of the (6,6)-linked genipin-methylamine version (*N*-methyl instead of *N*-glycine) of genipocyanin G1 was calculated using DFT theory along with the unconjugated C_1 linked and BR1 monomer for comparison. The conjugated C_1 linked dimer showed calculated visible absorption in the blue pigment range (Figure 98).

In summary, this analysis and observations together suggest that blue chromophoric moieties that occur within the gardenia blue polymer may be (6,6)-linked, (6,8)-linked or (8,8)-linked, contain an unsaturated C_1 or C_2 bridge, and the heterocyclic nitrogen may or may not be charged. As expected and

consistent with other blue pigments involving *N*-heterocyclic aromatic systems (Chapter 1 and Chapter 5), an extensive π electron system conjugated across at least two monomers is the critical property for the desired color in the gardenia blue polymer.

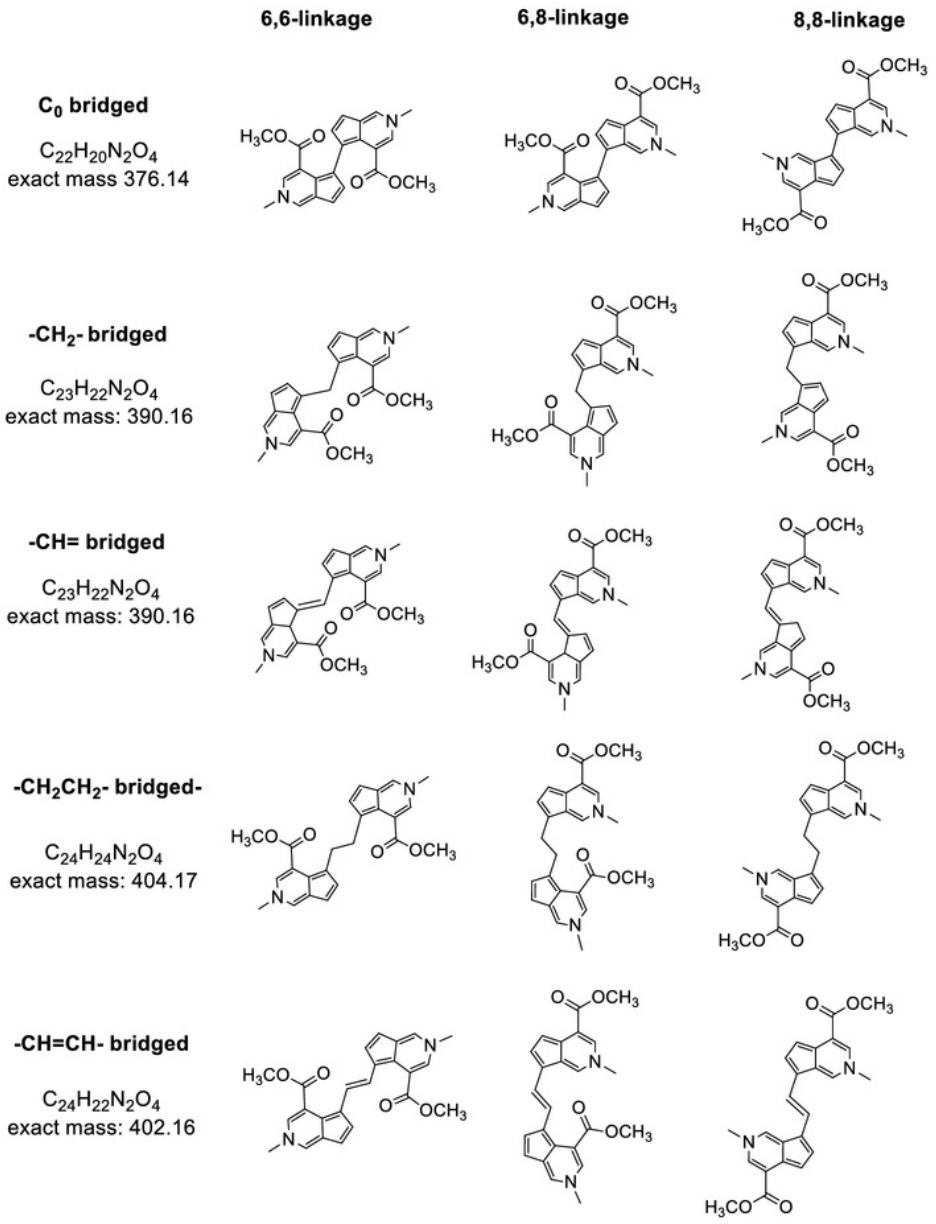

Figure 96. Dimer linkage possibilities for the primary monomer BR1

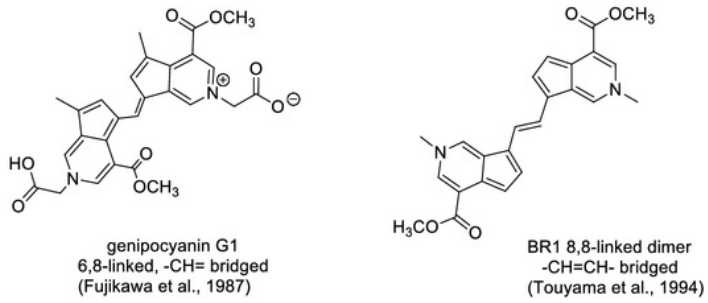

Figure 97: Chemical structures of published genipin-amine derived dimers with blue pigmentation

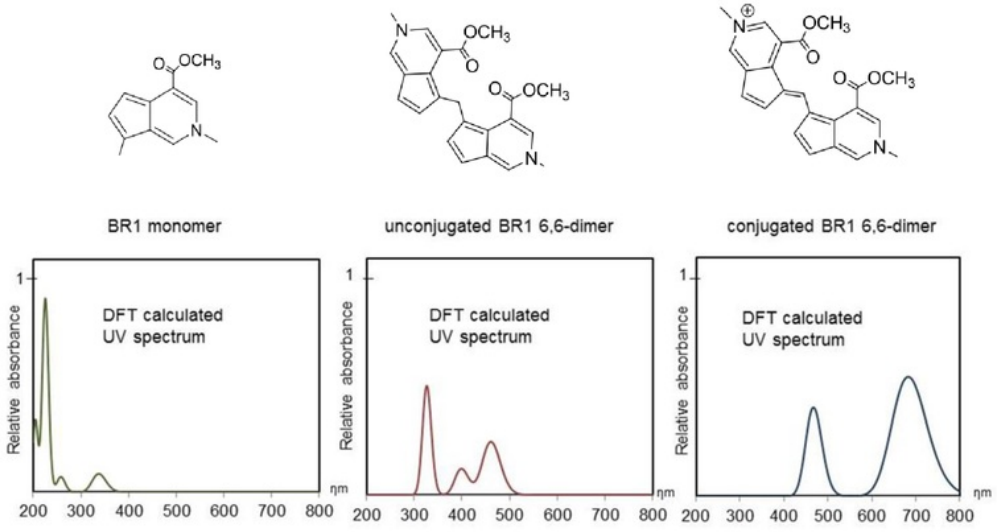

Figure 98: DFT calculated UV spectra of the BR1 monomer and (6,6)-linked conjugated and unconjugated BR1 dimer

6.3.2 Size exclusion chromatography and high resolution mass spectrometry of genipin-methylamine pigment

Genipin was reacted with methylamine to produce gardenia blue pigment material for study. The reaction solution became yellow immediately upon addition of methylamine, dark brown-red within 1 h, and then violet after 5 h. Prior to analysis, the reaction solution was split into two portions. One was stored at ambient temperature on the benchtop and the other at -20 °C protected from light for 48 h. Both samples were analyzed using size exclusion chromatography with UV absorbance detection (Figure 99). The solution that had been protected from light showed only one major blue pigmented product (named genipurin, t_R = 10.3 min). The UV spectra of the later eluting peaks showed characteristics of previously published red-brown intermediates or precursors such as monomer GM5 (Figure 95). The reaction product mixture stored at ambient temperature showed a decrease in precursors and genipurin along with an increase in high mass pigmented material near the column void time (>150 kD MW) suggesting the spontaneous formation of polymeric gardenia blue pigment from precursors. In the mass spectra, no ions of the high mass pigmented material were observed.

The genipurin pigment peak from the -20 °C stored sample was purified using size exclusion chromatography and then analyzed by using MALDI-TOF MS and IT-TOF MS. The IT-TOF positive ion electrospray mass spectra showed a series of doubly and triply charged ions (Figure 100). Table XV summarizes the high resolution accurate mass data for the purified genipurin peak. Figure 101 shows hypothetical ion structures consistent with the HRMS accurate masses and charge states of ions observed for the pigmented genipurin peak. The structures are only representative possibilities. Many isomers are possible due to the number of possible linkages, bridges, and charges. These data strongly support the genipurin pigment peak as being constructed of BR1 monomer units (203.1 Da) or slight variations thereof.

The MALDI negative ion mode signals around *m/z* 2,200 (Figure 100) suggest a degree of polymerization (DP_n) value near 10 for genipurin. The genipurin peak appears to be a reasonably stable oligomeric purple pigmented precursor to higher molecular weight polymeric gardenia blue pigment species. These are candidates for bulk purification and characterization by NMR spectroscopy in future work. In the next section, NMR analyses of a commercial gardenia blue product are described.

TABLE XV:

ELECTROSPRAY (+) HIGH RESOLUTION MASS SPECTROMETRIC DATA FOR THE ISOLATED PIGMENT PEAK (GENIPURIN) OF THE GENIPIN-METHYLAMINE REACTION

HRMS ion (charge)	$Mass_{obs}$	proposed formula	$Mass_{calcd}$	error (ppm)	[n] units
201.0828 (+2)	402.1656	$C_{24}H_{22}N_2O_4^{2+}$	402.1580	18.9	2
294.6164 (+2)	589.2328	$C_{35}H_{31}N_3O_6^{2+}$	589.2213	19.5	3
309.6224 (+2)	619.2448	$C_{37}H_{37}N_3O_6^{2+}$	619.2682	-37.8	3
316.1366 (+2)	632.2732	$C_{38}H_{38}N_3O_6^{2+}$	632.2761	-4.6	3
331.1412 (+2)	662.2824	$C_{39}H_{40}N_3O_7^{2+}$	662.2866	-6.3	3
395.1548 (+2)	790.3096	$C_{47}H_{42}N_4O_8^{2+}$	790.3003	11.8	4
410.1595 (+2)	820.3190	$C_{48}H_{44}N_4O_8^{2+}$	820.3108	10.0	4
340.1327 (+3)	1020.3981	$C_{60}H_{54}N_5O_{11}^{3+}$	1020.3820	15.8	5

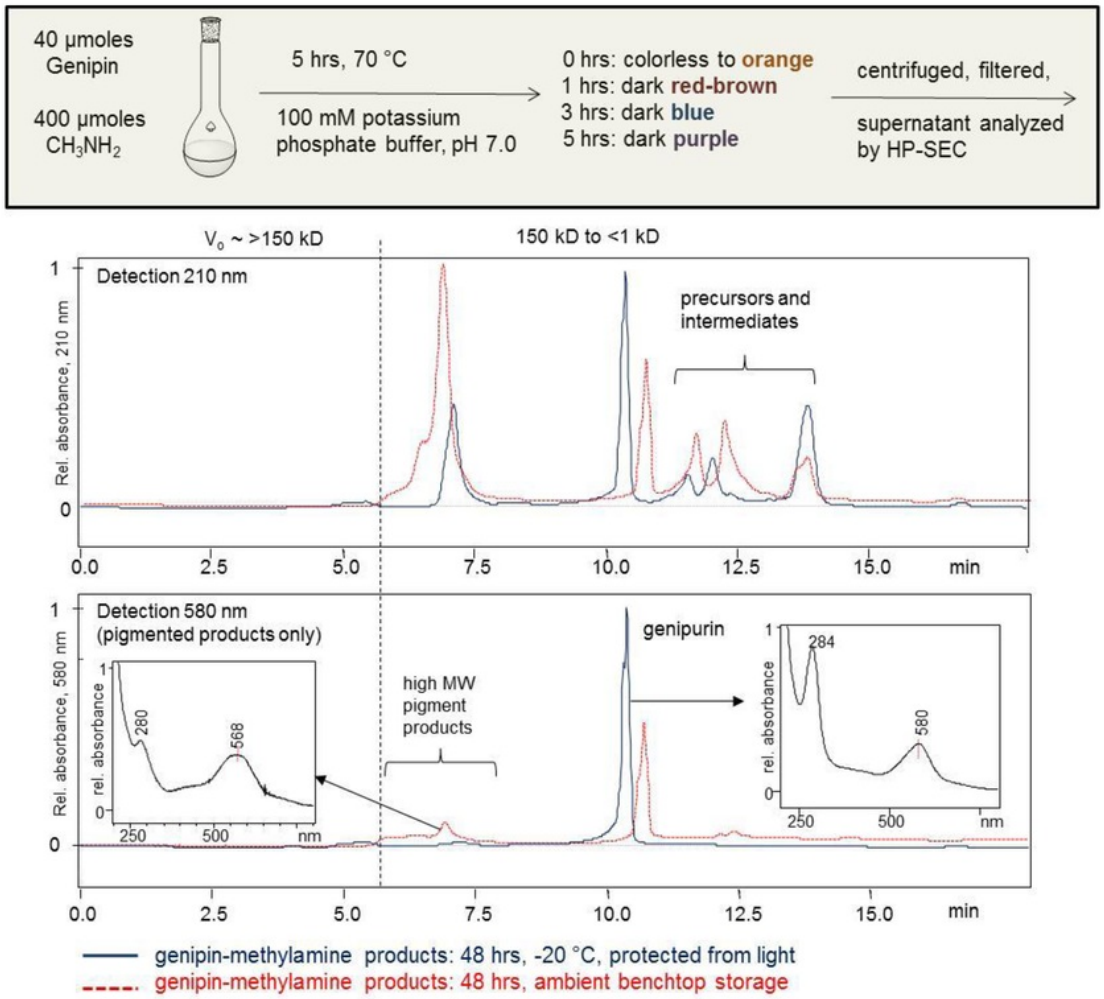

Figure 99. The reaction conditions and size exclusion LC-UV chromatograms for genipin-methylamine reaction products. The chromatogram for the sample stored at -20 °C and protected from light shows only one major pigment peak (genipurpin) whereas the sample left at ambient conditions for 48 h shows the formation of high mass pigmented products. The UV spectra of the purple genipurin peak and the high mass polymer peak are shown as insets. HP-SEC = high performance size exclusion chromatography

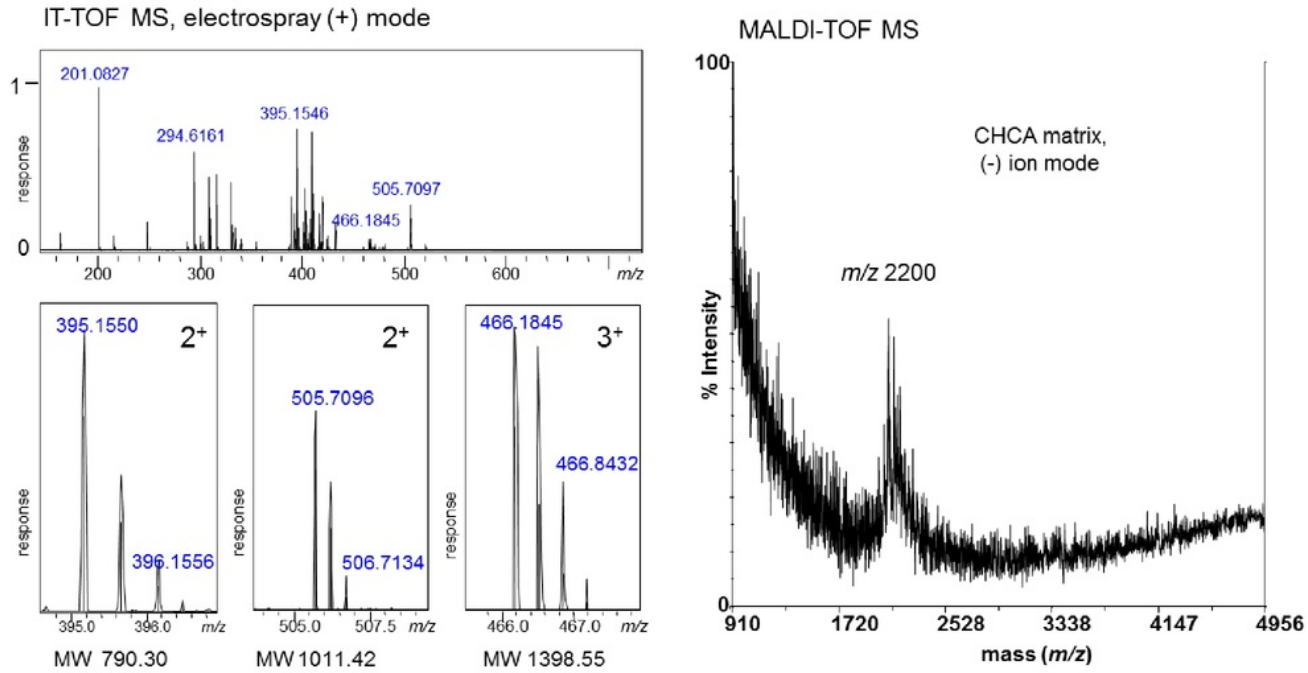

Figure 100. IT-TOF positive ion electrospray and MALDI mass spectra for the genipin-methylamine reaction product peak "genipurin" purified by size-exclusion chromatography.

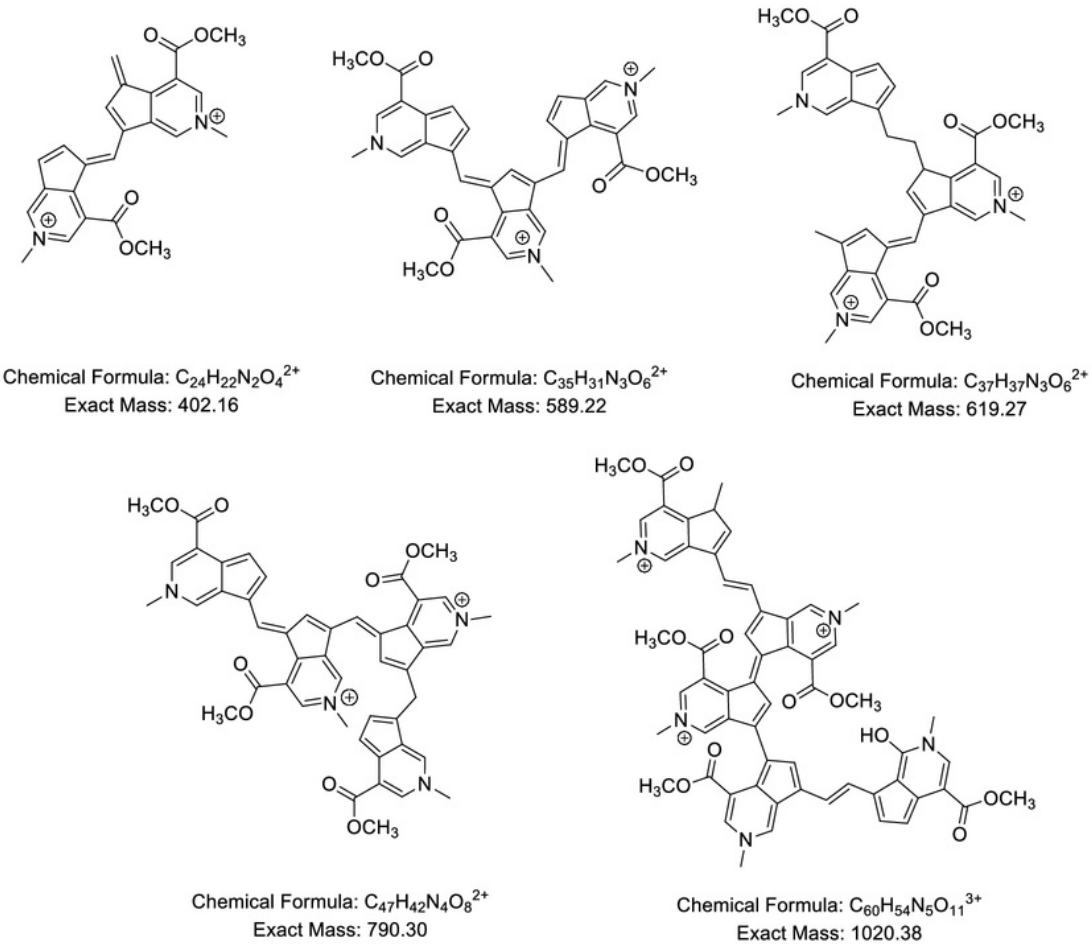

Figure 101. Hypothetical chemical structures consistent with the observed HRMS accurate masses, charge state, and linkage patterns known to occur between monomers in genipin-methylamine reaction products.

6.3.3 2D NMR analysis of commercial "gardenia blue" colorant

The commercial gardenia blue product analyzed by 900 MHz 2D NMR spectroscopy showed major signals fully consistent with the starting material genipin. The high quantity of unreacted genipin suggests that the primary amine was the limiting reagent with this particular product reaction process. The complete NMR assignments of genipin have been published previously (299). The high degree of complexity in the aromatic region is presumably due to a mixture of polymerized products of the 2-pyrindine BR1 monomer unit. As shown in Figure 102, a pair of doublet signals (7.12 ppm doublet, 8.22 ppm doublet) in the aromatic region may be consistent with either terminal or unreacted BR1 monomer or the presence of an ethene (–CH=CH-) bridge between two BR1 monomers similar to the linkage in the previously reported blue pigmented dimer isolate (299). The baseline singlet signals in the aromatic region (6-9 ppm) are consistent with aromatic protons attached to the pyrindine monomer skeleton. The baseline signals for the gardenia blue polymer were too weak relative to genipin for the analysis of 2D NMR correlations of the blue pigmented polymer. The ^{1}H, COSY, DEPTQ, HSQC and HMBC NMR spectra of the commercial gardenia blue pigment are shown in Figures 103-107.

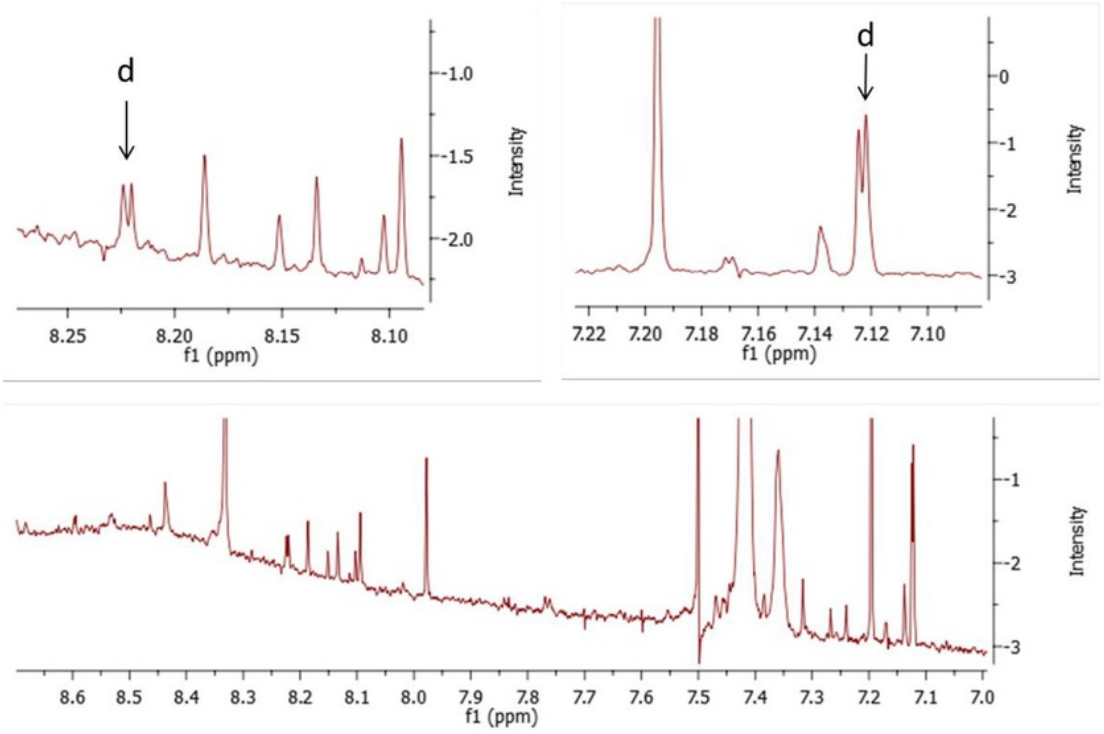

Figure 102. 900 MHz ^{1}H NMR spectra expansions showing aromatic region doublet (d) signals within the complex baseline of gardenia blue pigment.

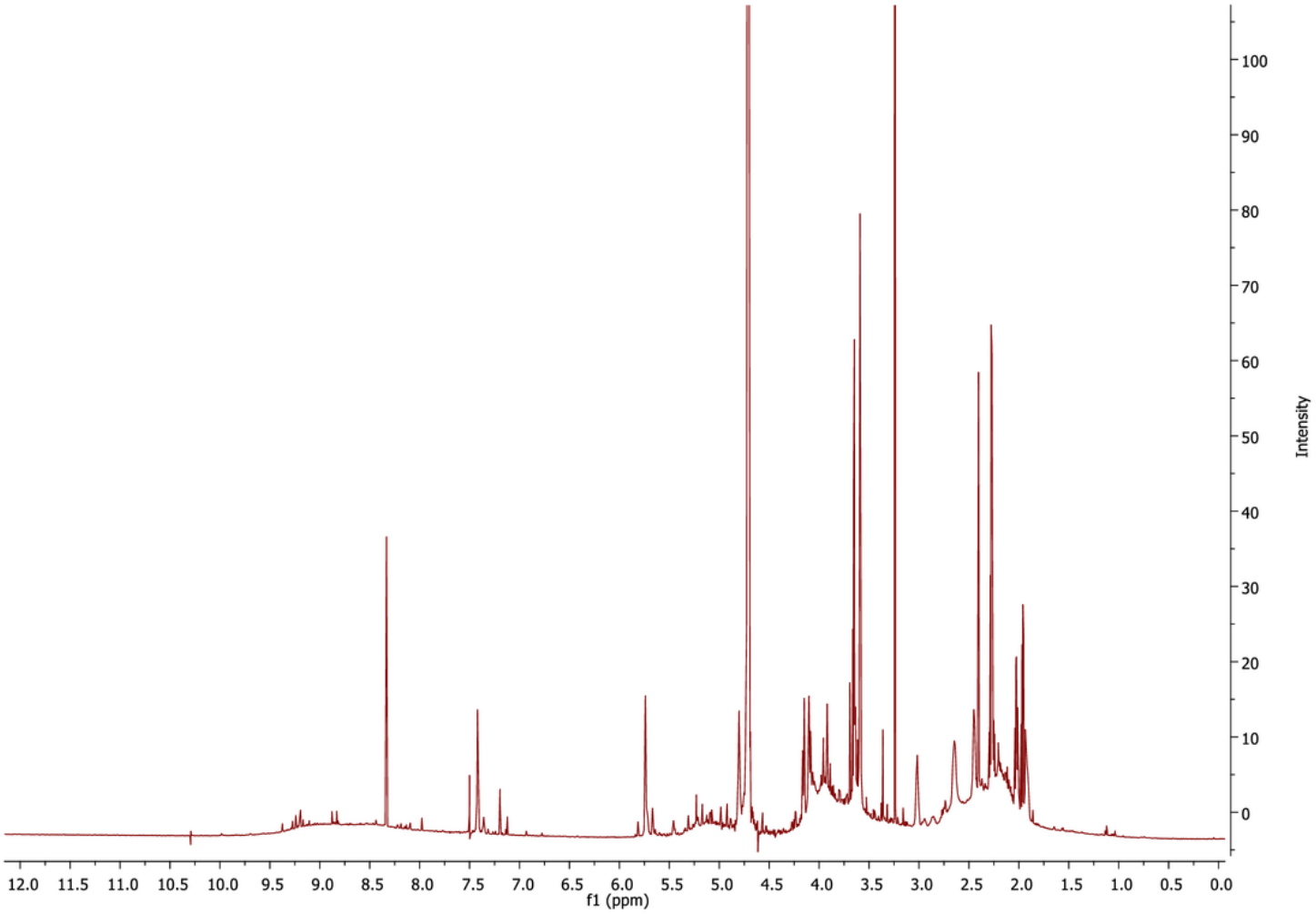

Figure 103. ^{1}H NMR 900 MHz of San Ei Gen "Gardenia Blue" in D_2O

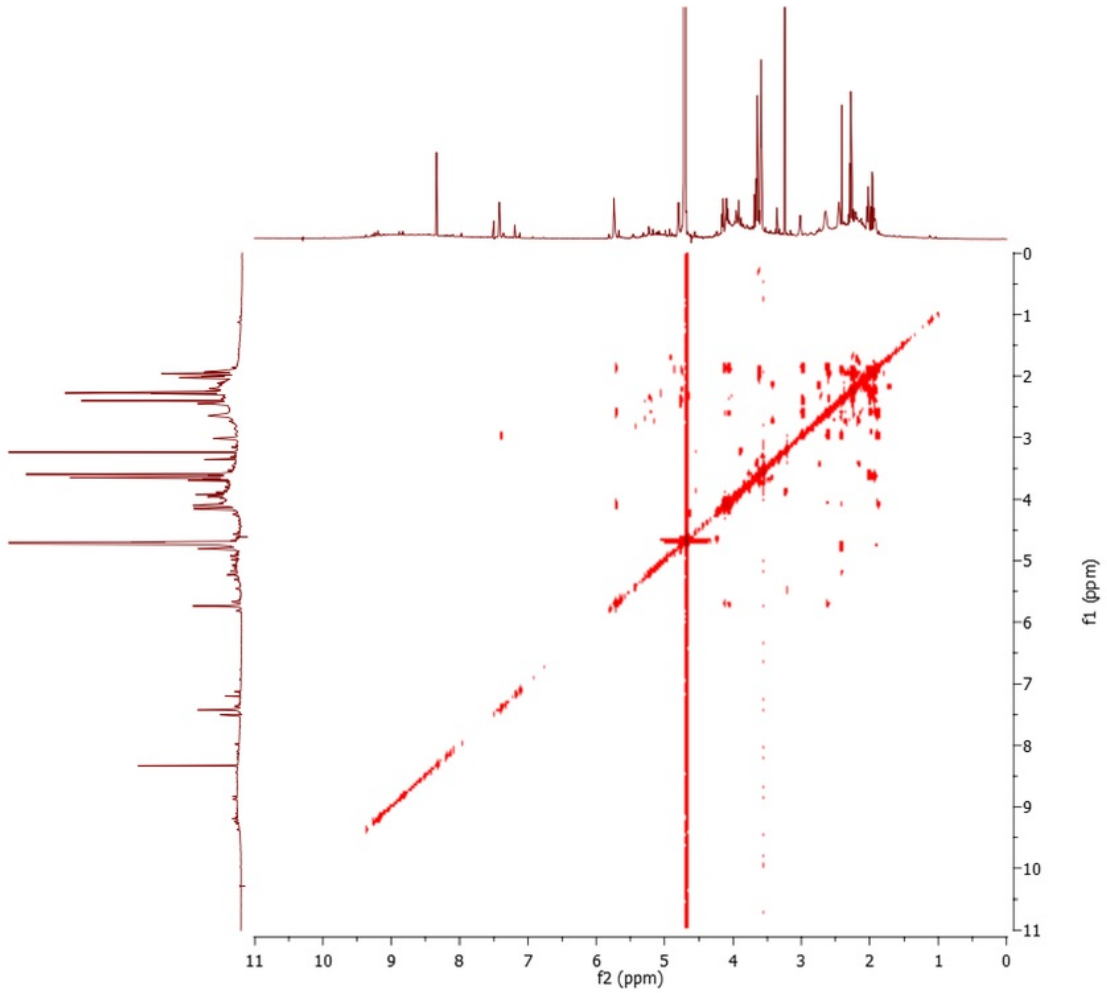

Figure 104. COSY 900 MHz NMR spectrum of San Ei Gen "Gardenia Blue" in D_2O

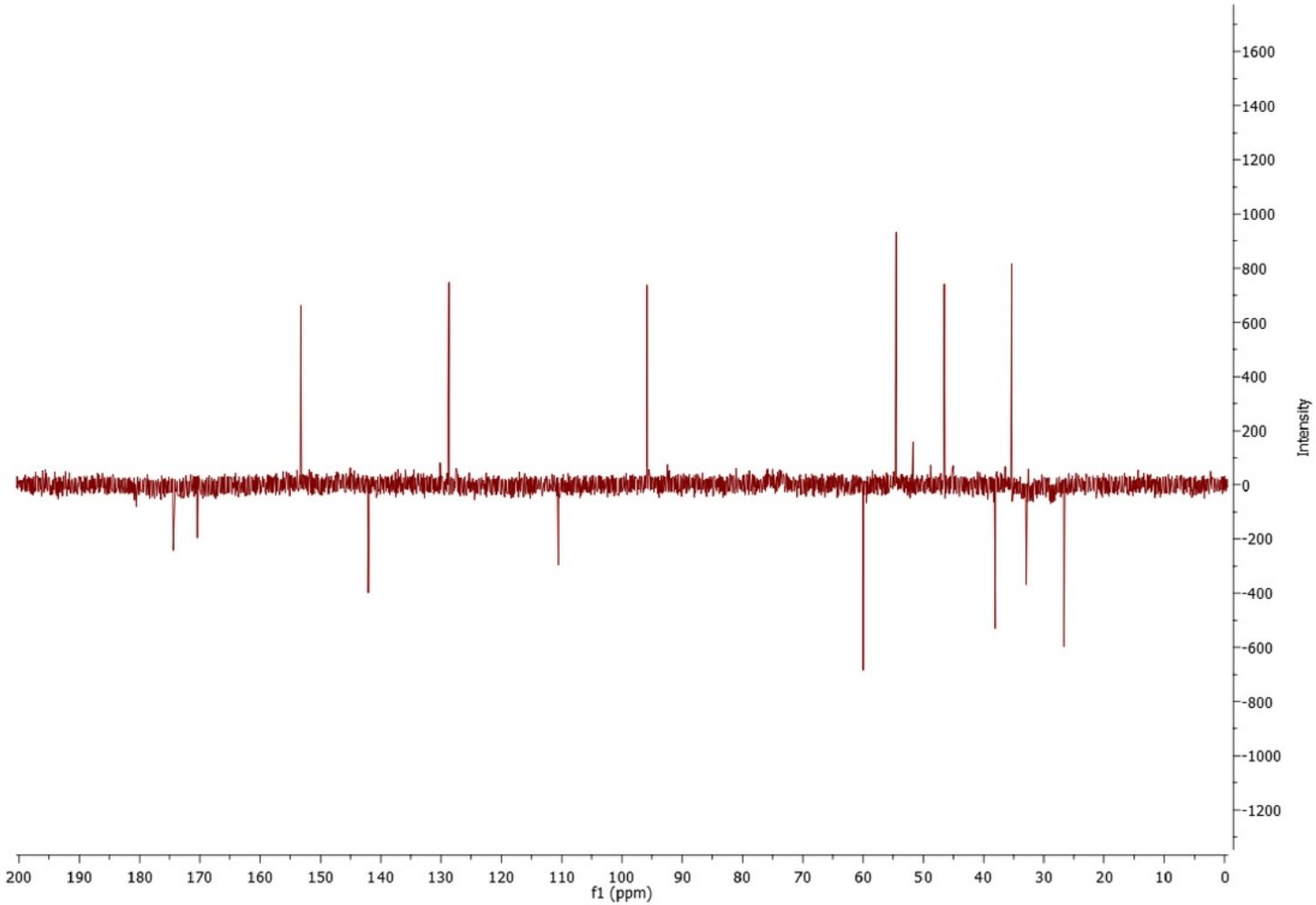

Figure 105. DEPTQ 900 MHz NMR spectrum of San Ei Gen "Gardenia Blue" in D_2O

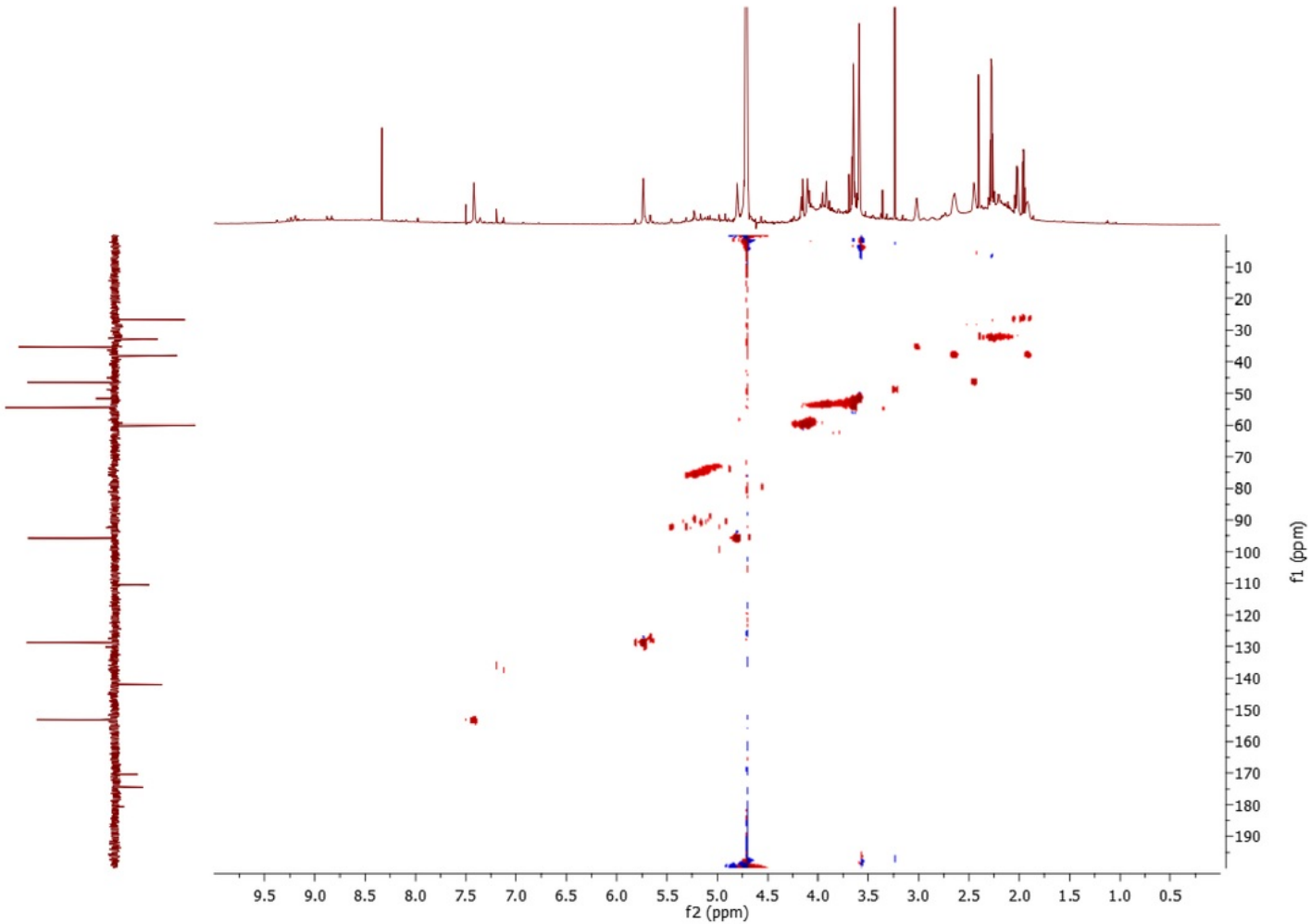

Figure 106. HSQC 900 MHz NMR spectrum of San Ei Gen "Gardenia Blue" in D_2O

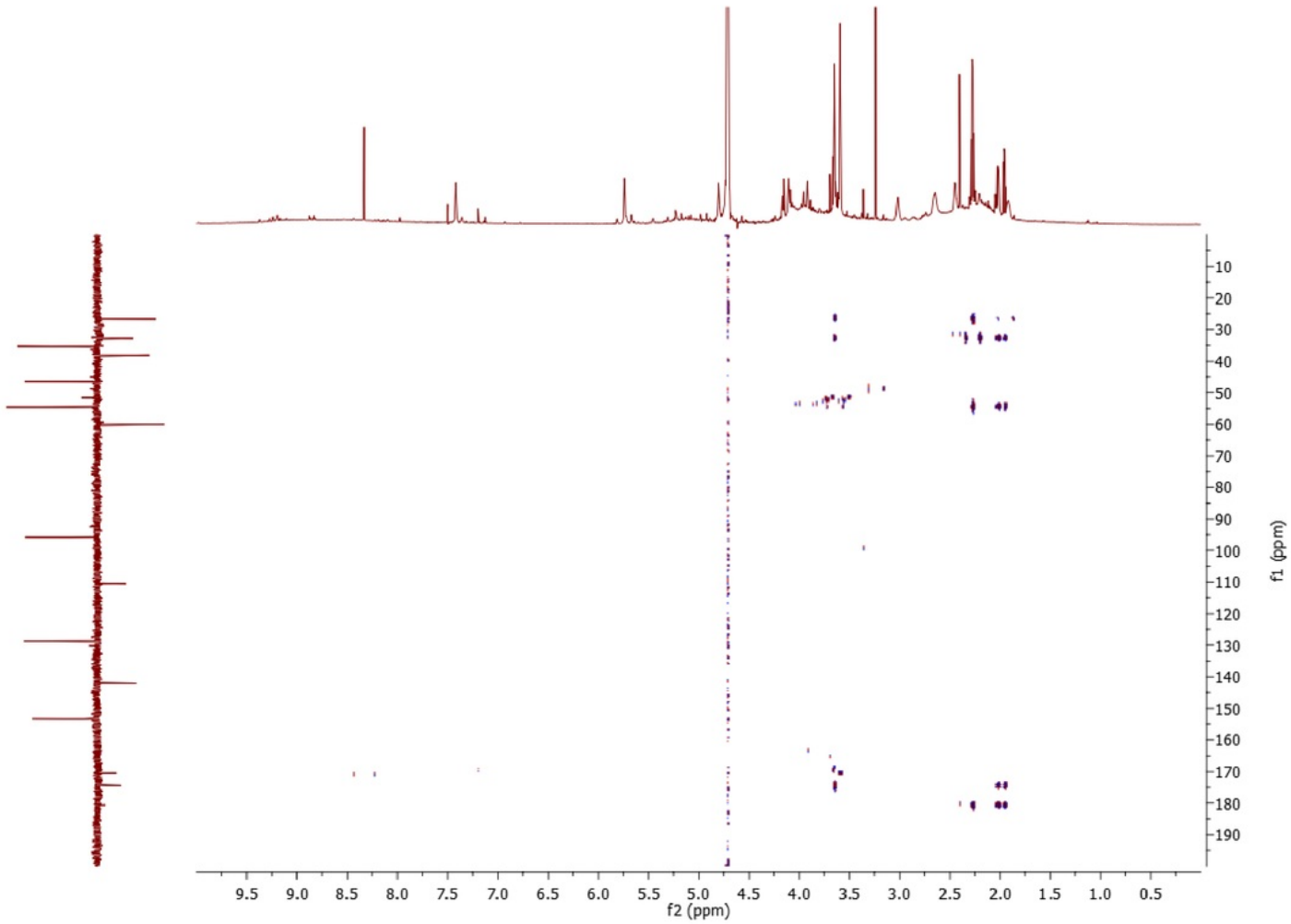

Figure 107. HMBC 900 MHz NMR spectrum of San Ei Gen "Gardenia Blue" in D_2O

6.3.4 Reaction of genipin with primary amines

Pure genipin was reacted with a variety of primary amines which are not typically used for the production of gardenia blue pigment using the same reaction protocol described for genpin and methylamine. Qualitative descriptions of the reaction products are shown in Table XVI. A comparison of the UV/Vis spectra of some of the primary amines which produced blue pigmented products is shown in Figure 108. An ideal natural colorant candidate for commercial beverage use would match the bright blue color hue of FD&C Blue No. 1. The product of genipin and L-glutathione uniquely displayed a bright sky blue hue. An invention disclosure was submitted to the UIC Office of Technology Management (see Appendix G) for the discovery of the sky blue pigment product of genipin and L-glutathione, but the university chose not to pursue a patent.

TABLE XVI. QUALITATIVE RESULTS OF REACTION PRODUCTS OF GENIPIN AND VARIOUS PRIMARY AMINES

genipin-amine reaction	description
genipin + guanidine	yellow-brown solution
genipin + cytidine	yellow-brown solution
genipin + hydroxylamine	clear, colorless
genipin + aniline	cloudy orange solution
genipin + L-tryptamine	cloudy orange solution
genipin + 4-guanidinobutyric acid	cloudy orange solution
genipin + L-dopamine	green solution, blue ppt
genipin + methylamine	dark purple solution
genipin + propane-1,3-diamine	purple solution
genipin + L-canavanine sulfate	dark blue solution
genipin + L-aspartame	blue solution
genipin + L-glutathione	sky blue solution
genipin + L-arginine	blue solution
genipin + γ-aminobutyric acid	blue-purple solution
genipin + L-glycine	blue-purple solution

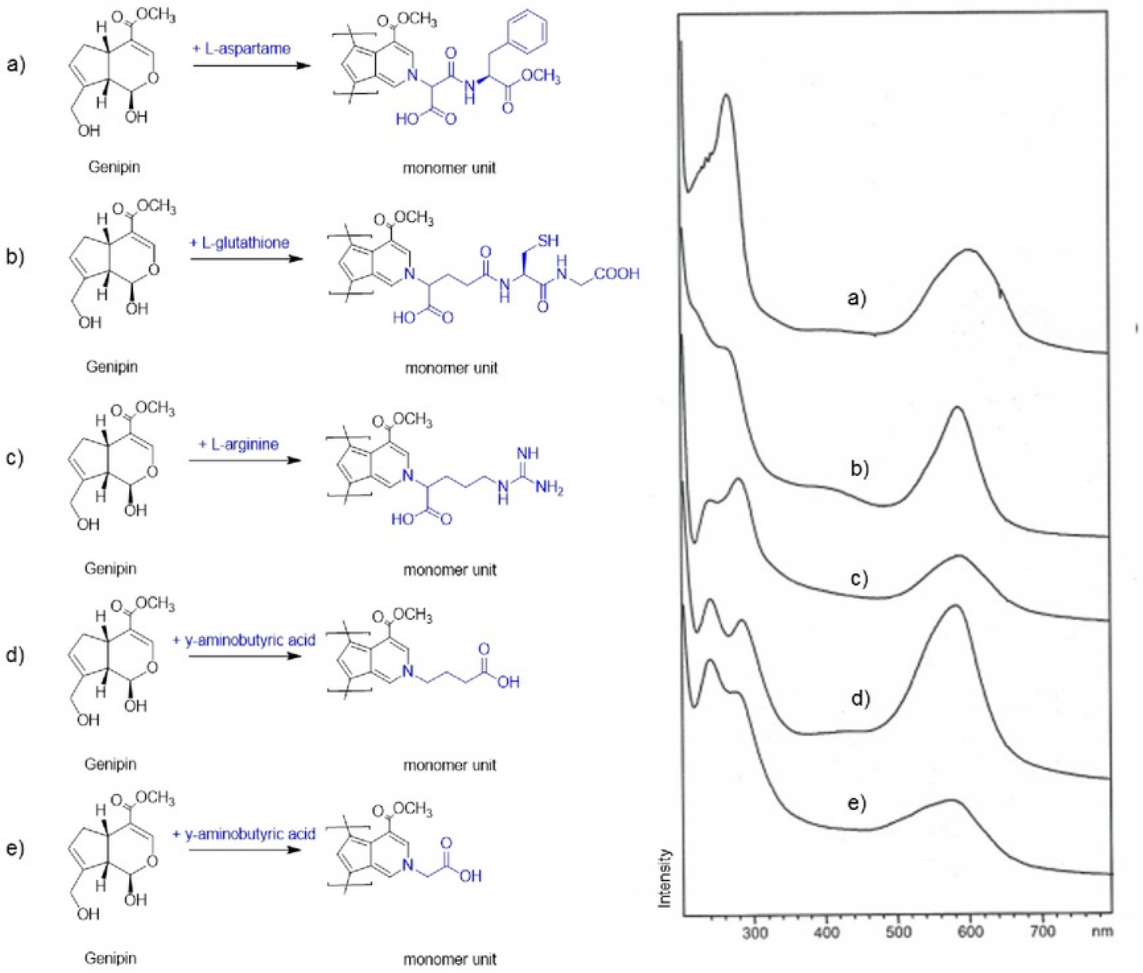

Figure 108. Comparison of UV absorbance spectra of blue pigments formed from the reaction of genipin with a) L-aspartame b) L-glutathione c) L-arginine d) γ-aminobutyric acid and e) L-glycine with putative monomer units.

6.4 Conclusion

The pigment "gardenia blue," the water soluble polymeric blue pigments derived from the reaction of genipin (from *Genipa americana* and *Gardenia jasminoides*) and a primary amine, is currently used by the food industry on a limited regulatory basis. The structural details of the polymeric mixture are still not well understood. The NMR analysis of a commercial "gardenia blue" product provided by San Ei Gen F.F.I. revealed mostly starting material genipin with unresolvable baseline complexity arising from the polymeric blue pigmented products. Additional gardenia blue pigment was generated by reaction of genipin with other primary amines resulting in the discovery of the genipin/L-glutathione sky blue pigment similar to FD&C Blue No. 1. For spectroscopic study, the gardenia blue pigment was generated by the reaction of genipin with methylamine. Possible structures were proposed based on high resolution tandem mass spectrometric analysis and MALDI mass spectrometric analysis of a 2.2 kDa purple intermediate isolated by size-exclusion chromatography. The UV spectra of a monomer and two dimers were predicted using density functional theory (DFT) calculations. These results together with previously reported work suggest that the blue chromophore sections of gardenia blue pigment involve a conjugated system of at least two 2-pyrindine ring systems linked at the 6 and 8 positions by an unsaturated C_1 or C_2 bridge

CHAPTER 7: CONCLUSION AND FUTURE DIRECTIONS

7 CONCLUSION AND FUTURE DIRECTIONS

The search for natural blue colorant alternatives to FD&C Blue No. 1has been ongoing for decades but has not been successful. Chapter 1 provided the first comprehensive review of natural blue pigmented organic compounds reported to date (172) and established major blue chromophore classes found in nature (flavonoid, quinoid, indole, tetrapyrrole, pyridyl, azulene, and phenazine). In addition to having a suitable blue hue and color intensity, a successful natural blue colorant requires excellent chemical stability and solubility in acidic solutions, must be available in bulk from natural sources at low cost, and must be completely safe for human consumption. No previously identified natural blue pigment meets all of these requirements.

Since the majority of the global search effort to date had focused on blue pigment molecules from flowers and fruits of plants, the current work sought to explore novel blue pigments from more obscure sources such as from the marine environment and extremophilic organisms which would be more likely to contain novel chromophores or pigments with greater heat and acid stability. Chapter 2 covered a variety of pigments explored and dereplicated from less accessible or underexplored biological sources. These included extracts of thermophilic microbes, microbes derived from aquatic (freshwater or marine) environments, cyanobacteria, and literature leads.

An exploratory pilot project was conducted with the goal of culturing marine-derived microbes from marine sediment samples using a variety of sample pretreatments and growth media to generate both pigment producing microbial strain leads and to explore conditions that might produce more pigmented strains. A variety of blue and purple pigmented secondary metabolites were dereplicated from marine-derived strains using microextraction and the HPLC-PDA-HRMS^2 analysis (section 2.3) and established methodology useful for rapid pigment dereplication. Other investigated pigments

included phycocyanin extracted from cyanobacteria (Orjala laboratory, UIC), an unknown and unstable black bacterial melanin derivative from a *Bacillus sp*. ATCC 6461, and prodigiosin-containing thermophilic microbial extracts (courtesy of Montana Polysaccharides Corp., Winnsboro, SC). The pigment ammosamide A was investigated and found unsuitable due to a lack of aqueous stability and solubility as well as having high general cytotoxicity. Much of the work presented in Chapter 2 was covered in a peer-reviewed book chapter (16).

The unidentified purple pigment of acidophilic *Zygogonium sp.* algae discussed in Chapter 3 (biomass obtained from Yellowstone National Park) was isolated and characterized by a variety of chemical and spectroscopic techniques. The purple pigmentation was found to arise from chelation of ferric iron by galloyl groups in the form of free gallic acid, galloyl glycosides and galloyl oligosaccharides. The need for an accurate quantitation of bound galloyl groups in this work led to the development of an improved LC/MS method for the determination of bound galloyl groups which was published (233) and presented in Chapter 4. As a water soluble and acid stable natural and putatively nontoxic organometallic complex, the purple pigment has some appeal for use as a natural colorant or dye but is very unlikely to be useful for consumable beverage colorant due to the low color intensity and high iron content. Aside from being a natural pigment, the chemical structure elucidation of the unusual ferric gallate complex was of fundamental ecological and chemical interest.

The intense blue hue, unique chromophore, apparent low toxicity, and minimal published information made the bis-indole pigment trichotomine from *Clerodendron trichotomum* (Japanese kusagi berry) a compelling natural blue colorant lead candidate. Chapter 5 covered the isolation, 2D-NMR structure elucidation, and pH and heat stability investigation of 3 new trichotomine glycosides (trichotomine G_3, trichotomine G_4, and trichotomine G_5) in an extract of the kusagi berry. Compared with the previously reported trichotomine monoglycoside (trichotomine G_1) and diglycoside

(trichotomine G_2), the novel analogs contained 6-*O*-malonyl attachments. Higher molecular weight trichotomine glycosides containing 3 sugar moieties were identified by $HRMS^n$ analysis. For all analogs, the glycosides were found to be attached to the trichotomine carboxylic acid groups (COOGlu) as opposed to the indole rings (NGlu) as was previously reported. Although the properties of the trichotomines are generally favorable, preliminary color stability testing indicated that acid and heat stability is insufficient for use as a consumer beverage colorant. Further research on trichotomine might include the elucidation of the trichotomine biosynthetic pathway, finding more stable natural analogs or discovering other means of enhancing trichotomine stability without compromising the "natural" criteria.

The blue iridoid-derived colorants from *Genipa americana* and *Gardenia jasminoides* are used in just a few food coloring applications because of limited regulatory approval. The chromophore structure of the blue pigment polymeric product derived from the reaction of the iridoid genipin and an amino acid was described in Chapter 6. The NMR analysis of a commercial "gardenia blue" product provided by San Ei Gen F.F.I. revealed mostly the starting compound genipin with unresolvable baseline complexity arising from the polymeric blue pigmented products. For further analysis, "gardenia blue" pigment was generated fresh by the reaction of genipin with methylamine, and the initial blue products were analyzed by size-exclusion chromatography (SEC) and HPSEC-UV-$HRMS^2$. The UV spectra of possible monomers and dimers were theoretically predicted using density functional theory (DFT) calculations. The experimental and theoretical results suggested that the "gardenia blue" pigment involves the transformation of genipin to 2-pyrindine monomers, and that the blue chromophore involves conjugated dimers of the 2-pyrindine ring system linked by an unsaturated C_1 or C_2 bridge.

Finding a naturally sourced replacement for synthetic FD&C Blue No. 1 food dye is extraordinarily difficult task. Blue pigmented molecules are relatively rare in nature and nearly all of

those that exist have critical failures with stability, safety, toxicity, hue, and and feasibility issues. In the opinion of the author, the most promising avenues for finding a successful replacement would be (1) continued lead discovery through a pigment screening program involving marine environment and (2) the pursuitt of a more heat and acid stable variant of the blue phycocyanin protein from extremophilic cyanobacteria. The rationale for (1) is towards the discovery of new natural blue pigmemt chromophoric scaffolds since all the known ones have failed. The marine environment is as promising a source of new chromophoric carbon skeletons for natural pigment leads as it is of new drugs. The pursuit of a more heat and/or acid stable varieties of phycocyanin protein is logical and feasible since the mesophilic cyanobacteria has been developed into a successful commercial blue pigment product (LinaBlue A) which only fails in beverages due to poor acidic solution stability.

In conclusion, a natural blue colorant suitable for consumer beverage applications has yet been found, but this dissertation contributes a foundation for future work towards that goal. In addition to contributing the first comprehensive literature review of natural blue pigment molecules, this work also contributes novel structures include intensely blue trichotomine malonylglycosides from *Clerodendron trichotomum,* and structural understanding of the unidentified purple pigment of *Zygogonium sp.* algae as an organoferric oligosaccharide complex involving galloyl oligosaccharides, a new class of biological molecules. Progress towards identifying blue chromophore structures within the complex mixture of polymeric iridoid-derived blue pigmented products derived from genipin (*Genipa americana*) was also presented. In future directions, investigation of natural means for increasing the stability of the trichotomine derivatives and investigation of more heat and acid stable versions of phycocyanin from extremophilic cyanobacteria are two promising areas for investigation of an acid stable natural blue colorant.

APPENDICES

APPENDIX H

Copyright Clearance Center RightsLink®

Home | Create Account | Help

ACS Publications
Most Trusted. Most Cited. Most Read.

Book: Physical Methods in Food Analysis
Chapter: Isolation and Characterization of Natural Blue Pigments from Underexplored Sources
Author: A. G. Newsome, B. T. Murphy, R. B. van Breemen
Publisher: American Chemical Society
Date: Jan 1, 2013
Copyright © 2013, American Chemical Society

LOGIN
If you're a copyright.com user, you can login to RightsLink using your copyright.com credentials.
Already a RightsLink user or want to learn more?

Quick Price Estimate

Permission for this particular request is granted for print and electronic formats, and translations, at no charge. Figures and tables may be modified. Appropriate credit should be given. Please print this page for your records and provide a copy to your publisher. Requests for up to 4 figures require only this record. Five or more figures will generate a printout of additional terms and conditions. Appropriate credit should read: "Reprinted with permission from {COMPLETE REFERENCE CITATION}. Copyright {YEAR} American Chemical Society." Insert appropriate information in place of the capitalized words.

I would like to...	reuse in a Thesis/Dissertation
Requestor Type	Author (original work)
Portion	make a selection
Format	Print
Select your currency	USD - $
Quick Price	Click Quick Price

QUICK PRICE | CONTINUE

This service provides permission for reuse only. If you do not have a copy of the article you are using, you may copy and paste the content and reuse according to the terms of your agreement. Please be advised that obtaining the content you license is a separate transaction not involving Rightslink.

To request permission for a type of use not listed, please contact the publisher directly.

APPENDIX H (continued)

Publication request: Thesis

JAFC Office <jafc@jafc.acs.org> Mon, Sep 8, 2014 at 6:43 PM
To: anewso2@gmail.com

Dear Mr. Newsome,

According to the terms of the ACS Journal Publishing Agreement, you do not need permission to reuse material from your manuscript in your dissertation. See Section II, part 1, reproduced below.

Securing written confirmation from the editor to avoid potential prior publication/embargo policy conflicts is needed. Since your manuscript has already been published, no prior publication conflict exists.

Best wishes for success in your career.

Sincerely,

Loreen Kleinschmidt for James N. Seiber, Editor

Journal of Agricultural and Food Chemistry

SECTION II: Permitted Uses by Author(s)

1. Reuse/Republication of the Entire Work in Theses or Collections:

Authors may reuse all or part of the Submitted, Accepted or Published Work in a thesis or dissertation that the Author writes and is required to submit to satisfy the criteria of degree-granting institutions. Such reuse is permitted subject to the ACS' "Ethical Guidelines to Publication of Chemical Research"

Isolation and Characterization of Natural Blue Pigments (reduced)

ORIGINALITY REPORT

0%

SIMILARITY INDEX

PRIMARY SOURCES

EXCLUDE QUOTES	ON	EXCLUDE MATCHES	OFF
EXCLUDE BIBLIOGRAPHY	ON		